EVALUATION OF A GAS-PHASE ATMOSPHERIC REACTION MECHANISM FOR LOW NO_x CONDITIONS

Final Report to the
California Air Resources Board
Contract No. 01-305

By

William P. L. Carter

May 5, 2004

Air Pollution Research Center and
Center for Environmental Research and Technology
College of Engineering
University of California
Riverside, California 92521

ABSTRACT

The ability SAPRC-99 atmospheric chemical mechanism to predict photochemical smog formation under low NO_x conditions was evaluated by comparing model predictions to results experiments from three different environmental chamber facilities. These included new experiments from our UCR EPA environmental chamber, and previous experiments at from the Tennessee Valley Authority (TVA) and the Australian Commonwealth Scientific and Industrial Research Organization (CSIRO) chambers. The facility and procedures for the new UCR EPA experiments, and the procedures for modeling data from all three chambers, are discussed.

The results indicated no apparent low NO_x mechanism performance problem for SAPRC-99 for simple chemical systems and for ambient surrogate reactive organic gas (ROG) - NO_x experiments with ROG/NO_x ratios high enough for maximum ozone formation potentials to be achieved. However, a consistent underprediction bias for NO oxidation and O_3 formation rates was found in simulations ambient surrogate ROG - NO_x experiments at low ROG/NO_x ratios. The widely used Carbon Bond 4 mechanism was even worse in this regard. Furthermore, new aromatic - CO - NO_x experiments indicate problems with current aromatic mechanisms that may be the cause of the low ROG/NO_x underpredictions. Integrated reaction rate calculations indicate that increasing the accuracy in representing combination reactions of organic peroxy radicals will probably have an insignificant effect on model predictions. It is concluded that at a minimum new aromatic mechanisms need to be developed for model predictions to be consistent with available data.

ACKNOWLEDGEMENTS AND DISCLAIMERS

The preparation of this report, all of the modeling and analysis work contained herein, and the UCR EPA chamber experiments carried out at NO_x levels of 10 ppb or lower and associated characterization runs were funded by the California Air Resources Board (CARB) through Contract No. 01-305. The remainder of the UCR EPA chamber experiments discussed in this report were funded by the United States Environmental Protection Agency cooperative agreement no. CR 827331-01-0.

The UCR EPA chamber experiments were carried out at the College of Engineering Center for Environmental Research and Technology primarily by Ms. Irina Malkina and Mr. Kurt Bumiller with the assistance of Claudia Sauer. Major contributions to the management of the UCR EPA chamber project was provided by Mr. Dennis Fitz, Manager of Atmospheric Processes at CE-CERT. Contributions to the design and construction of the UCR EPA facility were provided by Mr. Dennis Fitz, Mr. Kurt Bumiller, Mr. Charles Bufalino, Mr. Matt Smith and Mr. John Pisano.. Mr. John Pisano, Dr. Claudia Sauer, Mr. Kurt Bumiller, and Ms. Irina Malkina provided assistance in developing and assessing the analytical methods, with Mr. Pisano providing the lead in developing the TDLAS systems.

Helpful correspondence with Dr Robert Hynes of CSIRO regarding the CSIRO experiments is gratefully acknowledged. The author thanks Dr. Hynes for providing us with a copy of his conference paper on modeling the CSIRO experiments that proved to be extremely valuable in our modeling of those experiments. Dr. Deborah Luecken, the project officer for the above-referenced EPA cooperative agreement provided useful information and reports on the TVA and CSIRO chamber data that were used in this work. The author also thanks Dr. Roger Atkinson of the Air Pollution Research Center at UCR for helpful discussions concerning the chemical mechanism and atmospheric chemistry in general. Finally, we wish to thank the CARB staff for technical support and helpful discussions, specifically Dr. Dongmin Luo, the CARB project officer, and Dr. Luis Woodhouse, who was instrumental in initiating this project.

Although this work was funded primarily by the California Air Resources Board, it reflects only the opinions and conclusions of the author. Mention of trade names and commercial products does not constitute endorsement or recommendation for use.

TABLE OF CONTENTS

EXECUTIVE SUMMARY 1
Background 1
Results and Discussion 2
UCR EPA Chamber Experiments 2
TVA and CSIRO Experiments 2
Mechanism Performance 4
Alternative Low NO_x Mechanisms 5
Conclusions 6

INTRODUCTION 7

ENVIRONMENTAL CHAMBER EXPERIMENTS 10
Chamber Description 10
Analytical and Characterization Methods 12
Analytical Instrumentation 12
Sampling methods 16
Characterization Methods 16
Experimental Procedures 17
Summary of Experiments 18

MECHANISM EVALUATION METHODS 22
Chemical Mechanism Used 22
Evaluation Against UCR EPA Chamber Experiments 24
Characterization of Run Conditions 25
Chamber Effects Parameters 27
TVA Chamber Experiments 32
Description of Chamber and Experimental Procedures 32
Runs Modeled and Preparing of Data for Modeling 34
Characterization of Run Conditions 35
Derivation of Chamber Effects Parameters for Modeling 37
CSIRO Chamber Experiments 41
Chamber Description and Runs Modeled 41
Characterization of Run Conditions 43
Chamber Effects Parameters Used for Modeling 47
Results of Pure Air Simulation Test 48

MECHANISM EVALUATION RESULTS 49
UCR EPA Experiments 49
Characterization Runs 49
Single Compound Experiments 52
Ambient Surrogate Experiments 57
TVA Experiments 62
Characterization Runs 63
Single Compound Experiments 65
Mixture Experiments. 67
CSIRO Experiments 70

TABLE OF CONTENTS (continued)

DISCUSSION AND CONCLUSIONS 73
Smog Chamber Performance 73
TVA Chamber 73
CSIRO chamber 73
UCR EPA Chamber 74
Mechanism Performance 75
Low NO_x Conditions 75
Aromatics Mechanisms 76
Ambient Simulations 78
Assessment of Need to Modify Mechanism for low NO_x Conditions 82
Overall Conclusions and Recommendations 88

REFERENCES 90

APPENDIX A. LISTINGS AND TABULATIONS 95
UCR EPA Chamber Run Summary 95
Chamber Effects Model Summary 102

APPENDIX B. CHAMBER DATA PLOTS 105
UCR EPA Chamber Experiments 105
TVA Chamber Experiments 135
CSIRO Chamber Experiments 151

LIST OF TABLES

Table E-1. Summary of environmental chamber experiments used for mechanism evaluation. 3

Table 1. List of analytical and characterization instrumentation for the UCR EPA chamber. 13

Table 2. Summary of types of characterization experiments carried out in the UCR EPA chamber between January 4 and August 23, 2003 that were used for deriving characterization parameters in the mechanism evaluations using this chamber. 19

Table 3. Summary of mechanism evaluation experiments carried out in the UCR EPA chamber between January 4 and August 23, 2003. 20

Table 4. Average Compositions of the ambient reactive organic gas (ROG) surrogates in the UCR EPA surrogate - NO_x experiments modeled in this report. 21

Table 5. Composition the complex urban ROG surrogate mixture used in the TVA and CSIRO experiment and the condensed model species used to represent them. 23

Table 6. Summary of types of UCR EPA characterization experiments and chamber effects parameters they were used to derive chamber effects parameters. 28

Table 7. Summary of dark ozone decay measurements in the UCR EPA chamber. 28

Table 8. Summary of UCR EPA chamber characterization experiments that were modeled to determine radical source and formaldehyde offgasing parameters. 29

Table 9. Summary of TVA chamber runs used for mechanism evaluation in this project. Experimental and calculated predictions of O_3 formed and NO oxidized are also shown. 35

Table 10. Summary of types of TVA characterization experiments and chamber effects parameters they were used to derive chamber effects parameters for this chamber. 38

Table 11. Best fit characterization parameters for individual TVA characterization experiments. 39

Table 12. Summary of reactants, Δ([O3]-[NO]) results, and model biases for the CO - air and CO - formaldehyde - air characterization experiments in the UCR EPA chamber. 50

Table 13. Summary of reactants, Δ([O3]-[NO]) results, and model biases for the CO - air and CO - formaldehyde - air characterization experiments in the UCR EPA chamber. 51

Table 14. Summary of reactants, Δ([O3]-[NO]) results, and model biases for the single compound experiments in the UCR EPA chamber. 53

Table 15. Summary of reactants, Δ([O3]-[NO]) results, and model biases for the ambient surrogate - NO_x experiments in the UCR EPA chamber. 58

Table 16. Summary of the initial concentrations and the experimental and calculated amounts of O_3 formed and NO oxidized in the TVA characterization experiments modeled for this project. Figure numbers showing plots of the data in Appendix B are also shown. 64

Table 17. Summary of the initial concentrations and the experimental and calculated amounts of O_3 formed and NO oxidized in the TVA single compound experiments. 66

LIST OF TABLES (continued)

Table 18. Summary of the initial concentrations and the experimental and calculated amounts of O_3 formed and NO oxidized in the TVA mixture experiments. 68

Table 19. Summary of conditions and experimental and calculated NO oxidized and O_3 formed in the CSIRO experiments modeled for this program. 71

Table 20. Summary of input conditions of model scenarios used to calculate relative contributions of peroxy radical reactions. 85

Table A-1. Summary of environmental UCR EPA environmental chamber experiments carried out or modeled for this project. 95

Table A-2. Chamber wall effect and background characterization parameters used in the environmental chamber model simulations for mechanism evaluation. 102

LIST OF FIGURES

Figure E-1. Schematic of the UCR EPA environmental chamber reactors and enclosure. 3

Figure E-2 Plots of model underprediction error against normalized initial reactive organic gas / NO_x concentrations for the ambient surrogate - NO_x experiments modeled for this project. 5

Figure 1. Schematic of the UCR EPA environmental chamber reactors and enclosure. 11

Figure 2. Spectrum of the argon arc light source used in the UCR EPA chamber. Blacklight and representative solar spectra, with relative intensities normalized to give the same NO_2 photolysis rate as that for the UCR EPA spectrum, are also shown. 11

Figure 3. Matrix of initial reactive organic gas (ROG) and NO_x levels fir the ambient surrogate - NO_x experiments carried out in the UCR EPA chamber during the period covered by this report. Model calculations of MIR and MOIR conditions are also shown. 21

Figure 4. Plots of various measures of light intensity for the EPA chamber experiments against EPA run number. 26

Figure 5. Plot of temperature measurements made during run EPA123. 27

Figure 6. Plots of best fit HONO offgasing parameters against UCR EPA run number. 30

Figure 7. Diagram of the TVA indoor environmental chamber and associated laboratory 33

Figure 8. Spectra of the TVA chamber light source used for calculating photolysis rates for modeling. 34

Figure 9. Measured and assigned NO_2 photolysis rates for the TVA chamber experiments. 36

Figure 10. Time series plots for temperature during two example TVA chamber experiments. 37

Figure 11. Picture of the CSIRO Dual Outdoor Chamber and associated laboratory structures 42

Figure 12. Matrix of initial ROG and NO_x levels for the CSIRO chamber experiments modeled in this project. Different symbols are used to indicate maximum ozone concentration range. 43

Figure 13. Plots of experimental and model input temperatures for the CSIRO experiments. 45

Figure 14. Plots of experimental and calculated TSR data for the CSIRO experiments. Calculated TSR data are shown without adjustments and with total light intensity adjustments derived as discussed in the text. 46

Figure 15. Effect of increasing background methane from 1.8 to 5 ppm in simulations of $\Delta([O_3]-[NO])$ in the formaldehyde - NO_x experiment EPA069. 54

Figure 16. Experimental and calculated effects of CO additions in the toluene and m-xylene - NO_x experiments in the UCR EPA chamber. 56

Figure 17. Plot of $\Delta([O_3]-[NO])$ model underprediction bias against the ROG/NO_x ratio for the surrogate - NO_x experiments in the UCR EPA chamber. 59

LIST OF FIGURES (continued)

Figure 18. Effects of changing NO_x offgasing chamber parameter on calculations of selected species in the low NO_x ambient surrogate experiment EPA101A. 60

Figure 19. Plots of biases in model predictions of increases in formaldehyde concentration against initial ROG/NO_x ration and initial NO_x levels for the UCR EPA surrogate - NO_x experiments. 62

Figure 20. Plots of biases in model predictions of PAN against initial ROG/NO_x ratios and against biases in model predictions of $\Delta([O_3]-[NO])$ for the UCR EPA surrogate - NO_x experiments. 62

Figure 21. Plots of model underprediction error against ROG/NO_x ratio for the various types of mixture experiments carried out in the TVA chamber. 69

Figure 22. Plots of $\Delta([O3]-[NO])$ model overprediction error against ROG/NO_x ratio for the CSIRO experiments 72

Figure 23. Examples of results of reoptimizing SAPRC-99 toluene mechanism to fit different types of selected evaluation data. 77

Figure 24. Plots of model underprediction error for $\Delta([O_3]-[NO])$ in the ambient surrogate runs in the various chambers against the ROG/NO_x ratio normalized to the approximate ROG/NO_x ratios giving maximum O_3 concentrations for the conditions of the experiments. 79

Figure 25. Comparison of SAPRC-99 and CB4 underprediction errors for model simulations of the UCR EPA ambient surrogate experiments as a function of initial ROG and NO_x 79

Figure 26. Plots of underprediction error against OH reactivity-adjusted ROG/NO_x ratios in the SAPRC-99 model predictions of the surrogate experiments used in the Carter (2000) evaluation, with plots for the current UCR EPA experiments also shown for comparison. 81

Figure 27. (a) Plots of calculated maximum ozone as a function of NO_x input for the various test scenarios. (b) Calculated O_3 as a function of time for the test scenarios for a representative low NO_x input condition. 86

Figure 28. Plots of relative integrated reaction rates for various types of peroxy radical reactions as a function of NO_x levels for the various test scenarios. 87

Figure B-1. Experimental and calculated concentration-time plots for selected compounds in the CO– air experiments EPA055 and EPA056. 105

Figure B-2. Experimental and calculated concentration-time plots for selected compounds in the CO – air experiments EPA060 and EPA076. 106

Figure B-3. Experimental and calculated concentration-time plots for selected compounds in the CO– air experiments EPA079 and EPA087. Run EPA079 was not modeled because there is no chamber characterization model assigned to this experiment, because was carried out at a lower temperature than the other characterization runs. 107

Figure B-4. Experimental and calculated concentration-time plots for selected compounds in the CO - air experiments EPA112 and EPA160. 108

Figure B-5. Experimental and calculated concentration-time plots for selected compounds in the CO – formaldehyde – air experiments EPA063 and EPA115. 109

LIST OF FIGURES (continued)

Figure B-6. Experimental and calculated concentration-time plots for selected compounds in the CO - formaldehyde - air experiment EPA133 and the CO - NO experiment EPA057. 110

Figure B-7. Experimental and calculated concentration-time plots for selected compounds in the CO - NO experiments EPA058A, EPA061, and EPA070A 111

Figure B-8. Experimental and calculated concentration-time plots for selected compounds in the CO -NO experiments EPA070B, EPA071A, and EPA103. 112

Figure B-9. Experimental and calculated concentration-time plots for selected compounds in the CO - NO experiments EPA140 and the CO - NO_2 experiments EPA058B and EPA071B. 113

Figure B-10. Experimental and calculated concentration-time plots for selected compounds in the n-butane - NO_x experiment EPA064. 114

Figure B-11. Experimental and calculated concentration-time plots for selected compounds in the formaldehyde - NO_x experiment EPA068 and the formaldehyde - CO - NO_x experiment EPA069. 115

Figure B-12. Experimental and calculated concentration-time plots for selected compounds in the ethene - NO_x experiment EPA073. 116

Figure B-13. Experimental and calculated concentration-time plots for selected compounds in the propene - NO_x experiment EPA065. 117

Figure B-14. Experimental and calculated concentration-time plots for selected compounds in the toluene and toluene – CO - NO_x experiment EPA066. 118

Figure B-15. Experimental and calculated concentration-time plots for selected compounds in the toluene – CO - NO_x experiment EPA072. 119

Figure B-16. Experimental and calculated concentration-time plots for selected compounds in the toluene and toluene – CO - NO_x experiment EPA074. 120

Figure B-17. Experimental and calculated concentration-time plots for selected compounds in the toluene and toluene – CO - NO_x experiment EPA077. 121

Figure B-18. Experimental and calculated concentration-time plots for selected compounds in the m-xylene and m-xylene – CO - NO_x experiment EPA066. 122

Figure B-19. Experimental and calculated concentration-time plots for most monitored compounds in the low NO_x surrogate - NO_x experiment EPA101. 123

Figure B-20. Experimental and calculated concentration-time plots for most monitored compounds in the low NO_x surrogate - NO_x experiment EPA098. 124

Figure B-21. Experimental and calculated concentration-time plots for most monitored compounds in the low NO_x surrogate - NO_x experiment EPA097. 125

Figure B-22. Experimental and calculated concentration-time plots for most monitored compounds in the low NO_x surrogate - NO_x experiments EPA085A and EPA86A. 126

Figure B-23. Experimental and calculated concentration-time plots for most monitored compounds in the surrogate - NO_x experiments EPA095B and EPA114A. 127

Figure B-24. Experimental and calculated concentration-time plots for most monitored compounds in the surrogate - NO_x experiments EPA110B and EPA128A. 128

LIST OF FIGURES (continued)

Figure B-25. Experimental and calculated concentration-time plots for most monitored compounds in the surrogate - NO_x experiment EPA082. 129

Figure B-26. Experimental and calculated concentration-time plots for most monitored compounds in the surrogate - NO_x experiments EPA083A and EPA084B. 130

Figure B-27. Experimental and calculated concentration-time plots for most monitored compounds in the surrogate - NO_x experiment EPA081. 131

Figure B-28. Experimental and calculated concentration-time plots for most monitored compounds in the surrogate - NO_x experiments EPA113A and EPA108B. 132

Figure B-29. Experimental and calculated concentration-time plots for most monitored compounds in the surrogate - NO_x experiment EPA080. 133

Figure B-30. Experimental and calculated concentration-time plots for most monitored compounds in the surrogate - NO_x experiment EPA096. 134

Figure B-31. Plots of experimental and calculated ozone, formaldehyde (where available) and PAN results of the TVA acetaldehyde - air experiments. 135

Figure B-32. Plots of experimental and calculated Δ([O3]-[NO]), formaldehyde (where available) and representative CO results of the TVA CO - NO_x experiments. (Model data do not show where they overlap the experimental data.) 136

Figure B-33. Plots of experimental and calculated Δ([O3]-[NO]), formaldehyde (where available) and methane (where available) results of the TVA Methane - NO_x experiments. 137

Figure B-34. Plots of experimental and calculated Δ([O3]-[NO]) and formaldehyde (where available) results of the TVA NO_x - air experiments. 138

Figure B-35. Plots of experimental and calculated Δ([O_3]-[NO]) and formaldehyde results of the TVA formaldehyde - NO_x experiments. 139

Figure B-36. Plots of experimental and calculated Δ([O_3]-[NO]), formaldehyde, isopentane, and PAN results of the TVA isopentane - NO_x experiment. 139

Figure B-37. Plots of experimental and calculated Δ([O3]-[NO]), formaldehyde and ethylene results of the TVA ethylene - NO_x experiments. 140

Figure B-38. Plots of experimental and calculated Δ([O3]-[NO]), formaldehyde, PAN and propylene results of the TVA propylene - NO_x experiments. 141

Figure B-39. Plots of experimental and calculated Δ([O3]-[NO]), formaldehyde, PAN and transs-2-butene results of the TVA trans-2-butene - NO_x experiments. 142

Figure B-40. Plots of experimental and calculated Δ([O3]-[NO]), formaldehyde, PAN, and toluene results of the TVA toluene - NO_x experiments. 143

Figure B-41. Plots of experimental and calculated Δ([O3]-[NO]), formaldehyde, and m-xylene results of the TVA m-xylene - NO_x experiments. 144

Figure B-42. Plots of experimental and calculated Δ([O3]-[NO]) and formaldehyde results of the TVA paraffin and olefin mix experiments. 145

Figure B-43. Plots of experimental and calculated PAN (where available) and propene results of the TVA paraffin and olefin mix experiments. 146

LIST OF FIGURES (continued)

Figure B-44. Plots of experimental and calculated Δ([O3]-[NO]) and formaldehyde results of the TVA paraffin, olefin and aromatic mix experiments. 147

Figure B-45. Plots of experimental and calculated PAN and toluene results of the TVA paraffin, olefin and aromatic mix experiments. 148

Figure B-46. Plots of experimental and calculated Δ([O3]-[NO]) and formaldehyde results of the TVA synthetic urban mix experiments. 149

Figure B-47. Plots of experimental and calculated PAN results of the TVA synthetic urban mix experiments. 150

Figure B-48. Experimental and calculated Δ([O_3]-[NO]), O_3, NO, and NO_y-NO data for the CSIRO experiments 340, 342, and Side P of 342. The labels give Run ID, initial VOC in ppmC, and initial NOx in ppb. 151

Figure B-49. Experimental and calculated Δ([O_3]-[NO]), O_3, NO, and NO_y-NO data for the CSIRO experiments 342 (Side L), 343 and 344. The labels give Run ID, initial VOC in ppmC, and initial NOx in ppb. 152

Figure B-50. Experimental and calculated Δ([O_3]-[NO]), O_3, NO, and NO_y-NO data for the CSIRO experiments 345, 359, and Side P of 360. The labels give Run ID, initial VOC in ppmC, and initial NOx in ppb. 153

Figure B-51. Experimental and calculated Δ([O_3]-[NO]), O_3, NO, and NO_y-NO data for the CSIRO experiments 360 (Side L), 361 and 362. The labels give Run ID, initial VOC in ppmC, and initial NOx in ppb. 154

EXECUTIVE SUMMARY

Background

Despite improvements in urban air quality in recent years, ground-level ozone concentrations continue to exceed air quality standards in many areas of California. Ground level ozone is not emitted directly, but is formed in a complex and incompletely understood series of light-induced chemical reactions involving oxides of nitrogen (NO_x) and volatile organic compounds (VOCs) that are emitted from multiple sources. Because of these complexities, those responsible for developing plans and regulations for achieving air quality standards must rely on computer airshed models to assess the effectiveness of the strategies being considered. A critical component of models for predictions of ozone and other secondary pollutants is the gas-phase chemical mechanism, i.e., the portion of the model used to represent the gas-phase chemical reactions. This is because the chemistry is the source of much of the complexity and non-linearity involved. Because many of the chemical reactions are incompletely understood, these mechanisms cannot be relied upon to give accurate predictions until their predictive capabilities have been experimentally evaluated.

The most cost-effective and reliable way to test the predictive capabilities of the chemical mechanisms is to compare their predictions against results of environmental chamber experiments that simulate the range of conditions in the atmosphere. If a model cannot accurately predict observed changes in pollutant levels in experiments carried out under controlled and well characterized conditions, it cannot be expected to reliably predict effects of proposed control strategies on ambient air quality. Because of this, the chemical mechanisms used in current airshed models have been evaluated against an extensive set of existing environmental chamber data carried out at our laboratories and elsewhere.

The SAPRC-99 mechanism is currently the most up-to-date and chemically detailed mechanism utilized by the California Air Resources Board (CARB). This mechanism was evaluated against the results of over 1500 environmental chamber experiments carried out at our laboratories with many types of VOCs and mixtures, making it the most extensively evaluated mechanism currently in use. However, the chamber data used to evaluate it and other current mechanisms have a number of limitations that affect the range of conditions and comprehensiveness of the evaluations. Of particular concern is the fact that most of the chamber data used in previous evaluations were carried out with levels of NO_x and other pollutants that are significantly higher than currently occur in most areas. Even lower NO_x conditions are also expected as we approach eventual attainment of the air quality standards. The nature of the radical and NO_x cycles and the distribution of VOC oxidation products change as absolute levels of NO_x are reduced. Because of this, one cannot necessarily be assured that the current mechanisms developed to simulate results of relatively high NO_x experiments will satisfactorily simulate downwind or cleaner environments where NO_x is low.

Fortunately, there exist data that can be utilized to address this, and a new environmental chamber facility has been developed at our laboratory that can generate additional data of the kind that is needed. Environmental chamber experiments carried out at the Tennessee Valley Authority (TVA) and Australia's Commonwealth Scientific and Industrial Research Organization (CSIRO) include a number of mechanism evaluation experiments with NO_x levels in the 20-50 ppb range, which is significantly lower than the >100 ppb range in the experiments used previously. These data were not used when SAPRC-99 was first evaluated, but have since been made more readily available for this purpose.

In addition, to address the need for an improved environmental chamber facility for mechanism evaluation, in 1999 we obtained funding from the U.S. EPA to construct and evaluate a "next generation" environmental chamber facility capable of conducting well-characterized experiments at lower pollutant conditions than previously possible. The design and construction of this facility, called the "UCR EPA chamber", was completed in late 2002, and experiments for mechanism evaluation began in early 2003. Because of its design, data from this chamber should be useful for mechanism evaluation under low NO_x conditions. However, this UCR EPA facility has been operational for only a limited period, and the EPA funding was sufficient only for its characterization and a relatively small number of experiments. The use of these data for mechanism evaluation has not previously been reported.

Because of the importance of accurate model predictions under low NO_x conditions, the CARB funded us to carry out an experimental and modeling program to improve the evaluation of the SAPRC-99 mechanism for low NO_x conditions. The experimental work included carrying out very low NO_x experiments in the new UCR chamber developed for the EPA, to supplement the experiments conducted under EPA funding. The modeling work consisted of evaluating the SAPRC-99 mechanism utilizing the new data from the UCR EPA chamber and the low NO_x TVA and CSIRO chamber data that have not been used previously in its evaluation. The results of this project, and implications of the new evaluation results concerning the performance of this mechanism under low NO_x and other conditions, are discussed in this report.

Results and Discussion

UCR EPA Chamber Experiments

The UCR EPA chamber consists of two ~85,000-liter Teflon® reactors located inside a 16,000 ft^3 temperature-controlled "clean room" to designed minimize background contamination. The primary light source consists of a 200 KW argon arc lamp designed to give a UV and visible spectrum similar to sunlight. Moveable frameworks are used to collapse the reactors as samples are withdrawn to avoid dilution during experiments and to aid in cleaning. The dual reactor design permits two irradiation experiments to be carried out at the same time. A diagram of the enclosure and reactors is shown on Figure E-1.

The UCR EPA chamber experiments carried out or modeled for this project are summarized on Table E-1. In addition to the characterization runs needed to determine conditions of the experiments for modeling, the experiments included single compound - NO_x experiments, single compound - NO_x experiments with added CO, and a matrix of reactive organic gas (ROG) ambient surrogate - NO_x experiments at a variety of initial ROG and NO_x levels. The latter including experiments at very low NO_x levels carried out specifically for this project. Model performance in simulating the NO oxidation and O_3 formation in these experiments (as measured by $\Delta([O_3]-[NO])$, or $\{[O_3]_{final}-[NO]_{final}\}-\{[O_3]_{initial}-[NO]_{initial}\}$), which is a general measure of ozone forming potential), is also shown on Table E-1. This is discussed below.

TVA and CSIRO Experiments

The TVA experiments consisted of a number of characterization, single compound - NO_x, mixture - NO_x and ambient surrogate - NO_x experiments carried out in 1993 through 1995 in a 28,300-liter indoor Teflon® chamber irradiated with banks of blacklights and other types of fluorescent sunlamps combined to approximate the spectrum of sunlight. Available characterization information and the results of the various characterization experiments were used to derive the inputs needed to model these

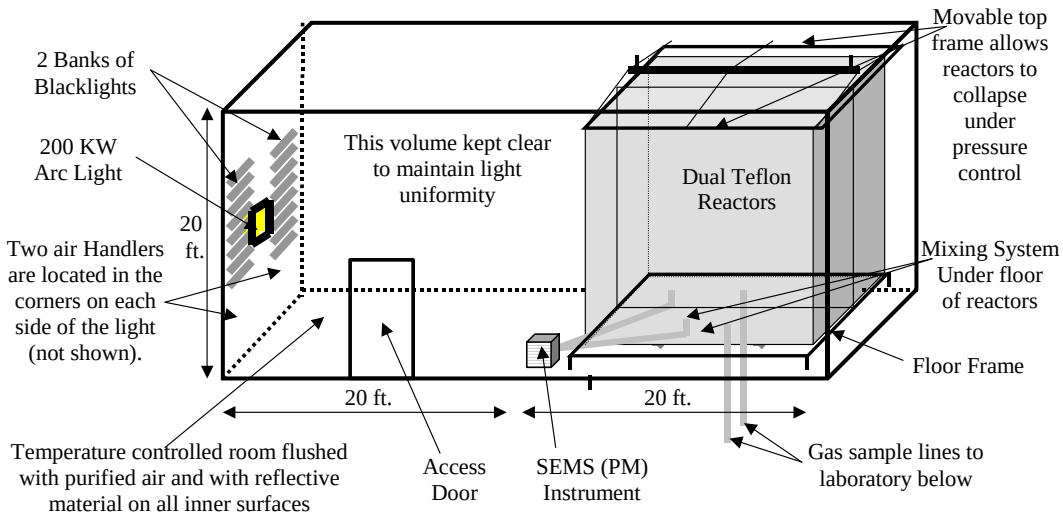

Figure E-1. Schematic of the UCR EPA environmental chamber reactors and enclosure.

Table E-1. Summary of environmental chamber experiments used for mechanism evaluation.

Run Type	Number of Runs	NO_x Range (ppb)	Average Δ([O3]-[NO]) Model Fits	
			Bias [a]	Bias [b]
UCR EPA Experiments				
Characterization	32	0 - 200	-2%	31%
HCHO - NO_x and HCHO - NO_x + CO [c]	4	8 - 25	-17%	17%
Ethene - NO_x	2	10 - 25	-15%	15%
Propene - NO_x	2	5 - 25	16%	16%
Toluene or m-Xylene - NO_x	4	5 - 25	10%	10%
Toluene or m-Xylene - NO_x + CO	6	5 - 30	-17%	18%
Ambient Surrogate - NO_x	24	2 - 110	-11%	15%
TVA Experiments				
Characterization		0 - 21		
Formaldehyde - NO_x	4	39 - 42	-4%	10%
Isopentane - NO_x	1	18	-28%	28%
Ethene, Propene, or trans-2-Butene - NO_x	7	22 - 54	10%	10%
Toluene or m-Xylene - NO_x	5	50 - 266	1%	8%
Simple Mixture - NO_x	23	50 - 100	6%	7%
Ambient Surrogate - NO_x	12	25 - 169	-8%	9%
CSIRO Experiments				
Ambient Surrogate - NO_x	20	17 - 100	-42%	42%

[a] Average of (model – experimental) / experimental
[b] Average of absolute value of (model – experimental) / experimental
[c] Two experiments with extremely high or extremely low biases are excluded from the average.

experiments. Some uncertainty was introduced because this chamber appears to have significant offgasing of formaldehyde and unknown formaldehyde precursors, so sensitivity calculations were conducted to assess this and other uncertainties. In general, these uncertainties were not sufficiently large to affect the major conclusions of this study.

The CSIRO experiments consisted of ambient mixture - NO_x irradiations carried out in dual 20,400-liter Teflon® reactors located outdoors and irradiated with natural sunlight. Characterization information for these experiments was more limited than for the other chambers, but sufficient information was available to derive or estimate the input data needed for modeling. The most uncertain inputs concerned the overall light intensity and the chamber radical source, and calculations were carried out to assess the effects of these uncertainties on mechanism evaluation results. Although these uncertainties had an impact on the result, they were not such that they changed the overall conclusions derived from modeling these experiments.

A summary of the types of TVA and CSIRO experiments modeled for this study is given in Table E-1 Model performance in simulating NO oxidation and O_3 formation in these experiments is also given on the table, and is discussed further below.

Mechanism Performance

In many respects the results of this SAPRC-99 mechanism evaluation study supported conclusions drawn from results of the previous evaluation of this mechanism. With a few important exceptions discussed below, the mechanism preformed as well or better in simulating these experiments as it did simulating the higher NO_x experiments used when it was originally evaluated. In addition, there was no obvious problem in simulating experiments carried out at the lowest NO_x levels, including experiments with aromatics, where this was a particular concern. Therefore these data extend downward, by at least an order of magnitude, the NO_x concentrations for which this mechanism has been shown to give satisfactory predictions of O_3 formation. However, the results of this study also revealed problems with the current mechanism that were not evident when it was previously evaluated. These are discussed below.

New UCR EPA experiments indicate a potentially significant problem with the aromatic mechanisms. Although the model preformed reasonably well in simulating O_3 formation in low NO_x aromatic - NO_x - air experiments in this and other chambers, other results are not satisfactorily simulated by the mechanism. The clearest indication of this is the fact that the model underpredicts, by about a factor of two, the change in amount of O_3 formed when CO is added to aromatic - NO_x irradiations. Aromatic - CO - NO_x experiments have not to our knowledge been conducted previously for mechanism evaluation, but these are expected to be useful test our model predictions of radical initiation processes. These results, and also other observations made during this evaluation, suggest that the SAPRC-99 (and probably other) mechanisms underpredict radical initiating processes in the aromatic photooxidation system. The fact that the mechanism could give good simulations of aromatic - NO_x and other experiments used in previous evaluations suggest that either there is cancellation of errors or these experiments are not sufficiently sensitive all the aspects of the mechanism that need to be tested.

The other potentially significant evaluation problem that was observed is that there is a consistent bias in the mechanism towards underpredicting NO oxidation and O_3 formation in the ambient simulations carried out at low ROG/NO_x ratios, with the bias getting worse as the ratio decreases. This is shown on Figure E-2, which gives plots of the model underprediction error for O_3 formation and NO oxidation against initial ROG/NO_x ratio. (To place the data from the different chambers on a comparable basis, the ROG/NO_x ratios are normalized to the ratio that the model predicts to the highest ozone

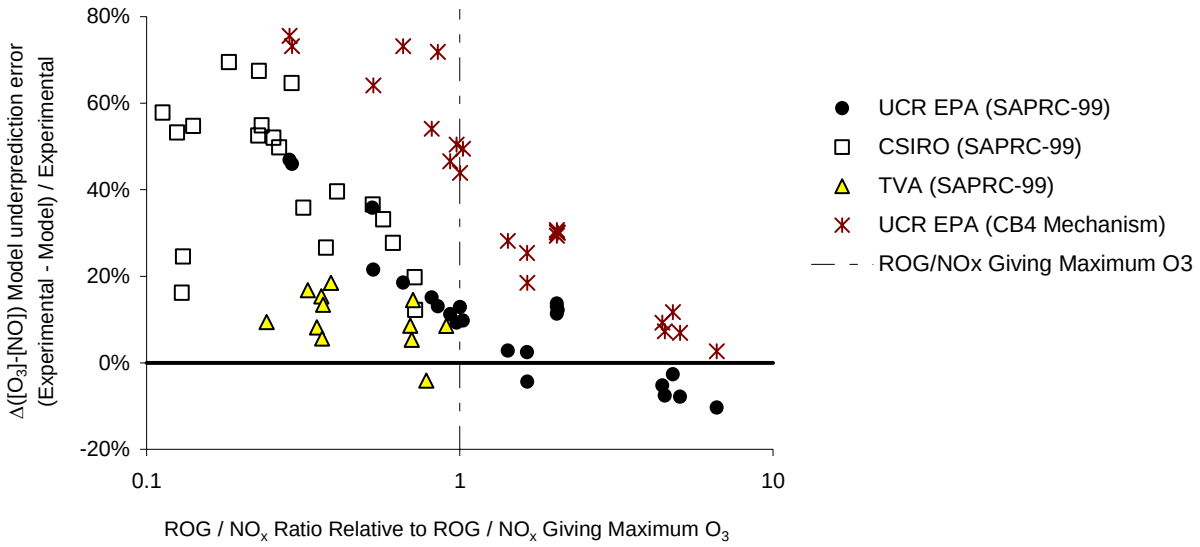

Figure E-2 Plots of model underprediction error against normalized initial reactive organic gas / NO_x concentrations for the ambient surrogate - NO_x experiments modeled for this project.

concentrations for the different sets of conditions.) The trend is most obvious for the UCR EPA chambers because of the relatively greater precision of the data and the wide range of ROG/NO_x ratios, but it can be seen in the experiments for the other chambers as well. In particular, the trend observed for the CSIRO experiments is entirely consistent with that for the UCR EPA chamber, with the large negative bias in the model in simulating those experiments as shown on Table E-1 being attributable to the fact that these experiments were carried out at a very low range of ROG/NO_x ratios.

This underprediction bias at low ROG/NO_x ratios is probably due to the problem with the aromatic mechanisms discussed above, because both are indications of insufficient radical formation being predicted. It is important to recognize that this is not just a problem with SAPRC-99; the RADM-2 mechanism has a similar representation of aromatic reactions as SAPRC-99, and the Figure E-2 shows that the low ROG/NO_x underprediction bias for the widely-used Carbon Bond 4 mechanisms is worse that that it is for SAPRC-99.

Alternative Low NO_x Mechanisms

Since the results discussed above did not indicate significant low mechanism evaluation problems that are necessarily associated with low NO_x conditions, development of alternative mechanisms specifically for low NO_x conditions was not given a high priority in this project. However, this evaluation did not assess model predictions of formation of organic photooxidation products other than formaldehyde and PAN, and the SAPRC-99 mechanism uses simplification that may result in incorrect predictions of organic photooxidation products when NO_x levels are sufficiently low peroxy + peroxy reactions become important. To assess the potential importance of these approximations, we carried out box model simulations of various single and multi-day simplified ambient scenarios to determine the relative importance of different types of peroxy + peroxy reactions.

The results of these calculations indicted that in terms of integrated reaction rates the reaction with HO_2 is the dominant fate of organic peroxy radicals under low NO_x conditions, with reactions with the other organic peroxy radials always being less than 10% of the total for peroxy radical reactions. Because of this, using more detailed representations of reactions of organic peroxy radials with other organic peroxy radicals is probably not a high priority for developing improved mechanisms for low NO_x conditions. A higher priority in this regard would be utilizing improved representations of the organic hydroperoxides believed to be formed when higher organic peroxy radials react with HO_2, which are currently represented in SAPRC-99 by only a single lumped species. However, this would require significantly larger mechanisms since multiple organic hydroperoxide species would need to be added, and the reactions of these compounds would be largely speculative.

Conclusions

This study was successful in significantly extending the range of conditions under which current atmospheric chemical mechanisms can be evaluated. The new or previously unutilized data extend the existing dataset into lower NO_x and lower VOC/NO_x conditions than previously used when evaluating such mechanisms, and the new UCR EPA data provide a higher level of precision for mechanism evaluation than previously available. The use of these data in this study has provided valuable insights concerning the predictive capabilities of the mechanisms used in current airshed models.

The results of this study include both good news and bad news regarding the predictive capabilities of the current mechanism. The good news is that there is no apparent low NO_x mechanism performance problems when simulating simple chemical systems and in ambient simulations where maximum ozone formation potentials can be achieved. The bad news is that new data indicate significant aromatic mechanism problems, and, probably because of this, the mechanism underpredicts NO oxidation and O_3 formation rates when ROG/NO_x ratios are low. This problem may not have been evident in previous evaluations in part because of scatter of the evaluation data, or, more likely, because all the lower ROG/NO_x ambient surrogate experiments were carried out at much higher NO_x levels than the experiments used in this study. This is significant because the NO_x levels used in the current evaluation are more representative of those in the atmosphere, and low ROG/NO_x ratios are characteristic of the more densely populated source areas.

Developing improved aromatic mechanisms that are consistent with all the available data needs to be given high priority, and the mechanism performance problem at low ROG/NO_x ratios needs to be addressed. This is one of the tasks in follow-on mechanism development project that has recently been approved by the CARB, and hopefully addressing this problem will also result in improvements in the performance at low ROG/NO_x ratios.

While the addition of the new or previously unexploited data discussed above expands the range of conditions covered by the now-available mechanism evaluation dataset, significant gaps still remain. Experiments are needed to assess possible inconsistencies between the high NO_x and low NO_x mechanism evaluation datasets. The aromatic mechanism performance problems are indicated by a relatively small set of experiments, and additional experiments will be needed to guide the development and fully evaluate any new aromatics mechanisms that are developed. Some experiments of this type are included in the follow-on mechanism development project for the CARB, but the resources for this are limited. Other aspects of mechanism performance, such as predictions of temperature effects or predictions of formations of condensable materials leading to the formation of secondary PM, are still not adequately evaluated.

INTRODUCTION

Despite improvements in urban air quality in recent years, unacceptable levels of ground-level ozone continues to be a persistent problem, which is not restricted to urban areas (NRC, 1991). To meet National Ambient Air Quality Standards, state and local agencies must implement additional regulations to control pollutant emissions. Ground level ozone is not emitted directly, but is formed in a complex and incompletely understood series of light-induced chemical reactions involving oxides of nitrogen (NO_x) and volatile organic compounds (VOCs) which are emitted from a variety of sources (NRC, 1991; Atkinson, 1990). Developing appropriate control strategies for ozone is complicated by the fact that reducing NO_x and VOCs have quite different effects on the ozone produced. Different types of VOCs also have very different effects on ozone. For example, reducing NO_x emissions may actually cause ozone concentrations to become higher in some urban areas, but NO_x reductions are probably the only means by which significant ozone improvement can be obtained in rural or downwind areas. VOC controls are often most effective in reducing ozone in urban areas, but VOC controls may have little effect on ozone in downwind areas where ozone is largely NO_x-limited. Furthermore, the relative effects of different VOCs on ozone formation also depend on the environment where they are reacting, with the NO_x levels being an important, but not the only factor (Carter and Atkinson, 1989; Carter, 1994).

Because of these complexities, those responsible for developing plans and regulations for achieving air quality standards must rely on computer airshed models to assess the effectiveness of the strategies they are considering. A critical component for predictions of pollutants such as ozone and other secondary pollutants is the gas-phase chemical mechanism, i.e., the portion of the model used to represent the gas-phase chemical reactions involved. This is because the chemistry is the source of much of the complexity and non-linearity involved. Because many of the chemical reactions are incompletely understood, these mechanisms cannot be relied upon to give accurate predictions of impacts on emissions on air quality until they have been shown to give accurate predictions of pollutant concentrations under realistic but controlled conditions.

Ozone is not the only secondary pollutant of interest to regulators. The reactions of organics in the atmosphere form formaldehyde and higher aldehydes, PAN and higher peroxynitrates, organic acids and other pollutants that can affect the environment and exposed populations and materials. They also form condensable species that contribute to the formation of secondary particulate matter (PM), which may have an even greater impact on health effects than ozone problem than ozone. The accurate prediction of these species in airshed models also critically depends on the chemical mechanism employed.

The most cost-effective and reliable way to test the predictive capabilities of the chemical mechanisms is to compare their predictions against results of environmental chamber experiments that simulate the range of conditions in the atmosphere. These involve adding known amounts of representative pollutants to large enclosures, and measuring the changes in concentrations and secondary pollutants formed when they are irradiated with either real or artificial sunlight under controlled conditions for periods of a day or longer. If a model cannot accurately predict observed changes in pollutant levels in such experiments, it cannot be expected to reliably predict effects of proposed control strategies on ambient air quality.

The available environmental chamber database for evaluating ozone mechanisms has been reviewed by Dodge (2000) as part of the 1998 NARSTO ozone assessment. A fairly extensive set of quality-assured data exist for experiments carried out at our facilities at UCR (Carter et al, 1993, 1995a,b,

1997, 2000, others[1]) and at the University of North Carolina (UNC) (Jeffries et al, 1982, 1985a-c, 1990; Jeffries, private communication, 1995). These experiments have used a variety of compounds and mixtures, and have been used as the basis for the development and evaluation of the major oxidant mechanisms currently used in the United States (Dodge, 2000; Carter and Lurmann, 1990, 1991; Gery et al, 1989; Stockwell et al, 1990). Smaller but potentially useful sets of sets of data are available from the chambers at the Tennessee Valley Authority (TVA) facility (Simonaitis and Bailey, 1995; Bailey et al, 1996) and the Commonwealth Scientific and Industrial Research Organization (CSIRO) chamber in Australia (Johnson et al, 1997); these are discussed further below. Several new facilities are being developed in Europe (Becker, 1996; Mentel et al, 1996; Wahner et al, 1998; Dodge, 2000, and references therein; IGC, 2002; CEAM, 2004), though most of the available data primarily involve specialized studies of specific chemical systems rather than general mechanism evaluation.

However, as also discussed by Dodge (2000), the then-available chamber data base has a number of serious limitations and data gaps that could be limiting the accuracy of the mechanisms used in the models to predict control strategies. Uncertainties exist concerning characterization of chamber conditions, particularly how wall artifacts affect the gas-phase reactions (Carter and Lurmann, 1990, 1991), and inappropriate treatment of these effects could cause compensating errors in the gas-phase mechanism (Jeffries et al, 1992). One important limitation is that because of chamber background and wall effects, and because of inadequate analytical equipment currently available at environmental chamber facilities, most of the current environmental chamber data base is not suitable for evaluating chemical mechanisms under the lower NO_x conditions[2] found in rural and urban areas with lower pollutant burdens. Relatively low NO_x conditions are also expected to become more typical in urban areas as we approach eventual attainment of the air quality standards. The nature of the radical and NO_x cycles and the distribution of VOC oxidation products changes as absolute levels of NO_x are reduced. Because of this, one cannot necessarily be assured that models developed to simulate urban source areas with high NO_x conditions will satisfactorily simulate downwind or cleaner environments where NO_x is low.

The TVA and CSIRO chamber database are potentially useful in this regard because they include a number of mechanism evaluation experiments with NO_x levels in the 20-50 ppb range. However, other than the evaluation of the Carbon Bond mechanism with the TVA data by Simonaitis et al (1997), these data have not been extensively used in mechanism evaluation studies. Because of this, under funding from the Reactivity Research Working Group[3], Jeffries et al (2000a,b) compiled data from these chambers and made them available for wider use.

To address the need for an improved environmental chamber facility for mechanism evaluation, in 1999 we obtained funding from the U.S. EPA to construct and evaluate a "next generation" environmental chamber facility capable of conducting well-characterized experiments at lower pollutant conditions than previously possible (Carter et al, 1999). The design and construction of this facility, designated the "UCR EPA" chamber, was completed in late 2002, and experiments useful for mechanism evaluation began in early 2003. Because of its design, data from this chamber would clearly be useful for mechanism evaluation under low NO_x conditions. However, this UCR EPA facility has been operational for only a limited period, and the EPA funding was sufficient only for its characterization and a relatively small number of experiments. The use of these data for mechanism evaluation has not previously been reported.

---

[1] See downloadable documents at http://cert.ucr.edu/~carter/bycarter.htm.

[2] In this report, the term "low NO_x conditions" will refer to conditions where total NO_x concentrations are less than about 50 ppb.

[3] See http://www.cgenv.com/Narsto/reactinfo.html for more information about the Reactivity Research Working Group.

The SAPRC-99 chemical mechanism (Carter, 2000a) is the most up-to-date and chemically detailed of the mechanisms currently in use by regulatory agencies in the United States. This mechanism includes the capability of representing the reactions of over 500 types of VOCs, either singly or in mixtures, and was used as the basis for calculating the Maximum Incremental Reactivity (MIR) scale for quantifying the effects of VOCs on ozone for regulatory applications in California (CARB, 1993, 2000). In addition to ozone, it can be used to predict the formation of a number of aldehyde, PAN, and organic acid species, and can potentially serve as the basis for developing mechanisms for predicting PM precursor formation.

Demonstrating the predictive capability of the SAPRC-99 mechanism is important to the California Air Resources Board (CARB) because of its use in California modeling applications and because of its use in calculating the ozone reactivity scales for VOCs in current and proposed CARB regulations (CARB, 1993, 2000, 2003a,b). This mechanism was evaluated against the full set of environmental chamber experiments carried out at UCR through 1999 (Carter, 2000) and earlier versions of this mechanism were evaluated against a large number of relatively high NO_x chamber experiments carried out at UNC (Carter and Lurmann, 1991; Carter and Atkinson, 1996). Almost all of the experiments used in our evaluation employed NO_x levels higher than about 80 ppb, which as indicated above do not represent the low NO_x conditions representative of many a and thus this evaluation did not include low NO_x conditions. Recently, Hynes et al (2003) reported evaluating SAPRC-99 using several lower NO_x CSIRO experiments, but the model performance was found to be unsatisfactory.

Because of the importance of accurate model predictions under low NO_x conditions, the CARB funded us to carry out an experimental and modeling program to improve the evaluation of the SAPRC-99 mechanism for low NO_x conditions. The experimental work included carrying out very low NO_x experiments in the new UCR chamber developed for the EPA, to supplement the existing low NO_x TVA and CSIRO experiments and the UCR EPA experiments conducted under EPA funding. The modeling work consisted of evaluating the SAPRC-99 mechanism utilizing the TVA and CSIRO chamber data that have not been used previously in its evaluation, and to evaluate the mechanism using the new data from the UCR EPA chamber. The results of this project, and implications of the new evaluation results concerning the performance of this mechanism under low NO_x and other conditions, are given in this report.

ENVIRONMENTAL CHAMBER EXPERIMENTS

All UCR experiments carried out or modeled for this project were carried out in the new "UCR EPA" environmental chamber. This chamber was constructed under EPA funding to address the needs for an improved environmental chamber database for mechanism evaluation (Carter, 1999). The objectives, design, construction, and initial evaluation of this chamber facility are described in more detail elsewhere (Carter et al, 1999, Carter, 2002a.b). Experiments in the current configuration useful for mechanism evaluation began in early 2003. The initial experiments were carried out under EPA funding and consisted not only of characterization runs but also experiments useful for mechanism evaluation. The latter included low NO_x experiments with simple chemical systems and ambient surrogate - NO_x experiments carried out at several total reactive organic gas (ROG) and NO_x levels, most being lower than previously employed in our chambers. For this project, we conducted ambient surrogate - NO_x experiments at even lower NO_x levels. The experimental methods, characterization, and results of these experiments are discussed in this section. Note that this also includes methods and results of the EPA experiments that were modeled for this project, since they are an essential part of this data set and they have not been described in sufficient detail previously. The methods used and characterization data for those experiments are also applicable to the experiments carried out specifically for this CARB program.

Chamber Description

The UCR EPA chamber consists of two ~85,000-liter Teflon® reactors located inside a 16,000 cubic ft temperature-controlled "clean room" that is continuously flushed with purified air. The clean room design is employed in order to minimize background contaminants into the reactor due to permeation or leaks. The primary light source consists of a 200 KW argon arc lamp with specially designed UV filters that give a UV and visible spectrum similar to sunlight. Banks of blacklights are also present to serve as a backup light source for experiments where blacklight irradiation is sufficient, but these were not used in the experiments discussed in this report. The interior of the enclosure is covered with reflective aluminum panels in order to maximize the available light intensity and to attain sufficient light uniformity, which is estimated to be ±10% or better in the portion of the enclosure where the reactors are located (Carter, 2002a). A diagram of the enclosure and reactors is shown on Figure 1, and the spectrum of the light source is shown on Figure 2.

The dual reactors are constructed of flexible 2 mil Teflon® film, which is the same material used in the other UCR Teflon chambers used for mechanism evaluation (Carter et al, 1995a; Carter, 2000a, and references therein). Tests indicated that other reactor film materials did not yield lower background effects (Carter et al, 2002a), and it was determined to be best to stay with the material for which there is already a large body of chamber characterization data. A semi-flexible framework design was developed to minimize leakage and simplify the management of large volume reactors. The Teflon film is heat-sealed into separate sheets for the top, bottom, and sides (the latter sealed into a cylindrical shape) that are held together and in place using bottom frames attached to the floor and moveable top frames. The moveable top frame is held to the ceiling by cables that are controlled by motors that raise the top to allow the reactors to expand when filled or lower the top to allow the volume to contract when the reactors are being emptied or flushed. These motors are in turn controlled by pressure sensors that raise or lower the reactors as needed to maintain slight positive pressure. During experiments the top frames are slowly lowered to maintain continuous positive pressure as the reactor volumes decrease due to sampling or leaks. The experiment is terminated once the volume of one of the reactor reaches about 1/3 the maximum value, which varied depending on the amount of leaks in the reactor, but the time involved was greater

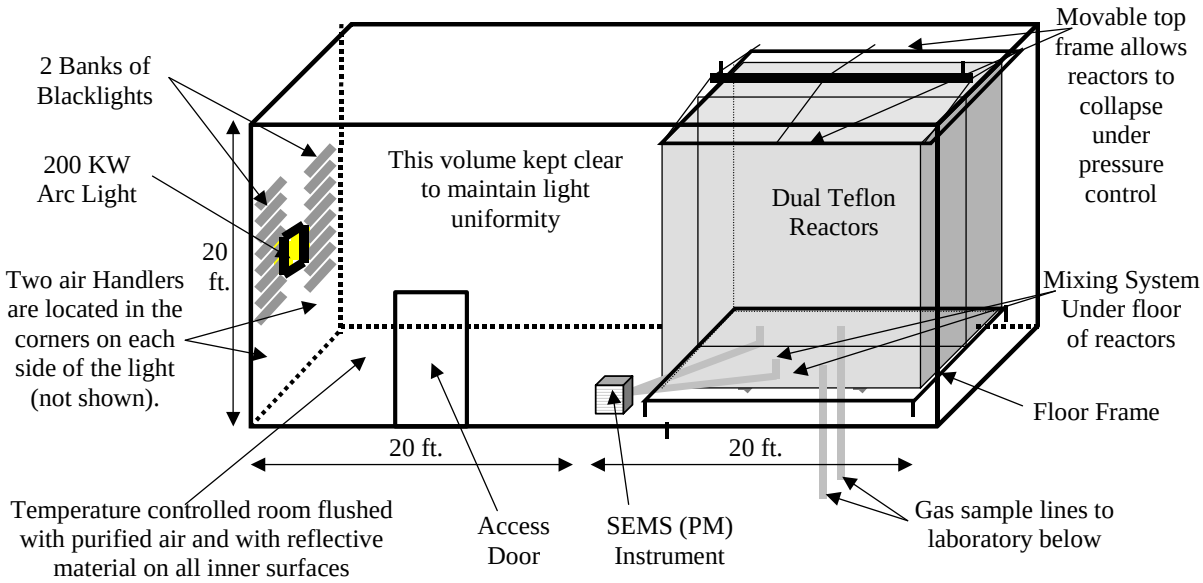

Figure 1. Schematic of the UCR EPA environmental chamber reactors and enclosure.

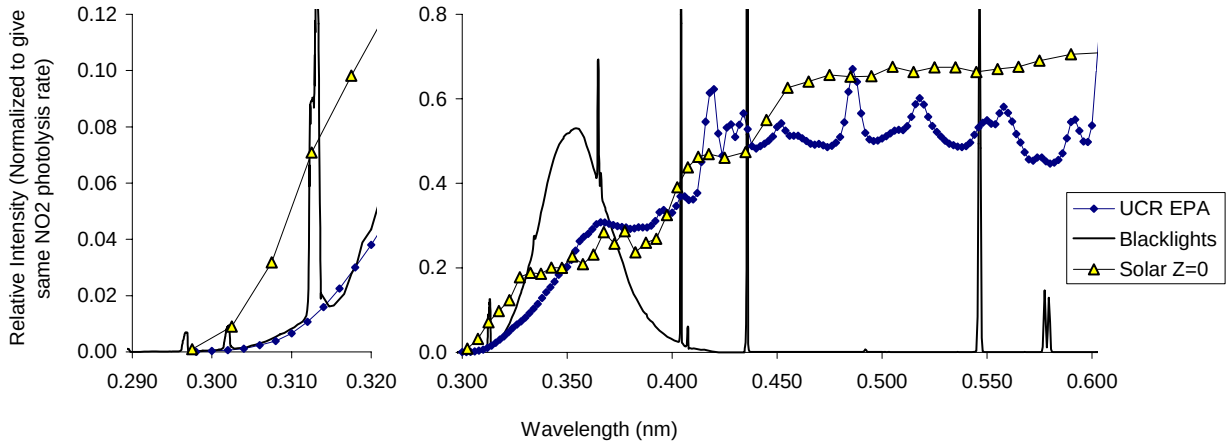

Figure 2. Spectrum of the argon arc light source used in the UCR EPA chamber. Blacklight and representative solar spectra, with relative intensities normalized to give the same NO_2 photolysis rate as that for the UCR EPA spectrum, are also shown.

than the ≥6-hour duration of most of the experiments discussed in this report. Since at least some leaks are unavoidable in large Teflon film reactors, the constant positive pressure is important to minimize the introduction of enclosure air into the reactor that may otherwise result.

As indicated on Figure 1, the floor of the reactors has openings for a high volume mixing system for mixing reactants within a reactor and also for exchanging reactants between the reactors to achieve equal concentrations in each. This utilizes four 10" Teflon pipes with Teflon-coated blowers and flanges to either blow air from one side of a reactor to the other, or to move air between each of the two reactors. Teflon-coated air-driven metal valves are used to close off the openings to the mixing system when not in use, and during the irradiation experiments.

An AADCO air purification system that provides dry purified air at flow rates up to 1500 liters min^{-1} is used to supply the air to flush the enclosure and to flush and fill the reactors between experiments. The air is further purified by passing it through cartridges filled with Purafil® and heated Carulite 300® which is a Hopcalite® type catalyst and also through a filter to remove particulate matter. The measured NO_x, CO, and non-methane organic concentrations in the purified air were found to be less than the detection limits of the instrumentation employed (see Analytical Equipment, below).

The chamber enclosure is located on the second floor of a two-floor laboratory building that was designed and constructed specifically to house this facility (Carter et al, 2002a). Most of the analytical instrumentation (except for the PM instrumentation, which is not discussed in this report) is located on the ground floor beneath the chamber, with sampling lines leading down as indicated on Figure 1.

Analytical and Characterization Methods

Table 1 gives a listing of the analytical and characterization instrumentation whose data were utilized for this project. Other instrumentation was available and used for some of these experiments, as discussed by Carter 2002a, but the data obtained were not characterized for modeling and thus not used in the mechanism evaluations for this project. The table includes a brief description of the equipment, species monitored, and their approximate sensitivities, where applicable. These are discussed further in the following sections.

Analytical Instrumentation

Ozone, CO, NO, and NO_y were monitored using commercially available instruments as indicated in Table 1. A second ozone analyzer, based on the chemiluminescence method, was utilized in some experiments, and its data were consistent with the UV absorption instrument listed on Table 1. The instruments were spanned for NO, NO_2, and CO and zeroed prior to most experiments using the gas calibration system indicated on Table 1, and a prepared calibration gas cylinder with known amounts of NO and CO. O_3 and NO_2 spans were conducted by gas phase titration using the calibrator during this period. Span and zero corrections were made to the NO, NO_2, and CO data as appropriate based on the results of these span measurements, and the O_3 spans indicated that the UV absorption instrument was performing within its specifications.

As discussed by Carter (2002a), two Tunable Diode Laser Absorption Spectroscopy (TDLAS) are available at our laboratories, with the potential for monitoring up to four different species. TDLAS analysis is described in detail elsewhere (Hastie et al., 1983; Schiff et al., 1994) and is based on measuring single rotational - vibrational lines of the target molecules in the near to mid infrared using

Table 1. List of analytical and characterization instrumentation for the UCR EPA chamber.

Type	Model or Description	Species	Sensitivity	Comments
Ozone Analyzer	Dasibi Model 1003-AH. UV absorption analysis. Also, a Monitor Labs Chemiluminescence Ozone Analyzer Model 8410 was used as a backup.	O3	2 ppb	Standard monitoring instrument.
NO - NO_y Analyzer	Teco Model 42 C with external converter. Chemiluminescent analysis for NO, NOy by catalytic conversion.	NO	1 ppb	Useful for NO and initial NO_2 monitoring. Converter close-coupled to the reactors so the "NO_y" channel should include HNO_3 as well as NO_2, PANs, organic nitrates, and other species converted to NO by the catalyst.
		NOy	1 ppb	
CO Analyzer	Dasibi Model 48C. Gas correlation IR analysis.	CO	50 ppb	Standard monitoring instrument
TDLAS #1	Purchased from Unisearch Inc. in 1995, but upgraded for this project. See Carter (2002a). Data transmitted to DAC system using RS-232.	NO2	0.5 ppb	NO_2 data from this instrument are considered to be interference-free.
		HNO3	~ 1 ppb	HNO_3 data not available for all of the experiments modeled in this report.
TDLAS #2	Purchased from Unisearch Inc. for this project. See Carter (2002a). Data transmitted to DAC system using RS-232.	HCHO	~ 1 ppb	Formaldehyde data from this instrument are considered to be interference-free.
		H_2O_2	~2 ppb	H_2O_2 data not taken during the experiments discussed in this report
GC-FID #1	HP 5890 Series II GC with dual columns, loop injectors and FID detectors. Various megabore GC columns available. Controlled by computer interfaced to network.	VOCs	~10 ppbC	Presently equipped with: 30 m x 0.53 mm GS-Alumina column used for the analysis of light hydrocarbons such as ethylene, propylene, n-butane and trans-2-butene and 30 m x 0.53 mm DB-5 column used for the analysis of C_{5+} alkanes and aromatics, such as toluene, n-octane and m-xylene. Loop injection suitable for low to medium volatility VOCs that are not too "sticky" to pass through valves.
GC-FID #2	HP 5890 Series II GC with dual columns and FID detectors, one with loop sampling and one set up for Tenax cartridge sampling. Various megabore GC columns available. Controlled by computer interfaced to network.	VOCs	~10 ppbC	30 m x0.53 mm GSQ column used during this period. Loop injection suitable for low to medium volatility VOCs that are not too "sticky". Not used as primary analysis for most of these experiments.
		VOCs	1 ppbC	Tenax cartridge sampling can be used for low volatility or moderately "sticky" VOCs that cannot go through GC valves but can go through GC columns. 30 m x 0.53 mm DB-1701 column is currently in use. Not used for experiments discussed in this report.

Table 1 (continued)

Type	Model or Description	Species	Sensitivity	Comments
Luminol GC	Developed and fabricated at CE-CERT based on work of Gaffney et al (1998). Uses GC to separate NO2 from PAN and other compounds and Luminol detection for NO2 or PAN. Data transmitted to the DAC system using RS-232.	NO_2	~0.5 ppb	NO_2 measurements were found to have interferences by O_3 and perhaps other species and were not used for mechanism evaluation.
		PAN	~0.5 ppb	Reliability of measurement for PAN not fully evaluated. Calibration results indicate about a 30% uncertainty in the spans. However, interferences are less likely to be a problem than for NO_2.
Gas Calibrator	Model 146C Thermo Environmental Dynamic Gas Calibrator	N/A	N/A	Used for calibration of NO_x and other analyzers. Instrument acquired early in project and under continuous use.
Data Acquisition Sytem	Windows PC with custom LabView software, 16 analog input, 40 I/O, 16 thermo-couple, and 8 RS-232 channels.	N/A	N/A	Used to collect data from most monitoring instruments and control sampling solenoids. In-house LabView software was developed using software developed by Sonoma Technology for ARB for the Central California Air Quality Study as the starting point.
Temperature sensors	Various thermocouples, radiation shielded thermocouple housing	Tempera -ture	~0.1 ^{o}C	Primary measurement is thermocouples inside reactor. However, comparison with temperature measurements in the sample line suggest that irradiative heating may bias these data high by ~2.5^{o}C. See text.
Humidity Monitor	General Eastern HYGRO-M1 Dew Point Monitor	Humidit y	Dew point range: -40 - 50°C	Instrument performing as expected, but dew point below the performance range for experiments discussed in this report.
Spectro-radiometer	LiCor LI-1800 Spectroradiometer	300-850 nm Light Spect-rum	Adequate	Resolution relatively low but adequate for this project. Used to obtain relative spectrum. Also gives an absolute intensity measurement on surface useful for assessing relative trends.
Spherical Irradiance Sensors	Biospherical QSL-2100 PAR Irradiance Sensor or related product. Responds to 400-700 nm light. Spectral response curve included.	Spherical Broad-band Light Intensity	Adequate	Provides a measure of absolute intensity and light uniformity that is more directly related to photolysis rates than light intensity on surface. Gives more precise measurement of light intensity trends than NO_2 actinometry, but is relatively sensitive to small changes in position.

laser diodes with very narrow line widths and tunability. The sample for analysis is flushed through closed absorption cells with multi-pass optics held at low pressure (~25 Torr) to minimize spectral broadening. Because of the narrow bandwidth of the diode lasers required to get the highly species-specific measurement, usually separate diode lasers are required for each compound being monitored. Both TDLAS systems have two lasers and detection systems, permitting analysis of up to four different species using this method. However, for most experiments discussed in this report, only one detector was operational for each instrument, one for monitoring NO_2 and the other for monitoring formaldehyde.

The TDLAS NO_2 measurements were calibrated as using the NO_2 span measurements made by gas phase titration with the gas calibrator at the same time the NO-NO_y analyzer was calibrated. Span data were taken in conjunction with most experiments, and these data were used to derive span factors for the entire data set. The TDLAS formaldehyde measurements were calibrated using a formaldehyde permeation source that in turn was calibrated based on Wet chemical calibration procedure using Purpald reagent (Jacobsen and Dickinson, 1974; Quesenberry and Lee, 1996; NIOSH, 1994)

A GC-luminol instrument, developed at our laboratories to monitor NO_2, PAN, and higher PAN analogues was also utilized during the experiments discussed in this report. This system, based on previous work by Gaffney et al (1998) uses luminol detection combined with GC column to separate NO_2 from PAN and other species that are detected by luminol to provide a specific analysis for those species. Unfortunately, there appears to be an O_3 interference in the NO_2 measurements by this instrument, and, even after attempts are made to correct for this, the NO_2 measurements from this instrument was consistently higher than those from the TDLAS during the latter stages of most experiments. Thus, the NO_2 data from this instrument were not considered to be sufficiently reliable for mechanism evaluation. This may be due to the fact that NO_2 is apparently not retained on the GC column.

On the other hand, since it is separated on the GC column, the PAN data from the GC-luminol instrument may not suffer from such interferences, and if appropriately calibrated may provide an unbiased measure of this compound. The PAN measurements were calibrated using PAN solution prepared by procedures based on condensed-phase synthesis of peracetic acid, sulfuric acid and powdered sodium nitrate in n-octane solution described by Holdren and Spicer (1984). PAN was injected into calibration bags, with the amount injected being determined by a NO_y analyzer, with the NO_2, as measured by the NO_2 channel on the GC-luminol, subtracted off. The PAN calibration data showed approximately ±20% variability.

Organic reactants other than formaldehyde were measured by gas chromatography with FID detection as described elsewhere (Carter et al, 1993, 1995a); see also Table 1. The gaseous compounds ethylene, propylene, n-butane and trans-2-butene were monitored by using 30 m megabore GS-Alumina column using the loop sampling system. The second signal of the same GC outfitted with FID and 30 m megabore DB-5 column was used to analyze toluene, n-octane and m-xylene. Both the GC instruments were controlled and their data were analyzed using HPchem software installed on a dedicated PC. The GC's were spanned using the prepared calibration cylinder with known amounts of ethylene, propane, propylene, n-butane, n-hexane, toluene, n-octane and m-xylene in ultrapure nitrogen. Analyses of the span mixture were conducted approximately every day an experiment was run, and the results were tracked for consistency.

Most of the instruments other than the GCs were interfaced to a PC-based computer data acquisition system under the control of a LabView program written for this purpose. The TDLAS and the GC-luminol instruments were controlled by their own computers, but the data obtained were sent to the LabView data acquisition system during the course of the experiments using RS-232 connections. These data, and the GC data from the HPchem computer, were collected over the CE-CERT computer network

and merged into Excel files that are used for applying span, zero, and other corrections, and preparation of the data for modeling (Carter, 2002c).

Sampling methods

Samples for analysis by the continuous monitoring instrument were withdrawn alternately from the two reactors, zero air, or (for the earlier experiments) the enclosure, under the control of solenoid valves that were in turn controlled by the data acquisition system discussed above. Sampling from the enclosure was discontinued after experiment EPA133 (conducted on July 2, 2003) because of it caused problems with the O_3 analysis in the subsequent sample mode, apparently due to a humidity effect on the O_3 analysis (the enclosure had some humidity due to exchange with outside air, while the air in the reactors were dry). For most experiments the sampling cycle was about 5 minutes for each reactor, the zero air, or (when applicable) the enclosure. The program controlling the sampling sent data to the data acquisition program to indicate which state was being sampled, so the data could be appropriately apportioned when being processed. Data taken less than 3-4 minutes after the sample switched were not used for subsequent data processing. The sampling system employed is described in more detail by Carter (2002a).

Samples for GC analysis in earlier experiments were taken manually at approximately 20-minute intervals from the sample line using 100 ml gas-tight glass syringes, which were then used to flush the sampling loop of the instrument with the air being sampled. After run EPA112 the samples for GC analyses were taken directly from the separate sample lines attached to each of the reactors by flushing for a certain time the sample loops with the air from reactors using pump.

Characterization Methods

Use of chamber data for mechanism evaluation requires that the conditions of the experiments be adequately characterized. This includes measurements of temperature and humidity and light and wall effects characterization. Wall effects characterization is discussed in the modeling method and results sections, below. The instrumentation used for the other characterization measurements is summarized in Table 1, above, and these measurements are discussed further below.

Temperature was monitored during chamber experiments using calibrated thermocouples attached to thermocouple boards on our computer data acquisition system. The temperature in each of the reactors was continuously measured using relatively fine gauge thermocouples that were located ~1' above the floor of the reactors. These thermocouples were not shielded from the light, though it was hoped that irradiative heating would be minimized because of their small size. In order to obtain information about possible radiative heating effects, for a number of experiments the thermocouple for one of the reactors was relocated to inside the sample line. The results indicated that radiative heating is probably non-negligible, and that a correction needs to be made for this by subtracting ~2.5^{o}C from the readings of the thermocouples in the reactors. This is discussed in the Mechanism Evaluation Methods section of this report.

Light Spectrum and Intensity. The spectrum of the light source in the 300-850 nm region was measured using a LiCor 1800 spectroradiometer, which is periodically calibrated at the factory. Spectroradiometer readings were taken several times during a typical experiment, though the relative spectra were found to have very little variation during the course of these experiments. Changes in light intensity over time were measured using a PAR spherical irradiance sensor that was located immediately in front of the reactors. In addition, NO_2 actinometry experiments were carried out periodically using the quartz tube method of Zafonte et al (1977) modified as discussed by Carter et al (1995a). In most cases the quartz tube was located in front of the reactors near where the PAR sensor was located. Since this

location is closer to the light than the centers of the reactors, the measurement at this location is expected to be biased high, so the primary utility of these data are to assess potential variation of intensity over time. However, several special actinometry experiments were conducted where the quartz tube was located inside the reactors, to provide a direct measurement of the NO_2 photolysis rates inside the reactors. The light spectrum and actinometry results obtained for the experiments of interest are discussed later in this report.

Humidity. Humidity was measured using an EG&G model Hygro M1 chilled mirror dew point sensor. Its lower limit of -40°C is above the expected dew point of the purified air used in the experiments described in this report, but adequate for humidified experiments to be carried out for other projects.

Experimental Procedures

The reaction bags were collapsed to the minimum volume by lowering the top frames, and then emptying and refilling them at least ten times after each experiment, and then flushing them with dry purified air on the nights before experiments. Span measurements were generally made on the continuous instruments prior to injecting the reactants for the experiments. The reactants were then injected through Teflon injection lines (that are separate from the sampling lines) leading from the laboratory below to the reactors. The common reactants were injected in both reactors simultaneously (except for the first few runs), and were mixed by using the reactor-to-reactor exchange blowers and pipes for 10 minutes. The valves to the exchange system were then closed and the other reactants were injected to their respective sides and mixed using the in-reactor mixing blowers and pipes for 1 minute. The contents of the chamber were then monitored for at least 30 minutes prior to irradiation, and samples were taken from each reactor for GC analysis.

Once the initial reactants are injected, stabilized, and sampled, the argon light is then turned on to begin the irradiation. During the irradiation the contents of the reactors are kept at a constant positive pressure by lowering the top frames as needed, under positive pressure control. The reactor volumes therefore decrease during the course of the experiments, in part due to sample withdrawal and in part due to small leaks in the reactor. A typical irradiation experiment ends after about 6 hours, by which time the reactors are typically down to about half their fully-filled volume. Larger leaks are manifested by more rapid decline of reactor volumes, and the run is aborted early if the volume declines to about 1/3 the maximum. This was not the case for most of the experiments discussed in this report. After the irradiation the reactors were emptied and filled ten times as indicated above.

The procedures for injecting the various types of reactants were as follows. The NO and NO_2 were prepared for injection using a vacuum rack. Known pressures of NO, measured with MKS Baratron capacitance manometers, were expanded into Pyrex bulbs with known volumes, which were then filled with nitrogen (for NO) or oxygen (for NO_2). The contents of the bulbs were then flushed into the reactor(s) with nitrogen. Some of the gaseous reactants such as propylene and n-butane (other than for surrogate experiments) were prepared for injection using a high vacuum rack as well. For experiments with added CO, the CO was purified by passing it through an in-line activated charcoal trap and flushing it into the reactor at a known rate for the amount of time required to obtain the desired concentration. Volatile liquid reactants were injected, using a micro syringe, into a 2 ft long Pyrex injection tube surrounded with heat tape and equipped with one port for the injection of the liquid and other ports to attach bulbs with gas reactants. Then one end of the injection tube was attached to the “Y”-shape glass tube (equipped with stopcocks) that was connected to reactors and the other to a nitrogen source.

Special procedures were used to simplify the injection of the hydrocarbon surrogate components. A cylinder containing n-butane, trans-2-butene, propylene and ethylene in nitrogen, was used for injecting the gaseous components of the surrogate. The cylinder was attached to the injection system and a gas

stream was introduced into reactors at controlled flow for certain time to obtain desired concentrations. A prepared mixture with the appropriate ratios of toluene, n-octane and m-xylene was utilized for injection of these surrogate components, using the procedures as discussed above for pure liquid reactants. All the gas and liquid reactants intended to be the same in both reactors were injected at the same time. The injection consisted of opening the stopcocks and flushing the contents of the bulbs and the liquid reactants with nitrogen, with the liquid reactants being heated slightly using heat that surrounded the injection tube. The flushing continued for approximately 10 minutes.

Formaldehyde was a reactant and a component of the surrogate used in many of these experiments, and different procedures were used for its injection. Because of the large volumes of the reactors it was impractical to use the method of formaldehyde preparation in a vacuum rack system by heating paraformaldehyde as employed in our previous chambers. In the experiments prior to EPA079 the formaldehyde was prepared by heating paraformaldehyde in a glass vessel while it was continuously flushed with nitrogen and injected in reactors until the measured concentration corresponded to the desired amount of formaldehyde. This procedure was discontinued after run 79 because it was difficult to make reproducible injections. After that time, formaldehyde was generated by catalytic decomposition of 1,3,5-trioxane, as described by Imada (1984). A diffusion tube at constant temperature was used as the source for a constant flow of 1,3,5-trioxane, which then is decomposed quantitatively to formaldehyde by a heated catalyst and injected in reactors for particular time depending of desired amount. This method was found to perform satisfactorily in reproducibly injecting the desired amounts of formaldehyde.

Summary of Experiments

All the UCR EPA chamber experiments discussed in this report were carried out between January 4 and August 19 of 2003. The run numbers ranged from 55 through 160[4]. A chronological listing of the experiments that are used either for chamber characterization or for the model evaluation discussed in this report is given in Table A-1 in Appendix A. Gaps in the run numbers indicate either experiments that were aborted because of experimental problems or experiments carried out for other purposes. Most of the latter consisted of blacklight irradiations of toluene or m-xylene - NO_x mixtures conducted to assess the PM formation potentials of these compounds, or incremental reactivity experiments on petroleum distillates carried out for our CARB coatings reactivity project[5]. In addition, some of the earlier surrogate experiments had either m-xylene or n-octane added to the other reactor to assess model predictions of incremental reactivities of these compounds under varying VOC or NO_x conditions. The results of these experiments will be described in separate reports, and are beyond the scope of this report. Note, however, that most or all of the characterization results here are relevant to modeling these experiments carried out for other purposes.

Characterization experiments consist of experiments whose results are used primarily to derive chamber characterization parameters that are needed when modeling the results of experiments from this chamber for mechanism evaluation. Table 2 gives a summary of the numbers and types of these runs, and indicates the chamber effect parameters that can be derived from them. These results, and the use of these data to derive the chamber effects parameters used when modeling the mechanism evaluation experiments for this study are discussed in the Mechanism Evaluation Methods section of this report. Table 7 and Table 8 in that section, and Table 12 in the Mechanism Evaluation Results section, summarizes the major results of the individual experiments.

[4] The characterization data are applicable through EPA168, carried out on August 29, 2003.
[5] CARB contract number 00-333, "Evaluation of Atmospheric Impacts of Selected Coatings VOC Emissions", William P. L. Carter, Principal Investigator.

Table 2. Summary of types of characterization experiments carried out in the UCR EPA chamber between January 4 and August 23, 2003 that were used for deriving characterization parameters in the mechanism evaluations using this chamber.

Run Type	Runs [a]	Sensitive Parameters	Comments [b]
Ozone Dark Decay	4 [c]	O_3 wall loss rate	The loss of O_3 in the dark is attributed entirely to a unimolecular wall loss process. See Table 7.
CO - Air	8	NO_x offgasing	Insensitive to radical source parameters but O_3 formation is very sensitive to NO_x offgasing rates. Formaldehyde data can also be used to derive formaldehyde offgasing rates. See Table 8.
CO - HCHO - air	2	NO_x offgasing.	Insensitive to radical source parameters but O_3 formation is very sensitive to NO_x offgasing rates. Also can be used to obtain formaldehyde photolysis rates (not discussed in this report). See Table 8.
CO - NO_x	6	Initial HONO, Radical source	O_3 formation and NO oxidation rates are very sensitive to radical source but not sensitive to NO_x offgasing parameters. Formaldehyde data can also be used to derive formaldehyde offgasing rates. See Table 8.
n-Butane - NO_x	1	Initial HONO, Radical source	O_3 formation and NO oxidation rates are very sensitive to radical source but not sensitive to NO_x offgasing parameters. See Table 8.

[a] For the purpose of this tabulation a "run" consists of a dual-sided irradiation experiment. Thus, data from two reactors are associated with a single experiment. This differs from the usage in Table 3 where results from each reactor are counted as separate experiments.

[b] References are made to tables in the Mechanism Evaluation Methods section of this report where the use of these data to derive characterization parameters for this chamber is discussed.

[c] Data from two of these experiments were not used because the results were out of the expected range. See discussion in the Mechanism Evaluation Methods of this report.

The types, numbers, and purposes of the UCR EPA experiments used for mechanism evaluation in this report are given in Table 3. Tabulations summarizing initial reactant concentrations and amounts of ozone formed and NO oxidized in the individual experiments are given in Table 14 and Table 15 in the Mechanism Evaluation Results section of this report. Concentration-time plots of measurement data in these experiments that were used in the mechanism evaluation are given in Figure B-1 through Figure B-30 in Appendix B. The discussion of these data is given in the Mechanism Evaluation Results section of this report in conjunction with the discussion of the results of modeling these experiments using the mechanism and methods discussed below.

Table 3 indicates that more than half the mechanism evaluation experiments used in this work consist of surrogate - NO_x experiments carried out at varying initial reactive organic gas (ROG) and NO_x levels. The matrix of ROG and NO_x levels for the experiments conducted during this period are shown on Figure 3. To give an indication of the approximate reactivity characteristics that correspond to these levels, the lines show SAPRC-99 model calculations ROG and NO_x levels that give maximum sensitivity

Table 3. Summary of mechanism evaluation experiments carried out in the UCR EPA chamber between January 4 and August 23, 2003.

Type	Runs [a]	NO_x Levels (ppb) [b]	Purpose and comments.
HCHO - NOx	2	10 - 25	Mechanism evaluation for simple chemical system at low to moderate NO_x levels. Also control experiments with chemical systems considered to be reasonably well characterized, useful for assessing the performance of the chamber model and measurement methods.
HCHO - CO - NOx	2	15 - 20	
Ethene - NOx	2	10 - 25	
Propene - NOx	2	5 - 25	
Toluene - NOx	3	5 - 25	Aromatic mechanism evaluation.
m-Xylene - NOx	1	5	
Toluene - CO - NOx	5	5 - 25	Determine effects of added CO on aromatic - NO_x systems. Sensitive to radical inputs from aromatic systems.
m-Xylene - CO - NOx	1	5	
Ambient ROG Surrogate - NOx	24 [c]	2 - 110	Evaluation of mechanism using experiments representing ambient chemical systems at low to moderate NO_x levels, and also evaluation of mechanism predictions of dependence of O_3 formation on changes in total VOC and NO_x levels in such systems. The average composition of the ROG surrogate for these experiments is given in Table 4.

[a] For the purpose of this tabulation a "run" consists of an irradiation of a single reactor in a dual-sided irradiation experiment. Thus, each dual-chamber irradiation gives two separate runs for mechanism evaluation. This differs from the usage in Table 2 where each dual-sided irradiation is counted as a single experiment.

[b] Approximate minimum and maximum initial NO_x concentrations

[c] Experiments carried out as the "base case" for petroleum distillate reactivity assessment at standard conditions are not included. Also, only data in the "base case" reactor in experiments with added n-octane or m-xylene are used in this studied. Modeling these experiments will be discussed in separate reports.

of initial ROG levels to O_3 concentrations and that give maximum final O_3 levels. These are referred to as Maximum Incremental Reactivity (MIR) and Maximum Ozone Incremental Reactivity (MOIR), following the terminology used when calculating ozone reactivity scales (Carter, 1994, 2000a). The model simulations of the conditions of these experiments are discussed later in this report.

The mixture used to represent ROGs in all of these UCR EPA experiments was based on the 8-component "full surrogate" as used in our previous incremental reactivity and mechanism evaluation experiments at UCR (e.g., Carter et al, 1995a,b, 1997; Carter, 2000a and references therein). This is designed to have one compound representative of each of the major lumped VOC model species used in condensed lumped-molecule mechanisms used in current airshed models. The relative compositions of the eight compounds in this mixture was derived to represent the distribution of compounds in the mixture used for the "base case" ROG mixture used when calculating VOC reactivity scales (Carter, 1994, 2000a), and also for deriving the parameters for model species in the "fixed parameter" version of

SAPRC-99 (Carter, 2000b). However, as indicated in Table A-1, five of the 24 experiments did not have formaldehyde injected because of experimental difficulties. This is calculated to have a relatively small but measurable effect on the O_3 formed and NO oxidized in the experiments, but the general trends in the results are expected to be essentially the same. The average compositions of surrogate components for the experiments discussed in this report are given in Table 4. The matrix on Figure 3 indicates the surrogate and NO_x levels of the experiments where formaldehyde was not injected.

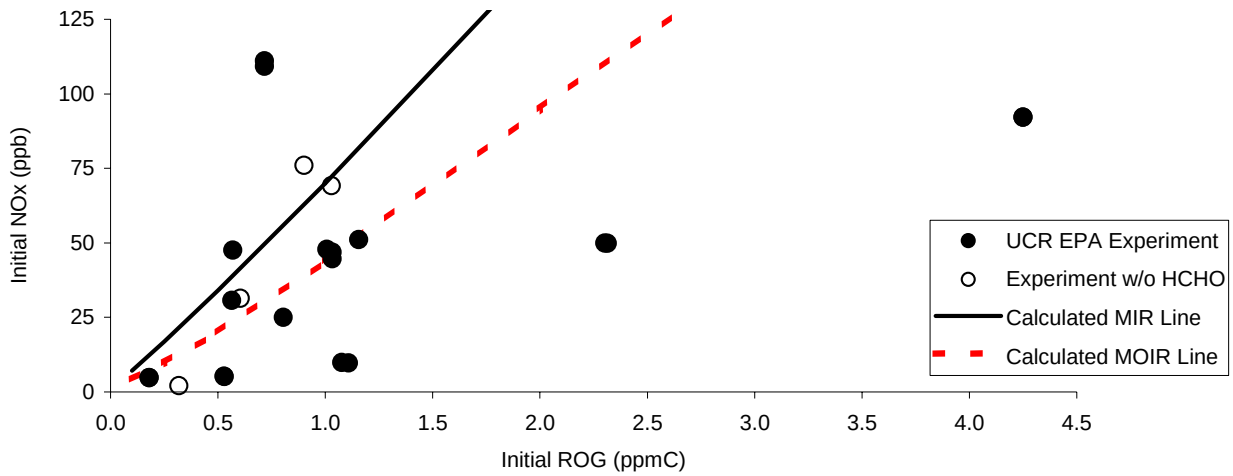

Figure 3. Matrix of initial reactive organic gas (ROG) and NO_x levels fir the ambient surrogate - NO_x experiments carried out in the UCR EPA chamber during the period covered by this report. Model calculations of MIR and MOIR conditions are also shown.

Table 4. Average Compositions of the ambient reactive organic gas (ROG) surrogates in the UCR EPA surrogate - NO_x experiments modeled in this report.

Component	Average Composition (ppm/ppmC)	
	Runs with Formaldehyde	Runs without Formaldehyde
n-Butane	0.092 ± 0.012	0.100 ± 0.009
n-Octane	0.024 ± 0.002	0.023 ± 0.001
Ethene	0.017 ± 0.003	0.017 ± 0.001
Propene	0.014 ± 0.001	0.015 ± 0.001
trans-2-Butene	0.013 ± 0.001	0.013 ± 0.001
Toluene	0.021 ± 0.001	0.021 ± 0.001
m-Xylene	0.020 ± 0.001	0.021 ± 0.001
Formaldehyde	0.025 ± 0.006	

MECHANISM EVALUATION METHODS

Chemical Mechanism Used

The chemical mechanism evaluated in this work is the SAPRC-99 mechanism as documented by Carter (2000a). A complete listing of this mechanism is given by Carter (2000a) and in subsequent reports from our laboratory where this mechanism was used, all of which are available either as previous reports to the CARB or on our web site[6]. Files and software implementing this chemical mechanism are also available at our web site[7], with the chemical mechanism simulation computer programs available there being essentially the same as those employed in this work. Although changes have been made to the mechanisms of some individual VOCs due to subsequent experimental studies and reactivity assessment projects (Carter, 2003a), the affected VOCs do not include the hydrocarbons or simple aldehydes employed in the experiments used for mechanism evaluation in this work. Because of this, a complete listing of this mechanism is not reproduced in this report.

As discussed previously (Carter, 2000a,b), the SAPRC-99 mechanism consists of a "base mechanism" that represents the reactions of the inorganic species and common organic products and lumped organic radical model species and "operators", and separate mechanisms for the initial reactions of the many types other organic compounds that are not in the base mechanism. The latter include all the alkane, alkene, and aromatic species used in the experiments modeled in this work. These can be represented either explicitly, with individual reactions or sets of reactions for each, or using lumped model species similar to those employed in the RADM-2 (Stockwell et al, 1990), such as employed in the "fixed parameter" version of SAPRC-99 (Carter, 2000b). The latter approach is useful when modeling complex mixtures in ambient simulations or simulations of experiments with complex ambient mixtures, but the other approach, representing each compound explicitly, is more appropriate when evaluating mechanisms for individual compounds or simple mixtures. This is because the purpose of mechanism evaluations against chamber data is to assess the performance of the mechanism itself, not to assess the performance lumping approaches. The latter is most appropriately assessed by comparing simulations of explicit and condensed versions of the same mechanism in ambient simulations.

All of the UCR EPA and most of the TVA chamber experiments discussed in this work all had no more than eight VOC reactants that are not in the base mechanism, so in those cases each of the reactant VOCs were represented separately when modeling those experiments. However, the TVA experiments included twelve runs with the "Synurban94" ambient reactive organic gas (ROG) surrogate mixture consisting of 52 hydrocarbons, and all of the CSIRO experiments employ similar mixtures of the same compounds, though with somewhat different relative compositions. The compounds in these mixtures are given in Table 5, along with the assigned or average relative compositions for each set of experiments. Because of the relatively large number of compounds, the reactions of each were not represented explicitly; instead they were represented using a condensation approach based on that employed in ambient models. This is appropriate because these mixtures are designed to represent those present in the atmosphere.

In view of this, when modeling the complex hydrocarbon mixtures in the TVA "Synurban94" and CSIRO experiments, we used the condensation approach of the condensed version of SAPRC-99 described by Carter (2000b). This version uses the same base mechanism to represent reactions of the

[6] These reports can be downloaded from http://www.cert.ucr.edu/~carter/bycarter.htm.

[7] Files and software implementing the SAPRC-99 mechanism are available at http://www.cert.ucr.edu/~carter/SAPRC99.htm.

Table 5. Composition the complex urban ROG surrogate mixture used in the TVA and CSIRO experiment and the condensed model species used to represent them.

Compound	Composition (ppb/ppmC) [a]			SAPRC-99 Model Species [b]	
	TVA	CSIRO #1	CSIRO #2	Detailed	Condensed
Ethane	23.63	21.74	21.74	ETHANE	ALK1*
Propane	20.04	16.38	16.38	PROPANE	ALK2*
n-Butane	21.94	20.70	20.70	N-C4	ALK3*
n-Pentane	7.37	6.10	6.10	N-C5	ALK4*
n-Hexane	2.02	2.41	2.41	N-C6	ALK4*
n-Heptane	2.17	2.36	2.36	N-C7	ALK5*
n-Octane	1.36	1.54	1.54	N-C8	ALK5*
n-Nonane	2.51	1.83	1.83	N-C9	ALK5*
n-Decane	1.60	2.06	2.06	N-C10	ALK5*
Isobutane	9.49	8.69	8.69	2-ME-C3	ALK3*
Isopentane	18.56	16.12	16.12	2-ME-C4	ALK4*
2,3-Dimethyl Butane	0.89	1.03	1.03	23-DM-C4	ALK4*
2-Methyl Pentane	4.04	3.78	3.78	2-ME-C5	ALK4*
3-Methylpentane	2.69	2.71	2.71	3-ME-C5	ALK4*
2,3-Dimethyl Pentane	2.35	2.50	2.50	23-DM-C5	ALK5*
3-Methyl Hexane	4.95	5.15	5.15	3-ME-C6	ALK5*
2,2,4-Trimethyl Pentane	1.66	1.67	1.67	224TM-C5	ALK4*
2,3,4-Trimethyl Pentane	1.18	1.29	1.29	234TM-C5	ALK5*
2,5-Dimethyl Hexane	1.29	1.43	1.43	25-DM-C6	ALK5*
4-Methyl Nonane	2.17	2.38	2.38	4-ME-C9	ALK5*
Cyclohexane	1.58	1.72	1.72	CYCC6	ALK5*
Methylcyclopentane	2.00	1.88	1.88	ME-CYCC5	ALK4*
Methylcyclohexane	0.81	0.88	0.88	ME-CYCC6	ALK5*
Ethene	15.60	14.34	14.34	ETHENE	ETHENE
Propene	3.72	2.49	2.49	PROPENE	OLE1*
1-Pentene	1.86	1.06	1.06	1-PENTEN	OLE1*
1-Octene	0.93	1.04	1.04	1-OCTENE	OLE1*
1-Nonene	0.81	0.80	0.80	1-C9E	OLE1*
Isobutene	1.47	1.21	1.21	ISOBUTEN	OLE2*
2-Methyl-1-Butene	1.01	0.90	0.90	2M-1-BUT	OLE2*
2-Methyl-1-Pentene	1.27	1.38	1.38	2M1-C5E	OLE2*
2,3,3-trimethyl-1-Butene	2.08	2.35	2.35	233M1BUT	OLE2*
trans-2-Butene	3.30	3.06	3.06	T-2-BUTE	OLE2*
cis-2-Pentene	2.96	1.91	1.91	C-2-PENT	OLE2*
2-Methyl-2-Pentene	0.49	0.51	0.51	2M-2-C5E	OLE2*
Cyclohexene	0.18	0.17	0.17	CYC-HEXE	OLE2*
1,3-Butadiene	1.16	0.55	0.55	13-BUTDE	OLE2*
Isoprene	0.60	0.63	0.63	ISOPRENE	ISOPRENE
a-Pinene	0.52	0.62	0.62	A-PINENE	TERP*
a-Methyl Styrene	0.97	0.28	0.28	AME-STYR	OLE2*
Benzene	3.53	3.78	3.78	BENZENE	ARO1*
Toluene	8.99	10.15	10.15	TOLUENE	ARO1*
Ethyl Benzene	1.22	1.41	1.41	C2-BENZ	ARO1*
n-Propyl Benzene	1.11	1.25	1.25	N-C3-BEN	ARO1*
s-Butyl Benzene	0.61	0.72	0.72	S-C4-BEN	ARO1*
m-Xylene	4.06	4.76	4.76	M-XYLENE	ARO2*

Table 5 (continued)

Compound	Composition (ppb/ppmC) [a]			SAPRC-99 Model Species [b]	
	TVA	CSIRO #1	CSIRO #2	Detailed	Condensed
o-Xylene	1.53	1.79	1.79	O-XYLENE	ARO2*
m-Ethyl Toluene	0.72	1.05	1.05	M-ET-TOL	ARO2*
p-Ethyl Toluene	0.72	1.55	1.55	P-ET-TOL	ARO2*
m-Diethyl Benzene	1.41	1.85	1.85	M-DE-BEN	ARO2*
1,2,4-Trimethyl Benzene	5.09	6.41	6.41	124-TMB	ARO2*
1,2,3,5 Tetramethyl Benzene	0.49	0.62	0.62	1235MBEN	ARO2*

[a] Composition used for the experiments in the indicated chamber. "CSIRO #1" refers to the mixture used in all CSIRO experiments except for 344P and 345P, and "CSIRO #2" refers to mixtures used in those two experiments, which had a different ratio of gas to liquid surrogate components.

[b] The condensed model species indicate the species used to represent them in the model calculations, and the detailed species indicate the species used to derive the parameters for the condensed species, where applicable. An asterisk indicates a condensed species whose kinetic and mechanistic parameters were derived based on the mixture of compounds it was used to represent. Note that these are different than those in the standard "fixed parameter" version of SAPRC-99, where the parameters of the model species were derived based on ambient VOCs (Carter, 2000b).

inorganics and the common organic products and radicals as the detailed mechanism, represents ethene and isoprene explicitly, and uses lumped species to represent the other organics. These include five lumped species (ALK1 … ALK5) to represent the alkanes and other non-aromatic compounds that react with OH radicals, two lumped species each (OLE1 and OLE2 and ARO1 and ARO2) to represent the alkenes and aromatics, respectively, and a separate lumped species (TERP) to represent the terpenes. The compounds are apportioned into the different model species according to their 300°K OH radical rate constants, with the dividing lines being as follows: alkanes: 0.5, 2.5, 5.0, and 10 x 10^3 ppm^{-1} min^{-1} (with compounds reacting slower than 0.2 x 10^3 ppm^{-1} min^{-1} being treated as inert); alkenes: 7 x 10^4 ppm^{-1} min^{-1}; and aromatics: 2 x 10^4 ppm^{-1} min^{-1}. Table 5 indicates the model species to which each compound was assigned.

The mechanistic parameters for these model species were derived based on the mixtures of the mixtures of compounds they were being used to represent in each of the experiments. Thus, the "adjustable parameter" version of the mechanism was employed. This means that all of the chemical detail contained in the detailed mechanism representing these species was incorporated into this mechanism. The only condensation consisted of grouping compounds with similar rate constants and types of mechanisms into a smaller number of model species. We have previously shown that if a lumping approach such as this is employed and if sufficient number of model species is employed (as is the case employed here), this condensation has almost no effect on simulations of O_3 and other species in chamber experiments with ambient mixtures (Carter, 1988). Therefore, we consider the effect of employing this approach on the results of this evaluation is not significant.

Evaluation Against UCR EPA Chamber Experiments

The UCR EPA chamber experiments used for mechanism evaluation for program were described in the previous section. In this section we discuss methods used for modeling these experiments, the methods for characterizing run conditions, and the utilization of the results of the characterization experiments to derive the chamber effects parameters for modeling. Relevant results of characterization experiments are also presented where applicable.

Characterization of Run Conditions

Initial Reactant Concentrations. For most experiments, the initial reactant concentrations used for modeling were based on measurements of the reactants immediately prior to the time the light was turned on. The spreadsheets used to organize and process the data had macros that derived initial reactant concentrations for modeling based on this. Many experiments had the same concentrations of some reactants injected into both reactors, and equivalent concentrations were assured not only by injecting equal amounts in both reactors, but also by rapidly mixing and exchanging contents of the two reactors during the injection process using the mixing system shown on Figure 1, above. Therefore, if reliable initial concentration data were available for only one reactor then the measurements on the other reactor were used to estimate the initial reactant concentrations for modeling. The derived or estimated initial reactant concentrations were checked for reasonableness by comparing model simulations with experimental measurements of the initially present reactants, and adjusting the initial value used for modeling if the subsequent measurements indicate another value is more reasonable.

Light Spectrum. The spectrum of the argon arc light source was measured during most experiments using a LiCor LI-1800, and was found to be relatively constant throughout the period of these experiments. The spectroradiometer was calibrated at the factory during the period of the experiments, and the spectra taken afterwards were slightly different due to the changed calibration settings. Since the spectra for the experiments after the calibration were also stable from run-to-run as was the case before, we assume that the spectra taken after the calibration were also applicable for the earlier experiments. For modeling purposes, we used the relative spectral distribution derived by averaging the LiCor measurements for runs EPA-163 through EPA-216, carried out between August 27 and October 30, 2003, for calculating the photolysis rates. This is the spectrum that is shown on Figure 2, above.

Light Intensity. All the UCR EPA experiments modeled in this work were carried out using the same Vortek solar simulator power (400 amps), so the light intensity should be essentially constant from run to run if the light is performing up to specifications. The results of the various light intensity measurements made during the course of these experiments were consistent with this expectation. This is shown on Figure 4, which shows plots of various light intensity measurements against EPA run number for the period of the experiments discussed during this report and for subsequent experiments where the same procedures were used. Most of the data concerning the variability in light intensity cam from the QSL PAR radiation meter, which was located in the enclosure about 1 meter in front of the reactors facing the light. These data showed less than 5% variability in total light intensity between run 60 through run ~250. In addition, periodic NO_2 actinometry (k_1) measurements were made with the quartz tube also located in the enclosure about 1 meter in front of the reactors, above the location of the PAR meter, These data also indicated run-to-run variability of less than 5%, and gave an average NO_2 photolysis rate of 0.284 ± 0.010 min^{-1}.

Since the location of the NO_2 actinometry tube for most of the experiments was outside the reactors and located somewhat closer to the light source than the gases in the reactor, one would expect the 0.285 min^{-1} average value from those measurements to be somewhat higher than that appropriate for modeling. To obtain measures of absolute light intensity of more direct relevance for modeling, occasional special actinometry experiments were conducted with the quartz actinometry tube located inside one of the reactors. The data obtained, shown on Figure 4, again indicate no trend in NO_2 photolysis rate during this period, and give an average of 0.260 ± 0.004 min^{-1}, with the differences in averages for the two reactors less than 3%. This is about 8% less than the measurement outside the reactor and slightly closer to the light, which is in the expected range.

Since the results of the actinometry measurements shown on Figure 4 indicate no significant changes in light intensity during the period of these experiments, they were all assumed to have the same

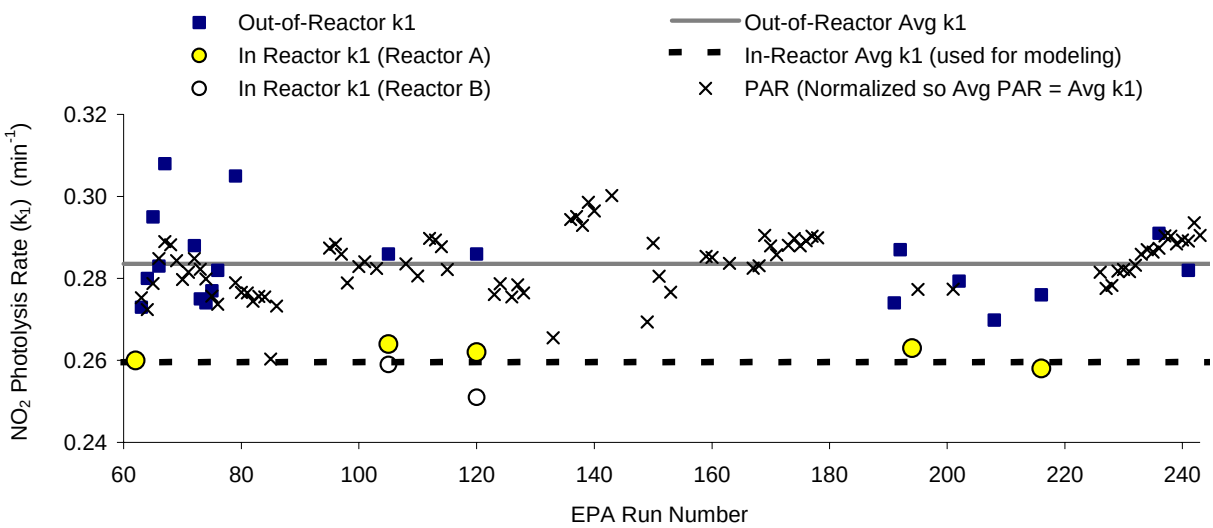

Figure 4. Plots of various measures of light intensity for the EPA chamber experiments against EPA run number.

NO_2 photolysis rate for modeling purposes, which was 0.26 min^{-1}, the average of the in-chamber actinometry results. The other photolysis rates were calculated using this, the assigned spectral distribution (shown on Figure 2) and the absorption cross-sections and quantum yields given with the mechanism.

Temperature. As discussed above, the temperature in each of the reactors was continuously measured using thermocouples located inside the reactor and also, for many experiments, using thermocouples located inside the sample line. It was found that the temperatures in the two reactors were essentially the same when their thermocouples were in comparable locations, but temperatures measured in the sample line were only the same as those in the reactors when the arc light was off. The temperatures monitored in both locations increased when the light was turned on, but the temperature measurement in the sample line rose much more slowly and stabilized at a lower level. An example of this is shown on Figure 5, which shows the measured temperature data for run EPA-123. This could be due to temperature inertia in the sample line, which takes a period of time to heat after the lights are turned on. However, the difference was consistent after about 4 hours of irradiation, with the average difference being 2.5^{o}C. Based on this, we conclude that temperature measured inside the reactor probably gives the better measure of how the temperatures changes with time, but that once it is stabilized the temperature in the sampling line is likely to have less bias because it is not exposed to the direct light.

Based on this, for modeling purposes we assume that the temperature inside the reactor is reflected by the readings of the thermocouples inside the reactor, corrected by subtracting 2.5^{o}C. Since the temperature appears to be relatively stable after about 1-2 hours for modeling in this work we represent the temperature as being constant at the average value. Although strictly speaking it would be better to represent the ~3°C rise in temperature during the first 1-2 hours in the model input, test calculations showed that using the more exact representation of the temperature variation had essentially no effect on predictions of O_3 and other species used in this evaluation. Figure 5 shows the average temperature used for modeling the example experiment shown there.

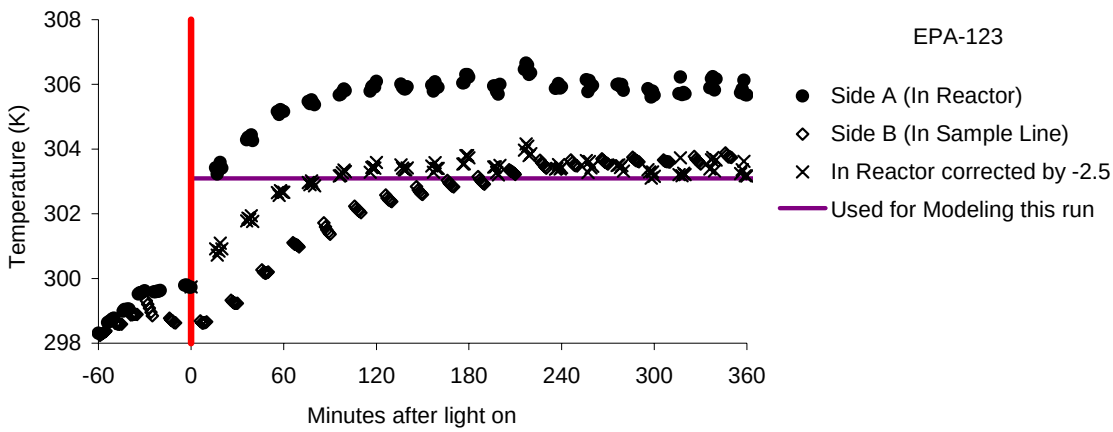

Figure 5. Plot of temperature measurements made during run EPA123.

Dilution. As discussed above, the UCR EPA chamber was constructed so that the reactors are always under positive pressure with respect to the enclosure, with the top framework moving down to maintain the positive pressure as air is removed due to sampling or leaks. Therefore, we assume that dilution is negligible when modeling this run. Measurements of CO and other slowly reacting species in applicable experiments are generally consistent with this assumption.

Humidity. The AADCO air used to flush and fill the reactors was not humidified in any of the experiments discussed in this report. The humidity of the AADCO output and in the reactors was too low to measure, indicating less than 1% RH. A H_2O level of 3.4 x 10^4 ppm, corresponding to ~1% RH at 300°K, was used for modeling these experiments. Results of model calculations were not sensitive to the assumed humidity at this level.

Chamber Effects Parameters

It is well recognized that mechanism evaluation against chamber data needs to take into account chamber wall effects and other chamber-dependent artifacts, some of which can be derived by modeling or analysis of appropriate characterization experiments and others of which can be estimated (Carter and Lurmann, 1991; Jeffries et al, 1992; Carter, 2000a and references therein). While the ozone wall loss rates can be derived directly from analysis of data from specific experiments designed for this purpose, other important parameters can be derived only by modeling characterization experiments that are particularly sensitive to the parameters of interest. For this study, the chamber effects parameters that were derived by modeling sensitive experiments were the NO_x and formaldehyde offgasing rates, initial HONO, and chamber radical source. Table 6 gives a summary of the types of experiments used to derive the chamber effects parameters for the UCR EPA chamber during the period of the experiments modeled in this report, and Table 7 and Table 8 give the best fit parameters for the individual experiments. The chamber effects parameters that were used when modeling the UCR EPA experiments are summarized in Table A-2 in Appendix A. These parameters, and the derivations of the values given in Table A-2 are discussed in more detail below.

Ozone Dark Decay. Table 7 summarizes the results of O_3 dark decay experiments carried out in the UCR EPA chamber. Because of the relatively limited number of such experiments, results of early experiments carried out using the single “pillow-bag” type reactors in the enclosure are also shown. These

Table 6. Summary of types of UCR EPA characterization experiments and chamber effects parameters they were used to derive chamber effects parameters.

Run Type	No. Runs	Sensitive Parameters	Comments
Ozone Dark Decay	4 [a]	O_3 wall loss rate	The loss of O_3 in the dark is attributed entirely to a unimolecular wall loss process. See Table 7.
CO - Air	8	NO_x offgasing	Insensitive to radical source parameters but O_3 formation is very sensitive to O_3 offgasing rates. Formaldehyde data can also be used to derive formaldehyde offgasing rates. See Table 8.
CO - HCHO - air	2	NO_x offgasing.	Insensitive to radical source parameters but O_3 formation is very sensitive to O_3 offgasing rates. Also can be used to obtain formaldehyde photolysis rates (not discussed in this report) . See Table 8.
CO - NO_x	6	Initial HONO, Radical source	O_3 formation and NO oxidation rates are very sensitive to radical source but not sensitive to NO_x offgasing parameters. Formaldehyde data can also be used to derive formaldehyde offgasing rates. See Table 8.
n-Butane - NO_x	1	Initial HONO, Radical source	O_3 formation and NO oxidation rates are very sensitive to radical source but not sensitive to NO_x offgasing parameters. See Table 8.

Table 7. Summary of dark ozone decay measurements in the UCR EPA chamber.

Run	Side	Decay (%/hr)	Comments
5		0.79	Single large pillow-bag reactor
6		0.80	Single large pillow-bag reactor
9		0.79	Single large pillow-bag reactor
59	A B	0.21 0.22	First O_3 decay experiment with chamber in current configuration.
156	A B	2.60 2.31	Data scattered
158	A B	0.66 0.44	
179	A B	0.83 0.67	The log book noted problems with framework control for the Side B reactor, which should have caused a high apparent decay rate. However, the results are in the expected range.

Table 8. Summary of UCR EPA chamber characterization experiments that were modeled to determine radical source and formaldehyde offgasing parameters.

Run No.	Run Type	Initial NOx (ppb)	Best fit chamber effects parameters [a]							
			HONO Emit/k1 (ppt) [b]				Init. HONO (ppb)		HCHO Emit/k1 (ppt)	
			RS Sens.		NOx Sens.					
			A	B	A	B	A	B	A	B
55	CO - Air	-			5	5	0.1	0.2	10	10
56	CO - Air	-			5	5	0.1	0.2	10	
57	CO - NOx	50	6	6			0		10	
58	CO - NO	91	5				0.1		10	
58	CO - NO2	80		5						10
60	CO - Air	-	4			2	0	0.1	10	10
61	CO - NOx	9	5	6			0	0	10	10
63	CO - HCHO - Air	-			3	1	0	0		
64	N-C4 - NO	49	5				0		10	
64	N-C4 - NO2	43		5						10
70	CO - NOx	28	5	5			0	0	20	15
71	CO - NO	266	3				0.1		10	
71	CO - NO2	204		[c]						
76	CO - Air	-			6	3			10	10
79	CO - Air [d]	-			5	5	0.1	0.1	10	10
87	CO - Air (BL) [e]				17	10			15	15
103	CO - NOx	28	25	15					10	10
112	CO - Air	-			25	8				
115	CO - HCHO - Air	-			10	7				
133	CO - HCHO - Air	-			8	5				
140	CO - NOx	24	12	10					20	20
160	CO - Air	-			14	11	0.2	0.1	15	10

[a] A blank indicates that the experiment was either insensitive to this parameter, or the modeling gave ambiguous results as to which set of parameter values gave best fits to the data.

[b] "RS Sens." refers to experiments that are sensitive to the radical source, while "NO_x Sens." refers to experiments that are sensitive to NO_x input rates. HONO wall emissions are used to represent both effects. "k1" is the NO_2 photolysis rate.

[c] Regardless of reasonable adjustment of chamber parameters, model predictions predict gradual decrease in NO and increase in NO_x during the experiment, but experimentally the NO increased and the NO_2 decreased. However, the changes were relatively slow and the model predictions were not sensitive to the chamber effects parameters considered here.

[d] Temperature for this run was ~7°C lower than usual.

[e] "(BL)" indicates that the blacklight light source was used. The runs were modeled using assigned NO_2 photolysis rates of 0.193 and 0.188 min^{-1} for runs 87 and 116, respectively, and the recommended blacklight spectral distribution of Carter et al (1995a).

have some relevance to the current configuration because the same wall material is used and the reactor volume is very similar.

The results of the experiments show some scatter, but if the data from the runs with the lowest and highest dark decay rates are discarded, then the results with the current reactor average about 0.65%/hour. This is the value used when modeling these experiments for this work. This is within the uncertainty of the results in the first reactor, and is only slightly lower than the 0.9%/hour dark decay rate that was recommended by Carter (1995a) for use when modeling the smaller UCR Teflon film chambers.

HONO Offgasing. As discussed previously, both NO_x offgasing and the continuous chamber radical source appear to occur at similar rates in Teflon film chambers, and can be modeled by a continuous HONO offgasing process. This is represented by the parameter "RN-I" (see Table A-2 in Appendix A), which is the HONO offgasing rate divided by the NO_2 photolysis rate in the experiment. The values of this parameter that gives best fits to the experiments are given in Table 8, where separate columns are used for runs that are sensitive to radical source and NO_x offgasing. These data are also plotted against run number in Figure 6. It can be seen that the magnitudes of the HONO offgasing rates that fit the radical-source sensitive runs are essentially the same as those that fit NO_x-offgasing sensitive runs, within the variability of the data. This supports our approach of representing these two effects by a single process in our chamber model.

The results indicate that the apparent HONO offgasing rates were considerably lower during the initial series of experiments than those carried out subsequently, with the dividing line being somewhere before run 87. Note that immediately before run 79 some construction was done in the chamber and enclosure that involved opening and entering the reactors to make modifications to the mixing and exchange system (see Table A-1 in Appendix A). Unfortunately, because of an apparent temperature control problem the average temperature in run 79, the NO_x offgasing experiment carried out immediately after these modifications were made, was ~7°C lower than that for all the other experiments in this study (296 vs. 303.4±0.6^{o}K). Therefore, although the apparent NO_x offgasing from that run was in the range expected from the experiments before the modifications, the data from that run could strictly speaking not

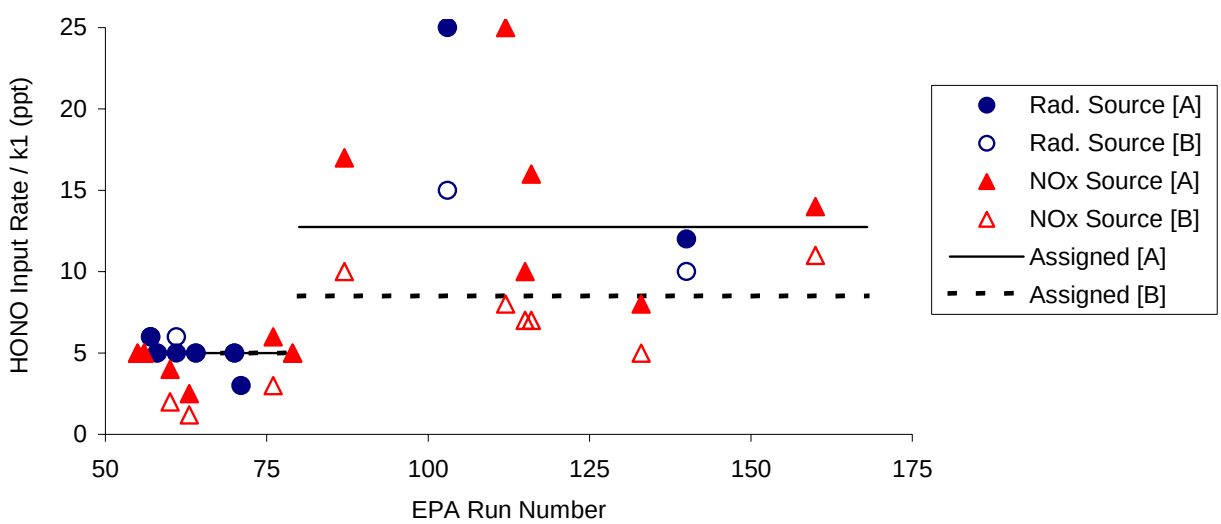

Figure 6. Plots of best fit HONO offgasing parameters against UCR EPA run number.

be used because the conditions of that experiment are not representative. The first relevant characterization experiment after the construction carried out with the normal temperature range was run 87, which was consistent with the subsequent runs that indicted the higher apparent NO_x offgasing and radical source rates. Thus the possibility that the construction and modifications caused the change cannot be ruled out.

Another possible explanation for the apparent change is that run 80 was the first ROG surrogate - NO_x experiment carried out in these reactors, and it was the first of a series of such runs (see Table A-1 in Appendix A). Run 80 was also the first time that the trioxane method was used to inject formaldehyde. However, it is difficult to understand how VOC exposure would affect an apparent HONO offgasing effect, especially since the reactor was exposed to most of the VOCs in the ROG surrogate in previous single compound or characterization runs.

The modeling of the characterization experiments carried out after run 79 also have higher apparent HONO offgasing rates in Side A than in Side B. Although the magnitude of the side-to-side differences are within the run-to-run variability, the side differences are consistent, with the average Side A/ Side B ratio being about 1.5, if the two runs with the greatest differences are excluded. The reason for this is unknown, though it should be noted that the reactor in Side A was constructed a number of months before that for Side B, and therefore might be expected to have higher backgrounds. However, the two reactors had very similar apparent HONO offgasing rates for the runs prior to 80. This side inequivalency is more consistent with the explanation of contamination introduced during the modifications prior to run 79 than contamination due to introduction of the surrogate components, since most of the experiments had the same levels of surrogate components in both of the reactors.

Based on the above considerations, the HONO offgasing parameters used for modeling in this work were assigned as follows: 5 ppt for runs 55 through 77, 12.8 and 8.5 ppt for runs 80 through 168, Sides A and B, respectively. No assignment is made for run 79 because of the lower temperature in that experiment, so there is no standard chamber model for that experiment. These assignments are shown as a function of run number and reactor on Figure 6.

Although the apparent radical source and NO_x offgasing rates after run 79 may appear to be high compared to those before this period, it should be noted that these are still very low compared to what was normally observed for previous UCR Teflon film chambers. For example, the radical source relative to NO_2 photolysis rates recommended by Carter et al (1995a) for modeling ITC, ETC, XTC, and DTC experiments were generally 80 ppt, and the NO_x offgasing parameters were in the 30-100 ppt range. The radical source input rates for other chambers were even higher (e.g., Carter and Lurmann, 1990, 1991).

Note that the NO_x offgasing rates assigned for Side A after run 80 correspond to NO_x input rates of 0.12 ppb/hour, or 0.7 ppb NO_x at the end of a 6-hour experiment. This is a non-negligible NO_x input in some of the lowest NO_x experiments carried out for this program. The sensitivities of these experiments to the NO_x offgasing rate assumed when modeling will be discussed in conjunction with the discussion of the evaluation results.

Initial HONO. Although there is no direct indication of significant levels of initially present HONO in our experiments, Table 8 indicates that some of the characterization experiments are somewhat better fit by models assuming relatively low but non-negligible levels of initial HONO. In particular, approximately half of the characterization runs that were modeled that were sensitive to initial HONO were better fit using initial HONO of 0.1 ppb, while the rest were better fit assuming no initial HONO. There is no apparent dependence on whether NO_x was injected in the experiments or initial NO_x levels. Based on this, for modeling these experiments we will assume initial HONO levels of 50 ppt

Formaldehyde offgasing. Evidence for formaldehyde offgasing in this chamber comes from the fact that measurable amounts of formaldehyde were formed in essentially all irradiations, including those where formaldehyde or formaldehyde precursors were not injected. The measured formaldehyde levels in such experiments were always low and close to the detection limit of the TDLAS, but were definitely nonzero. The formaldehyde offgasing rates that gave the best fit to the measured formaldehyde levels in such runs are indicated on Table 8, where it can be seen that most runs suggest ratios of formaldehyde offgasing to NO_2 photolysis rates of about 10 ppt. The determination for any given run is somewhat imprecise because of the scatter of the data due to the levels being near the detection limit, but the overall results are reasonably consistent in this regard, and there does not appear to be a significant change in formaldehyde offgasing rate with time. Therefore, a formaldehyde offgasing / NO_2 photolysis rate parameter of 10 ppt was assumed when modeling all these experiments.

Note that for most experiments with added VOCs this formaldehyde offgasing rate is very small compared to the formaldehyde present or formed in the gas-phase reactions. For the light intensities of our experiments, the offgasing is estimated to produce less than 1 ppb of formaldehyde input in a 6-hour irradiation. The effect of this formaldehyde input on experiments sensitive to the chamber radical source is small compared to the effect of the HONO offgasing, though it is not entirely negligible in the very low apparent HONO offgasing rate experiments prior to run 80. This is in contrast to the TVA experiments, discussed below, where the formaldehyde offgasing is a significant process and a major apparent contributor to the chamber radical source.

Note that although we have not used formaldehyde offgasing when modeling UCR chamber experiments previously, this is almost certainly due to limitations in the formaldehyde instrumentation used, which was far less sensitive than the TDLAS used in this experiment. It is reasonable to expect that the formaldehyde offgasing rates in the UCR EPA chamber are a lower limit for the smaller volume Teflon chambers employed previously in our laboratories.

TVA Chamber Experiments

As discussed in the Introduction, the TVA chamber was used to carry out a number of reasonably well-characterized experiments under relatively low NO_x conditions that are potentially useful for mechanism evaluation. Because these data have not been previously used to evaluate the SAPRC-99 mechanism, modeling these data was included among the tasks for this project. In this section, we discuss the methods used for modeling and deriving the chamber characterization parameters for the experiments from this chamber. First, we give a brief description of the chamber and the procedures employed for these experiments in order to provide an appropriate background and context for this discussion.

Description of Chamber and Experimental Procedures

In 1993 through 1995, Simonaitis and Bailey of the Tennessee Valley Authority (TVA) used a 28,000-liter indoor smog chamber to conduct a series of chamber experiments under lower NO_x conditions than employed previously (Simonaitis and Bailey, 1995; Bailey et al, 1996). The brief description of the chamber given below was taken primarily from the paper of Simonaitis et al (1996), and this and the other reports and publications of the TVA group should be consulted for details.

A diagram of the TVA chamber and its associated laboratory is shown on Figure 7. The reactor has a volume of 28,300 liters and is located above the laboratory with most of the monitoring instrumentation. The reactor is constructed of 0.13 mm FEP Teflon® film supported on an aluminum frame. Purified air is provided using an AADCO air purification system.

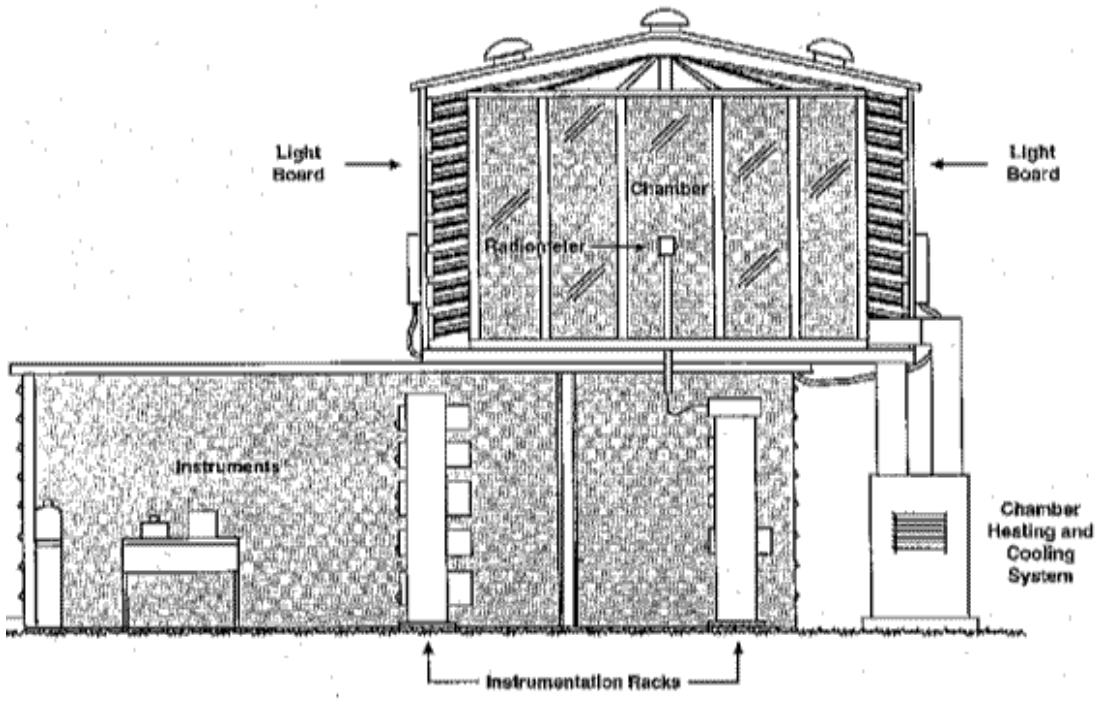

Figure 7. Diagram of the TVA indoor environmental chamber and associated laboratory

Irradiation is provided using banks of GE F40BL blacklamps, Q-Panel 340s and Phillips TL40W/O bulbs in a 4:3:1 ratio. The resulting spectrum is shown on Figure 8, where it is compared with that for the blacklights used for the UCR blacklight chamber experiments and that for direct overhead sunlight. The different spectra are normalized to give the same NO_2 photolysis rate, and thus they correspond to the same light intensity as measured this way. It can be seen that this spectrum gives a better simulation of the relative intensity of sunlight in the <325, ~350 and 400-450 nm regions than the blacklights used at UCR, though they still are deficient in the >400 nm region and also still have the sharp mercury lines.

Since an objective of the work with this chamber is to conduct experiments at lower concentrations than employed previously, a number of steps are taken to reduce background contamination. The chamber was purged with clean air with the lights on for at least two days before each experiment, and clean make-up air was added to the chamber during the experiments to maintain positive pressure. The volume of air input during the experiments was measured using a mass flow meter, permitting the dilution rate to be calculated from this and the known volume of the chamber. The average dilution rate determined in this way was ~15% per hour, and the CO loss rate during CO/NO_x experiments was consistent with this.

The compounds monitored during the experiments included O_3, NO, NO_x, and CO by commercial continuous instruments, PAN by GC-ECD, formaldehyde by DNPH, and individual hydrocarbons by GC. The light intensity was measured using a radiometer situated as indicated on Figure 7 and by conducting periodic NO_2 actinometry experiments. The temperature was measured continuously during the experiments and humidity was measured by dew point.

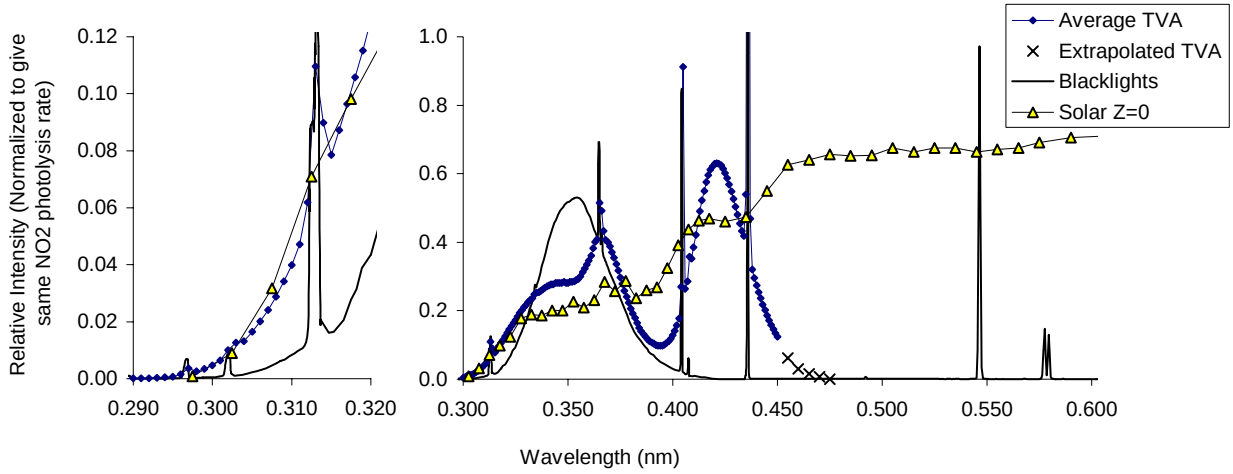

Figure 8. Spectra of the TVA chamber light source used for calculating photolysis rates for modeling.

Runs Modeled and Preparing of Data for Modeling

Some of the TVA chamber data were used by Simonaitis, et al (1997) to evaluate a version of the Carbon Bond mechanism, but to our knowledge no other use has been made of this data for mechanism evaluation. Because of its potential utility for this purpose, Jeffries and co-workers were given funding to make these data available for wider use. This included making these data available in a consistent format and preparing spreadsheets with summarizes of initial reactant concentrations, compositions of hydrocarbon surrogates used, and other relevant conditions, and making these data available at a public web site (Jeffries et al, 2000a). In order to take advantage of this effort, the UNC processed version of these data as the starting point for this project.

Table 9 summarizes the 80 TVA experiments whose data were made available by UNC for modeling. For use in this project, each run was given a number that indicates the order that it was carried out, and these are used in the presentation of the modeling results in this and the following section. Note that runs numbers 21, 23, 45, 46, and 76 were not modeled in this work because no files containing processed data for these runs were found. These include two photostationary state actinometry experiments, two SO_2/NO_x experiments, and one ethylene/NO_x run. The results of the photostationary state experiments are taken into account when determining the NO_2 photolysis rate for modeling, but the results of the other experiments with no data sets were not used for this project.

Computer programs were written to re-format the concentration-time data for these 80 experiments into files that can be read by existing SAPRC modeling programs. The various compound codes used by UNC were assigned to SAPRC-99 detailed model species. Excel macros were written to produce model simulation input files giving the initial reactant concentrations that were summarized in the run summary spreadsheet provided by UNC. For complex mixture experiments, UNC gave compositions of the various mixtures in terms of moles of compounds per mole carbon of mixture, and gave ppm carbon of mixtures used in the various experiments. The macro used this information to derive the initial concentrations of each compound used in each experiment. Model simulations of selected experiments indicated that the data were converted properly.

Table 9. Summary of TVA chamber runs used for mechanism evaluation in this project. Experimental and calculated predictions of O_3 formed and NO oxidized are also shown.

Run Type	Number of Runs	NO_x Range (ppb)
Acetaldehyde - Air	3	0
CO - NO_x	12	5 - 54
Methane - NO_x	13	19 - 21
NO_x - Air	11	9 - 11
Formaldehyde - NOx	4	39 - 42
Isopentane - NOx	1	18
Ethylene - NOx	3	25 - 52
Propylene - NOx	4	22 - 54
trans-2-Butene - NOx	3	20 - 41
Toluene - NOx	3	54 - 266
m-Xylene - NOx	2	98 - 100
Par - Ole Mix 2 - NOx	3	49 - 51
Par - Ole Mix 3 - NOx	3	50 - 100
Par - Ole - Aro Mix 1 - NOx	3	50 - 101
Par - Ole - Aro Mix 2 - NOx	7	50 - 54
SynUrban94 - NOx	12	25 - 169

Characterization of Run Conditions

Initial Reactant Concentrations. The distributed data files and the summary run conditions spreadsheet file distributed by the UNC researchers had recommended initial concentrations for each of the experiments that were modeled. These were used when modeling the experiments for this project in most cases. However, there were a number of cases where the UNC-specified initial concentrations did not correspond well to the measured concentrations, and corrections had to be made to the input data. The recommended initial VOC concentrations for the "SynUrban94" mixture had many discrepancies with the experimental data, so the initial concentrations for all the VOCs were recomputed from the measured data. The composition of this mixture, and the SAPRC-99 detailed model species assigned to each of the components, are given in Table 5, above. There were no measurement data for ethene, ethane, cyclohexene, and (for a few experiments) 1,2,3,5 tetramethylbenzene, so the initial concentrations for these were estimated from ratios of these compounds to other measured species in the recommended UNC composition and the measured concentrations of the other species.

Light Intensity. The light intensity used when modeling these experiments was derived from results of continuous NO_2 actinometry measurements using a flow system with NO_2 in N_2 in the experiments through July, 1994, and from results of occasional actinometry measurements using the photostationary state method after that. The results are shown on Figure 9, along with the NO_2 photolysis rate assignments in the data files, which presumably were made by the UNC researchers. The data (and UNC assignments) show considerable scatter in the 1993-1994 experiments, but do not indicate any

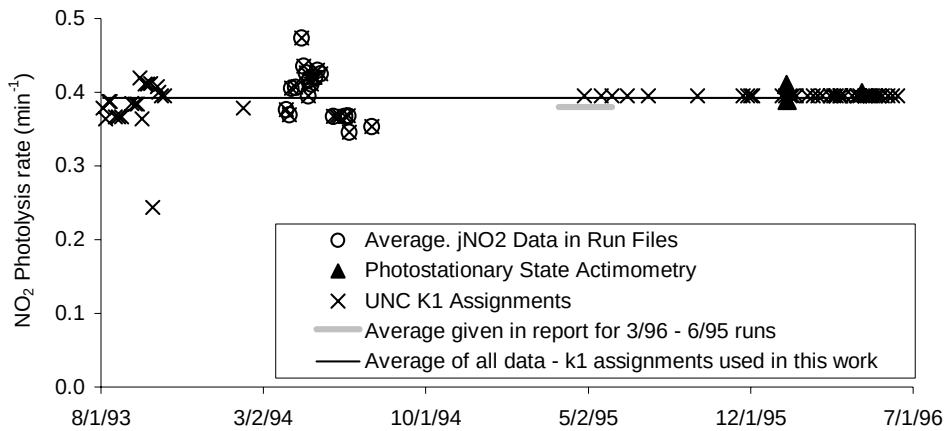

Figure 9. Measured and assigned NO_2 photolysis rates for the TVA chamber experiments.

consistent trend in light intensity during the overall period of the run. Based on our experience with fluorescent lights, we expect the intensity not to vary significantly from day to day, though declines in intensity can occur over time, especially with new lights. Since the data on Figure 9 indicate no significant long-term trend, we consider it most appropriate to use a single NO_2 photolysis rate when modeling all runs. The value assigned is 0.392 min^{-1}, which is the overall average of all the experimentally measured values shown on Figure 9. This is very close to the 0.390 min^{-1} value used by Simonaitis et al (1997) and the 0.395 min^{-1} value assigned by the UNC researchers for the latter runs, but quite different than the assignments for some of the earlier runs with the individual, somewhat variable, actinometry results.

Light Spectrum. Spectra of the light source were available for most of the experiments starting in late 1994, and were given in a spreadsheet file downloaded from the UNC web site. The results indicated no significant change in spectrum over time, as expected with fluorescent light sources. The average of these spectra, shown on Figure 8, above, was used for modeling these experiments. Relative spectral data after 450 nm were not provided, so the relative intensity at higher wavelengths had to be estimated. Note that the bimodal nature of the spectrum is due to the fact that they used a combination of lights in an attempt to provide a better approximation of the relative solar intensities at high and low wavelengths. The solar and blacklight spectra are shown on Figure 8 for comparison.

Temperature. Temperature measurements were made as a function of time during the course of most or all of the experiments, and representative results are shown on Figure 10. It can be seen that the temperature varies during the experiment by as much as 20°C, generally increasing during the first 1-2 hours, then becoming approximately constant after that. To represent this for modeling, the temperature data were fit to a series of line segments, and these were then used to specify the temperature for modeling. Examples of such lines are also shown on Figure 10. Note that the relatively large temperature variation means that using an average temperature when modeling these experiments, as done with the UCR EPA chamber runs discussed above, was not considered to be appropriate.

Dilution. The TVA experiments were continuously diluted with purified air during the experiments, and the rate of input of the make-up air was monitored. Based on these data, the UNC researchers provided summaries of the average dilution rates in the input files. These were used when modeling these experiments. Good fits between experimental and calculated methane and CO in the

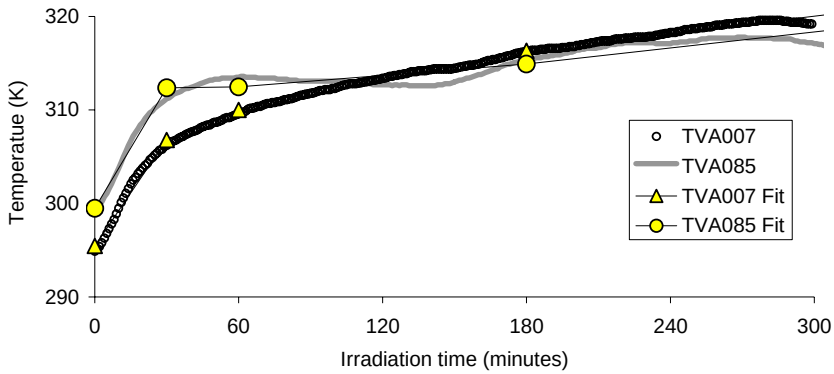

Figure 10. Time series plots for temperature during two example TVA chamber experiments.

model simulations of the experiments where these slowly reacting compounds were present indicated that these assigned dilution rates are appropriate (e.g., see Figure B-32 and Figure B-33 in Appendix B, below).

Humidity. The TVA experiments were carried out using humidified air, so the initial water concentration needs to be specified when modeling the runs. This was derived on a run-to-run basis from the averages of the temperature and dew point measurements made during the experiment. The calculated water concentrations increased very slightly during the course of the experiments, and were generally in the range of 0.8 – 1 x 10^4 ppm. This corresponds to an RH of ~15% for the temperature range of these experiments. Interpolation using least squares fit to the H_2O vs. run number data was used to estimate humidities for the few experiments without valid dew point data.

Derivation of Chamber Effects Parameters for Modeling

The chamber effects parameters used for modeling the TVA chamber experiments were, for the most part, derived using analogous procedures, and based on analysis of similar types of experiments, as employed for the UCR EPA chamber discussed above. The types of TVA characterization experiments whose data were available and used for this purpose are summarized on Table 10, and best fit characterization parameters for individual experiments are given in Table 11. Although in some cases somewhat different types of experiments were used to derive specific parameters than was the case for the UCR EPA chamber as indicated on Table 6, for the most part the analysis was similar. Comments in Table 10 indicate specific factors considerations involved with these TVA experiments.

Ozone Wall Loss. Information concerning the wall loss of O_3 is available only from measurements of O_3 decay in reacted mixtures in the dark after irradiation experiments were completed. By modeling the results of such experiments, Meagher et al (1990) derived a dark decay rate of 7 x 10^{-4} min^{-1}. This is somewhat higher than the ~1.5 x 10^{-4} min^{-1} value that is typical of most Teflon film reactors used at UCR, though it is less than the ~10^{-3} min^{-1} value used for the SAPRC EC (Carter, 2000, and references therein). This value was adopted in the model simulations for this study.

Initial HONO. In the previous modeling of these experiments, Simonaitis et al (1997) found it necessary to assume variable amounts of HONO present with the initial NO_x in order to simulate the rates of reaction in the first hour of the experiment. This was also found to be the case in this work. As shown on Table 11, the best fit initial HONO in the characterization runs where NO_x was injected varied from 0.1 to 1.5 ppb, with an average of 0.5 ±0.3 ppb. (Since HONO is detected as "NO_2" by commercial NO-

Table 10. Summary of types of TVA characterization experiments and chamber effects parameters they were used to derive chamber effects parameters for this chamber.

Run Type	No. Runs	Sensitive Parameters	Comments
Ozone Dark Decay	[a]	O_3 wall loss rate	The loss of O_3 in the dark is attributed entirely to a unimolecular wall loss process. The wall loss rate given by Meagher et al (1990) as used by Simonaitis et al (1997) was employed in this work.
Acetaldehyde – Air	3 [b]	NO_x offgasing	Insensitive to radical source and formaldehyde offgasing parameters. Used as only basis to get NO_x offgasing used in modeling.
CO - NO_x	12	Initial HONO, Radical source and formaldehyde offgasing	Only 3 runs had formaldehyde data. Data could be fit with initial HONO and Formaldehyde offgasing used to simulate radical source. Adjustments to fit formaldehyde data caused overpredictions of O_3 in some experiments. Unknown radical source may be needed to fit some of the experiments without formaldehyde data, but not experiments where formaldehyde measured.
NO_x - Air	11	Initial HONO, Radical source and formaldehyde offgasing	Only 4 runs had formaldehyde data. Data could be fit with initial HONO and Formaldehyde offgasing used to simulate radical source. Most runs could bed fit without assuming an unknown radical source if the initial HONO is adjusted and the formaldehyde offgasing parameters are in the range that fit the formaldehyde data.
Methane - NO_x	5	Initial HONO	Once initial HONO was adjusted the data could be fit using formaldehyde offgasing rates that fit the formaldehyde data in the CO - NO_x and NO_x – air runs with such data without a need to assume an additional radical source.

[a] The TVA O_3 dark decay experiments were not part of the database prepared by UNC.

[b] The O_3 data from the first acetaldehyde – air run, TVA-004, appeared to be anomalous and the data from that run were not used.

NO_x analyzers, the initial NO_2 used when modeling the experiments consisted of the measured "NO_2" minus the adjusted initial HONO. Note that this is a non-negligible correction when modeling some very low NO_x experiments.) No apparent dependence of initial HONO on initial NO_x levels, temperature, or type of experiment was found. The default initial HONO of 0.5 ppb was used for modeling experiments for mechanism evaluation, but the effects of varying this within its variability was also assessed for runs where this was found to be a sensitive parameter.

Table 11. Best fit characterization parameters for individual TVA characterization experiments.

Run		NOx (ppb)	CO or CH_4 (ppm)	Best Fit Parameters [a]			
No.	Date			Init. HONO (ppb)	NO_2 Offg. (ppb/hr)	HCHO Offg. Adj. Fac. [b]	Note
				Acetaldehyde - Air Runs			
43	6/23/94			0.1	0.21		
52	9/22/95			0.1	0.09		
85	6/11/96			0.1	0.19		
				CO - NOx runs			
2	8/7/93	53	47	0.9		(3.1)	
3	8/11/93	5	5	0.3		(1.8)	
12	9/24/93	51	41	1.0		(2.0)	
18	10/16/93	51	43	0.6		(2.0)	
19	10/19/93	8	5	0.3		(1.0)	
41	6/17/94	54	44	0.5		(1.7)	
42	6/21/94	12	5	0.2		(1.2)	
54	11/27/95	5	4	0.1		(0.9)	
55	12/1/95	51	41	0.6		(1.2)	
70	3/28/96	51	44	0.3		0.75	[c]
82	5/22/96	5	4	0.2		1.3	
83	5/29/96	52	43	0.6		1.0	
				Methane - NOx runs			
1	8/4/93	21	125	0.3			[d]
20	10/23/93	20	124	0.2			[d]
32	5/2/94	19	134	0.1			[d]
58	1/16/96	19	118	0.2			[d]
84	6/4/96	20	41	0.4			[d]
				NOx - Air Runs			
7	8/28/93	10		0.6		(1.2)	
10	9/18/93	10		1.2		(1.4)	
17	10/14/93	11		1.5		(1.2)	
22	2/4/94	9		0.1		0.8	[c]
34	5/7/94	10		0.6		(0.7)	
40	6/10/94	10		0.6		(0.8)	
44	7/22/94	11		0.7		(1.2)	
53	11/21/95	11		0.5		1.1	
57	1/11/96	10		0.5		(0.8)	
69	3/27/96	11		0.7		0.75	
81	5/17/96	11		0.8		0.75	

[a] If no data are sown then either the run was insensitive to the parameter or there were insufficient data to make the adjustment A "0" indicates that best fits are obtained if it is assumed that the process is negligible.

[b] If the value is in parentheses, then there is no formaldehyde data for the experiment and the parameter was adjusted to fit the O_3 and NO data. Otherwise, the formaldehyde offgasing parameter was adjusted to fit the formaldehyde data.

[c] The O_3 and NO data are better fit by using a lower formaldehyde offgasing rate.

[d] The results of these experiments are not sufficiently sensitive to the formaldehyde offgasing rates to serve as a basis for adjusting the parameter. However, most of these experiments are slightly better fit using the default formaldehyde offgasing rates than assuming no formaldehyde offgasing is occurring at all.

Formaldehyde Offgasing. As discussed by Simonaitis et al (1997), measurable formation of formaldehyde is observed in the CO - NO_x and NO_x - air experiments where there is no expected formaldehyde source in the gas-phase chemistry. In order to fit the formaldehyde concentration-time profile data in these experiments, it is necessary to assume both direct formaldehyde offgasing and also offgasing of some formaldehyde precursor compound. Based in part on the model developed by Simonaitis et al (1997) and in part on our own modeling of these experiments, most of the data were reasonably well fit by the following formaldehyde offgasing model:

Walls $\rightarrow$ HCHO	Rate = f x k_1 x 0.05 ppb
Walls $\rightarrow$ WallVOC	Rate = f x 0.15 ppb min^{-1}
WallVOC + OH $\rightarrow$ HO_2 + 0.2 HCHO	k = 2 x 10^4 ppm^{-1} min^{-1}

where k_1 is the NO_2 photolysis rate in min^{-1}, and "f" is "formaldehyde offgasing adjustment factor" that was adjusted from run to run. The values of "f" that best fit the formaldehyde data in the experiments where formaldehyde was measured are given in Table 11, and ranged from 0.75 to 1.3, with an average of 0.9 ±0.2. The default value of f = 0.9 was used when modeling the experiments for mechanism evaluation, but the effect of varying this to within this variability is also assessed. This corresponds to default formaldehyde and formaldehyde precursor offgasing rates of 0.018 and 0.059 ppb min^{-1} for the light intensity of these experiments.

NO_x Offgasing. It is necessary to assume some NO_x offgasing in order to explain the formation of O_3 and PAN in the acetaldehyde – air experiments. Four acetaldehyde – air experiments are part of the TVA data set, but the data from one appeared to be anomalous and were not used. The data in the other three experiments were best fit by NO_x offgasing rates are shown in Table 11. The average NO_x offgasing rates that fit the data in these experiments was 0.17±0.06 ppb/hour. This was used as the default for modeling. Note that the other characterization experiments were not particularly sensitive to this parameter, and the modeling of the acetaldehyde – air experiments was not very sensitive to the other characterization parameters. In order to evaluate the NO_x offgasing and radical source effects separately, the NO_x offgasing was represented by offgasing of NO_2 rather than HONO.

Continuous Radical Source. The NO oxidation and O_3 formation rates in the CO - NO_x and the NO_x – air experiments are extremely sensitive to chamber effects involving radical sources. These include initial HONO, offgasing of HONO, formaldehyde, or other photoreactive species, or the "unknown radical source" first discussed by Carter et al (1982), and used in previous mechanism evaluation studies, including the evaluation of the SAPRC-99 mechanism (Carter, 2000). However, model simulations of most of the TVA NO_x – air and CO - NO_x experiments in which formaldehyde was monitored could adequately fit the NO oxidation and O_3 formation rates if no other radical source is assumed other than the initial HONO required to fit the initial data, and the formaldehyde offgasing parameters necessary to fit the formaldehyde data. Indeed, the O_3 formation in a few of these experiments is slightly overpredicted even with no unknown radical source, i.e., the radicals predicted to be formed from the observed formaldehyde is more than enough to account for the observed reactivity.

Based on the result of modeling the experiments where formaldehyde data were available, the radical-sensitive characterization experiments without formaldehyde data were modeled with the formaldehyde offgasing parameter ("f" in the equations above) adjusted to fit the O_3 formation and NO oxidation data. The formaldehyde offgasing parameter that best fit most of the NO_x - air experiments without formaldehyde data were within the range of those with formaldehyde data, as expected. However, for many of the CO - NO_x experiments without formaldehyde data it was necessary to assume formaldehyde offgasing parameters that were higher than the range of those that fit runs with formaldehyde data. This suggests that there may be an additional radical source in at least some of these

CO - NO_x experiments. This may be due to impurities in the CO, since in chamber experiments in our laboratory we found high apparent chamber radical sources if care is not taken to purify the formaldehyde prior to injection. Therefore, the results of these anomalously reactive CO - NO_x experiments were not considered to be a sufficiently reliable basis to revise our assumption that additional chamber-dependent radical sources probably do not need to be represented when modeling these experiments.

Chamber effects parameters used for modeling. The chamber effects parameter used for modeling the TVA experiments are summarized in Table A-2 in Appendix A. In order to provide an indication of the sensitivity of the mechanism evaluation results to what we consider to be the most important uncertain variable chamber parameters, the experiments were modeled using different assumptions concerning amounts of formaldehyde offgasing and initial HONO in the experiments. The "Standard" model used our best estimates of the values of these parameters, derived as discussed above. The "High Aldehyde" model used the formaldehyde offgasing adjustment parameter, f, set at a value of 2.0, which is a factor of 2.2 higher than that used in the standard model, but within the range of variability of the parameter that best fit the characterization runs, as shown on Table 11. The "Low HONO" model assumed initial HONO levels at only 0.1 ppb, a factor of 5 lower than the value used in the default model but also within the variability of the characterization data. (Note that an initial HONO of 0.1 ppb is what was assumed for the UCR EPA chamber, as discussed above.) The differences between the simulations using the standard model and these alternative chamber effects models indicate the sensitivity of the model calculations to the uncertainties in these characterization parameters. This is discussed in the "Mechanism Evaluation Results" section, below.

CSIRO Chamber Experiments

The CSIRO chamber was used to carry out a number of ambient surrogate - NO_x experiments under relatively low NO_x conditions, and the data are also potentially useful for mechanism evaluation. Because these data have not been used to evaluate the SAPRC-99 mechanism at the time this project was initiated, modeling these data was also included among the tasks for this project. Subsequently, Hynes et al (2003) reported modeling a number of CSIRO chamber experiments, and noted discrepancies between model predictions and the experimental results. Therefore, it is still useful for us to conduct an independent modeling study of these data to determine if such problems are also indicated by our results.

In this section we discuss the methods used for modeling and deriving or estimating the chamber characterization parameters when modeling experiments from this chamber. A brief description of the chamber and the procedures employed for these experiments is also given to provide an appropriate background for this discussion.

Chamber Description and Runs Modeled

The CSRIO chamber facility was designed to simulate photochemical smog production under conditions approximating those of the urban atmosphere (Johnson, 1983, Johnson et al, 1983). It consists of two separate 20,400-liter outdoor reactors, named Levante (L) and Ponente(P), located in a suburb of Sydney, Australia. The reactors are constructed of 5 mil FEP Teflon® mounted to cubic rigid frameworks. The reactors are located on rails so they can be moved inside an enclosure for storage and during reactant injection and moved outside to begin the irradiations. An air purification system with non-methane organics < 50 ppb and NO_x < 10 ppb, with a CO scrubber and with an output rate of 0.5 m^3 min^{-1} was employed to purge the reactors between the experiments. The chamber and facility is described by Hess et al (1992) and Johnson et al (1997) and its major features are also summarized by Johnson (1983) and Hynes et al (2003). A photograph of the reactors during an irradiation is shown on Figure 11.

Figure 11. Picture of the CSIRO Dual Outdoor Chamber and associated laboratory structures

A number of earlier experiments in this facility were carried out for the purpose of developing Johnson's "Extent of Reaction" parameterization method (Johnson, 1983). Although the data from these earlier experiments are now available in tabular and graphical form (Johnson et al, 1997), preparing these data in a form suitable for modeling was beyond the scope of this project. However, under EPA funding a limited number of ambient surrogate - NO_x experiments for mechanism evaluation were carried out in 1995 and 1996, and under funding from a RRWG project these data were made available for modeling by Jeffries et al (2000b). These were the runs that were modeled for this project.

The procedures employed for the CSIRO experiments are described by Johnson (1983) and Johnson et al (1997). The reactors were purged with dry, purified air overnight after each experiment and purged in daylight and again overnight before each experiment. The reactants, consisting of NO and a complex organic mixture designed to represent photochemical smog precursors measured in ambient air were injected while the reactors were still in the enclosure, and water vapor was also injected to bring the humidity to the desired level. The irradiation was begun by rolling the reactors out into sunlight and terminated at the end of the day by rolling the reactors back into the enclosure. The experiments were performed without dilution.

Jeffries et al (2000b) made available data from a total of 10 CSIRO chamber experiments, carried out between September 21 through October 19, 1995, and between March 15 through March 26, 1996. Figure 12 shows the matrix of initial NO_x and VOC concentrations for these experiments, where it can be seen that the initial NO_x ranged fro 20 to 100 ppb, the surrogate concentrations ranged fro 50 to 400 ppmC. The experiments covered a range of VOC/NO_x ratios as well, ranging from 1.6 to 10.2. The conditions and selected results of individual experiments are given in Table 19 in the Mechanism

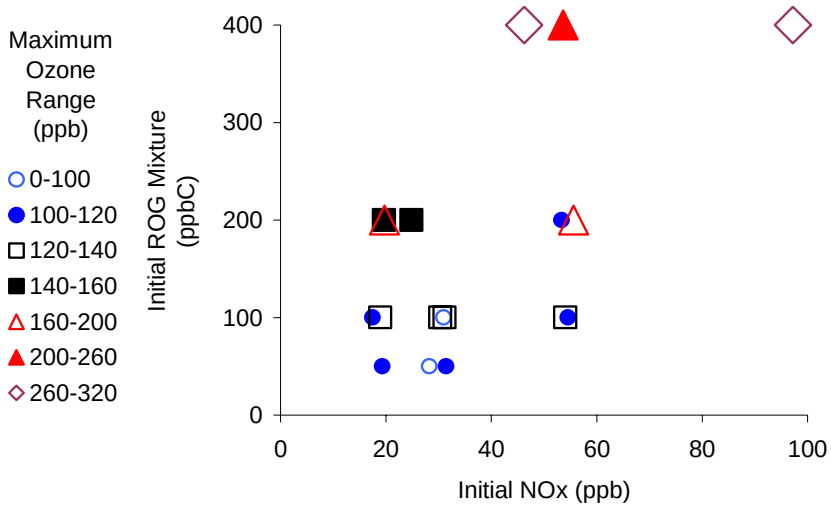

Figure 12. Matrix of initial ROG and NO_x levels for the CSIRO chamber experiments modeled in this project. Different symbols are used to indicate maximum ozone concentration range.

Evaluation Results section, where they are discussed in the context of the model performance in simulating their results.

Characterization of Run Conditions

All of the experiments made available for modeling were surrogate - NO_x runs, and no characterization data were included in this dataset. Some characterization information is given by Johnson (1983) and Johnson et al (1997), but this is insufficient for deriving characterization parameters using the procedures discussed above for the TVA or the UCR EPA experiments. Pure air irradiations were carried out periodically, with final concentrations being in the 40 - 80 ppb range, and averaged ~50 ppb (Johnson, 1983). Experiments using smaller reactors suggest that the effects of the walls on overall reactivity are not large compared to the reactivity due to the VOC and NO_x reactants, suggesting that chamber effects such as the radical source may not be a dominant factor affecting surrogate - NO_x runs (Johnson et al, 1997). In addition, information presented by Hynes et al (2003), and characterization data for other Teflon film chambers, are useful for estimating characterization parameters for these reactors. This is discussed below.

Initial Reactant Concentrations. The initial NO, NO_x, and total ROG surrogate concentrations injected into the CSIRO experiments were given in the data files provided by Jeffries et al (2000b), and these were used to determine the initial reactant concentrations when modeling these experiments. The amounts of injected ROG surrogate were specified as total ppmC each of liquid surrogate and gas surrogate, which were injected separately. The compositions of these surrogates were also provided by Jeffries at al (2000b), and this, combined with the total ppmC of each injected, could be used to derive the concentrations of the individual injected VOCs. It was found that all but two experiments had the same ratio of total gas to liquid surrogate, which meant that the same relative distribution of VOCs was used in those runs. This composition, and the SAPRC-99 model species assigned to each of the components, is given in Table 5, above. As indicated there, the same composition was used when modeling all experiments except for runs 344P and 345P, where the ratio of liquid to gas VOCs was a factor of 1.7

higher than for the other experiments. Note that for these experiments the "gas" mixture consisted of all $C_{\leq 5}$ alkanes and alkenes except for isoprene, and the "liquid" mixture consisted of isoprene and all $C_{\geq 6}$ alkanes and alkenes and all aromatics, and this is reflected in the differences in relative composition as indicated on Table 5.

Temperature. Temperature was measured as a function of time in both chambers during the experiments, and temperature data for all but two of the experiments are included with the data provided by Jeffries et al (2000b). These data are plotted against time (given as minutes after midnight, which is the time unit we use when modeling outdoor chamber experiments) on Figure 13. For most of these experiments, the temperature at the beginning of the experiment was around 280°K, and it leveled off at about 300°K in the afternoon. For modeling purposes, several line segments were derived based on least squares fits to the temperature data, and these were used to derive the simulated temperature during the experiments. These are also shown on Figure 13, where they can be compared with the measurement data. Temperature data were not available for runs 344 and 345, so for modeling those experiments the temperature fits for run 343, which was carried out the day before run 344 and about a week before run 345, was used.

Humidity. Although the CSIRO chamber was flushed with dry air prior to the experiments, water vapor was injected along with the reactants in the experiments (Johnson, 1993, Hynes et al, 2003). The files prepared by UNC give 9.5 x 10^{-3} ppm as the water concentration for these experiments, and that was assumed in our modeling. This is consistent with the 10,000 ppm H_2O concentration given by Johnson (1993) for earlier experiments.

Light Intensity and Spectrum. The CSIRO experiments were carried out using natural sunlight, so both the intensity and the spectrum of the irradiating light varied with time. Although the spectrum and intensity of sunlight can be calculated using actinic flux models (e.g, Peterson, 1976, Jeffries, 1991), these do not take into account effects of local meteorology and albedos and also effects of chamber walls. The only information available about local light effects during CSIRO experiments are measurements by total solar radiation (TSR) and UV radiation instruments. We have found data from UV radiometer instruments vary significantly from instrument to instrument, making them useless for light characterization unless each instrument's spectral response has been determined (Fitz et al, 2000), so the only useable light characterization information available for the CSIRO chamber runs consists of the TSR data.

Fortunately, there appears to be useful information about how to derive NO_2 photolysis rates from TSR data, thus converting them effectively into NO_2 actinometry data. Hynes et al (2003), when modeling the CSIRO experiments, used the following experimentally-derived relationship between TSR and the NO_2 photolysis rate from previous work by Demerjian and Schere:

$$k_1 = (0.295 + 0.076/\cos z) \times TSR \qquad z < 47^o$$
$$k_1 = 0.4064 \times TSR \qquad 47^o < z < 64^o$$
$$k_1 = [-0.0696 + 0.835(1-\cos z)] \times TSR \qquad z > 64^o$$

Here, k_1 is the NO_2 photolysis rate in min^{-1}, TSR is the TSR reading in cal cm^{-2} min^{-1}, and z is the solar zenith angle in the range of 0 to 90 degrees. The solar zenith angle is calculated from the time of day, the latitude of the experiment, and the correction time for the difference between calculated solar time and reported time of the experiment.

The above relationship was used to estimate the NO_2 photolysis rates when modeling these experiments. The ratios of the other photolysis rate constants to that of NO_2 being calculated as a function of time in the experiment using the solar actinic fluxes given by Peterson (1977) for his "best estimate" surface albedos for the calculated zenith angle, and the absorption cross sections and quantum yields of

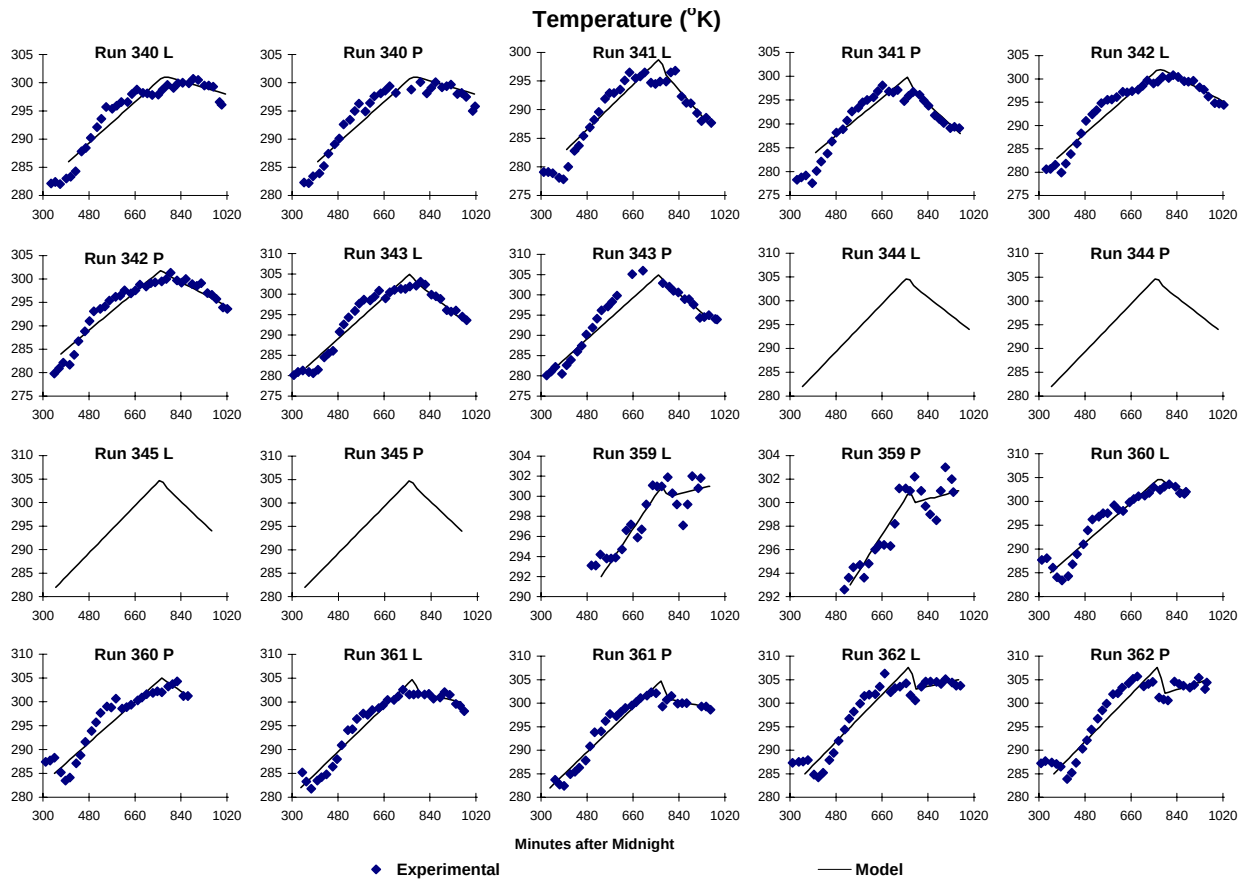

Figure 13. Plots of experimental and model input temperatures for the CSIRO experiments.

the mechanism. In practice, however, the TSR data were not used to derive the NO_2 photolysis rates directly. Instead the model simulation program was used to calculate the TSR values from the calculated NO_2 photolysis rates using the inverse of the k_1 vs. TSR relationship above, with the NO_2 photolysis rates being calculated as a function of zenith angle using the Peterson (1977) actinic fluxes and the SAPRC-99 NO_2 absorption cross sections and quantum yields (Carter, 2000a). The TSR values so calculated were compared with the experimental results, and total light intensity adjustment factors were used to make the calculated TSR values consistent with the experimental measurements.

Figure 14 shows the experimental and calculated TSR values for the CSIRO experiments modeled in this study. Note that the calculation is only for the time period of the irradiation experiment, as indicated in the files provided by Jeffries et al (2000b), so early morning and late evening calculated values are not shown. The dotted lines show the calculation without adjustment, derived using the date and time of the experiments and using 33.867° south as the latitude of the chamber. It can be seen that for most times of the experiments the theoretical and experimental TSR values agree remarkably well, and that no solar vs. experimental time correction is needed[8]. However, for certain times in most experiments the experimental TSR was different (usually lower) from the theoretical values, presumably due to clouds

[8] The need for a time correction would be indicated by the calculated and experimental TSR values for clear-sky experiments having maxima at different times.

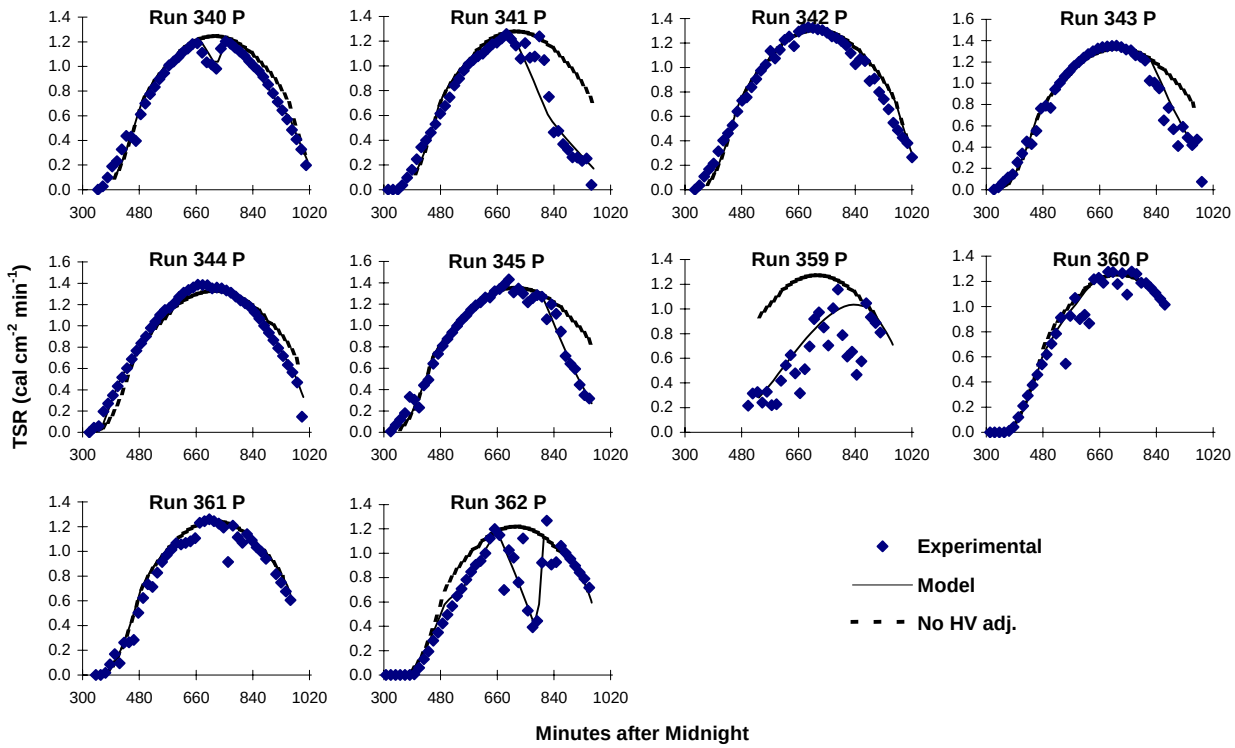

Figure 14. Plots of experimental and calculated TSR data for the CSIRO experiments. Calculated TSR data are shown without adjustments and with total light intensity adjustments derived as discussed in the text.

or haze. To account for this, adjustments were made to the total light intensity parameter "HV", by which the calculated TSR values and all photolysis rates was multiplied, which was varied throughout the experiments when needed. This was done by manually assigning values at certain times so the calculated and experimental TSR agree, and having the program linearly interpolate the HV for times between when the values were manually adjusted. The resulting adjusted TSR values are shown as the solid lines on Figure 14.

Note that this adjustment does not take into account any changes in light spectrum that may occur during less-than-clear-sky conditions, which would result from different photolysis rates changing by different factors, depending on their action spectrum. This also does not take into account any effects of the chamber walls on light intensity or spectrum, or differences between the albedo within the chambers and the "best estimate" albedos used by Peterson (1977). The latter may result in the actual in-chamber photolysis rates possibly being higher than calculated, if reflective surfaces are present. Therefore, although the calculated and experimental TSR values agree well, there is a possibly non-negligible uncertainty in the accuracy of the calculated in-chamber photolysis rates.

In order to assess the effects of any light intensity uncertainty on the evaluation results, experiments were modeled not only using the best-fit light intensity adjustment factors derived as discussed above, but also with the light adjustment factors increased by 15%. The former is used in the "standard" calculations while the latter is referred as to the "high HV" model in the discussion of the results.

Chamber Effects Parameters Used for Modeling

The chamber effects used for modeling the CSIRO experiments are given in Table A-2 in Appendix A. No data from characterization experiments were made available to us for this project, so we were unable to derive these parameters in the same way as done for the UCR and TVA experiments discussed above. The most important of these is probably the chamber radical source, which is represented by HONO offgasing or light induced conversion of NO_2 to HONO in the EPA chamber experiments, and by similar processes when modeling experiments in most other Teflon wall chambers. In the case of the TVA chamber the radical effect appears to be dominated by an unusually high formaldehyde and formaldehyde precursor offgasing processes, but these are assumed not to be important in the CSIRO chamber.

Chamber Radical Source. The chamber radical source and NO_x offgasing can both be represented by a HONO offgasing process whose rate is determined by the parameter RN-I, which is the rate of NO_x offgasing divided by the NO_2 photolysis rate. For indoor Teflon chamber experiments at UCR, the value of RN-I that best fits the characterization data is about 0.001 - 0.02 ppb for the EPA chamber and is about 0.06 - 0.1 ppb for the older UCR chambers where experiments are generally conducted at higher concentrations. When modeling CSIRO experiments, Hynes et al (2003) used 0.066 ppb for RN-I, which is in the low end of the range of that used for the earlier UCR chambers, but higher than that appropriate for the EPA chamber, where steps are taken to minimize background effects. (Hynes et al, 2003, also used RS-I, the rate of OH input relative to the NO_2 photolysis rate, of 0.001 ppb. This is small compared to the RN-I value they use, and in effect can be incorporated by using a value of RN-I of 0.067 ppb.)

However, use of indoor chamber radical source parameters may not be appropriate for modeling outdoor chamber experiments, where the temperature varies widely. When modeling SAPRC outdoor Teflon chamber (OTC) experiments, we found that the chamber data were much better fit using a radical source parameterization incorporating a significant temperature dependence for RN-I (Carter et al, 1995a,b). Based on updated modeling of these experiments, the current parameterization used for the OTC is

$$\text{RN-I (ppb)} = 6.0\text{x}10^{-9} \text{ x } e^{-19.3/(0.0019872 \text{ x } T)}$$

where T is the temperature in degrees K. For 300°K, which is typical of afternoon conditions in the CSIRO experiments modeled here, this yields a RN-I of 0.079 ppb, which is very close to the 0.066 ppb value used by Hynes et al (2003).

Although one might expect the CSIRO chamber to have lower or at least no higher radical source levels than the SAPRC OTC because generally lower concentration experiments are carried out, the results of modeling these experiments, discussed below, indicate that the model consistently underpredicts the NO oxidation and O_3 formation rates in essentially all experiments. This suggests that the actual radical source for the CSIRO chamber could be higher than used for the SAPRC OTC.

Therefore, when modeling these runs we show results of calculations using two assumptions regarding the chamber radical source. In the “standard” model we use the OTC radical source parameters, shown above, which are not inconsistent with that used by Hynes et al (2003). In the second, “High RS” model, we use a RN-I value that is three times higher than this. The latter is probably higher than a reasonable upper limit for the chamber radical source for chambers with Teflon film reactors, but is useful for the purpose of evaluating whether this uncertainty can account for the problems with modeling these runs as discussed below.

Initial HONO. Another component of the chamber radical source is the initial HONO levels in the experiments, which can affect NO oxidation rates during the initial stages of the experiments. Since no characterization data are available that can be used to derive this parameters, the model simulations were carried out assuming either no initial HONO, or with an initial HONO level of 2 ppb, the latter being considered to be higher than a reasonable upper limit for this parameter. The higher value is used because as discussed below the standard and even the high radical source model underpredicts initial NO oxidation rates in most of the CSIRO experiments modeled.

Results of Pure Air Simulation Test

As indicated above, Johnson (1983) stated that pure air irradiations in the CSIRO chamber yielded final O_3 concentrations in the 40 - 80 ppb range. Simulation of temperature conditions and lighting conditions of run 352 (without light intensity adjustments), without injected reactants, yielded a final O_3 concentration of 66 ppb. This is within the range given by Johnson (1983) and not far from the stated average concentration. Calculations using the high radical source or the 20% increase in light intensity result in calculated maximum O_3 concentrations of 75-80 ppb, which is in the high end of this range given by Johnson (1983). Thus the chamber models used in this work are not inconsistent with the results of the pure air simulations in these reactors.

MECHANISM EVALUATION RESULTS

UCR EPA Experiments

A total of 78 UCR EPA chambers were used in this mechanism evaluation study, of which 36 were used for characterization, 18 were for mechanism evaluation using simple chemical conditions, and 24 were ambient surrogate - NO_x experiments at various surrogate and NO_x levels. A relatively large number of characterization experiments were carried out during the period of the evaluation experiments of interest in this report because this chamber had not been previously characterized. The 42 mechanism evaluation experiments included 14 carried out at NO_x levels lower than 10 ppb and 24 at levels less than 25 ppb, making this probably the lowest NO_x set of chamber data sufficiently well characterized for mechanism evaluation. All these experiments were modeled using the SAPRC-99 mechanism and the characterization described in the previous section. The evaluation results for the different types of experiments are discussed separately below.

Characterization Runs

Table 12 and Table 13 list all the UCR EPA characterization experiments that were modeled in this study, gives the initial reactant concentrations, the final amounts of NO oxidized and O_3 formed in the experiments (as measured by $\Delta([O_3]\text{-}[NO])$, or $\{[O_3]_{final}\text{-}[NO]_{final}\}\text{-}\{[O_3]_{initial}\text{-}[NO]_{initial}\}$)), and the model performance in simulating these results. More details about the model performance in simulating the results of the experiments is available in Figure B-1 through Figure B-10 in Appendix B, which shows concentration-time plots for $\Delta([O_3]\text{-}[NO])$, O_3, NO, NO_2, formaldehyde and (where applicable) n-butane for all the experiments.

Because of the sensitivity of the characterization runs to potentially variable chamber effects, one may expect some scatter in the quality of the fits of model to the characterization data, but the average biases should be small because the characterization parameters were adjusted to minimize overall biases in the model fits to the data. The results shown on Table 13 are consistent with this expectation, where the average error is in model predictions of $\Delta([O3]\text{-}[NO])$ is ~30%, but the average bias is near zero. However, an average error in the 30% range is better than the model performance in simulating characterization runs that are sensitive to variable chamber effects in previous comprehensive mechanism evaluation studies (e.g., Carter and Lurmann, 1990, 1991; Carter, 2000a), suggesting that there may be less variability in the characterization of this chamber than those used in previous evaluations.

However, there are individual experiments or sets of experiments where biases are sufficiently large compared to the scatter that they may indicate problems with the mechanism or the characterization model. The O_3 is overpredicted in all the formaldehyde - CO - air, with EPA063A (Figure B-5) being the most extreme example of this. This may be due to some problem with the formaldehyde mechanism under very low NO_x conditions rather than reflecting actual NO_x offgasing. If this were the case, it may have been more appropriate not to include “best fit” NO_x offgasing parameters in these runs when deriving the HONO offgasing parameter used when modeling these experiments, but given the relatively large number of other experiments the effect of this on the overall results would be small.

The inability of the model to simulate the results of the relatively high NO_x CO - NO_2 experiment EPA071B (see Table 13 and Figure B-9) is also a concern. In this case, it is probably not due to characterization uncertainty as much as either a mechanism or an experimental problem. Note, however,

Table 12. Summary of reactants, Δ([O3]-[NO]) results, and model biases for the CO - air and CO - formaldehyde - air characterization experiments in the UCR EPA chamber.

Run	HCHO (ppb)	CO (ppm)	Hours	$[O_3]$ (ppb)	Model Bias [a]	Plot Figures
			CO - Air			
EPA055A	-	60	7	10	-21%	Figure B-1
EPA055B	-	60	7	12	-36%	"
EPA056A	-	77	10	13	14%	"
EPA056B	-	68	10	18	-20%	"
EPA060A	-	168	9	8	51%	Figure B-2
EPA060B	-	64	10	10	40%	"
EPA076A	-	72	10	20	-27%	"
EPA076B	-	73	10	12	18%	"
EPA079A [b]	-	72	10	16		Figure B-3
EPA079B [b]	-	76	10	15		"
EPA087A [c]	-	75	10	27	-15%	“
EPA087B [c]	-	75	10	17	-6%	“
EPA112A	-	100	7	34	-40%	Figure B-4
EPA112B	-	101	7	10	33%	"
EPA160A	-	95	7	26	-21%	"
EPA160B	-	95	7	20	-32%	"
				Average Bias:	-9%	
				Average Error [d]:	22%	
			Formaldehyde - CO - Air			
EPA063A	220	80	10	20	67%	Figure B-5
EPA063B [e]	71	64	10	12	155%	"
EPA115A	99	72	6	24	13%	"
EPA115B	73	73	6	11	77%	"
EPA133A	79	73	6	24	13%	Figure B-6
EPA133B	80	73	7	15	63%	"
				Average Bias:	31%	
				Average Error:	34%	

[a] Model bias is (calculation - experimental) / experimental Δ($[O_3]$-[NO]) data for the indicated hour of the experiment. Calculations used the SAPRC-99 mechanism and the standard chamber model.

[b] Temperature was ~7°C lower than the other experiments discussed in this report. The run was not modeled because no characterization model for that temperature was developed.

[c] Blacklight light source used. However, these data are counted in the average biases and errors because the light source is assumed not to affect the characterization model.

[d] Average of absolute values of the model biases

[e] This large model bias is due to an unusually low experimental Δ($[O_3]$-[NO]) in the experiment. This bias not counted when computing the average biases and errors.

Table 13. Summary of reactants, Δ([O3]-[NO]) results, and model biases for the CO - air and CO - formaldehyde - air characterization experiments in the UCR EPA chamber.

Run	NO (ppb)	NO_2 (ppb)	n-C_4 (ppb)	CO (ppm)	Hours	Δ([O_3]-[NO]) (ppb)	Model Bias [a]	Plot Figures
				CO - NO_x (where NO>NO_2)				
EPA057A	54	2	-	81	10	114	-13%	Figure B-6
EPA057B	48	2	-	82	10	113	-7%	"
EPA058A	81	13	-	90	10	94	-7%	Figure B-7
EPA061A	7	0	-	86	10	104	-5%	"
EPA061B	9	1	-	68	10	116	-7%	"
EPA070A	25	1	-	87	10	145	-10%	"
EPA070B	26	1	-	77	10	120	1%	Figure B-8
EPA071A	189	13	-	81	10	66	13%	"
EPA103A	16	10	-	46	6	114	-28%	"
EPA103B	18	9	-	46	6	91	-29%	"
EPA140A	14	9	-	44	6	83	2%	Figure B-9
EPA140B	14	9	-	44	6	72	-6%	"
						Average Bias:	-8%	
						Average Error [b]:	11%	
				CO - NO_2				
EPA058B	-	76	-	74	10	51	9%	Figure B-9
EPA071B [c]	-	180	-	85	10	-23	-212%	"
				n-Butane - NOx				
EPA064A	47	2	490	-	7	18	-13%	Figure B-10
EPA064B	0	41	350	-	10	12	-20%	"
						Average Bias:	-16%	
						Average Error [d]:	16%	
				All Characterization experiments [d]				
						Average Bias:	-3%	
						Average Error [d]:	19%	

[a] Model bias is (calculation – experimental) / experimental Δ([O_3]-[NO]) data for the indicated hour of the experiment. Calculations used the SAPRC-99 mechanism and the standard chamber model.

[b] Average of absolute values of the model biases

[c] This run could not be fit by any reasonable chamber model. The results are considered to be anomalous and the data are not used when computing the overall average and bias.

[d] Includes all experiments in Table 12 and Table 13 except EPA079, EPA063B, and EPA071B. Note that including EPA063B and EPA071B changes the average bias and error to –4% and 28%, respectively.

that the changes in the NO and O_3 data in that experiment, which determines the model bias as indicated on Table 13, are relatively small in magnitude compared to the total amount of NO_x present, which is mostly in the form of NO_2. Therefore, the apparent model problem is due to the model's inability to simulate relatively small changes in NO_x species compared to the total amount present.

Although the NO_x offgasing parameters in the CO - air and CO - formaldehyde - air experiments were derived based on fits to O_3 data, the most direct evidence for NO_x offgasing in those experiments come from the NO_2 data, which are shown in the concentration - time plots for those experiments in Appendix B[9]. Detectable amounts of NO_2 were formed in most of those experiments, at levels that were generally consistent with model predictions. The quality of the NO data in the NO_x offgasing experiments was variable, since there was a CO interference on the instrument that lead to invalid or readings from the NO analyzer. However, in the experiments with reasonable appearing NO data the results were also not inconsistent with the model predictions of the very low NO levels present in photostationary state with the NO_2 and O_3.

The formaldehyde data in the experiments with no injected formaldehyde are also of interest, since they were used to derive the formaldehyde offgasing parameter. The amount of formaldehyde formed in those experiments was close to the detection limit of the instrument, but, as discussed above, were definitely above zero in most of these experiments. Overall, the amounts formed were consistent with model prediction, as is expected given that the formaldehyde offgasing parameter was adjusted to fit these data. There is relatively little variability from run to run in the apparent formaldehyde offgasing, indicating that it is unlikely to be a memory effect from reactants in prior experiments.

Overall, although there is variability and some biases, the model simulations of the characterization runs for this chamber is considered to be as good as can reasonably be expected given our current state of knowledge and ability to model chamber effects. Although the uncertainties and variability are obviously of concern, this model performance in simulating the characterization experiments is considered to be sufficient for the purpose of mechanism evaluation. Sensitivity calculations where the more important chamber effects are varied within the range indicated by the variability of the characterization data indicate that the mechanism evaluation experiments, discussed in the following section, are generally much less sensitive to the uncertain or variable characterization parameters than these characterization experiments. This suggests that small or moderate biases or uncertainties the characterization data probably will not have a large effect.

Single Compound Experiments

Although the number of single compound experiments carried out to date in this chamber are relatively limited, they include a representative set of compounds, and they were carried out at lower NO_x levels than previously used in mechanism evaluations. The individual experiments, the final amounts of NO oxidized and O_3 formed, and the performance of the model in simulating these data are summarized on Table 14, and experimental and calculated concentration-time plots of measured species are given in Figure B-11 through Figure B-18 in Appendix B. The results for the various types of compounds are discussed below.

<u>Formaldehyde - NO_x and Formaldehyde - CO - NO_x</u>. One dual chamber formaldehyde - NO_x and one dual chamber formaldehyde - CO - NO_x, with NO_x levels ranging from less than 10 to ~25 ppb. The results are shown in Figure B-11. Good model performance is obtained in simulating the formaldehyde -

[9] Note that the NO_2 data shown in the figures are obtained using the TDLAS, giving a specific measurement for this compound. The "NO_y" data obtained from the chemiluminescence NO-NO_x analyzer were generally much higher than these specific NO_2 readings (see Carter, 2002b).

Table 14. Summary of reactants, Δ([O3]-[NO]) results, and model biases for the single compound experiments in the UCR EPA chamber.

Run	NOx (ppb)	VOC (ppb)	CO (ppm)	Hours	Δ([O_3]-[NO]) (ppb)	Model Bias [b]	Plot Figure
			Formaldehyde - NOx				
EPA069A	8	35	-	10	49	-27%	Figure B-11
EPA069B	23	50	-	10	49	-19%	"
EPA068A	21	49	76	4	225	-12%	"
EPA068B	16	39	14	4	123	-8%	"
			Ethene - NOx				
EPA073A	25	617	-	6	300	-13%	Figure B-12
EPA073B	10	650	-	6	194	-17%	"
			Propene - NOx				
EPA065A	24	52	-	10	115	17%	Figure B-13
EPA065B	5	42	-	10	81	15%	"
			Toluene - NOx				
EPA066B	5	61	-	10	61	18%	Figure B-14
EPA074A	24	151	-	6	145	7%	Figure B-16
EPA077A	23	152	-	6	139	9%	Figure B-17
			Toluene - CO - NOx				
EPA066A	4	55	24	10	77	4%	Figure B-14
EPA072A	14	155	25	5	161	-19%	Figure B-15
EPA072B	15	155	27	5	172	-20%	
EPA074B	27	157	45	6	284	-23%	Figure B-16
EPA077B	26	165	50	6	278	-21%	Figure B-17
			M-Xylene - NOx and m-Xylene - CO - NOx				
EPA067A	5	18	-	6	63	6%	Figure B-18
EPA067B	6	18	47	6	125	-21%	"

[a] Model bias is (calculation – experimental) / experimental Δ([O_3]-[NO]) data for the indicated hour of the experiment. Calculations used the SAPRC-99 mechanism and the standard chamber model.

CO - NO_x experiments, but there is a tendency for the model to underpredict the final O_3 concentrations in the runs without the added CO. The formaldehyde consumption rates are reasonably well simulated in both types of experiments.

It is interesting to compare EPA069B and EPA068A because these experiments have similar levels of formaldehyde and NO_x, and differ only in the level of CO. The addition of the CO causes an increase in the NO oxidation and O_3 formation rates, but a decrease in the rate of formaldehyde consumption. This is as expected since the CO causes reactivity towards NO oxidation and O_3 formation, but suppresses HO levels because of the OH + CO reaction, and is reasonably well simulated by the model.

Given that the formaldehyde system is reasonably well studied and the better model performance in simulating the formaldehyde - CO - NO_x experiments, the relatively poor performance in simulating the final O_3 in the formaldehyde - NO_x runs may be somewhat surprising. However, this may be due to a high sensitivity of formaldehyde - NO_x experiments to background VOCs that may be present. This sensitivity is shown o Figure 15, which shows the effect of increasing the background methane in the calculation from the default of 1.8 to 5 ppm. It can be seen that increasing the background methane to this extent causes the final $\Delta([O_3]-[NO])$ to be correctly simulated. Although our pure air system removes non-methane organics to undetectable levels, it does not remove methane[10]. The background methane is assumed to be 1.8 ppm when modeling our experiments, based on the limited number of measurements that were done, but it may vary from day-to-day. Although other experiments with added VOCs are insensitive to these low levels of methane, the formaldehyde - NO_x experiments are apparently very sensitive to any small amounts of background VOCs that may be present. Note that if the model discrepancy is indeed due to background VOC it may not necessarily be methane. For example, similar results are obtained if it is assumed that about 1 ppm of CO is present rather than the increased methane. In any case, this indicates the level of reactivity that would be involved.

Because of the extreme sensitivity of formaldehyde - NO_x experiments to background VOCs, they probably should be considered more as characterization runs than mechanism evaluation experiments. On the other hand, the formaldehyde - CO - NO_x runs were found not to be sensitive to background VOCs or other chamber effects, and thus provide a clearer test of the mechanism. Simulating these experiments indicate satisfactory mechanism performance at NO_x levels down to ~15 ppb.

Ethene - NO_x. One dual chamber ethene - NO_x experiment was carried out, with 10 ppb NO_x in one reactor and 20 ppb NO_x in the other. The results are plotted in Figure B-12. The model performed moderately well in simulating these data, though it gave slightly low final O_3 yields on both sides. Reasonably good simulations of formaldehyde yields are obtained, as expected since this is a major ethene reaction product and the atmospheric reactions of ethene have been reasonably well studied (Atkinson, 1990, 2000). There does not appear to be any greater problem in model performance in simulating ethene - NO_x experiments under low NO_x conditions than in the higher concentration experiments used in previous mechanism evaluations. Indeed, the model performs slightly better in

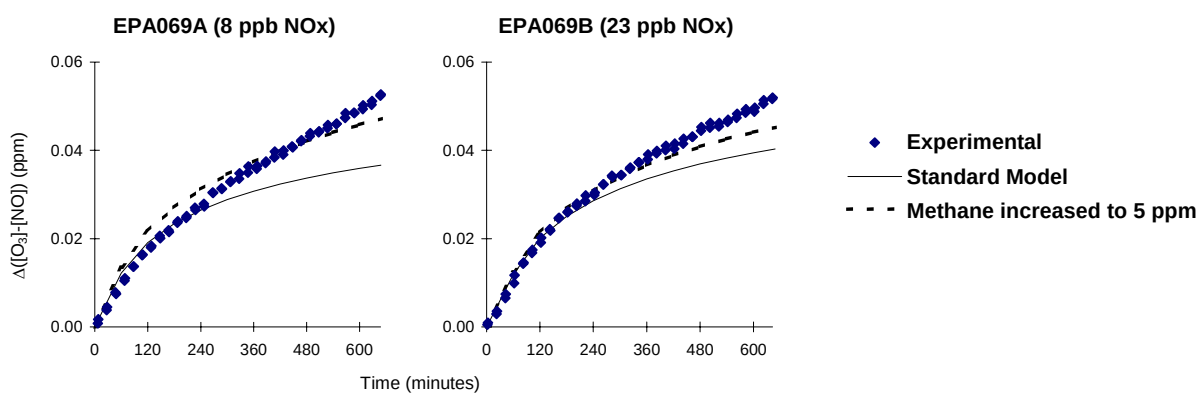

Figure 15. Effect of increasing background methane from 1.8 to 5 ppm in simulations of $\Delta([O_3]-[NO])$ in the formaldehyde - NO_x experiment EPA069.

[10] The air purification system has a catalytic combustor that should remove methane as well as any small amounts of ethane or propane that may pass through the main system. However, the combustor as delivered from AADCO was not effective, and it was not made functional until after the period of the experiments discussed in this report.

simulating the initial NO oxidation and O_3 formation rates in the experiment with the lower NO_x levels in the case of these two runs.

Propene - NO_x. A dual chamber propene - NO_x experiment was also carried out, in this case with only 5 ppb NO_x in one reactor and 25 ppb in the other. The concentration - time plots for this experiment are shown in Figure B-13. Fairly good model performance is seen in simulating all species, including formaldehyde. There is a consistent bias in overpredicting O_3 and the initial NO oxidation rate; somewhat better fits are obtained if the radical source in the chamber model is reduced. The good fits to the PAN data are also of interest because the reliability of the GC luminol method we use to measure this species has not been fully established. The propene - NO_x system is reasonably well studied in previous chamber studies, and available data indicate that the model should perform reasonably well in predicting PAN levels in such experiments (e.g., Carter and Lurmann, 1991). Therefore, the fact that the experimental PAN measurements are in good agreement with the model prediction (in cases where the model fits O_3) tends to support the support the validity of the measurement as much as the other way around.

Again, there is no indication with problems with mechanism evaluation under low NO_x conditions in the propene - NO_x system. The performance of the model is as good or better than its performance in simulating propene - NO_x experiments at higher NO_x levels (Carter, 2000a), and the model performance in simulating the data in the reactor with only 5 ppb NO_x is essentially the same as that simulating the reactor where the NO_x level is five times higher.

Toluene - NO_x. Three toluene - NO_x experiments were carried out, with NO_x levels ranging from ~5 to ~25 ppb, and the results of these experiments are shown on Figure B-14 through Figure B-17. (The experiments with added CO, carried out in the other reactor in each case, are discussed separately, below.) Fairly good model performance is obtained in simulating O_3 formation and NO oxidation these experiments, though there is a small but consistent bias towards overpredicting O_3. However, the model performance in other respects is not totally satisfactory. The model also underpredicts formaldehyde yields in all three experiments, predicts it takes longer for NO_2 to be consumed following the peak than is observed experimentally, and tends to underpredict toluene consumption rates later in the experiment. Both of the latter two observations can be related to an underprediction of OH radicals at the later stages of the experiment, since reaction with OH is the only known toluene consumption process and is also an important sink for NO_2. The performance of the model in simulating PAN is inconsistent; good fits to PAN levels are obtained in the lowest NO_x experiment, while PAN is underpredicted by about a factor of two in the other runs. However, the possibility that this inconsistency could be due to nonlinearity in the luminol PAN detection system cannot be ruled out. The PAN calibrations were carried out at ~20 ppb, which is closer to the concentrations in the experiments where the model underpredicts PAN levels.

Other than the differences in model performance in predicting PAN yields, the model performance in simulating the very low NO_x experiment is comparable to the simulations of the higher NO_x experiments in this set, and it is also comparable to the mechanism's performance in simulating toluene experiments carried out in other chambers (Carter and Lurmann, 1991; Carter, 2000a). This is significant because the parameterized mechanisms used to represent aromatics and their unknown reactive products were derived based on simulations of these higher NO_x experiments, and there was a concern that the parameterization may not be valid at lower NO_x levels because the actual chemical processes is represented were unknown.

m-Xylene - NO_x. One m-xylene - NO_x experiment was carried out during this period, at NO_x levels of ~20 ppb, and the results are shown on Figure B-18. The performance of the model in simulating this experiment is very much like its performance in simulating the toluene - NO_x runs discussed above, except that the PAN levels appear to be much better predicted. As with the toluene runs, the model has a tendency to slightly overpredict O_3 and to underpredict the reactant aromatic and the NO_2 consumption

rates in the later stages of the experiment, indicating an underprediction of OH levels. This performance is also consistent with the performance of the mechanism in simulating m-xylene - NO_x experiments in other chambers carried out at higher NO_x levels (Carter, 2000a).

Effect of CO on Aromatic - NO_x Experiments. Model calculations carried out prior to the experiments discussed here suggested that adding CO to aromatic - NO_x experiments would result in a significant enhancement in O_3 formation because the presence of CO enhances the effects of the radicals formed in the aromatic CO systems. In addition, CO acts as a chemically simple surrogate for the less reactive VOCs present in ambient air in the presence of CO, whose reactions provide a means to test predictions of effects of radicals from aromatics with minimum complexities and uncertainties in the reactions of the other VOCs. Therefore, most of the toluene and the m-xylene experiments discussed above were carried out with the other reactor having the same aromatic and NO_x levels, but with 25-50 ppm CO added. The results of these experiments are shown on Figure B-14 through Figure B-18, where they can be compared with the experiments in the other reactor without the added CO. A separate experiment, where CO was added to both reactors by mistake, is shown on Figure B-17. The effects of CO in the two toluene and the m-xylene experiment where this was directly assessed is also shown on Figure 16, where the experimental and O_3 data in the reactors with and without the added CO are more directly compared, and where the experimental and calculated changes in O_3 caused by the adding CO are also shown.

It can be seen that, as predicted by the model, the addition of CO indeed causes a large increase in the amount of O_3 formed, far more than one would expect based on the results of the CO - NO_x irradiations in the absence of the aromatic. For example, run the CO - NO_x experiment EPA106 had

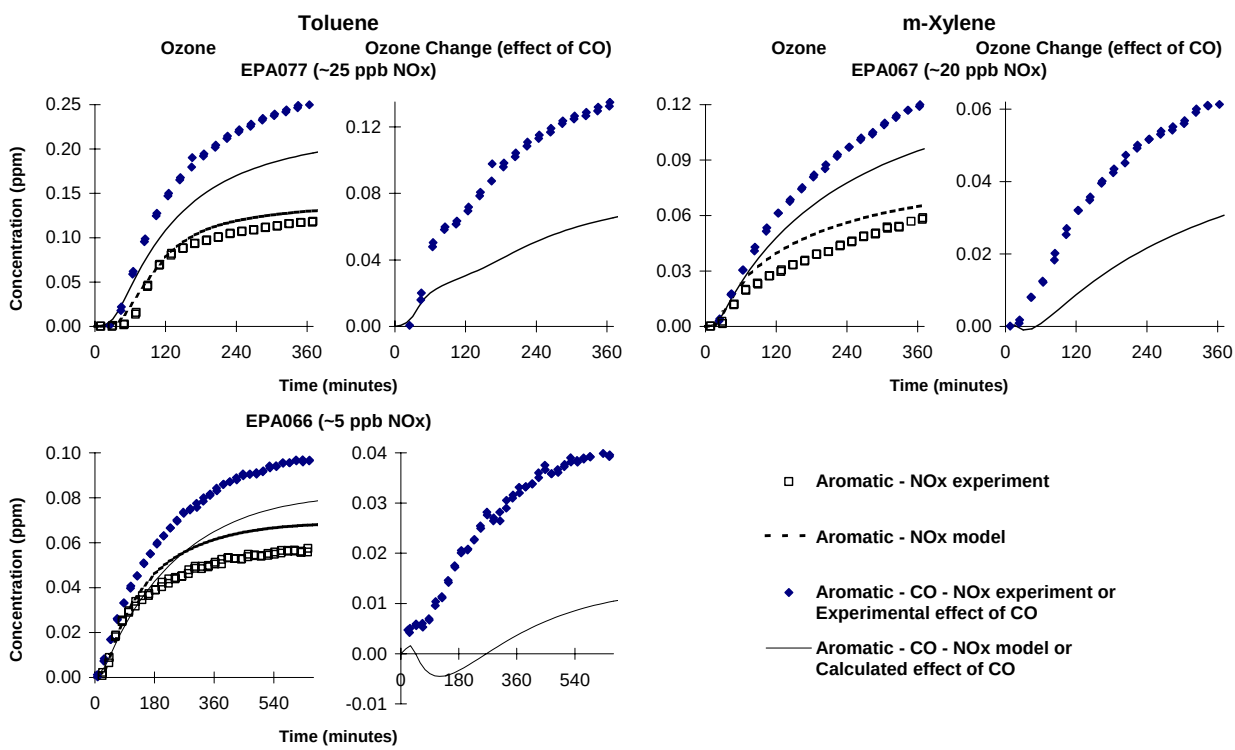

Figure 16. Experimental and calculated effects of CO additions in the toluene and m-xylene - NO_x experiments in the UCR EPA chamber.

similar amounts of CO and NO_x as the m-xylene experiment and the toluene experiment EPA077, and yet Figure B-8 shows it formed only ~10 ppb O_3, and yet the added CO caused the O_3 to increase by ~60 to 120 ppb in the presence of the aromatics. On the other hand, the added CO significantly decreases the OH radical levels in the experiments, as can be seen by the decrease in the toluene and (especially) the m-xylene consumption rates in these experiments. This is expected because of the reaction of CO with OH radicals, and is consistent with model predictions.

Although the *qualitative* effects of the CO addition are consistent with model predictions, it is significant that the *quantitative* effects are not correctly predicted. In particular, the mechanism significantly underpredicted the effect of the added CO in all the experiments where this was examined. While the model has a tendency to slightly overpredict O_3 in the aromatic - NO_x experiments, it consistently underpredicted the O_3 in the experiments with the added CO, and the change in O_3 caused by the CO addition is underpredicted by a factor of two or more. The results are similar in the two toluene and the m-xylene experiments where the reactant levels are similar. The discrepancy appears to be even larger in the lowest NO_x toluene experiment, but additional experiments would be needed to confirm whether this is a general trend.

It should be noted that it is extremely unlikely that this discrepancy can be attributed to problems with the characterization runs. In the first place, these aromatic experiments are relatively insensitive to the uncertain or variable chamber effects parameters. In addition, the discrepancy discussed here concerns a *difference* between two experiments, where differences in chamber effects should at least to some extent cancel out. Sensitivity calculations with chamber effects parameters varied within their uncertainty range gave results that were consistent with these expectations.

Ambient Surrogate Experiments

Ambient surrogate - NO_x experiments were carried out at a number of initial ROG and NO_x levels, including NO_x levels as low as 2 and 5 ppb. The matrix of experiments that were carried out is shown in Figure 3, above. Because of the range of ROG and NO_x conditions, these experiments are useful not only for low NO_x mechanism evaluation using ambient simulations, but also for evaluating how well the mechanism predicts how O_3 changes with changing ROG and NO_x levels. Table 15 summarizes the initial ROG and NO_x levels of the individual experiments modeled in this study, gives the final amounts of O_3 formed and NO oxidized, and indicates the ability of the model to simulate the final $\Delta([O_3]-[NO])$ results. Experimental and calculated concentration-time plots of the selected measured species are given in Figure B-19 through Figure B-30 in Appendix B. Table 15 indicates the figure number where the experimental and calculated data for the individual experiments can be found.

The model performance in simulating final O_3 levels and rates of O_3 formation and NO oxidation varied from run-to-run, with the model performing reasonably well in about half the experiments and underpredicting it in the others, in a few cases significantly so. The cases of poor model performance do not have a clear relationship to initial NO_x or initial ROG levels by themselves, but are strongly correlated to the ROG/NO_x ratio. This is shown on Figure 17, which gives plots of the model underprediction bias for $\Delta([O_3]-[NO])$ against the ROG/NO_x ratio. (A logarithmic axis is used for ROG/NO_x because of the extremely high ratio in some of the lower NO_x experiments.) The dotted and dashed lines on the plot shows the approximate ROG/NO_x ratio corresponding to MIR and MOIR conditions, i.e., conditions where final O_3 levels in the experiments are most sensitive to increases in ROG levels, and conditions where NO_x levels are most favorable for O_3 formation, respectively[11]. The MIR levels are of relevance

[11] These ratios were derived by model calculations of the effects of changing initial ROG and NO_x levels on O_3 formation under averaged conditions representing these experiments.

Table 15. Summary of reactants, Δ([O3]-[NO]) results, and model biases for the ambient surrogate - NO_x experiments in the UCR EPA chamber.

Run	NOx (ppb)	VOC (ppmC)	VOC / NOx	Hours	Δ([O_3]-[NO]) (ppb)	Model Bias	Plot Figures
EPA101 [b,c]	2	0.32	149	6	38	10%	Figure B-19
EPA098A	5	0.18	37	5	52	-3%	Figure B-20
EPA098B	5	0.18	37	6	52	4%	"
EPA097B	5	0.53	102	6	67	8%	Figure B-21
EPA097A	5	0.53	100	5	66	5%	"
EPA085A	10	1.11	114	6	95	8%	Figure B-22
EPA086A	10	1.08	108	6	103	3%	"
EPA095B	25	0.80	32	5	167	-3%	Figure B-23
EPA114A	31	0.57	18	4	154	-15%	"
EPA110B [c]	31	0.60	19	5	167	-13%	Figure B-24
EPA128A	48	0.57	12	5	162	-22%	"
EPA082A	45	1.03	23	4	225	-10%	Figure B-25
EPA082B	47	1.03	22	4	225	-9%	"
EPA083A	48	1.01	21	6	269	-11%	Figure B-26
EPA084B	51	1.16	23	6	290	-13%	"
EPA081A	50	2.31	46	6	295	-12%	Figure B-27
EPA081B	50	2.30	46	6	293	-11%	"
EPA113A [c]	69	1.03	15	6	297	-19%	Figure B-28
EPA108B [c]	76	0.90	12	5	257	-36%	"
EPA080A	92	4.25	46	6	435	-13%	Figure B-29
EPA080B	92	4.25	46	6	438	-14%	"
EPA096A	109	0.72	7	6	246	-46%	Figure B-30
EPA096B	111	0.72	6	5	209	-47%	"

[a] Model bias is (calculation - experimental) / experimental Δ([O3]-[NO]) data for the indicated hour of the experiment. Calculations used the SAPRC-99 mechanism and the standard chamber model.

[b] Average of results for both of the reactors, which had the same mixture. The Side B 6 hour value was extrapolated from data from 240 to 355 minutes.

[c] No formaldehyde in ROG surrogate.

because of the importance of the MIR scale in California's current and proposed regulations (CARB, 1993, 2000, 2003). The MOIR levels are of relevance because they indicate the approximate levels where the formation of O_3 becomes NO_x limited.

It can be seen that the correlation between model bias for predicting Δ([O_3]-[NO]) and ROG/NO_x ratio is remarkably good, being almost perfect except for run EPA081. Note that this also suggests a higher standard of precision in the model evaluations, since we are seeing model discrepancies of no more than ±20% except for the three runs with the lowest ROG/NO_x ratios. In previous evaluations, model predictions to within ±30% have been considered to be satisfactory. If the variability of the model performance were ±30% in the simulations of these the correlation that is so obvious on Figure 17 may not have been evident at all, and the lower ROG/NO_x experiments may have been considered as outliers. However, in this case the precision is sufficiently good that the trends in the bias is clear, and it is equally

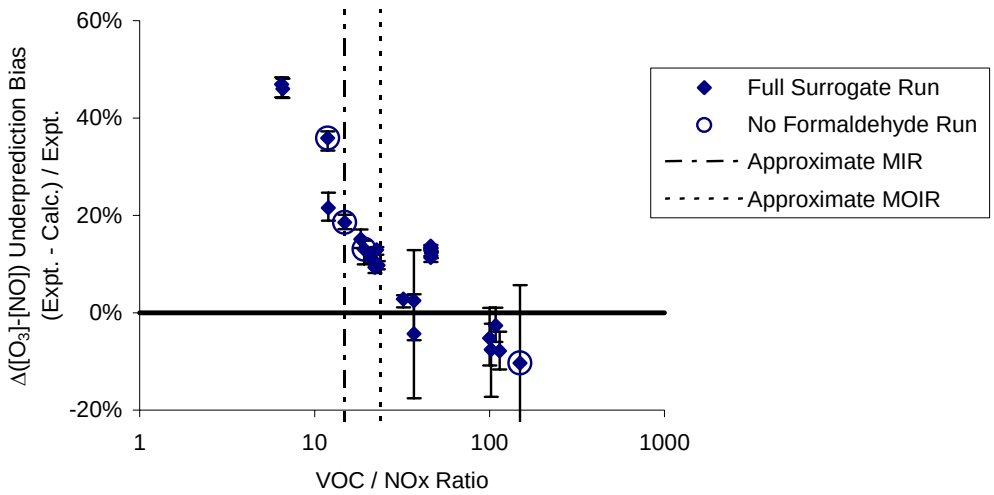

Figure 17. Plot of $\Delta([O_3]-[NO])$ model underprediction bias against the ROG/NO_x ratio for the surrogate - NO_x experiments in the UCR EPA chamber. Error bars show the effects of varying the HONO offgasing characterization parameter within its range of uncertainty.

clear that the experiments with the very large underprediction errors are not outliers but are simply confirmations of the trends indicated by the other experiments, where the errors were less than ±20%. The scatter in the data in Figure 17 suggest that the actual run-to-run variability in model performance in simulating these runs, after the general bias is factored out, is only ±10%.

In any case, these data clearly show a problem with the SAPRC-99 mechanism in underpredicting rates of NO oxidation O_3 formation and under conditions where the ROG/NO_x ratio is at MIR or lower levels. It is unlikely to be due to uncertainties in the chamber effects, because the chamber effect parameter that is most likely to affect this is the HONO offgasing rate, and as shown on Figure 17 varying this parameter within its range of uncertainty[12] does not significantly affect this bias. On the other hand, the model performs reasonably well (within ±10% in most cases) in simulating experiments with MOIR or higher ROG/NO_x ratios. This appears to be the case regardless of the total absolute levels of NO_x in the experiment.

On the other hand, if the above-mentioned dependence of model performance on the ROG/NO_x ratio is taken into account, the model appears to perform as well in simulating NO oxidation and O_3 formation the very low NO_x experiment as it does in the experiments at the higher NO_x levels. This can be seen on Figure B-19 through Figure B-21 which show plots of experimental and calculated data for the experiments with total NO_x levels of ~5 ppb or lower, and Figure B-22, which show the data for the experiments with NO_x levels of ~10 ppb. Note that all of these experiments have ROG/NO_x ratios above the MOIR level of ~25, so one would not expect biases on this basis. It can be seen that the model fits in simulating these data is of comparable quality to its performance in simulating the other runs in this set with ROG/NO_x above MOIR.

[12] The range shown indicates the differences in bias between assuming no HONO offgasing and assuming a maximum HONO offgasing parameter of 25 ppt (see Figure 6).

One of the reasons why very low NO_x experiments have not been conducted previously in our chambers is because of concern about NO_x-related chamber effects. The- NO_x offgasing effects are of particular concern when simulating experiments with initial NO_x as low as 2 ppb. The effects of varying the NO_x-related parameters within their uncertainties in the model simulations of selected species in the ~2 ppb NO_x experiment EPA101A are shown on Figure 18. The left hand series of plots shows calculations where the HONO offgasing parameter RN-I is varied from zero to 25 ppt, which is the maximum value indicated by the characterization experiments sensitive to this parameter (see Table 8, above). The right hand plots show the effects of assuming that none of the initial NO_x is present as HONO. The standard model assumes that 50 ppt of the initial NO_x is in the form of HONO, which is 2.5% of the initial NO_x in this 2 ppb NO_x experiment.

It can be seen from Figure 18 that the NO_x related chamber effects parameters do affect the results of the simulations of these experiments. The data appear to be better fit using the standard model, as may be expected since the sensitivity calculations use extreme assumptions concerning the chamber effects. The model simulations of the NO_y data are of interest, though the measurements are uncertain

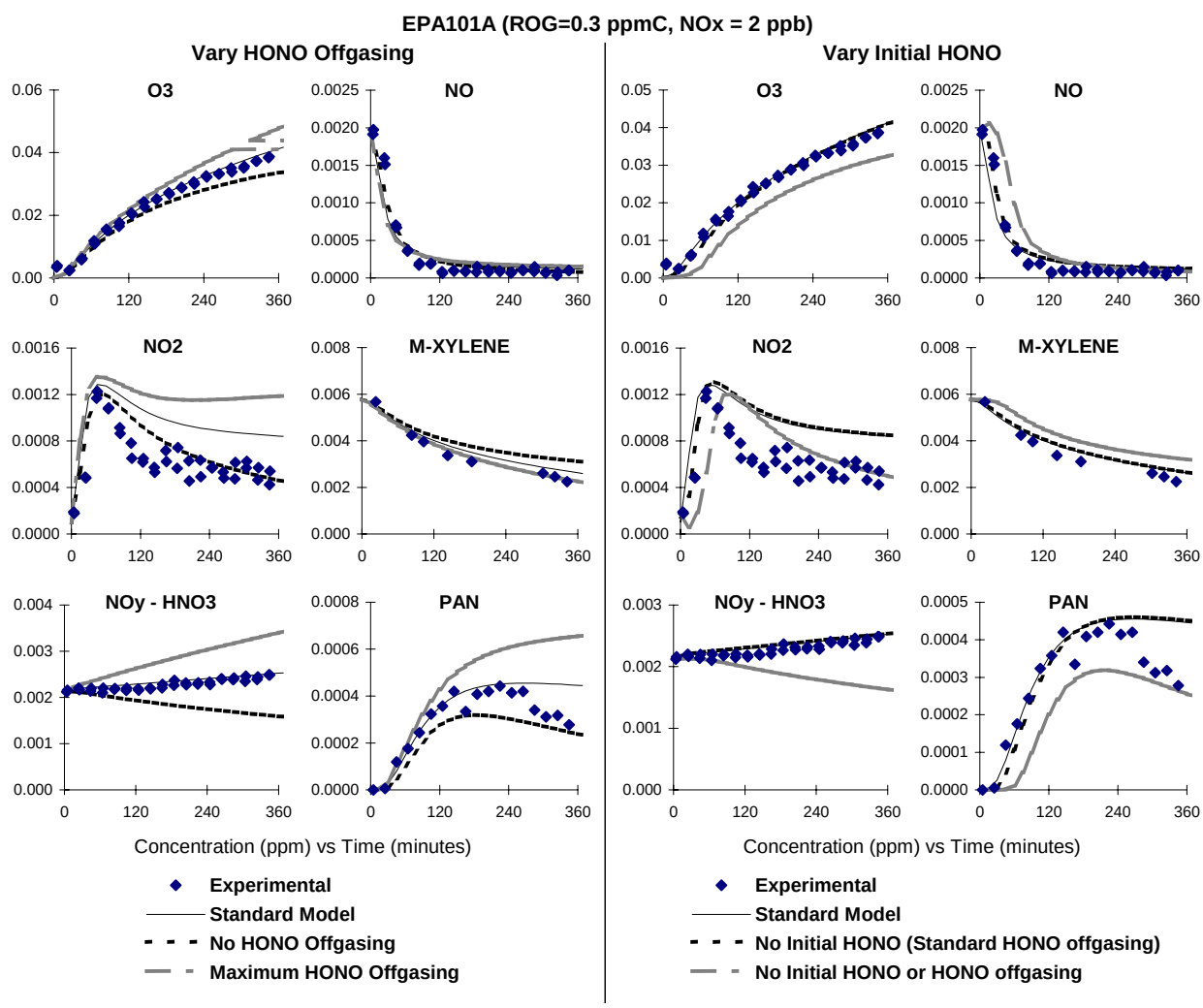

Figure 18. Effects of changing NO_x offgasing chamber parameter on calculations of selected species in the low NO_x ambient surrogate experiment EPA101A.

because of the uncertainty concerning the extent of interference by HNO_3. If it is assumed that the NO_y measurements do not respond to HNO_3, the NO_y data are consistent with predictions of the standard model and not with the models assuming no or maximum NO_x offgasing. If it is assumed that the NO_y includes HNO_3, then the data fall halfway between the predictions of the standard model and the model assuming no NO_x offgasing (not shown). The right hand plots show that the simulations of the ambient surrogate experiment are insensitive to reasonable assumptions concerning initial HONO if the standard NO_x offgasing is assumed, but if no radical source (as HONO offgasing) is assumed then the model is significantly affected by assuming no initial HONO, and the initial NO oxidation rate is significantly underpredicted. Therefore, at least some chamber radical sources must be assumed for the model to satisfactorily simulate this experiment.

Model simulations of other species. The plots on Figure B-19 through Figure B-10 also show the performance of the model in simulating NO_2, formaldehyde, PAN, HNO_3 (in some cases), and consumption rates of the more reactive VOCs. The most useful comparisons is in the simulations of the higher ROG/NO_x experiments where the performs satisfactorily in simulating NO oxidation and O_3 formation, since if it is biased in simulating these then it may be expected to have comparable biases in simulating other species as well. The performance in simulating these measurements is briefly summarized below.

NO_2. Although the mechanism simulates the formation rate and maximum concentration of NO_2 reasonably well, there appears to be a consistent tendency to underpredict its consumption rate following its maximum, This is greatest in the experiments where the O_3 formation rate is underpredicted, but it is seen in most other experiments as well. Note that the simulations of the aromatic experiments have similar biases, and these problems may be related.

Formaldehyde. The model gives reasonably good simulations of the formation of formaldehyde in some of the experiments, but in some cases the formaldehyde formation is significantly underpredicted. In contrast with the case for O_3 (and also PAN, discussed below) the bias appears to be better correlated to the initial NO_x levels than to the initial ROG/NO_x ratio. This is shown in Figure 19. The correlation with initial ROG levels, not shown, is relatively poor. The best fits are obtained in the experiments with the lowest NO_x levels, where the fits to the simulated changes in formaldehyde are ±25%. The underpredictions appear to become above the scatter of the data at NO_x levels above ~25 ppb.

PAN. As with O_3 and formaldehyde, the model simulates PAN formation reasonably well in some experiments and underpredicts it in others. This is expected since PAN and O_3 formation is generally correlated in ambient simulations, and similar performance is seen in the model predictions of O_3, as discussed above. The relationship between the model performance in the PAN and O_3 formation simulations is shown on Figure 20, which plots the model underprediction bias against the initial ROG/NO_x concentration and also against the model underprediction bias for $\Delta([O_3]-[NO])$, as discussed above. It can be seen that the correlation between the underprediction biases for PAN with ROG/NO_x is similar to that for $\Delta([O_3]-[NO])$, and also that the biases for these two measurements are strongly correlated. However, it is also of interest to note that there may be a slight bias towards underpredicting PAN in experiments where there is no bias in $\Delta([O_3]-[NO])$ simulations, though the bias may be within the scatter of the data.

HNO_3. Several of the ambient surrogate experiments have HNO_3 data from our TDLAS instrument, allowing model predictions of this compound to be evaluated probably for the first time in reasonably well characterized chamber runs. However, the data are highly scattered for the lower NO_x experiments because of limitations of sensitivity, so useful evaluation data are available only for experiments with NO_x levels greater than about 50 ppb. The results indicate reasonably good model performance in simulating HNO_3 in these experiments. There may be a slight bias towards

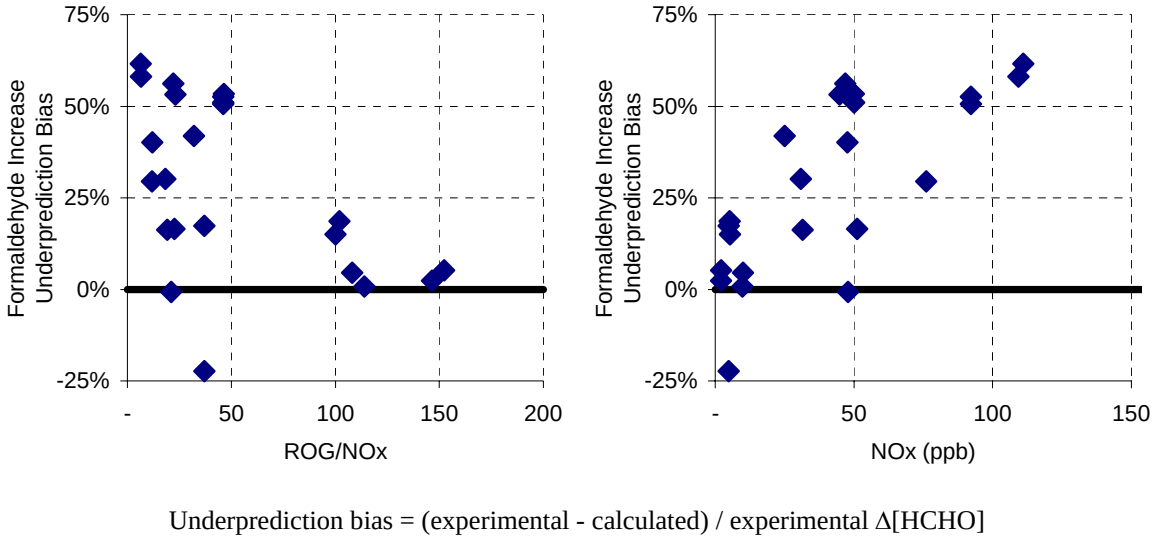

Figure 19. Plots of biases in model predictions of increases in formaldehyde concentration against initial ROG/NO_x ration and initial NO_x levels for the UCR EPA surrogate - NO_x experiments.

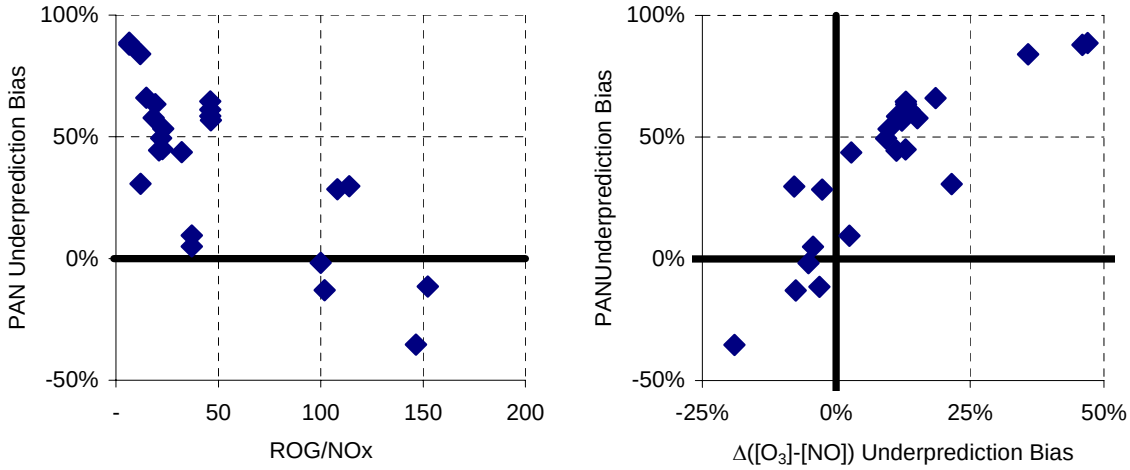

Figure 20. Plots of biases in model predictions of PAN against initial ROG/NO_x ratios and against biases in model predictions of Δ([O_3]-[NO]) for the UCR EPA surrogate - NO_x experiments.

underprediction many of the experiments, but given the uncertainties in the measurement this is not considered to be significant. The possibility of some HNO_3 loss on the sample lines has also not been completely evaluated, though it should be noted that the calibrations are carried out using the same sample lines. Although the data are limited, overall the results indicate no significant problem with the model in simulating formation of this compound.

TVA Experiments

A total of 79 TVA experiments were used in this mechanism evaluation study, of which 31 were used for characterization, 30 were single compound - NO_x experiments, and 28 used various mixtures, of which the latter included 12 using a highly complex ambient ROG surrogate. The mechanism evaluation experiments with the simpler systems were carried out at NO_x levels ranging to ~100 ppb, and the ambient surrogate experiments were carried out at NO_x levels ranging from 25 to 170 ppb and with total ROG levels ranging from 0.2 to 0.7 ppmC. The results of the evaluations with the various types of experiments are discussed in the following sections.

Characterization Runs

Table 16 summarizes the initial reactant concentrations and the experimental and calculated final amounts of O_3 formed and NO oxidized in the experiments used for characterizing the run conditions for modeling the TVA chamber runs. Experimental and calculated concentration-time plots of the major measurement data are shown on Figure B-31 through Figure B-34 in Appendix B. As discussed above, the results of the characterization experiments indicate that the formaldehyde offgasing rates and the initial HONO levels used the characterization model are somewhat uncertain. To assess the impacts of these uncertainties, the plots in Appendix B show model calculations assuming the upper limit formaldehyde offgasing rates and also calculations assuming no initial HONO. A comparison of these plots with those calculated using the standard chamber model indicate the sensitivity of the simulations of the data for different types of experiments to the uncertainties in the in these characterization parameters.

Table 16 shows that the overall biases in the $\Delta([O_3]-[NO])$ simulations of the characterization runs are low, and generally within the run-to-run variability. Small average biases are expected because the chamber characterization parameters were adjusted to minimize this. However, there is an overall bias for the model to somewhat overpredict $\Delta([O_3]-[NO])$ in the methane / NO_x runs, which is offset by the small bias towards underprediction in the larger number of CO - NO_x runs. The results of the NO_x -air experiments are highly scattered but considering the scatter the bias is relatively low.

The scatter in the fits of the model to the characterization runs can be taken as an indication of the run-to-run variability of the major chamber effects. As discussed above, the formaldehyde offgasing and the initial HONO appear to be the most important source of the variability. A comparison of the data on Figure B-34 with those on Figure B-31 through Figure B-33 indicates that the $\Delta([O_3]-[NO])$ data in the NO_x -air experiments are the most sensitive to these variable parameters, which is consistent with the observed greater variability in the model performance in simulating these runs.

<u>Fits to Formaldehyde</u>. A significant fraction of the characterization experiments had formaldehyde data, and the figures show these data for all experiments where they are available. As discussed above, the formaldehyde levels in the runs with no injected formaldehyde or formaldehyde precursors indicated significant formaldehyde and formaldehyde precursor offgasing. The variability in the model simulations of formaldehyde in these experiments indicate the run-to-run variability of formaldehyde offgasing in TVA runs.

The formaldehyde data in the TVA methane - NO_x runs are relatively insensitive to different assumptions of the for formaldehyde offgasing parameters because most of the formaldehyde comes from the photooxidation of methane. The relatively good fits of the model predictions to the formaldehyde yields in these experiments indicate that the model is giving appropriate predictions of OH radicals, whose reactions with methane results in the observed formaldehyde levels.

Table 16. Summary of the initial concentrations and the experimental and calculated amounts of O_3 formed and NO oxidized in the TVA characterization experiments modeled for this project. Figure numbers showing plots of the data in Appendix B are also shown.

Run No	Date	NOx (ppb)	Total VOCs (ppmC)	Final Δ([O_3]-[NO]) [a] Hour	Expt.	Calc.	Bias.	Plot Figure
				Acetaldehyde - Air				
43	6/23/94		28.0	4	20	14	-28%	
52	9/22/95		2.5	5	10	12	20%	Figure B-31
85	6/11/96		2.2	5	20	20	-1%	
						Average Model Bias:	-3%	
						Average Model Error [b]:	16%	
				CO - NO_x				
2	8/7/93	52.5	47.2	6	214	169	-21%	
3	8/11/93	5.4	5.3	4	48	45	-5%	
12	9/24/93	51.3	41.4	6	191	158	-17%	
18	10/16/93	51.4	43.2	5	172	146	-15%	
19	10/19/93	7.8	5.3	4	52	52	1%	
41	6/17/94	53.5	43.5	5	178	153	-14%	Figure B-32
42	6/21/94	11.9	53.9	3	51	47	-9%	
54	11/27/95	5.4	4.3	4	49	54	12%	
55	12/1/95	51.4	41.1	5	181	165	-9%	
70	3/28/96	51.0	44.0	8	198	246	24%	
82	5/22/96	5.0	4.0	5	50	56	11%	
83	5/29/96	51.8	43.5	6	211	207	-2%	
						Average Model Bias:	-4%	
						Average Model Error:	12%	
				Methane - NO_x				
1	8/4/93	21.3	125	4	129	137	6%	
20	10/23/93	20.2	124	4	119	132	11%	
32	5/2/94	19.1	134	4	127	137	8%	Figure B-33
58	1/16/96	19.4	118	6	115	125	9%	
84	6/4/96	19.6	41	5	98	100	2%	
						Average Model Bias:	7%	
						Average Model Error:	7%	
				NO_x - Air				
7	8/28/93	9.7		4	26	21	-18%	
10	9/18/93	9.7		4	29	20	-32%	
17	10/14/93	11.1		4	25	20	-19%	
22	2/4/94	9.2		4	13	20	59%	
34	5/7/94	10.1		5	22	27	23%	
40	6/10/94	10.0		6	29	32	11%	Figure B-34
44	7/22/94	10.7		4	28	21	-24%	
53	11/21/95	10.7		5	30	28	-6%	
57	1/11/96	9.7		4	19	22	15%	
69	3/27/96	10.8		5	22	29	29%	
81	5/17/96	10.9		5	26	29	11%	
						Average Model Bias:	4%	
						Average Model Error:	22%	

[a] Results for last full hour where data available. Bias = (calculated - experimental) / experimental.
[b] Average model error is average of absolute value of biases.

Fits to PAN. PAN data are available for all three of the acetaldehyde - air experiments, and the results are shown on Figure B-31. Although the NO_x offgasing parameters were adjusted to fit the O_3 data in these experiments, the model simulates the PAN to within its experimental variability for the two experiments where it also gives reasonable predictions of O_3. As expected, it underpredicts PAN in the experiment where O_3 is also underpredicted. This indicates that the model is appropriately representing PAN formation from acetaldehyde under the very low NO_x conditions of these experiments.

Single Compound Experiments

The TVA mechanism evaluation experiments include single compound experiments with formaldehyde, isopentane, ethylene, propylene, toluene and m-xylene. Table 17 summarizes the initial reactant concentrations and the experimental and calculated final amounts of O_3 formed and NO oxidized in these experiments, and the experimental and calculated concentration-time data for the major measured species are shown on Figure B-35 through Figure B-41. As with the characterization runs, the figures also show calculations with the higher formaldehyde offgasing rates and with no initial HONO, to indicate the sensitivity of these calculations to these uncertain chamber characterization parameters. With the exception of a slight tendency to overpredict O_3 in the propene and trans-2-butene runs and a consistent tendency of the model to underpredict PAN in most of the experiments where this is measured, the model performance in simulating these experiments is reasonably good. The results for the various compounds are discussed in more detail below.

Formaldehyde. Figure B-35 shows that the model simulates the $\Delta([O_3]-[NO])$ and formaldehyde data for the formaldehyde - NO_x experiments reasonably well. The simulated results have no sensitivity to the assumed initial HONO, but are slightly sensitive to the formaldehyde offgasing parameters. However, this sensitivity is not large enough to affect conclusions on model performance in simulating this system.

Isopentane. Figure B-36 shows plots of the data for the single isopentane experiment. Alkane - NO_x experiments are known to be highly sensitive to chamber radical sources and because of this they do not provide very good data for mechanism evaluation (Carter and Lurmann, 1991). In the case of this experiment, the model somewhat underpredicts the NO oxidation and O_3 formation rate, but given the sensitivity of this to variable chamber effects this is probably within the uncertainty of the evaluation. The formaldehyde is also underpredicted, though the underprediction is comparable to the amount of underprediction of O_3. On the other hand, the significant underprediction of PAN is probably more than can be accounted for by the variable chamber effects, and suggests that the SAPRC-99 isopentane mechanism may have a problem in this regard. However, better characterized data than a single radical-source-sensitive chamber experiment would be needed to adequately assess this.

Ethylene. The data for the three ethylene - NO_x experiments are shown on Figure B-37. The results indicate reasonably good simulations of NO oxidation, O_3 formation, formaldehyde formation, and ethylene consumption. Although varying the chamber parameters has some effect on the simulations, the effect is not sufficiently large to affect conclusions about model performance in simulating this system.

Propylene. The data for the four propylene - NO_x experiments are shown on Figure B-38. The model performance is generally satisfactory, though there is a slight but consistent tendency to overpredict O_3 in these experiments. The formaldehyde and the propene consumption data are reasonably well simulated. The uncertain chamber parameters have some effect on the model simulations, with the initial HONO being the more important in this case, but the effect is not excessive.

The fits of the model to the PAN data in the propene experiments are variable, with the PAN yields being reasonably well simulated in run 13 but underpredicted in the other two runs. Note that the better fits are obtained in the runs with the greater biases towards overpredicting O_3, which, in view of the

Table 17. Summary of the initial concentrations and the experimental and calculated amounts of O_3 formed and NO oxidized in the TVA single compound experiments.

Run No	Date	NOx (ppb)	VOC (ppmC)	Final Δ([O_3]-[NO]) [a]				Plot Figure
				Hour	Expt.	Calc.	Bias	
				Formaldehyde / NOx				
5	8/20/93	40.4	0.15	3	118	105	-11%	Figure B-35
6	8/24/93	38.8	0.05	3	53	48	-10%	
31	4/30/94	41.0	0.17	1	116	103	-11%	
38	6/2/94	41.9	0.09	5	67	73	10%	
						Average Model Bias:	-4%	
						Average Model Error [b]:	10%	
				Isopentane / NOx				
50	6/22/95	17.9	0.18	7	110	75	-32%	Figure B-36
				Ethylene / NOx				
8	9/10/93	51.5	0.50	4	242	252	4%	Figure B-37
9	9/15/93	25.0	0.26	3	138	142	3%	
11	9/21/93	48.7	0.24	4	168	174	4%	
						Average Model Bias:	4%	
						Average Model Error:	4%	
				Propylene / NOx				
13	9/28/93	21.5	0.22	4	112	134	20%	Figure B-38
14	10/1/93	52.7	0.45	4	208	241	16%	
15	10/5/93	54.2	0.02	5	178	198	11%	
16	10/8/93	53.5	0.20	5	172	178	3%	
						Average Model Bias:	13%	
						Average Model Error:	13%	
				trans-2-Butene / NOx				
63	2/21/96	19.5	0.10	8	99	114	15%	Figure B-39
64	2/27/96	40.0	0.10	8	126	138	10%	
65	3/4/96	40.7	0.10	8	125	138	11%	
						Average Model Bias:	14%	
						Average Model Error:	14%	
				Toluene / NOx				
47	4/27/95	104.9	0.52	8	187	188	1%	Figure B-40
71	4/2/96	265.6	2.48	4	508	424	-16%	
80	5/13/96	54.3	0.41	6	156	179	15%	
						Average Model Bias:	1%	
						Average Model Error:	12%	
				m-Xylene / NOx				
48	5/19/95	99.8	0.29	7	232	238	3%	Figure B-41
49	6/2/95	98.4	0.29	7	233	241	3%	
						Average Model Bias:	4%	
						Average Model Error:	4%	

[a] Results for last full hour where data available. Bias = (calculated - experimental) / experimental.

[b] Average model error is average of absolute value of biases.

correlation between O_3 and PAN, suggests that the model may actually underpredict PAN in experiments where O_3 is well simulated. However, the variability in model performance in simulating PAN in these experiments is much greater than its variability in simulating O_3. The possibility of experimental factors affecting these fits cannot be ruled out.

Trans-2-Butene. Figure B-39 shows the data for the three trans-2-butene - NO_x experiments in the TVA chamber. Overall, the model performance is comparable to that for propene. As with propene, there is a small but consistent tendency of the model to overpredict O_3, but the fits to formaldehyde and the olefin consumption rates are good. There is also a tendency for the model to underpredict PAN levels, with the extent of underprediction again being variable. The sensitivity to the uncertain chamber parameters is not excessive.

Toluene. Figure B-40 shows the data for the three toluene experiments. The simulations of NO oxidation and O_3 formation are reasonably good, with no consistent overall bias in the case of this compound. The fits to formaldehyde are variable, but in this case the results are somewhat more sensitive to the formaldehyde offgasing parameters than is the case for the olefins, which may account in part to the greater variability. PAN is again underpredicted, with the underprediction appearing to be greater than is the case for the olefins. The toluene consumption rate is reasonably well simulated in run 47 but is underpredicted at the end of the other two experiments. This is consistent with the results we have seen in the simulations of the toluene in the UCR EPA chamber and indicates a likely problem with the mechanism in underpredicting OH levels at the end of aromatic - NO_x experiments.

m-Xylene. The experimental and simulated data for the two TVA m-xylene experiments are shown in Figure B-41. The model gives reasonably good fits to the NO oxidation and O_3 formation data and the m-xylene consumption rates, and these predictions are relatively insensitive to the uncertain chamber characterization parameters. On the other hand, there is a moderate bias of the model towards underpredicting formaldehyde and a relatively large bias towards underpredicting PAN. The ability of the mode to simulate the m-xylene consumption throughout the experiment is not necessarily inconsistent to its tendency to underpredict m-xylene consumption at the end of the UCR EPA runs. This is because in the UCR EPA experiments there is m-xylene remaining to react at the end of the experiment, while in these TVA runs essentially all the m-xylene is consumed after three hours.

Mixture Experiments.

Four different types of mixture - NO_x experiments were carried out the TVA chamber, one with only alkanes and alkenes, two with mixtures of alkanes, alkenes, and aromatics in relative amounts approximating their levels in ambient mixtures, and one with a very complex mixture of organics representing VOCs measured in ambient air. Table 18 gives a summary of the initial concentrations and experimental and calculated amounts of O_3 formed and NO oxidized these experiments, and Figure B-42 through Figure B-47 show experimental and calculated concentration-time plots of selected data. These results are discussed below.

As indicated on Table 18, the model did not have large overall biases in simulating O_3 formed and NO oxidized in these mixture experiments, with the average biases for each of the four types of runs being less than 10%, and the Δ([O3]-[NO]) prediction errors for individual experiments being less than 25% in all cases. This is better than the ±30% performance in simulating the overall dataset in the SAPRC-90 and RADM-2 evaluations of Carter and Lurmann (1990, 1991), and comparable to the overall performance in the simulation of SAPRC-99 with the earlier UCR chamber data (Carter, 2000a).

However, as with the UCR EPA surrogate experiments, discussed above, there is an apparent correlation between the model performance and the ROG/NO_x ratio that indicates a potential systematic

Table 18. Summary of the initial concentrations and the experimental and calculated amounts of O_3 formed and NO oxidized in the TVA mixture experiments.

Run No	Date	NOx (ppb)	VOC (ppmC)	Final Δ([O_3]-[NO]) [a]				Plot Figure
				Hour	Expt.	Calc.	Bias	
				Par / Ole Mix / NOx				
56	12/4/95	50.6	0.22	7	82	83	2%	Figure B-42 and Figure B-43
51	7/20/95	49.3	0.23	6	79	79	1%	
59	1/22/96	48.9	0.49	8	135	163	21%	
66	3/14/96	50.2	0.51	8	161	188	17%	
67	3/19/96	85.0	0.41	8	128	129	0%	
68	3/22/96	99.6	0.41	7	112	113	2%	
						Average Model Bias:	7%	
						Average Model Error:	7%	
				Par / Ole / Aro Mix #1 / NOx				
60	1/25/96	49.9	0.51	8	136	165	21%	Figure B-44 and Figure B-45
61	1/30/96	100.6	0.40	8	122	123	0%	
62	2/14/96	100.0	0.42	8	143	130	-8%	
						Average Model Bias:	4%	
						Average Model Error:	10%	
				Par / Ole / Aro Mix #2 / NOx				
72	4/12/96	49.8	0.45	8	168	186	11%	Figure B-44 and Figure B-45
73	4/18/96	50.0	0.19	8	119	122	2%	
74	4/22/96	49.9	0.20	8	129	132	2%	
76	4/29/96	53.5	0.52	8	186	205	10%	
77	5/2/96	49.9	0.22	8	168	177	5%	
78	5/6/96	51.4	0.21	8	170	175	3%	
79	5/9/96	50.9	0.40	8	185	204	10%	
						Average Model Bias:	6%	
						Average Model Error:	6%	
				SynUrban94 / NOx				
24	4/1/94	89.5	0.43	8	149	122	-18%	Figure B-46 and Figure B-47
25	4/5/94	104.0	0.45	8	143	131	-8%	
26	4/8/94	51.9	0.45	6	135	123	-9%	
27	4/13/94	51.5	0.23	7	95	89	-6%	
28	4/21/94	25.4	0.22	4	82	70	-15%	
29	4/24/94	55.6	0.62	5	163	149	-9%	
30	4/27/94	51.8	0.23	6	90	76	-15%	
33	5/4/94	51.8	0.45	6	126	119	-5%	
35	5/9/94	104.0	0.47	7	151	131	-13%	
36	5/12/94	76.5	0.23	7	98	89	-9%	
37	5/16/94	25.0	0.24	6	82	86	4%	
39	6/6/94	169.0	0.68	8	239	199	-17%	
						Average Model Bias:	-8%	
						Average Model Error:	9%	

[a] Results for last full hour where data available. Bias = (calculated - experimental) / experimental.

[b] Average model error is average of absolute value of biases.

bias in the mechanism in simulating mixture runs. This is shown on Figure 21, which gives plots of the $\Delta([O_3]-[NO])$ overprediction error for the various types of TVA mixture experiments against the initial ROG/NO_x ratio. As with the UCR EPA surrogate experiments, the underprediction error gets more positive (or less negative) as the ROG/NO_x ratio decreases, though the trend is somewhat less evident because of the limited number of experiments in case of the simple mixture TVA runs, or because of the scatter in the simulations of the SynUrban94 runs. The fact that this trend occurs with the Par / Ole mix runs is of particular interest because of the lack of aromatics in those experiments. As discussed below, problems with the aromatics mechanisms is given as an explanation of the model performance problems in simulating the mixture experiments at low ROG and NO_x ratios.

The model performance in simulating the TVA simple mixture experiments differ from the simulations of the SynUrban runs and the ambient surrogate experiments in the other chambers (discussed above and below) in that the best performance is obtained at the low range of the ROG/NO_x ratios. This suggests that the model is underpredicting the final O_3 in the high ROG/NO_x experiments where O_3 is NO_x -limited. On the other hand, the SynUrban runs are more similar to the ambient mixture runs in the UCR EPA and CSIRO chambers in that the best fits are obtained at the higher ROG/NO_x ratios.

Although these data support the finding of a dependence of the model bias in ambient mixture simulations on ROG/NO_x, the range of ROG/NO_x ratios examined in these experiments is not large, and neither is the range in model biases over the range of ratios examined compared to the expected run-to-run variability. Because of this, these runs do not provide as definitive a test of the dependence of model biases as the experiments in the other chambers examined in this work.

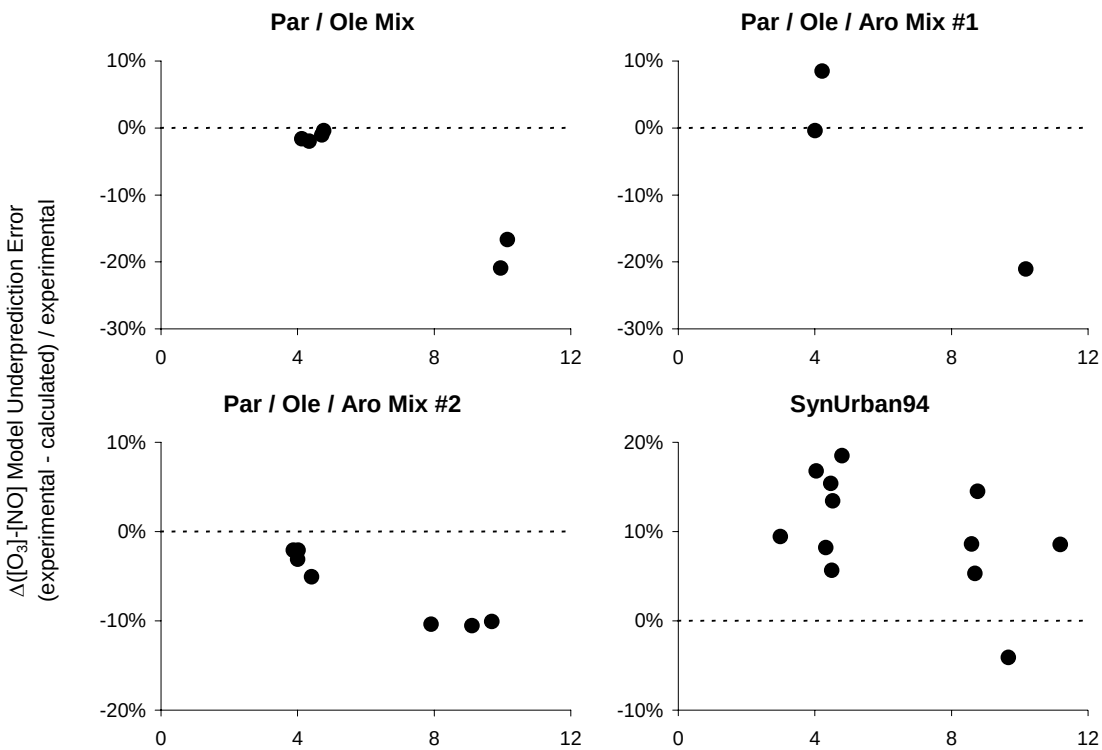

Figure 21. Plots of model underprediction error against ROG/NO_x ratio for the various types of mixture experiments carried out in the TVA chamber.

The model simulations of formaldehyde formation for the various types of mixture experiments are also shown on the figures referenced in Table 18. Overall, the model tends to somewhat underpredict formaldehyde in most of the mixture runs, though the fit is probably within the uncertainty of the data. In particular, although the calculations using the standard or default characterization model usually underpredicts the formaldehyde, the calculations with the higher formaldehyde offgasing parameters tend to fit or overpredict the data. Therefore, if there is a bias towards underpredicting formaldehyde, it is probably not significant or definitive.

On the other hand, there is a very significant tendency for the model to underpredict PAN in almost all of the TVA mixture experiments. The underprediction is approximately a factor of 2 in the simple mixture experiments, but is much greater than that in the SynUrban94 experiments, as is show on Figure B-47. The poor performance for the SynUrban94 experiments cannot be attributed entirely to calibration uncertainty since even if the PAN yields were increased by a factor of two to fit the simple mixture (and also most of the single compound) runs, the PAN in the SynUrban94 experiments would still be significantly underpredicted. This poor performance in PAN simulations also cannot be attributed to problems in O_3 simulations, since as indicated above the overall bias in O_3 simulations in these runs is relatively small.

CSIRO Experiments

A total of 10 dual-reactor CSIRO chamber experiments, amounting to irradiations of 20 separate mixtures, were modeled in this study, all complex ambient surrogate - NO_x irradiations carried out at a variety of initial ROG and NO_x levels. The initial reactant concentrations, maximum temperatures and integrated light intensities, and experimental and calculated amounts of O_3 formed and NO oxidized in these experiments are summarized on Table 19. The experimental and calculated $\Delta([O_3]-[NO])$, O_3, NO, and NO_y-NO data for these experiments are shown on Figure B-48 through Figure B-51 in Appendix B. (Note that no other measurement data for reacting species are available for these experiments.) Plots of model underprediction errors against the initial ROG/NO_x ratio for these experiments are shown in Figure 22.

Because of uncertainties in characterizing run conditions, the figures also show results of calculations with the light intensity increased by 20% (“High HV”) and calculations assuming an upper limit chamber radical source (“High RS”). As discussed previously, these are considered to be the greatest uncertainty in modeling these experiments.

It can be seen from these results that the SAPRC-99 mechanism with the standard chamber effects representation underpredicts O_3 formation and NO oxidation rates in all these CSIRO experiments. The light intensity and radical source sensitivity calculations both employ assumptions that tend to increase the reactivity of the system. To see if this bias can be explained by these uncertainties, calculations were carried out making “upper limit” assumptions for these parameters. The effects of making these assumptions are shown on Figure B-48 through Figure B-51. It can be seen that making these upper limit assumptions for these parameters improves the fit for some experiments and even result in overpredictions for others, but that O_3 is still underpredicted in the majority of experiments. This underprediction of reactivity is consistent with the results of Hynes et al. (2003), who had similar results when modeling CSIRO surrogate - NO_x experiments with the SAPRC-99 mechanism.

Figure 22 shows that the underprediction bias increases with decreasing ROG/NO_x ratio. This is consistent with the results seen in the modeling of the surrogate - NO_x runs in the other UCR EPA and the TVA chambers. Increasing the model predicted reactivity by increasing light intensity or radical source tends to decrease the underprediction bias about equally regardless of the ROG/NO_x ratio, and thus does

Table 19. Summary of conditions and experimental and calculated NO oxidized and O_3 formed in the CSIRO experiments modeled for this program.

Date	Run	Side	NOx (ppb)	ROG (ppbC)	Max T (^oK)	Time (hrs)	Int'd TSR (cal cm^{-2})	Final $\Delta([O_3]-[NO])$ (ppb)	Model Err. [a]	Plot Figure
9/21/95	340	P	20	200	301	10.0	524	156	-12%	Figure B-48
		L	20	200	301	10.0	521	171	-20%	"
9/28/95	341	P	53	200	300	10.0	438	117	-50%	"
		L	25	200	299	9.5	434	138	-33%	"
10/5/95	342	P	54	100	302	10.5	607	126	-25%	"
		L	56	200	302	11.0	612	167	-52%	Figure B-49
10/10/95	343	P	54	400	305	10.0	558	251	-37%	"
		L	55	100	305	10.0	548	110	-16%	"
10/11/95	344	P	45	200	305	11.0	611	232	-36%	"
		L	46	400	305	10.5	619	314	-28%	"
10/19/95	345	P	100	200	305	10.0	559	201	-55%	Figure B-50
		L	97	400	305	9.5	549	300	-65%	"
3/15/96	359	P	31	100	301	6.0	294	84	-67%	"
		L	28	50	301	6.5	307	69	-53%	"
3/19/96	360	P	31	50	305	8.5	439	101	-58%	"
		L	30	100	305	9.5	454	131	-55%	Figure B-51
3/21/96	361	P	17	100	305	9.6	517	120	-40%	"
		L	31	100	305	10.1	528	130	-53%	"
3/26/96	362	P	19	50	308	10.5	426	113	-70%	"
		L	19	100	308	10.5	415	131	-27%	"

[a] (Calculated – experimental) / calculated $\Delta([O_3]-[NO])$ data. The calculations used the SARPC-99 mechanism with the standard chamber effects model for CSIRO experiments.

affect the underlying dependence of the bias on this ratio. The correlation between model underprediction error and ROG/NO_x ratio is almost perfect for all experiments except for runs 342P and 343L, which appear to be outliers. The reason these are outliers is unclear, since there do not appear to be any apparent additional characterization problems or other factors that distinguish them from the other experiments.

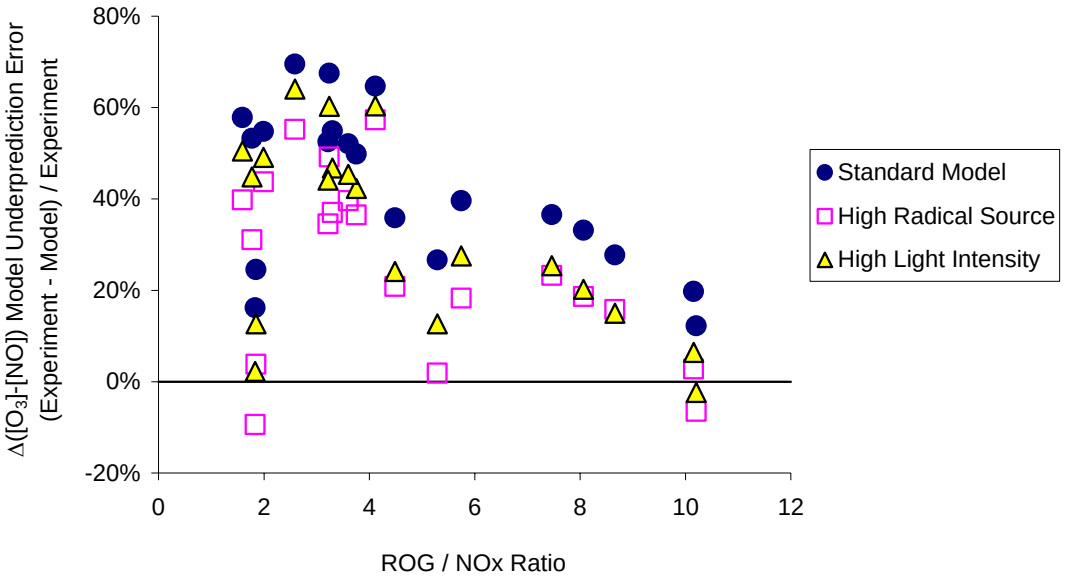

Figure 22. Plots of Δ([O3]-[NO]) model overprediction error against ROG/NO_x ratio for the CSIRO experiments

DISCUSSION AND CONCLUSIONS

Smog Chamber Performance

TVA Chamber

The TVA chamber represents the first significant attempt to produce well-characterized mechanism evaluation data at lower pollutant concentrations than previously available. Although no longer operational, during its period of operation this chamber produced a sizeable dataset that had not been fully exploited. The data obtained are reasonably well characterized, though we would have preferred to have a somewhat larger number of no-NO_x characterization experiments to assess NO_x offgasing effects. The characterization results indicate a significant formaldehyde contamination problem that overwhelms other chamber radical sources and dominates many of the characterization runs. In some ways this is an advantage because it reduces effects of uncertainties in the NO_x -related chamber radical source, but unfortunately it had sufficient apparent run-to-run variability that it provided a non-negligible source of uncertainty in the characterization model. This resulted in a run-to-run variability in the evaluation results that could have been reduced had this contamination been eliminated. The NO_x offgasing results suggests that the NO_x offgasing and NO_x -related radical source in this chamber is within the variability of those obtained in the UCR EPA chamber.

Overall, the TVA chamber data appear to be of comparable or better quality as the chamber data used previously for mechanism evaluation. These data extend downward the range of concentrations for which the mechanisms can be evaluated. In particular, it provides a larger dataset of low NO_x experiments for single compounds than is currently the case for the UCR EPA chamber. The results of modeling these experiments are consistent with the results of modeling comparable experiments in other chambers at higher concentrations. The results of the ambient mixture experiments tend to support the observations from the UCR EPA and CSIRO experiments that there is a dependence of model underprediction bias on ROG/NO_x, though the evidence would have been stronger had the characterization precision been better or had a larger range of ROG/NO_x conditions been examined.

Since the TVA chamber is no longer operational, the experiments discussed here constitute the full dataset available from this chamber. Although the data are useful and provide a valuable addition to the mechanism evaluation dataset, because of the limited number of experiments and the characterization uncertainties they are not, by themselves, sufficient for comprehensive mechanism evaluations.

CSIRO chamber

The CSIRO chamber experiments modeled in this study amount to only a subset of the data from this chamber (Johnson et al, 1997), but they are probably the best characterized and appear to be reasonably representative. They provide a unique dataset of ambient surrogate experiments at relatively low NO_x levels and also low ROG/NO_x ratios. Only a few such experiments are available from other chambers; essentially none if the new UCR EPA and the TVA experiments discussed in this report are excluded.

The CSIRO dataset is clearly not sufficient for comprehensive mechanism evaluation because of its relatively large characterization uncertainties and the limited number of experiments with simpler chemical systems. However, despite the characterization uncertainties, these experiments have provided valuable confirmation of the dependence of model results on ROG/NO_x ratio and the problem of the mechanism in simulating the experiments at the lowest ratios, which are lower than those in any other

dataset. Any revised mechanism developed to address these problems should include modeling of these CSIRO experiments as part of its evaluation.

At present, because of the characterization uncertainties, the main utility of the CSIRO data are to evaluate relative changes in model performance as the ROG/NO_x ratio changes, rather than to predict absolute NO oxidation or O_3 formation rates in any particular experiment. Additional work in improving the characterization data and characterization model for this chamber will increase the value of the CSIRO dataset, as well as any new data that may be obtained. It is probable that we did not fully exploit the available characterization information when developing the CSIRO characterization model for this project, and additional work may have reduced the uncertainty. However, light characterization for outdoor chamber experiments is always problematic, and a significant effort to evaluate this will be required to reduce the characterization uncertainties to the levels attainable for indoor chamber experiments.

UCR EPA Chamber

This is the first report of a systematic mechanism evaluation study using data from the new UCR EPA chamber. This chamber facility was designed to provide more precise and comprehensive mechanism evaluation data, and at lower simulated pollutant concentrations, than previously possible. Although the dataset from this chamber is still limited, the results of this study demonstrate its utility for providing valuable data for mechanism evaluation. The major background effects parameters in the UCR EPA chamber appear to be lower than those observed in other chambers used for mechanism evaluation, including the TVA chamber, which was also designed for experiments at lower pollution levels.

The lower background levels in this chamber permitted successful mechanism evaluation experiments to be carried out with NO_x levels as low as 2 ppb. This is at least an order of magnitude lower than in the mechanism evaluation dataset from other chambers, including the TVA and CSIRO chambers discussed above. Modeling of these experiments did have some sensitivity to chamber effects parameters, but this was not so large that the data could not provide an adequate test for the mechanism. But these NO_x offgasing effects would become relatively more important if NO_x levels were reduced further, and ~2 ppb NO_x probably represents a reasonable lower limit for low NO_x mechanism evaluation for the UCR EPA chamber as currently configured.

It may be possible with some effort to use this chamber for mechanism evaluation at even lower NO_x levels than employed in the experiments discussed here, should this be required. The radical source and NO_x offgasing rate during the period of most of the UCR EPA experiments used in this evaluation study about a factor of two higher than observed when the reactor was new, and even lower apparent NO_x offgasing rates were observed in large pillowbag reactors inside flushed Teflon bag enclosures (Carter, 2002a). This suggests that it may be possible to reduce background effects in this chamber further, by determining the source of the increase around the time of run 79 and by taking further steps to reduce the background pollutant levels in the enclosure which, while low, are not as low as can be achieved using Teflon bag enclosures. However, this would require significant effort and expense, and probably making major modifications to the present enclosure. Nevertheless, the background levels currently achieved represent an important advance and were sufficiently low for the experiments used in this study.

In addition to providing data at lower NO_x levels than previously available, we believe that the lower background effects attainable in this chamber provided an improvement in the precision of the mechanism evaluation dataset. The results of modeling the relatively large number of surrogate - NO_x experiments give some information regarding this. Although the model had systematic biases in simulating many of these experiments, as shown in Figure 17, above, plots of model biases against ROG/NO_x ratios had relatively little scatter, suggesting fits to within ±10% could be obtained if the

current problem(s) with the mechanism can be corrected. This is less than the scatter for the fits to the TVA and the CSIRO data (see Figure 21 and Figure 22), though the scatter for the CSIRO runs may be comparable if the two outliers were removed. This is important since if the scatter in these fits were on the order of ±30%, which was observed mechanism evaluation studies using other chamber data sets (e.g., Carter and Lurmann, 1990, 1991), the ROG/NO_x dependences may not have been statistically significant, and the mechanism performance would have been concluded to be satisfactory. With this more precise dataset the low ROG/NO_x problem with the mechanism is evident.

The results presented in this report reflect only the first series of mechanism evaluation experiments carried out in this chamber, and these only begin to utilize its full capabilities. Under EPA funding we subsequently carried out an extensive matrix of surrogate - NO_x experiments with enhanced measurements in order to test utility of indicator species to predict sensitivities of O_3, including measurements of H_2O_2, and OH and HO_2 radicals (Tonnesen et al, 2002). These experiments are completed and are the results are currently being analyzed. Under CARB funding we are using this facility to assess ozone formation potentials of selected petroleum distillates and other solvents in architectural coatings, and these experiments are currently underway. We are also utilizing this chamber to assess PM formation potentials of aromatics and test models for PM formation, and results to date indicate this chamber has unique capabilities in this regard. We hope to carry out experiments to utilize the unique capabilities of this chamber to provide mechanism evaluation data on temperature effects, once funding for this becomes available. Temperature is an important factor affecting rates of gas-phase reactions and PM formation processes, yet this important aspect of mechanism performance remains to be evaluated.

Mechanism Performance

In many respects the results of this SAPRC-99 mechanism evaluation study supported conclusions of the previous evaluation of this mechanism. In general, the evaluation using the new data from the UCR EPA chamber and the previously unexploited data from the TVA and CSIRO chamber was consistent with the evaluation carried out previously, and with types of experiments simulated well in the previous evaluations being simulated equally well (or better) in the current data set. However the new or previously exploited data that extend the range of conditions used in previous evaluations, or, in the case or the new UCR EPA chamber data, improve its precision, indicate mechanism problems that were not previously apparent. These are discussed below.

Low NO_x Conditions

In most cases, the SAPRC-99 mechanism was found to perform reasonably well in simulating experiments carried out under low NO_x conditions. One of the major concerns that lead to this project was that current mechanisms were not previously evaluated for NO_x conditions lower than about 200 ppb, which is much higher than ambient levels in many areas where ambient ozone modeling is important. The TVA and CSIRO experiments reduced the NO_x levels for evaluation experiments to about 20 ppb, and the UCR EPA experiments, while more limited in number, included experiments with NO_x levels as low as 2 ppb, with most in the 5-30 ppb range. The model performance in simulating these experiments was comparable (and in some cases better) than its performance in simulating the experiments used previously for mechanism evaluation.

The fact that the mechanism performance in simulating representative aromatic experiments at NO_x levels as low as 5 ppb is comparable to its performance for higher NO_x runs is significant. The actual chemical processes involved for much of the aromatic photooxidation process remain highly uncertain, and these are represented by parameterized mechanisms adjusted to fit relatively high NO_x chamber data.

Because of possible competitions between unimolecular, O_2, or NO_x reactions with some of the intermediate radicals, the possibility exists that the parameterization may not be valid for lower NO_x levels, where competing unimolecular or O_2 reactions may be more important. These results suggest that this is not a factor, at least at NO_x levels down to about 5 ppb, and tend to support the conclusion that the current aromatics mechanisms may be appropriate for low NO_x conditions.

Aromatics Mechanisms

Although the model preformed reasonably well in simulating low NO_x aromatic experiments of the type carried out previously, new results indicate problems with the aromatic mechanisms at all NO_x conditions. The most obvious indication of this is the fact that the model underpredicts, by about a factor of two, the change in amount of O_3 formed when CO is added to aromatic - NO_x irradiations. Sensitivity calculations indicate that this is unlikely to be due to uncertainties in chamber effects. These experiments, which were not to our knowledge conducted previously for mechanism evaluation, were carried to test our model predictions that the addition of CO acts as a "radical amplifier" to enhance the amount of ozone formation caused by radicals formed in the aromatic photooxidation, would significantly enhance O_3 formation in aromatic - NO_x experiments. In fact they acted as a greater radical amplifier than the model predicted.

These data therefore indicate that the current aromatics mechanisms do not supply enough radicals in their NO_x -air photooxidations. Further evidence for this comes from the fact that the consumption rates for the reacting aromatic and NO_2 are generally greater than predicted in aromatic - NO_x experiments. This is despite the fact that the formation yields and photolysis rates of unknown photoreactive aromatic product are adjusted to fit aromatic - NO_x experiments. Apparently there are compensating errors in parameterizations used in the aromatic mechanisms that allow them to simulate the aromatic - NO_x experiments in the absence of CO, but become evident when CO is added to the system.

This is a significant problem because in many ways the presence of CO in the aromatic - NO_x experiments have analogous effects on the aromatic system as the presence of alkanes and other reactive but non-radical-initiating species present in real atmospheric systems. This aromatic mechanism problem may be the reason that the model tends to underpredict NO oxidation and O_3 formation rates in low ROG/NO_x ambient surrogate experiments, which is another significant finding of this study. Low ROG/NO_x experiments are highly sensitive to radical levels, and the failure of the aromatics mechanisms to supply sufficient radicals when reacting in the presence of other species may be the reason for the underprediction bias. The sensitivity to radicals increase as the ROG/NO_x ratio decreases, and this may explain the observed strong correlation of the underprediction bias with this ratio.

In a previous study (Carter and Malkina, 2002) we found that the "direct reactivity" of aromatics, i.e., the amount of NO oxidized and O_3 formed by the direct aromatic reactions, was about half what the mechanism predicted. This suggests that the compensating error allowing data to be fit with inappropriately low radical production rates may be the mechanism assuming too many NO to NO_2 conversions in the initial aromatic photooxidation reactions.

However, modifying the mechanism to reduce the direct reactivity and fit the data of Carter and Malkina (2002) and re-adjusting radical initiation rates in the mechanism to simulate aromatic - NO_x experiments did not significantly improve the model performance in simulating the effects of added CO. Even increasing the yield of the major model species representing unknown photoreactive aromatic products beyond the point where NO oxidation rates in aromatic - NO_x experiments are overpredicted does not result in satisfactory predictions of the effects of CO predictions. This is shown on Figure 23, which shows results of simulations of various types of toluene experiments using the standard toluene

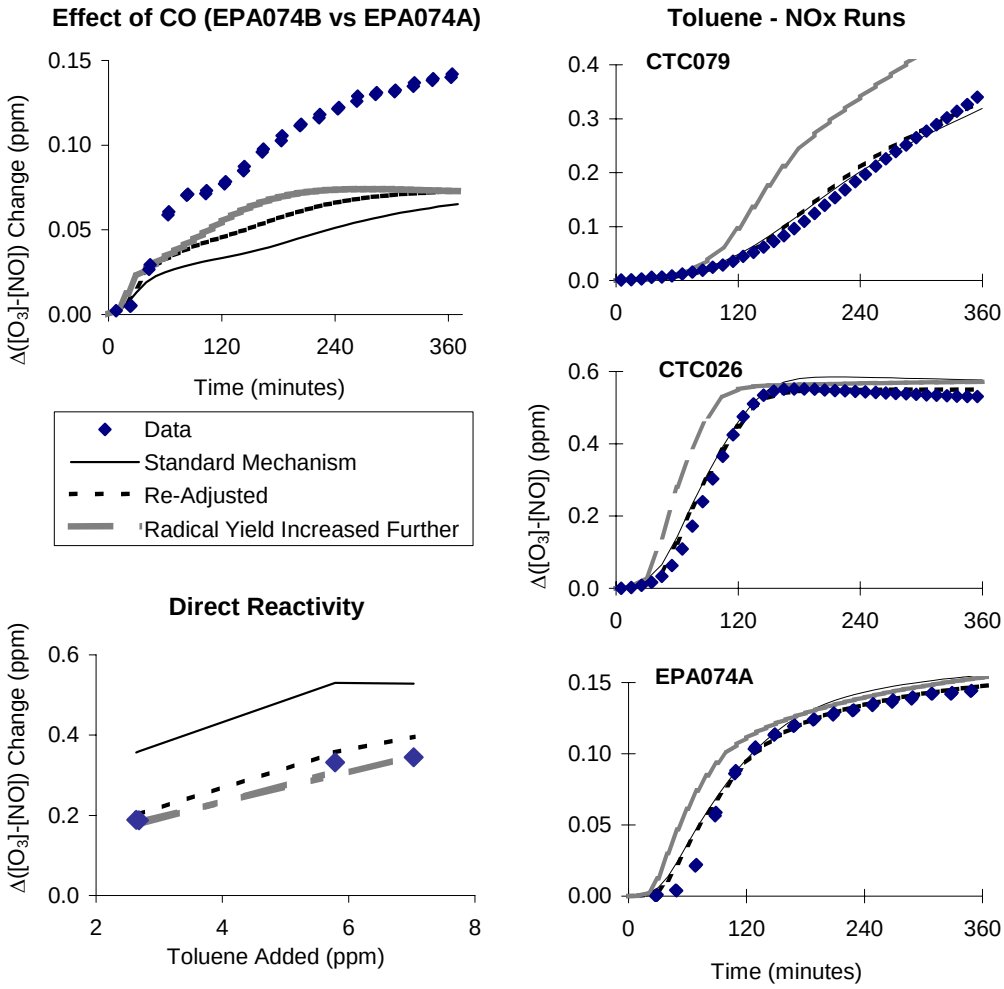

Standard Mechanism:	SAPRC-99 mechanism without modifications
Re-Adjusted:	NO to NO_2 conversions in initial reaction reduced from 1.8 to 0.56 to fit direct reactivity data. Yield of DCB2 increased from 0.156 to 0.2 to fit toluene - NO_x experiments.
Radical Yield Adjusted Further:	DCB2 yield increased to 0.2 and NO to NO_2 conversions further reduced to 0.24 to fit direct reactivity data.

Figure 23. Examples of results of reoptimizing SAPRC-99 toluene mechanism to fit different types of selected evaluation data.

mechanism and with the mechanism modified as indicated above. Other variations and re-optimizations of the current mechanism parameters were attempted, but no reasonable combination of parameters were found that could yield acceptable fits to the types of data shown on Figure 23.

It is clear that major modifications to how the these are represented in the current mechanism is needed before aromatic mechanisms are needed before satisfactory model performance can be obtained. Simply adjusting and reoptimizing the parameters in the current mechanism do not appear to be sufficient to fit the available data. Unfortunately, the level of effort required to develop entirely new aromatic

mechanisms exceeded the time and resources available to this project. This work will be carried out in a follow-on mechanism development project that has recently been approved by the CARB (Carter, 2003b).

Ambient Simulations

The mechanism evaluation experiments used in this study included three datasets of ambient ROG surrogate - NO_x simulations carried out at a range of ROG and NO_x levels, including NO_x levels significantly lower than used in previous mechanism evaluations. As discussed above, the model performance in simulating the lowest NO_x experiments was comparable to, or (usually) better than, the simulations of the experiments at the higher NO_x levels. However, modeling this dataset indicates a significant tendency for the model to underpredict NO oxidation and O_3 formation rates in experiments at low ROG/NO_x ratios, with the magnitude of the underprediction increasing as the ratio decreases. This is seen in the datasets from all three chambers, though the trend is most obvious in the case of the UCR EPA and CSIRO datasets. Varying chamber effects parameters within their ranges of uncertainty or variability does not correct this problem.

Figure 24 shows a comparison of the trends in model underprediction errors as a function of ROG/NO_x ratio for the ambient surrogate experiments in the different chambers. Since the reactivity characteristics at a given ROG/NO_x ratio depend on other experimental conditions such as light intensity, temperature, and duration of the irradiation, etc, the data are put on a comparable basis by dividing the ROG/NO_x ratios with that yielding the highest O_3 concentration for the conditions of the experiment[13]. It can be seen that this normalization of ROG/NO_x ratios puts the trend for the CSIRO experiments in line for that for the experiments in the UCR EPA chamber, with the agreement being remarkably good if the two outliers in the CSIRO dataset are removed. On the other hand, the data from the TVA experiments indicate somewhat lower model underprediction error in simulating experiments with comparable normalized ROG/NO_x ratios.

The UCR EPA dataset gives the strongest indication of this dependence of model performance on ROG/NO_x ratios because it incorporates a relatively wide range of reactant conditions and also the data show relatively little scatter once this trend is taken into account. However, the CSIRO data provide useful confirmation to this trend since they tend to fall on the same trend line, and also they extend the range of ROG/NO_x ratios to lower levels than in the current UCR EPA dataset. Modeling the CSIRO data alone is probably not sufficient by itself to convince us of this evaluation problem because of the uncertainty in chamber characterization and because the extreme biases might lead one to suspect large characterization problems. However, in conjunction with the UCR EPA data they provide important confirmation of the observed trend using entirely different experimental conditions and a more complex, and presumably more representative, ROG surrogate mixture. The extremely poor performance of the mechanism in simulating the CSIRO data is entirely expected in light of the results in the UCR EPA chamber.

The underprediction bias in the SAPRC-99 for low ROG/NO_x ambient surrogate experiments is not unique to SAPRC-99 and we suspect the performance of other mechanism may be similar or worse. For example, Figure 25 compares the UCR EPA Δ([O3]-[NO]) model underprediction errors for Carbon Bond 4 (CB4) mechanism (Gery et al, 1988) with that obtained with SAPRC-99. It can be seen that the low ROG/NO_x underprediction biases are even greater with CB4 than obtained with SAPRC-99, and the

[13] The maximum O_3 (MOIR) ROG/NO_x ratio for each type of experiment was determined by varying the initial NO_x concentration in a hypothetical experiment with the average initial ROG surrogate level to determine the NO_x level that gave the highest O_3 concentration. The other inputs used were those for a selected experiment where the temperature and (for CSIRO runs) integrated TSR were closest to the average. Note that the MOIR ROG/NO_x ratio may have some dependence on the ROG level, but this dependence is not expected to be large and is ignored.

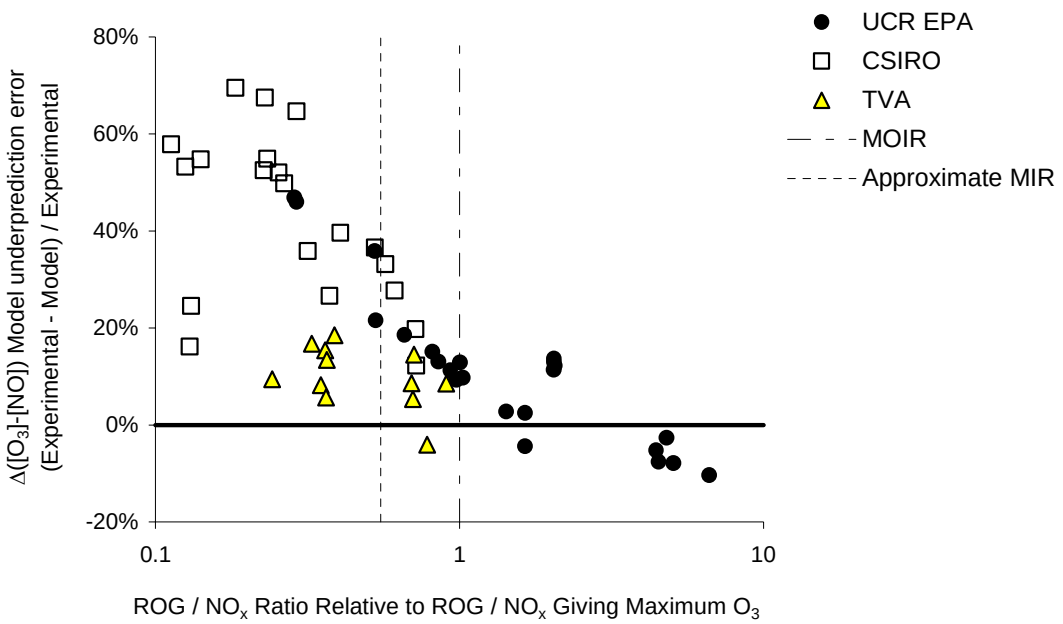

Figure 24. Plots of model underprediction error for $\Delta([O_3]-[NO])$ in the ambient surrogate runs in the various chambers against the ROG/NO_x ratio normalized to the ROG/NO_x ratios estimated to give maximum O_3 concentrations for the conditions of the experiments.

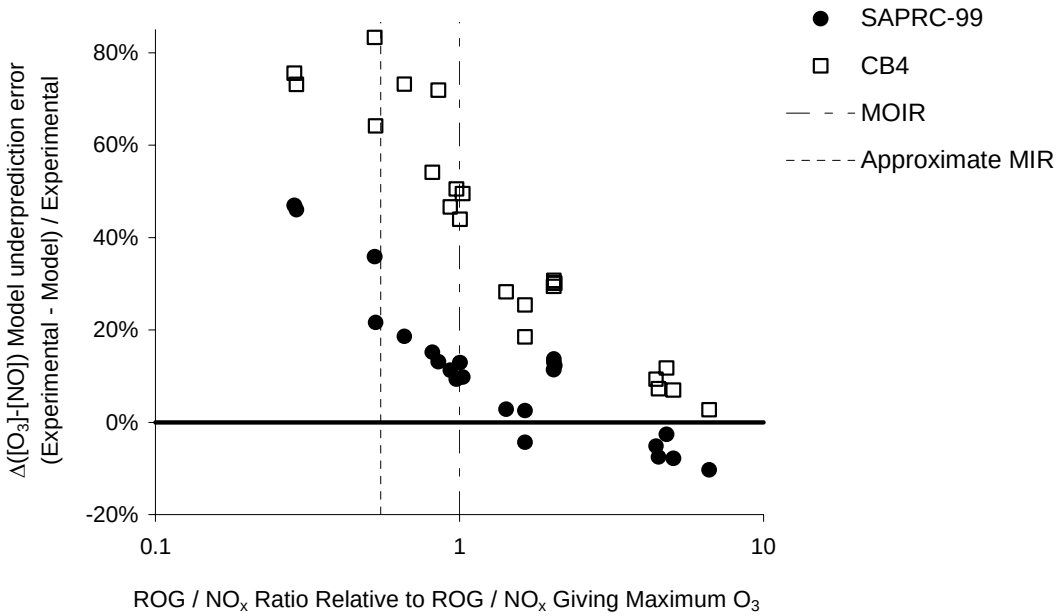

Figure 25. Comparison of SAPRC-99 and CB4 underprediction errors for model simulations of the UCR EPA ambient surrogate experiments as a function of initial ROG and NO_x

slope of the trend line for that mechanism is also a factor of two larger. Although we did not evaluate the RADM-2 mechanism with these data, in most respects it is more like SAPRC-99 than CB4, so we expect its performance to be similar. Note that we did not optimize our chamber effects model for the CB4 mechanism, and doing so may have an effect on the biases obtained, though we suspect the effect will be relatively small. But the modeling of the CSIRO experiments with alternative chamber effects assumptions suggests that modifying the chamber effects model would not affect the prediction of the general trend of underprediction biases with ROG/NO_x, nor would it significantly improve the model predictions at the lowest ratios.

It is surprising that this underprediction trend was not apparent in previous mechanism evaluation studies. Indeed, with one exception, the trend in model underprediction bias with ROG/NO_x was not evident in the modeling of the various types of surrogate experiments used in the initial SAPRC-99 mechanism evaluation of Carter (2000a). This is shown in Figure 26, which gives plots of model underprediction error against OH reactivity-adjusted ROG/NO_x ratios for the various types of UCR ambient surrogate experiments used in the Carter (2000a) evaluation. The UCR EPA results are shown on the same scale at the bottom right for comparison. No such trend can be seen except perhaps for the 8-component surrogate experiments carried out in 1983-84. This is despite the fact that the 8-component surrogate used in the 1993-99 experiments shown in the right-top plot is the same surrogate used in the UCR EPA studies. Although we did not examine modeling of UNC chamber experiments in this work, Carter and Lurmann (1990, 1991) did not observe any such bias when evaluating SAPRC-90 or RADM2 with these data.

The reason why the modeling of the earlier ambient surrogate - NO_x experiments did not show this same trend with ROG/NO_x is unclear. It could in part be due to trends being hidden by run-to-run variability in model simulations, and in part due to the relatively limited number of experiments carried out at the lowest ratios where the trend is the most apparent. It could also be due to the fact that the earlier experiments were carried out at higher NO_x levels than the UCR EPA, TVA, and CSIRO experiments evaluated here. Most of the experiments in the ambient simulations modeled in this work had NO_x levels of less than 100 ppb, while those used in the earlier evaluations had NO_x levels ranging from ~100 ppb to over 500 ppb. In addition, most of the earlier experiments in the lowest ROG/NO_x range, where the underprediction error is most apparent, had NO_x levels on the order of 500 ppb.

Therefore, it is possible that this model underprediction bias at low ROG/NO_x levels may not be as great in experiments carried out at higher NO_x levels than used in these relatively low NO_x runs. This needs to be verified by conducting high NO_x, low ROG/NO_x experiments in the UCR EPA chamber, with the concentration ranges used in the previous mechanism evaluation runs. Since reasonably good consistency was obtained when reproducing earlier lower NO_x full surrogate runs, we have no reason to expect that different results will be obtained with higher NO_x experiments. If this is the case, then this low ROG/NO_x model underprediction bias can be concluded to be a low NO_x mechanism performance problem.

We believe that this low ROG/NO_x underprediction bias is most likely due to problems with the aromatic mechanism discussed above. However, results of modeling the “paraffin/olefin” mixture TVA experiments, shown on Figure 21, suggested a similar trend in bias with ROG/NO_x ratio, though in this case it was due to the model overpredicting NO_x at the higher ROG/NO_x ratios, which may be due to a different problem. This will need to be evaluated once an aromatic mechanism is developed that successfully simulates the various types of aromatic - NO_x experiments discussed above.

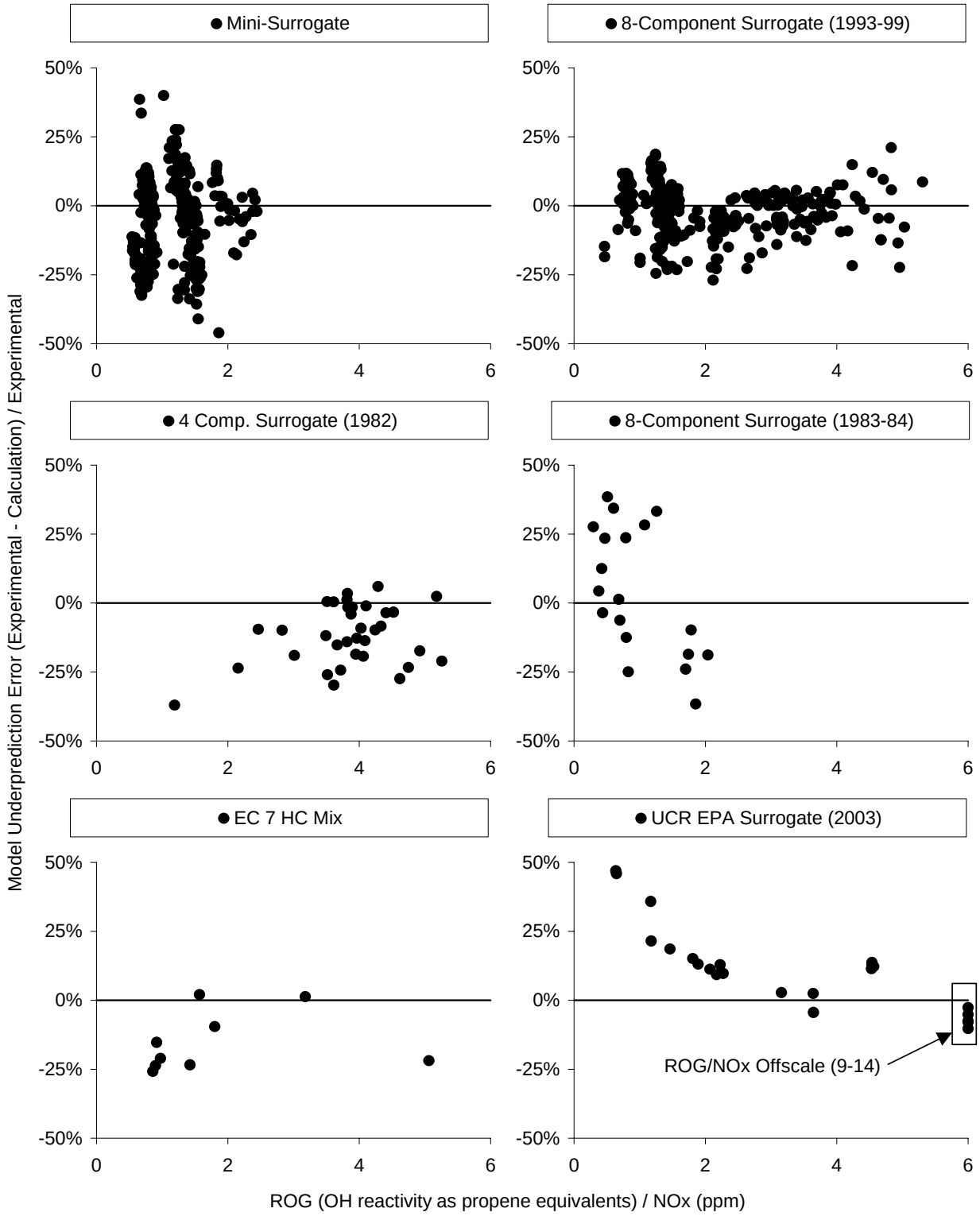

Figure 26. Plots of underprediction error against OH reactivity-adjusted ROG/NO_x ratios in the SAPRC-99 model predictions of the surrogate experiments used in the Carter (2000) evaluation, with plots for the current UCR EPA experiments also shown for comparison.

Assessment of Need to Modify Mechanism for low NO_x Conditions

One of the ways in which that lower NO_x levels affect the VOC and NO_x photooxidation process is through the reactions of the peroxy radicals that are formed when VOCs react. These are critical intermediates because they are involved in the oxidation processes of almost all VOCs and it is their reactions with NO that are primarily responsible for the fact that VOCs promote ozone formation. When NO_x levels are relatively high and O_3 formation is not NO_x limited, this reaction with NO is the only important loss processes for these radicals. However, when NO_x levels become sufficiently low, reactions with other peroxy radicals, such as HO_2, acetylperoxy (RCO_3) or alkyl peroxy (RO_2) radicals become competitive. These competing reactions affect not only ozone formation, but also the distribution of organic products formed in the VOC's atmospheric reactions.

Because of the relatively large number of different type of peroxy radicals formed in even relatively condensed mechanisms, explicitly representing all the possible peroxy + peroxy combination reactions in a mechanism is quite burdensome. Since these reactions are relatively unimportant under conditions where O_3 formation is occurring, approximate approaches to represent these processes are generally employed. In the case of the SAPRC-99 mechanism, a "chemical operator" method is used to represent the effects of the peroxy radical reactions on radical propagation and termination, NO_x cycles, and O_3 formation. This method represents the products formed when the VOCs react as being the same as those formed when peroxy + peroxy reactions occur as they are under high NO_x conditions. Although this approximation does not affect predictions of O_3 (Carter and Lurmann, 1990), it does not given an accurate representation of organic product formation under very low NO_x conditions.

To illustrate the problems with the current chemical operator approach for representing peroxy + peroxy reactions, consider the simple example of the reactions of ethane. Under relatively high NO_x conditions, the major reactions are as follows,

$$CH_3CH_3 + OH \rightarrow CH_3CH_2\cdot + H_2O$$
$$CH_3CH_2\cdot + O_2 \rightarrow CH_3CH_2O_2\cdot$$
$$CH_3CH_2O_2\cdot + NO \rightarrow NO_2 + CH_3CH_2O\cdot$$
$$CH_3CH_2O\cdot + O_2 \rightarrow CH_3CHO + HO_2$$

This results in the overall formation of acetaldehyde as the only organic oxidation product, the conversion of one molecule of NO to NO_2, and the formation of hydroperoxy radicals, whose subsequent reactions will regenerate OH. In the current documented versions of SAPRC, this overall process is represented by

$$\text{Ethane} + OH \rightarrow CCHO + RO2\text{-}R\cdot$$
$$RO2\text{-}R\cdot + NO \rightarrow NO_2 + HO_2$$

where CCHO is the model species for acetaldehyde and RO2-R· is the chemical "operator" representing the formation of peroxy radicals that convert NO to NO_2 and form HO_2. An analogous approach is used in other mechanisms such as CB4. This gives the same overall process as the explicit mechanism when reaction with NO is the major fate of peroxy radicals. However, if NO_x levels are sufficiently low, then the following reactions also compete with the reaction with NO, and eventually become dominant.

$$CH_3CH_2O_2\cdot + HO_2\cdot \rightarrow CH_3CH_2OOH + O_2$$
$$CH_3CH_2O_2\cdot + CH_3CH_2O_2\cdot \rightarrow 2\ CH_3CH_2O\cdot + O_2$$
$$CH_3CH_2O_2\cdot + CH_3CH_2O_2\cdot \rightarrow CH_3CHO + CH_3CH_2OH + O_2$$

where analogous reactions can occur between ethyl peroxy and the many other types of peroxy radicals. Note that these reactions result in the formation of ethanol and ethyl hydroperoxide and lower yields of

acetaldehyde than is the case in the higher NO_x conditions. These loss processes for the peroxy radical center are represented in the mechanism by

$$\text{RO2-R}\cdot + HO_2 \rightarrow \text{Lumped hydroperoxide model species}$$
$$\text{RO2-R}\cdot + \text{RO2-R}\cdot \rightarrow HO_2$$

plus analogous reactions of RO2-R· with other peroxy radical operators. Although this representation may give a reasonably accurate representation of the effects of NO_x levels on the total peroxy radical concentration and the amount of NO to NO_2 conversion and radical propagation and termination caused by their reactions, it does not take into account the fact that products other than acetaldehyde can be formed in the ethane photooxidation process. This representation can represent the formation of total lumped hydroperoxide species from the peroxy + HO_2 reactions, but not the fact that these hydroperoxides are formed in the place of the high NO_x products such as acetaldehyde, rather than in addition to them.

An alternative approach that was investigated when SAPRC-99 was initially developed was to use separate peroxy radical model species for each type of reaction forming a peroxy radical, and use peroxy radical operators only for determining the total rate at which they react with other peroxy radicals. In this approach, the reactions of ethane is represented as follows:

$$\text{Ethane} + OH \rightarrow \text{Ethane-}RO_2\cdot + [\text{total } RO_2]$$
$$\text{Ethane-}RO_2\cdot + NO \rightarrow NO_2 + CCHO + HO_2$$
$$\text{Ethane-}RO_2\cdot + HO_2 \rightarrow \text{Ethyl Hydroperoxide or lumped hydroperoxide species}$$
$$\text{Ethane-}RO_2\cdot + [\text{total } RO_2] \rightarrow [\text{total } RO_2] + 0.75\ CCHO + 0.25\ ETOH + 0.5\ HO2$$
$$\text{Ethane-}RO_2\cdot + [\text{total } RCO_3] \rightarrow [\text{total } RCO_3] + CCHO + HO_2$$

where [total RO_2] and [total RCO_3] are species used to represent the total peroxy or acyl peroxy radicals which are formed in conjunction with the individual peroxy radical formations, and whose loss processes are represented in separate reactions. This approach allows the representation of different products formed in the peroxy + peroxy reactions than in the peroxy + NO reaction, but at the cost of having a separate model species for each type of reaction forming peroxy radicals. However, the computational demand can be reduced somewhat by using the steady state approximation for the individual peroxy radical species such as Ethane-RO_2, with only the total RO_2 or RCO_3 counter species being integrated and transported.

Note that while this approach permits a more accurate representation of the products formed in the reactions of organic peroxy radicals with other organic peroxy radicals, it still uses an approximate representation of the products formed from the peroxy + HO_2 reaction. In particular, a lumped species is used to represent the hydroperoxide compounds formed. Representing these explicitly would place significant burden on the mechanism, and their subsequent reactions, other than photolysis, would be largely speculative. Their photolysis reactions would be expected to form OH and the same types of alkoxy radicals as formed when the parent peroxy radical reacted with NO, with the ultimate product distribution being that predicted using the “operator” approach of the current mechanism. Therefore, if reaction with HO_2 were the dominant fate of peroxy radicals under low NO_x conditions, further development of the alternative representation discussed above would probably not be worthwhile. Depending on the approach used to represent the hydroperoxide reactions, either a much larger mechanism would need to be developed than would be acceptable in current airshed models used by the CARB, or the model predictions of ultimate products would be essentially the same as in the current me mechanism or not necessarily any more accurate.

To assess whether it was worthwhile to undergo the major effort of completing the development and evaluation of the alternative version of SAPRC-99, we conducted a series of box model calculations to assess the relative importance of the various peroxy radical reactions under low NO_x conditions. Three types of scenarios were employed, whose major inputs and conditions are summarized on Table 20. As indicated there, the first was the one-day "Averaged Conditions" scenario developed based on those used by Carter (1994a, 2000a) to calculate the MIR and other reactivity scales, whose specific inputs are given by Carter (1994b), with the NO_x levels varied as discussed below. Because factors affecting peroxy + peroxy reactions may be different in the multi-day transport or stagnation conditions that may occur in regional models, additional simulations were carried out using two multi-day variants of this EKMA model. In the first, designated "Multi Day #1", the same emissions and inversion height changes occurred on five consecutive days, with the air mass being diluted from the air from aloft as the inversion height rose during each day. This can be taken as a simple representation of a stagnant air mass over an urban area, or one that moves from one urban area to another in consecutive days. In the second, designated "Multi-Day #2," emissions and dilution occur only on the first day, and on the subsequent four days the pollutants react without additional emissions or dilution. This can be taken as representing an air mass that is transported out of polluted areas, where effects of multi-day processes are maximized. Additional details are given on Table 20, its footnotes, and references cited therein.

To maximize the importance of organic peroxy + peroxy reactions, which are the processes most affected by the mechanism modification being considered, these scenarios employed the relatively high total VOC emissions levels that are used in the standard "averaged conditions" scenarios of Carter (1994a,b). For each type of scenario, the NO_x inputs were varied from MOIR levels (i.e., NO_x levels giving the highest maximum O_3 concentration) down to near zero. The maximum ozone concentrations calculated for these scenarios are sown as a function of NO_x levels relative to MOIR NO_x on Figure 27a, and O_3 concentration-time plots for representative low NO_x scenarios of the three types are compared on Figure 27b.

For each scenario, the integrated rates of the various types of reactions of a representative peroxy radical model species were calculated, and the ratios of these integrated rates relative to the total integrated rates of all reactions of this species, and relative to the total peroxy + peroxy rates, were then derived[14]. These integrated reaction rate ratios are shown as a function of NO_x inputs on Figure 28. Note that the NO_x inputs are shown on logarithmic scale, and thus show results over three orders of magnitude of NO_x levels. Note also that highest NO_x levels shown represent MOIR conditions (NO_x = MOIR NO_x), which represents the start of NO_x-limited conditions. Above these NO_x levels the peroxy + NO reaction is by far the dominant peroxy radical reaction.

The reactions with NO and HO_2 were calculated to be the dominant loss processes for the peroxy radicals under all NO_x conditions of these scenarios. The third most important is the reaction with acetyl peroxy radicals (RCO3), but this is never more than 10% of the total or 20% of the peroxy + peroxy reactions in all these scenarios. The integrated rates of reactions with other alkyl proxy radicals are essentially negligible under all conditions. The integrated rates of reaction with NO_3 radicals become non-negligible in the multi-day scenarios with the higher NO_x levels, presumably due to reactions at nighttime when NO_3 levels are high. But the NO_3 reaction forms the same alkoxy radicals as the reaction with NO, and thus is not a factor in the mechanism modifications under consideration.

[14] The RO2-R. model species was taken as representative. The specific integrated rates shown were derived from the integrated rates of the following reactions of SAPRC-99 model species: RO2+NO: RO2-R. + NO; RO2+HO2: RO2-R.+HO2.; RO2+RCO3: sum of (RO2-R.+CCO-O2.. RO2-R.+RCO-O2.; RO2-R.+BZCO-O2., and RO2-R.+ MA-RCO3.); RO2+RO2: sum of (RO2-R.+C-O2., RO2-R.+RO2-R., and RO2-R.+RO2-N.); RO2+NO3: RO2-R.+ NO3).

Table 20. Summary of input conditions of model scenarios used to calculate relative contributions of peroxy radical reactions.

Input Parameter	Avg. Cond. EKMA	Multi Day #1	Multi Day #2
Latitude	36.22	34.1	Same as #1
Solar declination angle	16.5	23.5	Same as #1
Solar time offset (min) [a]	-75.81	-60	Same as #1
Start time	8:00 AM	6:00 AM	Same as #1
Number of Days	1	5	Same as #1
End Time	6:00 PM	9:00 PM	1:00 PM
Temperature (^oK)	[b]	300	Same as #1
H_2O (ppm)	[b]	2.08e+4	Same as #1
ROG Emissions (mmol C/m2)		15.38	
ROG Composition		SCOS 97 emissions [c]	
NOx Emissions		Varied -- see text.	
Aloft VOCs (ppbC)		30	
Aloft NO_x		0	
Aloft O_3 (ppb)		70.4	
Fraction VOC initially present	60%	0	Same as #1
Fraction NO_x initially present	46%	0	Same as #1
Initial NO_2/NO_x	25%	n/a	Same as #1
Emitted NO_2/NO_x	5%	25%	Same as #1
Initial $HONO/NO_x$	2%	n/a	Same as #1
Emitted $HONO/NO_x$	0.1%	0	Same as #1
Day 1 Emissions Schedule	[b]	[d]	Same as #1
Emissions on Days 2-5	n/a	Same as Day 1	None
Inversion Height Schedule	[b]	[e,f]	[e,g]
Initial height (M)	293	100	100
Final height (M)	1823	540	540
Days 2-5 inversion heights	n/a	Same as Day 1	Does not change

[a] The solar time offset is the difference between solar time and simulated local clock time. This accounts for daylight saving time (used for all scenarios) and effects of longitude difference. Time offset of -60 means that daylight time is used for local clock time and there is no longitude effect.

[b] See Carter (1994b) for a the schedules used for water, emissions schedule, and inversion height changes for the "averaged conditions" scenario..

[c] The ROG composition was derived from a total emissions profile based on SCOS-97 emissions that was provided by Paul Allen of the CARB on 2/20/2001.

[d] Emissions for multi-day scenarios begin at 6 AM, the rates increase linearly until 8 AM and then are constant until 6:30 PM, at which time their rates decrease linearly until 7:30 PM, when they are zero. No emissions after 7:30 PM until the next day.

[e] The inversion height is constant until 8 AM, then rise linearly to the maximum at 9 PM.

[f] The nighttime inversion height decreases linearly from 9 PM until 8 AM the following day.

[g] The inversion height is constant at its maximum value after 9 PM on day 1.

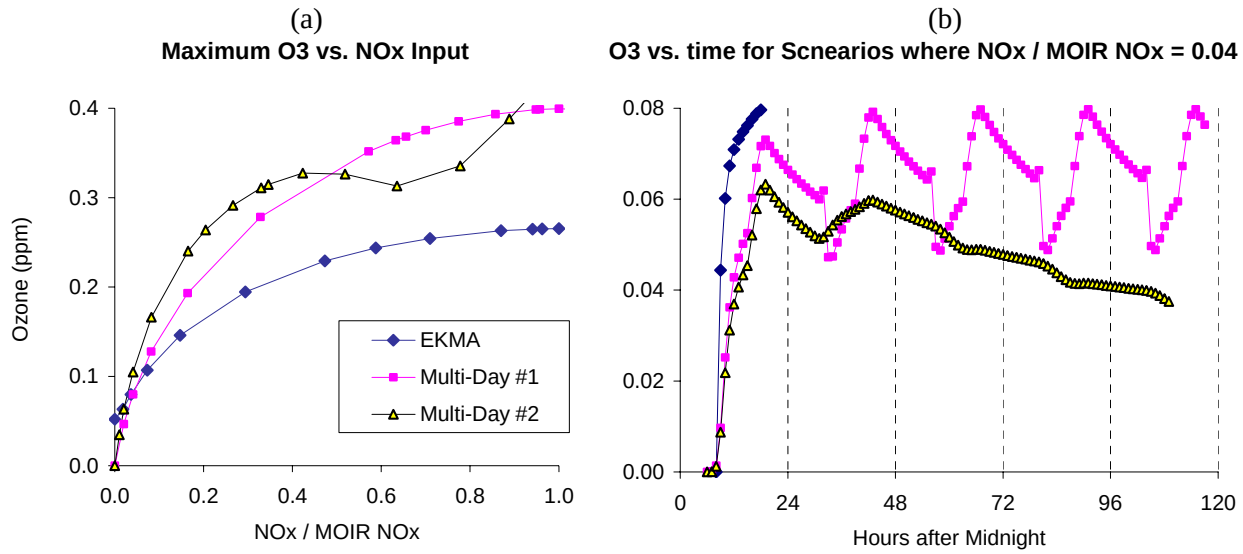

Figure 27. (a) Plots of calculated maximum ozone as a function of NO_x input for the various test scenarios. (b) Calculated O_3 as a function of time for the test scenarios for a representative low NO_x input condition.

Although these scenarios are probably significant simplifications of reality, and represent relatively high VOC pollution conditions, they are probably reasonably representative of the range of conditions that may affect the relative importances of the various types of peroxy radical reactions being considered. The relatively high VOC pollutant levels should bias the simulations towards over-representing the organic peroxy + peroxy processes, and under lower VOC conditions the relative importances of the "RO2+RCO3" and "RO2+RO2" should be even less than shown on Figure 28. Since these two types of reactions are calculated to contribute no more than 10% of the total product formation in the reactions of organics regardless of NO_x conditions, it is concluded improving the representation of these two types of reactions is not, by itself, sufficient reason to make modifications to the mechanism that increase its size, complexity, and computational overhead.

This does not mean that improving the accuracy of the mechanism in representing these low-NO_x peroxy radical reactions would not be beneficial. Improved representations of reactions of hydroperoxides or (if applicable) other products formed from peroxy + HO_2 reactions would clearly be appropriate for models where long term transport or ultimate fates of VOCs are of concern. This would be a major effort and require an improved understanding of peroxy + HO_2 reactions and the hydroperoxide products they are believed to form. While the organic peroxy + peroxy reactions are not calculated to be significant in ambient simulations, they may be non-negligible in certain types of mechanism evaluation experiments, and may also occur near source areas or under "upset" conditions where VOC levels are very high. In general, having better representations of these processes would extend the range of validity and applicability of the mechanism, and enhance the credibility of its predictions when applied to unusual or extreme situations.

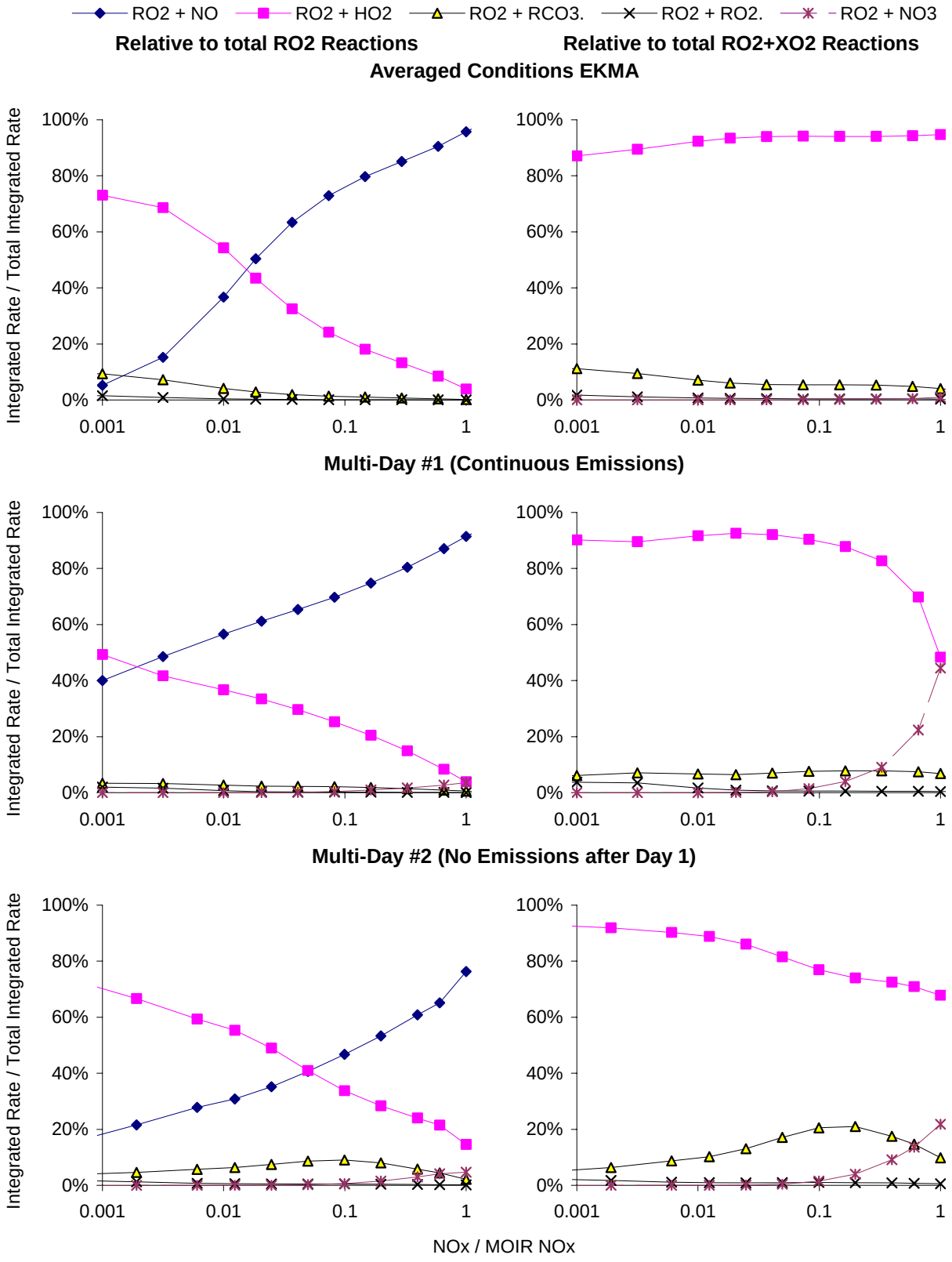

Figure 28. Plots of relative integrated reaction rates for various types of peroxy radical reactions as a function of NO_x levels for the various test scenarios.

Overall Conclusions and Recommendations

This study was successful in significantly extending the range of conditions under which current atmospheric chemical mechanisms can be evaluated. The existing TVA and CSIRO and the new UCR EPA data extend the existing dataset into lower NO_x and (in the case of CSIRO) lower VOC/NO_x conditions than previously used when evaluating such mechanisms, and the new UCR EPA data provide a higher level of precision for mechanism evaluation than previously available. The use of these data in this study has provided valuable insights concerning the predictive capabilities of the mechanisms used in current airshed models.

The results of this study include both good news and bad news in this regard. The good news is that there is no apparent low NO_x mechanism performance problem in simulating simple chemical systems and in simulating ambient simulation experiments where maximum ozone formation potentials can be achieved. The good performance in simulating the simpler chemical systems is important because it indicates no evident problems with the base inorganic or simple organic product mechanism, which is essential to the validity of the mechanism as a whole. The good performance in simulating O_3 in experiments where maximum ozone formation potentials can be achieved, i.e., where O_3 levels are limited by the availability of NO_x, is important because this is representative of much of the atmosphere.

The bad news is twofold. New UCR EPA chamber experiments, of the type not previously used for aromatic mechanism evaluation, indicate that there are fundamental problems with how the unknown processes in the aromatic photooxidation reactions are represented in the current mechanism, No adjustments of the parameters in the mechanism could be found to give acceptable fits to all the data. This indicates that the parameterization employed is incorrect or incomplete. The second problem is that the current mechanism underpredicts NO oxidation and O_3 formation rates at low ROG/NO_x ratios in experiments carried out in all three of the chambers used in the present evaluation. This problem may not have been evident in previous evaluations in part because of scatter of the evaluation data, or, more likely, because all the lower ROG/NO_x ambient surrogate experiments were carried out at much higher NO_x levels than the experiments used in this study. This is significant because the NO_x levels used in the current evaluation are more representative of those in the atmosphere, and low ROG/NO_x ratios are characteristic of the more densely populated source areas.

Although this evaluation focused on the SAPRC-99 mechanism, many of its conclusions are probably applicable to other current mechanisms as well. The CB4 mechanism has even worse problems simulating low ROG/NO_x experiments as SAPRC-99, and unpublished results in our laboratory indicate it also performs poorly in simulating the new aromatics data (Chao-Jung Chien, personal communication, 2003). The RADM-2 mechanism has very similar characteristics as SAPRC and previous studies indicated it had comparable performance in simulating available chamber data (Carter and Lurmann, 1990).

Development of improved aromatic mechanisms that are consistent with all the available data needs to be given high priority, and the mechanism performance problem at low ROG/NO_x ratios needs to be addressed. Development of an improved aromatics mechanism is one of the tasks in follow-on mechanism development project that has recently been approved by the CARB (Carter, 2003b), and hopefully addressing this problem will also result in improvements in the performance at low ROG/NO_x ratios. However, attempts to incrementally improve the current aromatics representation to be able to simulate current data have not been successful, and it is clear that a complete re-formulation of how aromatics are represented is required. Additional research in this area is almost certainly needed.

While the addition of the new or previously unexploited data discussed in this report significantly expands the range of conditions covered by the now-available mechanism evaluation dataset, significant

gaps still remain. Experiments are needed to assess whether the inconsistencies between low NO_x and high NO_x experiments concerning model performance at low ROG/NO_x ratios are due to differences in total NO_x levels or other problems. Experiments are needed to assess the extent to which the model performance problems at low ROG/NO_x conditions are due to problems with the aromatics mechanisms or to a more general problem with the mechanism at a whole. Our conclusions about aromatic mechanism performance problems are based on a relatively small set of experiments and additional experiments will be needed to guide the development and fully evaluate any new aromatics mechanisms that are developed. Other aspects of mechanism performance, such as predictions of temperature effects or predictions of formations of condensable materials leading to the formation of secondary PM, are still not adequately evaluated.

REFERENCES

Atkinson, R. (1990): "Gas-Phase Tropospheric Chemistry of Organic Compounds: A Review," Atmos. Environ. 24A, 1-24.

Atkinson, R. (2000): "Atmospheric Chemistry of VOCs and NO_x," Atmos. Environ., 34, 2063-2101.

Becker , K. H. (1996): "The European Photoreactor EUROPHORE: Design and Technical Development of the European Photoreactor and First Experimental Results," Final Report of the EC-Project Contract EV5V-CT92-0059, February.

CARB (1993): "Proposed Regulations for Low-Emission Vehicles and Clean Fuels -- Staff Report and Technical Support Document," California Air Resources Board, Sacramento, CA, August 13, 1990. See also Appendix VIII of "California Exhaust Emission Standards and Test Procedures for 1988 and Subsequent Model Passenger Cars, Light Duty Trucks and Medium Duty Vehicles," as last amended September 22, 1993. Incorporated by reference in Section 1960.

CARB (2000): "Initial Statement of Reasons for the Proposed Amendments to the Regulation for Reducing Volatile Organic Compound Emissions from Aerosol Coating Products and Proposed Tables of Maximum Incremental Reactivity (MIR) Values, and Proposed Amendments to Method 310, 'Determination of Volatile Organic Compounds in Consumer Products'," California Air Resources Board, Sacramento, CA, May 5.

CARB (2003): "Architectural Coatings – Reactivity Page," California Air Resources Board web page at http://www.arb.ca.gov/coatings/arch/reactivity/reactivity.htm, November.

Carter, W. P. L. (1988): "Documentation of a Gas Phase Photochemical Mechanism for Use in Airshed Modeling," Final report on California ARB Contract No. A5-122-32, October.

Carter, W. P. L. (1994): "Development of Ozone Reactivity Scales for Volatile Organic Compounds," J. Air & Waste Manage. Assoc., 44, 881-899.

Carter, W. P. L. (2000a): "Documentation of the SAPRC-99 Chemical Mechanism for VOC Reactivity Assessment," Report to the California Air Resources Board, Contracts 92-329 and 95-308, May 8. Available at http://cert.ucr.edu/~carter/absts.htm#saprc99 and http://www.cert.ucr.edu/~carter/reactdat.htm.

Carter, W. P. L. (2000b): "Implementation of the SAPRC-99 Chemical Mechanism into the Models-3 Framework," Report to the United States Environmental Protection Agency, January 29. Available at http://www.cert.ucr.edu/~carter/absts.htm#s99mod3.

Carter, W. P. L. (2002a): "Development of a Next-Generation Environmental Chamber Facility for Chemical Mechanism and VOC Reactivity Research," Draft Research Plan and First Progress Report to the United States Environmental Protection Agency Cooperative Agreement CR 827331-01-0. January 3.

Carter, W. P. L. (2002b): "Development of a Next Generation Environmental Chamber Facility for Chemical Mechanism and VOC Reactivity Research," Summary of Progress and Current Status, October 20. Available at http://www.cert.ucr.edu/~carter/epacham.

Carter, W. P. L. (2002c): “Data Processing Procedures for UCR EPA Environmental Chamber Experiments, Appendix B To Quality Assurance Project Plan.” Prepared for the United States Environmental Protection Agency Cooperative Agreement CR 827331-01-0, April 25. Available at http://www.cert.ucr.edu/~carter/epacham.

Carter, W. P. L. (2003a): “The SAPRC-99 Chemical Mechanism and Updated VOC Reactivity Scales,” http://www.cert.ucr.edu/~carter/reactdat.htm. Last modified February 5.

Carter, W. P. L. (2003b): “Updated Chemical Mechanism for Airshed Model Applications,” Research Proposal to the California Air Resources Board, October.

Carter, W. P. L., R. Atkinson, A. M. Winer, and J. N. Pitts, Jr. (1982): “Experimental Investigation of Chamber-Dependent Radical Sources,” Int. J. Chem. Kinet., 14, 1071.

Carter, W. P. L. and R. Atkinson (1987): "An Experimental Study of Incremental Hydrocarbon Reactivity," Environ. Sci. Technol., 21, 670-679

Carter, W. P. L. and R. Atkinson (1987): “Development and Implementation of an Up-to-Date Photochemical Mechanism for Use in Airshed Modeling,” Final Report, California Air Resources Board Contract No. A5-122-32, October.

Carter, W. P. L., and F. W. Lurmann (1990): “Evaluation of the RADM Gas-Phase Chemical Mechanism,” Final Report, EPA-600/3-90-001.

Carter, W. P. L. and F. W. Lurmann (1991): “Evaluation of a Detailed Gas-Phase Atmospheric Reaction Mechanism using Environmental Chamber Data,” Atm. Environ. 25A, 2771-2806.

Carter, W. P. L., J. A. Pierce, I. L. Malkina, D. Luo and W. D. Long (1993): “Environmental Chamber Studies of Maximum Incremental Reactivities of Volatile Organic Compounds,” Report to Coordinating Research Council, Project No. ME-9, California Air Resources Board Contract No. A032-0692; South Coast Air Quality Management District Contract No. C91323, United States Environmental Protection Agency Cooperative Agreement No. CR-814396-01-0, University Corporation for Atmospheric Research Contract No. 59166, and Dow Corning Corporation. April 1.

Carter, W. P. L., D. Luo, I. L. Malkina, and D. Fitz (1995a): “The University of California, Riverside Environmental Chamber Data Base for Evaluating Oxidant Mechanism. Indoor Chamber Experiments through 1993,” Report submitted to the U. S. Environmental Protection Agency, EPA/AREAL, Research Triangle Park, NC., March 20..

Carter, W. P. L., D. Luo, I. L. Malkina, and J. A. Pierce (1995b): “Environmental Chamber Studies of Atmospheric Reactivities of Volatile Organic Compounds. Effects of Varying Chamber and Light Source,” Final report to National Renewable Energy Laboratory, Contract XZ-2-12075, Coordinating Research Council, Inc., Project M-9, California Air Resources Board, Contract A032-0692, and South Coast Air Quality Management District, Contract C91323, March 26. Available at http://www.cert.ucr.edu/~carter/absts.htm#explrept.

Carter, W. P. L., D. Luo, and I. L. Malkina (1997): “Environmental Chamber Studies for Development of an Updated Photochemical Mechanism for VOC Reactivity Assessment,” final report to California Air Resources Board Contract 92-345, Coordinating Research Council Project M-9, and National Renewable Energy Laboratory Contract ZF-2-12252-07. November 26.

Carter, W. P. L., J. H. Seinfeld, D. R. Fitz, and G. S. Tonnesen (1999): “Development of a Next-Generation Environmental Chamber Facility for Chemical Mechanism and VOC Reactivity Evaluation,” Proposal to the U. S. Environmental Protection Agency, February 22. Available at http://www.cert.ucr.edu/~carter/epacham.

Carter. W. P. L., D. Luo and I. L. Malkina (2000): “Investigation of Atmospheric Reactivities of Selected Consumer Product VOCs,” Report to California Air Resources Board, May 30. Available at http://www.cert.ucr.edu/~carter/absts.htm#cpreport.

Carter, W. P. L. and I. L. Malkina (2002): “Development and Application ff Improved Methods for Measurement of Ozone Formation Potentials of Volatile Organic Compounds,” Final report to California Air Resources Board Contract 97-314, May 22.

CEAM (2004): “CEAM Foundation Webpages; Research Area: ‘Atmospheric Chemistry’,” Web page at http://www.gva.es/ceam/index_i.htm, January 30.

Dodge, M. C. (2000): “Chemical Oxidant Mechanisms for Air Quality Modeling, Critical Review Paper for 1998 Ozone Assessment,” Atmos. Environ, 34, 2103-2130.

Fitz, D., L., W. P. L. Carter, and E. C. Tuazon (2000): “Measurement of Nitrogenous Species and Solar Intensity during the 1997 Southern California Oxidant Study,” Final Report to California Air Resources Board Contract No. 96-540, March 1.

Gaffney, J. S, Bornick, R. M., Chen, Y-H and Marley, N. A. (1998): “Capillary gas chromatographic analysis of nitrogen dioxide and PANs with luminol chemiluminescent detection,” Atmos. Environ. 32, pp.1445-1454.

Gery, M. W., G. Z. Whitten, and J. P. Killus (1988): "Development and Testing of the CBM-IV For Urban and Regional Modeling,", EPA-600/ 3-88-012, January.

Hess G. D., F. Carnovale. M. E., Cope. and G. M. Johnson (1992)” ‘The evaluation of some photochemical smog reaction mechanisms – 1 temperature and initial composition effects’, Atmos. Environ., 26A, 625-641.

Hastie, D. R, Mackay, G. I., Iguchi, T., Ridley, B. A.; and Schiff, H. I. (1983): “Tunable diode laser systems for measuring trace gases in tropospheric air,” Environ. Sci. Technol. 17, 352A-364A.

Hynes,R., M. Azzi, and M. Cope (2003): “Simulating Environmental Chamber Experiments with Photochemical Models,” National Clean Air Conference: Linking Air Pollution Science, Policy and Management CASN03, November 23-27 2003 Newcastle, NSW, Australia.

IGC (2002): “Institute of Chemistry And Dynamics of the Geosphere, SAPHIR, Simulation of Atmospheric PHotochemistry In a large Reaction Chamber,” Web page at http://www.fz-juelich.de/icg/icg-ii/saphir/home, last modified December 9.

Imada, M. R. (1984): “Formaldehyde Gas Generation System,” Report #249, CA/DOH/AIHL/R-249, Air and Indusrial Hygiene Laboratory, Laboratory Services Branch, California Department of Health and Services, January,

Jacobsen, N. W. and R. G. Dickinson (1994): “Spectrometric Assay of Aldehydes as 6-Mercapto-3-substituted-s-triazolo(4,3-b)-s-tetrazines,” Analytical Chemistry 46/2 (1974) 298–299.

Jeffries, H. E. (1991): “UNC Solar Radiation Models,” unpublished draft report for EPA Cooperative Agreements CR813107, CR813964 and CR815779”.

Jeffries, H. E., Sexton, K. G., Kamens, R. M. and Holleman, M. S. (1985a): "Outdoor Smog Chamber Experiments to Test Photochemical Models: Phase II," Final Report, EPA-600/3-85-029.

Jeffries, H. E., Sexton, K. G., Morris, T. P., Jackson, H., Goodman, R. G., Kamens, R. M. and Holleman, M. S. (1985b): "Outdoor Smog Chamber Experiments Using Automobile Exhaust," Final Report, EPA-600/3-85-032.

Jeffries, H. E., K. G. Sexton, and M. S. Holleman (1985c): "Outdoor Smog Chamber experiments: Reactivity of Methanol Exhaust", Final Report, EPA-600/3-85-009a, September

Jeffries, H. E., K. G. Sexton, J. R. Arnold, Y. Bai, J. L. Li, and R. Crouse (1990): “A Chamber and Modeling Study to Assess the Photochemistry of Formaldehyde,” Report on EPA Cooperative Agreement CR-813964, Atmospheric Research and Exposure Assessment Laboratory, EPA, Research Triangle Park, NC.

Jeffries, H.E.; Gery, M.W.; and Carter, W.P.L. (1992): “Protocol for evaluating oxidant mechanisms for urban and regional models.” Report for U.S. Environmental Protection Agency Cooperative Agreement No. 815779, Atmospheric Research and Exposure Assessment Laboratory, Research Triangle Park, NC.

Jeffries et al (2000a): “Tennessee Valley Authority's Indoor Smog Chamber Data for Low NOx and VOC Conditions,” Available at Available at http://airchem.sph.unc.edu/Research/Products/ ChamberData/TVAData/default.htm. Undated. Last accessed July, 2002

Jeffries et al (2000b): “CSIRO's Outdoor Smog Chamber Data for Low NOx and VOC Conditions,” Available at http://airchem.sph.unc.edu/Research/Products/ChamberData/CSIROData/default .htm. Undated. Last accessed July, 2002.

Johnson, G. M. (1983): "Factors Affecting Oxidant Formation in Sydney Air," in "The Urban Atmosphere -- Sydney, a Case Study." Eds. J. N. Carras and G. M. Johnson (CSIRO, Melbourne), pp. 393-408.

Holdren, M. W. and C. W. Spicer (1984): “Field Compatible Calibration Procedure for Peroxyacetyl Nitrate,” Environ. Sci. Technol., 18, 113-115.

Mentel T.F., D. Bleilebens. and A. Wahner (1996): “A study of nighttime nitrogen oxide oxidation in a large reaction chamber - the fate of NO_2 , $N_2 O_5$, HNO_3 , and O_3 at different humidities.” Atmos. Environ., 30, 4007-4020.

NIOSH (1994): “Sulfite titration of formaldehyde stock solution: modified Method 3500,” NIOSH Manual of Analytical Methods, NMAM, fourth edition, August 15.

Peterson, J. T. (1976): “Calculated Actinic Fluxes (290 - 700 nm) for Air Pollution Photochemistry Applications”, EPA-600/4-76-025, June.

Quesenberry, M. S. and Y. C. Lee (1996): “A Rapid Formaldehyde Assay Using Puprald Reagent: Application under Periodation Conditions,” Analytical Biochemistry. 234, 50–55.

Schiff, H.. I., Mackay, G. I. and Bechara, J. (1994): "The Use of Tunable Diode Laser Absorption Spectroscopy for Atmospheric Measurements", Res. Chem. Intermed. 20, 1994, pp 525-556.

Simonaitis, R., J. Meagher, and E. M. Bailey (1997): "Evaluation of the condensed Carbon Bond Mechanism against smog chamber data at low VOC and NOx Concentrations," Atm. Environ. 31, 27-43

Simonaitis, R. and E. M. Bailey (1995): "Smog Chamber Studies at Low VOC and NO_x Concentrations: Phase I," Report on Interagency Agreement DW64936024 to EPA/NREL, Research Triangle Park, NC.

Stockwell, W. R., P. Middleton, J. S. Chang, and X. Tang (1990): "The Second Generation Regional Acid Deposition Model Chemical Mechanism for Regional Air Quality Modeling," J. Geophys. Res. 95, 16343- 16376.

Tonnesen, G. S., Carter, W. P. L., and Brune, W. H. (2002): "Experimental Evaluation of Observation Based Methods for Assessing the Sensitivity of Ozone to VOC and NO_x", Proposal to the United States Environmental Protection Agency, December 4. Available at http://www.cert.ucr.edu/ ~carter/epacham/obmprop.pdf

Wahner, A. (1998): Private communication to M. C. Dodge. See also http://www.kfa-juelich.de/icg/icg3/ KOOP/atmoskam.html.

Wahner, A., T. F. Mentel and M. Sohn (1998): "Gas-Phase Reaction of N_2O_5 with water vapor: Importance of Heterogeneous Hydrolysis of N_2O_5 aand Surface Desorption of HNO_3 in a Large Teflon Chamber," Geophys. Res. Lett. 25, 2169-2172.

APPENDIX A. LISTINGS AND TABULATIONS

UCR EPA Chamber Run Summary

Table A-1. Summary of environmental UCR EPA environmental chamber experiments carried out or modeled for this project.

Run	Date	Type	Purpose and Applicable Conditions.	Results
55	1/10/03	CO - Air	Determine NO_x and formaldehyde offgasing	Some problems with lamp and reactor, but results useable. Results on Table 8 and Figure B-1
56	1/14/03	CO - Air	Repeat of previous experiment	See Table 8, Table 12 and Figure B-1
57	1/15/03	CO - NO_x	Determine radical source and formaldehyde offgasing at ~50 ppb initial NOx. NO injected on one side, NO_2 the other to vary NO_2 but not NO_x.	See Table 8, Table 12and Figure B-6
58	1/16/03	CO - NO_x	Similar to previous run but with higher (~90 ppb) initial NO_x.	See Table 8, Table 12 and Figure B-7.
59	1/17/03	O_3 Dark decay	CO added to test for dilution and O_3 added to test for O_3 loss on walls in dark.	No measurable dilution. Results on Table 7
60	1/21/03	CO - Air	Determine reproducibility and consistency of NO_x and formaldehyde offgasing	See Table 8, Table 12 and Figure B-2
61	1/22/03	CO - NO_x	Determine radical source with low (~10 ppb) initial NO_x	See Table 8, Table 12 and Figure B-7.
62	1/24/03	Actinometry	NO_2 photolysis rate measured inside one of the reactors and some light uniformity measurements made in same reactor.	Results indicated NO_2 photolysis rate in the reactor at the power setting used in these experiments was 0.26 min^{-1}; see Figure 4. Light uniformity was within ±~15% or better in most measurements, but additional measurements will be needed to completely characterize this.
63	1/28/03	CO - HCHO - Air	This amounts to formaldehyde actinometry because photolysis is calculated to be the major loss process. Also provides data on NO_x offgasing rate independent of radical source parameter.	Formaldehyde consumption rate consistent with NO_2 photolysis rate measured in previous run. See Table 8, Table 12and Figure B-5.
64	1/30/03	n-Butane - NO_x	Measure radical source rate using a somewhat different chemical system. 50 ppb NO_x.	Apparent radical source comparable to those indicated by the CO - NO_x runs. See Table 8, Table 12 and Figure B-10.

Table A-1 (continued)

Run	Date	Type	Purpose and Applicable Conditions.	Results
65	2/3/03	Propene - NO_x	Test performance of mechanism and characterization data with simple, reasonably well tested, chemical system, but at variable and low NO_x. ~6 ppb NO_x on one side, ~15 ppb NO_x on the other. Also test mechanism for proposed base ROG surrogate component.	See Table 14 and Figure B-13.
66	2/4/03	Toluene - NO_x + CO	Obtain a preliminary test of the toluene mechanism under low NO_x conditions. ~5 ppb NO_x both sides. CO added to one side only to determine effect of "radical amplifier" species. Also test mechanism for proposed base ROG surrogate component.	Model does not correctly predict effect of adding CO. See Table 15 and Figure B-14.
67	2/7/03	m-Xylene - NO_x + CO	Similar purpose and procedure as for previous run, except with m-xylene. Also test mechanism for proposed base ROG surrogate component.	Model does not correctly predict effect of adding CO. See Table 15 and Figure B-18.
68	2/10/03	HCHO - CO - NO_x	Evaluate basic mechanism for formaldehyde and CO under conditions that should be relatively insensitive to chamber effects. Initial CO varied. NO_x ~20 ppb.	See Table 14 and Figure B-11
69	2/11/03	HCHO - NO_x	Sensitive to background VOC contamination. Also basic mechanism and characterization evaluation.	See Table 14 and Figure B-11. Assuming non-negligible background VOCs does not improve model fit, indicating that this is probably not important.
70	2/12/03	CO - NO_x	Evaluate consistency of radical source after experiments with various systems.	See Table 8, Table 12 and Figure B-7.
71	2/14/03	CO - NO_x (high NO_x)	Evaluate radical source at much higher NO_x levels than previous experiments, to determine NO_x dependency. Also vary NO_2. ~260 ppb NO added to one side, ~200 ppb NO_2 added to the other.	Results of added NO experiment reasonably well fit by default model, but results of high NO_2 experiment were unexpected and could not be well fit using any reasonable chamber effects parameters. See Table 8, Table 12, and Figure B-8.
72	2/19/02	Toluene - CO - NO_x	This was intended to be like EPA066 except with larger amounts of NO_x (~15 ppb), but CO was injected on both sides by mistake, so the same toluene - CO - ~15 ppb NOx mixture was irradiated on both sides.	The results were similar to the lower NO_x toluene - CO - NO_x experiment. See Table 14 and Figure B-15.

Table A-1 (continued)

Run	Date	Type	Purpose and Applicable Conditions.	Results
73	2/21/03	Ethene - NO_x	Test performance of mechanism and characterization data with simple chemical system, but at variable and low NO_x. ~10 ppb NO_x on one side, ~25 ppb NOx on the other. Also test mechanism for proposed base ROG surrogate component.	See Table 14 and Figure B-12.
74	2/25/03	Toluene - NO_x + CO	Repeat of previous toluene experiments with higher NO_x levels. Approximately 25 ppb NOx and 150 ppb toluene injected to both reactors, with ~45 ppm CO added to one reactor.	The results were similar to the previous experiments with toluene. See Table 14 and Figure B-16.
76	2/27/03	CO - Air	Determine if change in NO_x offgasing parameter after conducting a number of experiments with added NO_x. Approximately 75 ppm CO injected into both sides with no NO_x injections.	Results consistent with previous experiments. See Table 8, Table 12 and Figure B-2
77	2/28/03	Toluene - NO_x + CO	Repeat of previous higher NO_x toluene experiment EPA074, except with particle measurement instrumentation on line. Irradiation carried out for longer period than EPA074 but data after the first 6 hours not suitable for modeling because of problems with the light source.	The results were similar to the previous experiments with toluene. See Table 14 and Figure B-16. Discussion of the particle measurements is beyond the scope of this report.
	3/3/03 – 3/7/03	Construction	The reactors were opened to fix the mixing and exchange system, which leaked excessively when used. Also, the framework for the backup blacklight system was installed in the enclosure.	
79	3/11/03	CO - Air	Characterization run to evaluate NO_x offgasing. Also, check for changes in NOx offgasing after repairs to mixing system. ~75 ppm CO injected into both reactors with no NOx injection. <u>The average temperature in this experiment was ~7 degrees lower than for all the other experiments carried out around this time.</u>	The results indicated no increase in apparent NO_x offgasing compared to the previous runs. However, higher apparent NO_x or radical source offgasing in subsequent experiments suggests that the construction could have affected these parameters. See discussion in the text and Table 8, Table 12 and Figure B-3.
80	3/13/03	Old Standard "Low NO_x Full Surrogate"	Replicate reactants and approximate conditions of the standard "Low NO_x Full Surrogate" experiments used in previous reactivity studies. Injected ~100 ppb NO_x and ~4 ppmC "Full Surrogate" components, to duplicate approximate average for previous low NO_x full surrogate experiments. Irradiation for 6 hours.	Results are reasonably well simulated by the model, as was the case for the experiment when carried out in the older chambers. Good side equivalency. See Table 15 and Figure B-29.

Table A-1 (continued)

Run	Date	Type	Purpose and Applicable Conditions.	Results
81	3/17/03	ROG=2 ppmC and NOx=50 ppb	Variable ROG and NO_x surrogate evaluation. Same reactants on both sides.	Good side equivalency. See Table 15 and Figure B-27.
82	3/18/03	ROG=1 ppmC, NO_x=50 ppb Surrogate	Variable ROG and NO_x surrogate evaluation. Same reactants on both sides.	Good side equivalency. See Table 15 and Figure B-25.
83	3/20/03	ROG=1 ppmC, NO_x=50 ppb Surrogate + n-Octane	Incremental reactivity test experiment with a previously studied VOC as part of the variable ROG and NO_x surrogate evaluation. 250 ppb n-octane added to Side B.	See Table 15 and Figure B-26 for the results of the base case experiment. Added n-octane causes significant reduction in m-xylene consumption rates and slight reduction in O_3 formation in initial states of experiment, which is consistent with model prediction. Results of these n-octane reactivity experiments will be discussed in a subsequent report.
84	3/21/03	ROG=1 ppmC, NO_x=50 ppb Surrogate + m-Xylene	Incremental reactivity test experiment for variable ROG and NO_x surrogate evaluation. 30 ppb m-xylene added to Side A.	See Table 15 and Figure B-26 for results of the base case experiment. Added m-xylene causes increased initial O_3 formation but slight reduction in final O_3 level, which is consistent with model predictions. Results of these m-xylene reactivity experiments will be discussed in a subsequent report.
85	3/25/03	ROG=1 ppmC, NO_x=10 ppb Surrogate + n-Octane	Low NO_x incremental reactivity test experiment for variable ROG and NO_x surrogate evaluation. 200 ppb n-octane added to Side B.	See Table 15 and Figure B-22 for the results of the base case experiment. Effect of added n-octane qualitatively similar to the other n-octane reactivity experiments.
86	3/27/03	ROG=1 ppmC, NO_x=10 ppb Surrogate + m-Xylene	Low NO_x incremental reactivity test experiment for variable ROG and NO_x surrogate evaluation. 25 ppb m-xylene added to Side B.	See Table 15 and Figure B-22 for the results of the base case experiment. Effect of added m-xylene qualitatively similar to the other m-xylene reactivity experiments.
87	3/28/03	CO - Air	Characterization run to evaluate NO_x offgasing. Blacklight light source used. Although other blacklight runs are not modeled in this study, this was included for characterization purposes because of the uncertainty in when the apparent NO_x offgasing and radical source increased.	Results indicated the higher NO_x offgasing rates than observed in previous experiments, and higher NO_x offgasing on Side A than B. This results is characteristic of subsequent experiments. See Table 8, Table 12 and Figure B-3
95	4/15/03	ROG=1 ppmC, NO_x=25 ppb Surrogate + n-Octane	Incremental reactivity test experiment for variable ROG and NO_x surrogate evaluation. 200 ppb n-octane added to Side A. Note that this base case will become the standard "MOIR/2" base case for the coatings reactivity study. (This study will be discussed in a separate report.)	See Table 15 and Figure B-23 for the results of the base case experiment. Effect of added n-octane qualitatively similar to the other n-octane reactivity experiments.

Table A-1 (continued)

Run	Date	Type	Purpose and Applicable Conditions.	Results
96	4/16/03	ROG=1 ppmC, NO_x=100 ppb Surrogate	Variable ROG and NO_x surrogate evaluation. Same reactants on both sides for side equivalency test. (Desired initial NO_x was 50 ppb, but 100 ppb injected because of injection calculation error.)	Good side equivalency. Very significant model underprediction of O_3 formation. See Table 15 and Figure B-30.
97	4/17/03	ROG=0.5 ppmC, NO_x=5 ppb Surrogate	Low NO_x variable ROG and NO_x surrogate evaluation. Same reactants on both sides for side equivalency test.	Fair side equivalency, with slightly more O_3 on Side A. See Table 15 and Figure B-21.
98	4/18/03	ROG=0.1 ppmC, NO_x=5 ppb Surrogate	Low NO_x variable ROG and NO_x surrogate evaluation. Same reactants on both sides for side equivalency test.	Fair side equivalency; slightly more O_3 on Side A. See Table 15 and Figure B-20.
100	4/22/03	ROG=0.25 ppmC, NO_x=5 ppb Surrogate + m-Xylene	Low NO_x incremental reactivity test experiment for variable ROG and NO_x surrogate evaluation. 15 ppb m-xylene added to Side B. Initial formaldehyde uncertain because of lack of formaldehyde data and possible problems with formaldehyde injection.	The results of this experiment were reasonably consistent with model predictions, but were not used for model evaluation in this work because of the uncertainty in the initial formaldehyde concentration.
101	4/23/03	ROG=0.25 ppmC, NO_x=2 ppb Surrogate	Low NO_x variable ROG and NO_x surrogate evaluation. Same reactants on both sides for side equivalency test. No formaldehyde injected because formaldehyde injection system was not functioning.	Fair side equivalency, with slightly more O_3 on Side A. See Table 15 and Figure B-19.
103	4/25/03	CO - NO_x Irradiation	Characterization run to evaluate chamber radical source. 50 ppm CO and 25 ppb NO_x injected in both sides.	The results indicated relatively high radical source compared to most previous experiments and higher radical source on Side A than Side B. This is consistent with the blacklight run 87 and subsequent characterization experiments. See Table 8, Table 12 and Figure B-9
105	4/29/03	Actinometry	The NO_2 photolysis rate was measured at various locations, including inside each reactor.	The measured NO_2 photolysis rates were 0.264 and 0.259 min^{-1} inside Sides A and B, respectively. These are the same to within the experimental uncertainty, and within the range observed in previous and subsequent in-reactor actinometry experiments. The data indicate no trend in light intensity during the period of these experiments.
108	5/7/03	ROG=1 ppmC, NO_x=70 ppb Surrogate + m-Xylene	Incremental reactivity test experiment with a previously studied VOC as part of the variable ROG and NO_x surrogate evaluation. 20 ppb m-xylene added to Side A.	See Table 15 and Figure B-28 for the results of the base case experiment. Effect of added m-xylene qualitatively similar to the other m-xylene reactivity experiments.

Table A-1 (continued)

Run	Date	Type	Purpose and Applicable Conditions.	Results
110	5/9/03	ROG=0.5 ppmC, NO_x=30 ppb Surrogate + m-Xylene	Incremental reactivity test experiment for variable ROG and NO_x surrogate evaluation. 10 ppb m-xylene added to Side A. Note that this base case will become the standard "MIR" base case for the coatings reactivity study.	See Table 15 and Figure B-24 for the results of the base case experiment. Effect of added m-xylene qualitatively similar to the other m-xylene reactivity experiments.
112	5/12/03	CO - Air	Characterization run to evaluate apparent NO_x offgasing rates. 100 ppm CO added to both sides. No NO_x injected.	Results consistent with other characterization experiments carried out after run 79. See Table 8, Table 12 and Figure B-4
113	5/13/03	ROG=1 ppmC, NO_x=70 ppb Surrogate + n-Octane	Incremental reactivity test experiment with a previously studied VOC as part of the variable ROG and NO_x surrogate evaluation. 200 ppb n-octane added to Side B.	See Table 15 and Figure B-28 for the results of the base case experiment. Effect of added n-octane qualitatively similar to the other n-octane reactivity experiments.
114	5/14/03	ROG=0.5 ppmC, NO_x=30 ppb Surrogate + n-Octane	Incremental reactivity test experiment with previously studied VOC using the standard “MIR” base case used for the coatings reactivity study. 100 ppb n-octane added to Side B.	See Table 15 and Figure B-24 for the results of the base case experiment. Effect of added n-octane qualitatively similar to the other n-octane reactivity experiments.
115	5/15/03	CO - HCHO - Air	Characterization and control experiment that is sensitive to NO_x offgasing rates and is useful for actinometry because HCHO consumption is expected to be due only to photolysis. 80 ppm CO and 100 ppb formaldehyde injected into both sides. No NO_x injected.	The formaldehyde consumption rates were 9.2 and 7.1 x 10^{-4} min^{-1} on Sides A and B, respectively. These correspond to calculated NO_2 photolysis rates of respectively 0.25 and 0.19 min^{-1}, which are within the uncertainty range of the measurement. Somewhat more O_3 was formed in Side A. The data were fit with apparent NO_x offgasing rates, relative to the NO_2 photolysis rate, of 10 and 5 ppt, respectively. See Table 8, Table 12 and Figure B-5.
120	5/29/03	Actinometry	The NO_2 photolysis rate was measured at various locations, including inside each reactor.	The measured NO_2 photolysis rates were 0.262 and 0.251 min^{-1} inside Sides A and B, respectively. These are within the range observed in previous and subsequent in-reactor actinometry experiments, and indicate no trend in light intensity during the period of these experiments.
128	6/16/03	ROG=0.5 ppmC, NO_x=50 ppb Surrogate + n-Octane	Low ROG/NO_x Incremental reactivity test experiment with a previously studied VOC as part of the variable ROG and NO_x surrogate evaluation. 20 ppb m-xylene added to Side B.	See Table 15 and Figure B-24 for the results of the base case experiment. Effect of added n-octane qualitatively similar to the other n-octane reactivity experiments.

Table A-1 (continued)

Run	Date	Type	Purpose and Applicable Conditions.	Results
133	7/2/03	CO - HCHO - Air	Characterization and control experiment that is sensitive to NO_x offgasing rates and is useful for actinometry because HCHO consumption is expected to be due only to photolysis. 80 ppm CO and 100 ppb formaldehyde injected into both sides. No NO_x injected.	The formaldehyde consumption rates were 1.2 x 10^{-3} on both sides, which was about 25% higher than in the previous such experiment and also higher than expected from the NO_2 actinometry data. The apparent NO_x offgasing results were consistent with other characterization runs during this period. See Table 8, Table 12 and Figure B-6.
140	7/16/03	CO - NO_x Irradiation	Characterization run to evaluate chamber radical source. 50 ppm CO and 25 ppb NO_x injected in both sides.	Results consistent with other radical and NO_x source characterization runs carried out during this period. See Table 8, Table 12 and Figure B-9.
156	8/14/03	O_3 Decay	Ozone dark decay determination and control experiment for effect of dark O_3 on PM measurements. ~300 ppb O_3 injected in both sides and monitored for only 2 hours because of equipment problems.	Ozone decay rates much higher than expected based on other experiments, but the data were scattered. Results given on Table 7. Data not used for chamber characterization purposes.
158	8/16/03	O_3 Decay	Repeat of previous O_3 decay experiment but with longer exposure time. ~300 ppb O_3 injected in both sides and monitored for 2 hours.	Data are much less scattered and the results are in the expected range. Results given on Table 7
160	8/19/03	CO - Air	Characterization run to evaluate apparent NO_x offgasing rates. 100 ppm CO added to both sides. No NO_x injected.	Results consistent with other radical and NO_x source characterization runs carried out during this period. See Table 8, Table 12 and Figure B-4.

Chamber Effects Model Summary

Table A-2. Chamber wall effect and background characterization parameters used in the environmental chamber model simulations for mechanism evaluation.

Cham.		Value	Discussion
RN-I (ppb)			Ratio of the rate of wall + hν → HONO to the NO_2 photolysis rate. Assumed to account for the continuous, light-induced radical and NO_x source.
EPA 55-80		0.005	Derived from simulations of radical source and NO_x offgasing characterization experiments during this period. See Table 8. Note that for runs 81-168 the HONO input rates appear to be approximately a factor of 1.5 higher in Side A than Side B.
EPA 81-168	A	0.0085	
	B	0.0128	
TVA		(Not used)	Data for most experiments can be fit without assuming additional radical source. Probably there is some radical source, but its magnitude appears to be negligible compared to that resulting from the photolysis of the offgassed formaldehyde.
CSIRO (standard)		$6.0e\text{-}9 \times e^{-19.3/RT}$ where R=0.0019872 and T in ^oK.	Based on chamber effects model currently used for modeling the SAPRC Outdoor Teflon Chamber (OTC). The temperature dependence is necessary to simulate SAPRC OTC results at varying temperatures. At 300_oK, this gives a RN-I value not greatly different than the temperature-independent value of 0.066 ppb used by Hynes et al (2003).
CSIRO (high RS)		3 x CSIRO (std)	Because the standard model consistently underpredicted rates of O_3 formation and NO oxidation when simulating the CSIRO experiments, "High RS" calculations were conducted to determine the sensitivity to a threefold increase in the radical source.
Initial HONO (ppb)			Initial concentration of HONO in the experiments, either due to wall offgasing or injection with NO_x. For these chambers, it is assumed that the initial HONO is not injected with the NO_x.
EPA		0.05	This is based on the fact that approximately half of the characterization experiments between EPA 55 and 168 that are sensitive to initial HONO are somewhat better fit using initial HONO of 0.1 ppb, and most of the rest are better fit by no initial HONO.
TVA		0.5	Average of initial HONO that gives best fits in model simulations of the CO - NO_x, methane - NO_x, and NO_x – air characterization experiments. See text.
CSIRO		0 - 2	No information is available to derive initial HONO. To assess sensitivities to this, the "Standard" model assumed no initial HONO while the "High HONO" model assumed an initial HONO of 2 ppb, The latter is probably higher than the likely upper limit.
E-NO2/K1 (ppb)			Ratio of the rate of wall + hν → NO_2 to the NO_2 photolysis rate. Used to account to NO_x input from the walls when it is assumed to be a separate process than HONO offgasing
EPA and CSIRO		(Not used)	The NO_x offgasing caused by representing the radical source by HONO offgasing appears to be sufficient for accounting for NOx offgasing effects. Results of model simulations of characterization experiments in the EPA chamber are generally consistent with this assumption.

Table A-2 (continued)

Cham.	Value	Discussion
TVA	0.0072	Average of NO_x input rate that gives best fits to O_3 formed in the acetaldehyde – air experiments.
k(NO2W) (min^{-1})		Rate of unimolecular loss (or hydrolysis) of NO_2 to the walls.
All Teflon Film Chambers	1.6e-4	Based on dark NO_2 decay and HONO formation measured in a ~3000-liter Teflon chamber by Pitts et al. (1984). Assumed to be the same in all chambers with Teflon film walls, regardless of volume.
YHONO		Yield of HONO in the unimolecular reaction (hydrolysis) of NO_2 on the walls.
All Teflon Film Chambers	0.2	Based on dark NO_2 decay and HONO formation measured in a ~3000-liter Teflon chamber by Pitts et al. (1984). Assumed to be the same in all chambers with Teflon film walls, regardless of volume.
k(O3W) (min^{-1})		Unimolecular loss rate of O3 to the walls.
EPA	1.08e-4	Based on results of O_3 decays in O_3 dark decay experiments EPA-158 and EPA-179, which gave reasonably consistent results and within the expected range based on O_3 decays in other reactors. Two other O_3 dark decay experiments were carried out with these reactors, but these are not used because one gave unexpectedly low and one gave unexpectedly high O_3 decay rates.
TVA	7.0e-4	From Meagher et al (1990) as used by Simonaitis et al (1997). Based on O_3 decay experiments in this chamber.
CSIRO	1.32e-4	Information concerning the O_3 decay rate in this chamber was not available. The O_3 decay rate is assumed to be similar to that in the EPA chamber.
Initial Formaldehyde (ppb)		Default initial concentration of formaldehyde in experiments where it is not measured. Represents effect of formaldehyde offgasing prior to start of experiment. Primarily needed for modeling the TVA chamber, where formaldehyde offgasing is significant.
EPA and CSIRO	0	No evidence of significant formaldehyde contamination in the beginning of the experiments in the EPA chamber. No information available about formaldehyde offgasing in the CSIRO chamber, but it is assumed to be negligible.
TVA	1	Based on formaldehyde measurements in experiments where formaldehyde was not injected but formaldehyde data are available.
k(N26I) (min^{-1})		Rate constant for N2O5 $\rightarrow$ 2 Wall-NOx. This represents the humidity-independent portion of the wall loss of N_2O_5, or the intercept of plots of rates of N_2O_5 loss against humidity.
All Teflon Film Chambers	2.8e-3	Based on N_2O_5 decay rate measurements made by Tuazon et al (1983) for a ~3000-liter Teflon film chamber. Assumed to be independent of chamber size (Carter et al, 1995c).
E-ALD/K1 (ppb)		Ratio of the rate of wall + hν $\rightarrow$ HCHO to the NO_2 photolysis rate. Used to account to direct formaldehyde offgasing from the walls.
EPA	0.010	Consistent with formaldehyde levels measured in characterization experiments carried out in 2003 with no injected formaldehyde or formaldehyde precursors.

Table A-2 (continued)

Cham.	Value	Discussion
TVA	0.045	Based on simulations of formaldehyde formation in experiments where no formaldehyde or formaldehyde source is injected. This is only part of the formaldehyde offgasing in this chamber, since the data also require assuming offgasing a reactive formaldehyde precursor. See text.
CSIRO	~0	This is not represented in modeling the CSIRO experiments. The effects of formaldehyde offgasing in surrogate experiments should be relatively small, and can be represented by using an appropriate magnitude of the chamber radical source parameter.
Formaldehyde Precursor Offgasing Rate (ppb/min)		Rate of reaction Walls → WallVOC, where WallVOC is used to represent an unknown reactive formaldehyde precursor compound that reacts via WallVOC + OH → HO2 + 0.2 HCHO, with a rate constant of 2×10^4 ppm^{-1} min^{-1}. This representation was derived by Simonaitis et al (1997) to fit the TVA formaldehyde data, and was adopted in our modeling of these data.
TVA	0.135	Based on simulations of formaldehyde formation in experiments where no formaldehyde or formaldehyde source is injected. This is only part of the formaldehyde offgasing in this chamber, since the data also require assuming continuous direct formaldehyde offgasing. See text.
All other chambers	0	There is no evidence of a formaldehyde offgasing problem similar to that observed in the TVA chamber in any other chambers we have modeled to date. The formaldehyde data in the EPA chamber in runs where it is not formed from gas-phase processes is adequately modeled assuming only direct formaldehyde offgasing.
k(N26S) (ppm^{-1} min^{-1})		Rate constant for N2O5 + H2O -> 2 Wall-NOx. This represents the humidity dependent portion of the wall loss of N_2O_5, or the slope of plots of rates of N_2O_5 loss against humidity.
All Teflon Film Chambers	1.1e-6	Based on N_2O_5 decay rate measurements made by Tuazon et al (1983) for a ~3000-liter Teflon film chamber. Assumed to be independent of chamber size (Carter et al, 1995d).
H2O (ppm)		Default water vapor concentration for runs where no humidity data are available.
EPA	3.4e+2	Only dry air experiments in the EPA chamber are modeled in this work. The humidity was too low to measure, indicating less than 1% RH. A H_2O level corresponding to ~1% RH at 300°K is used for modeling.
TVA	5.6e+3 – 1.0e+4	Derived on a run-to-run basis from the average temperature and average dew point given for the experiment in the UNC data summary.
CSIRO	9.5e+3	Default value given in datasets prepared by Jeffries et al (2003). This corresponds to a RH of 28% at 300°K. Although dried air was used when flushing the chamber, water vapor was injected along with the other reactants.

[a] Set refers to the characterization set, which refers to the group of experiments assumed to have the same run conditions and represented using the same chamber-dependent parameters. See Carter et al (1995) for more discussion. All experiments in this program were in DTC characterization set 18.

APPENDIX B. CHAMBER DATA PLOTS

UCR EPA Chamber Experiments

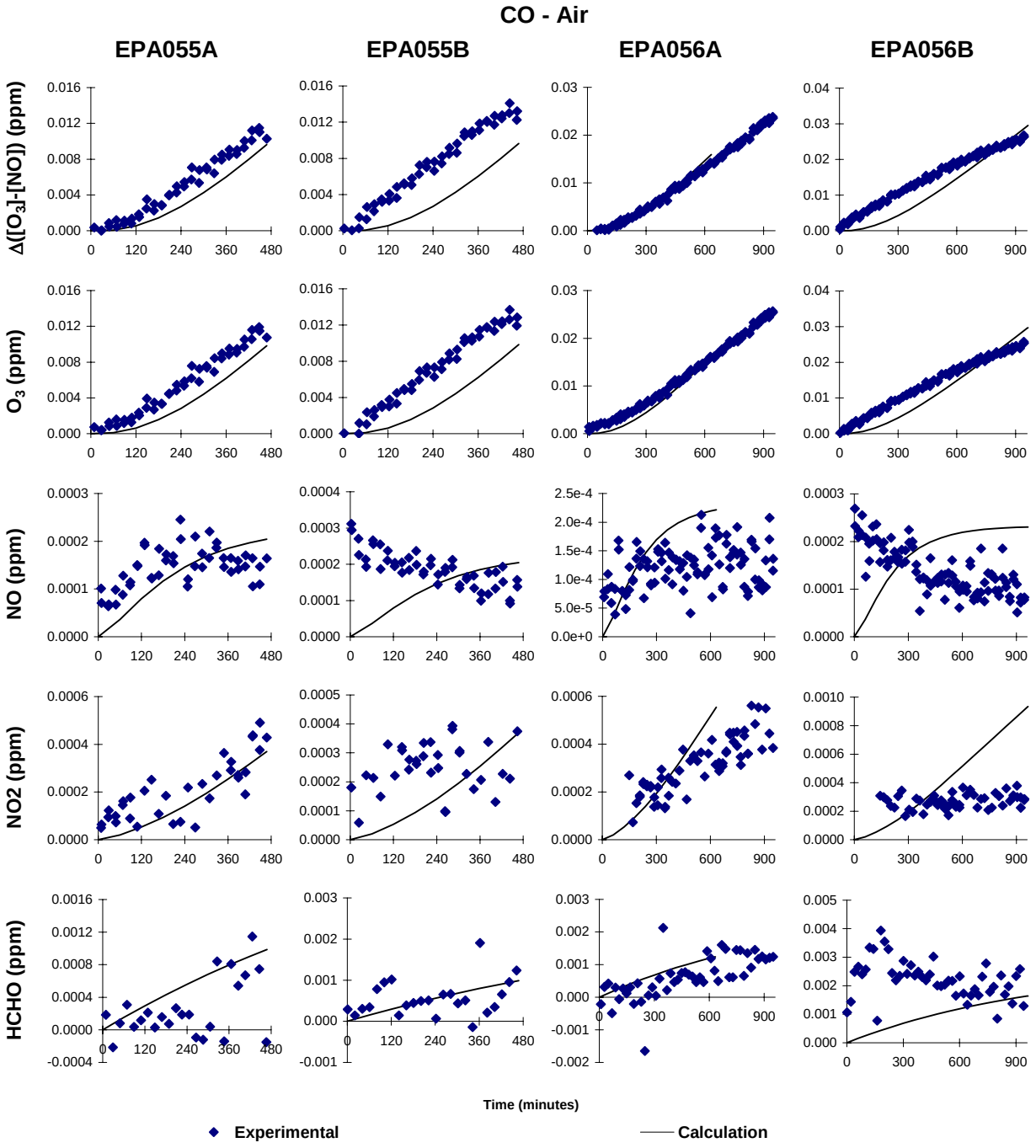

Figure B-1. Experimental and calculated concentration-time plots for selected compounds in the CO–air experiments EPA055 and EPA056.

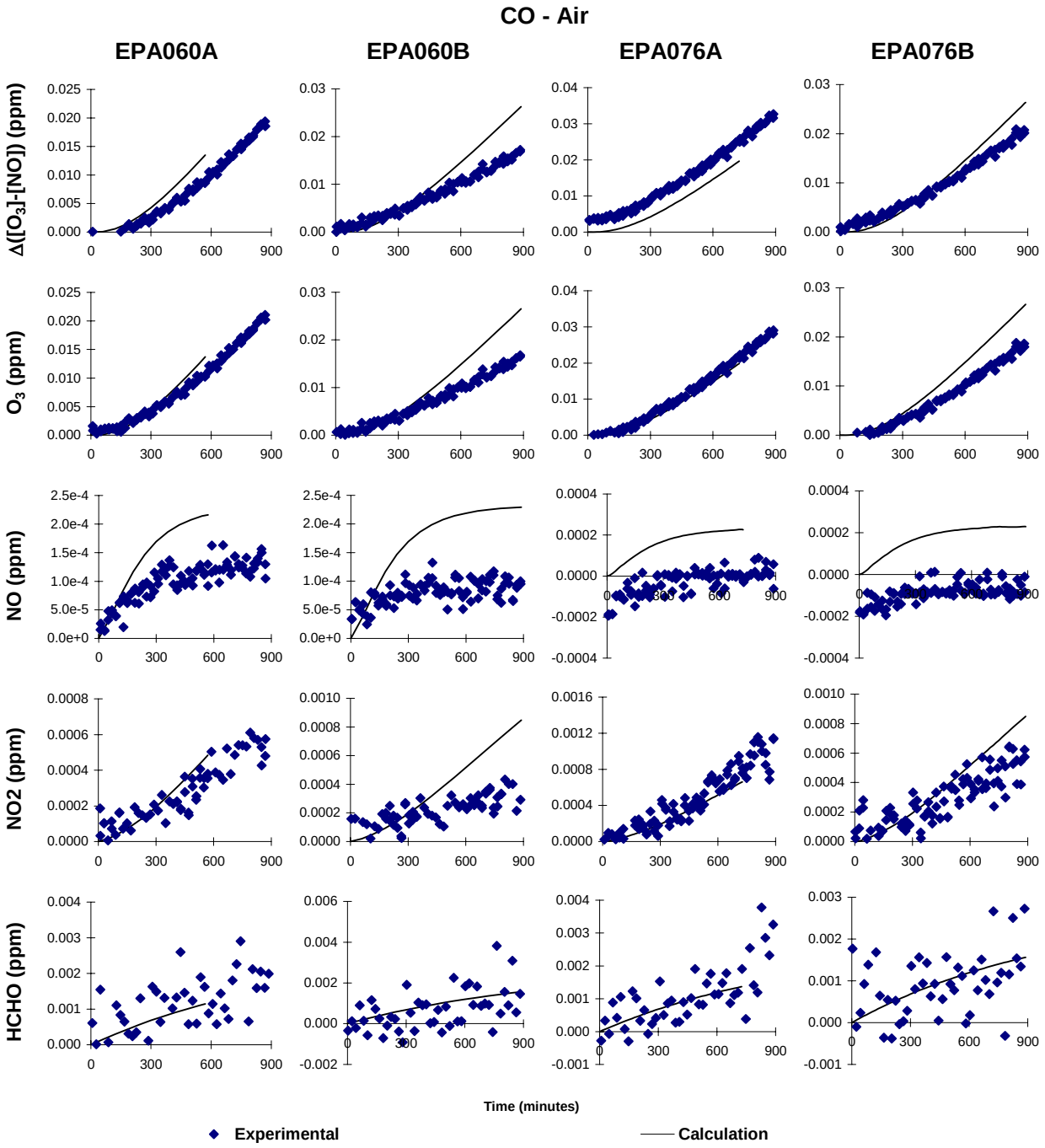

Figure B-2. Experimental and calculated concentration-time plots for selected compounds in the CO – air experiments EPA060 and EPA076.

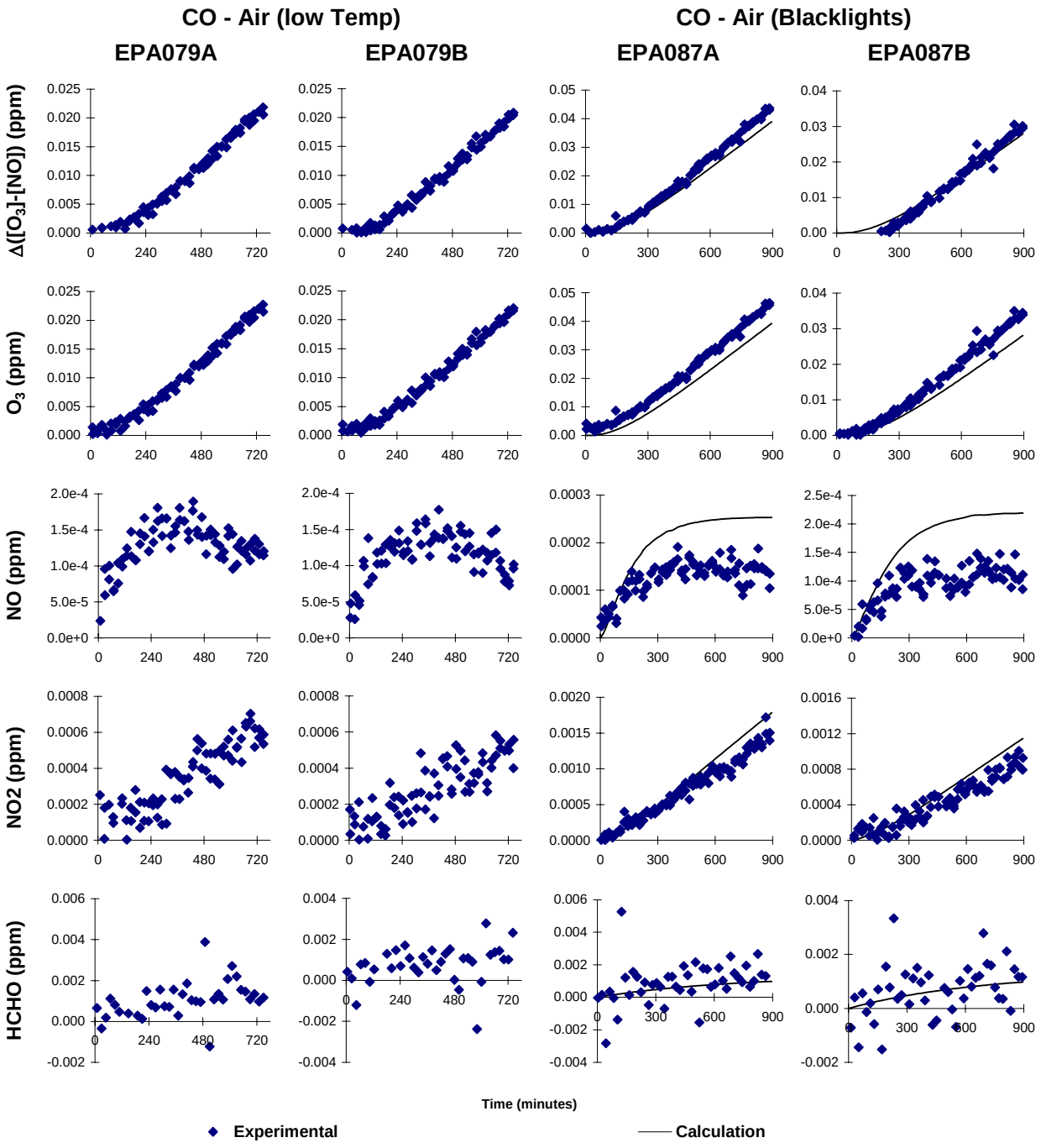

Figure B-3. Experimental and calculated concentration-time plots for selected compounds in the CO–air experiments EPA079 and EPA087. Run EPA079 was not modeled because there is no chamber characterization model assigned to this experiment, because was carried out at a lower temperature than the other characterization runs.

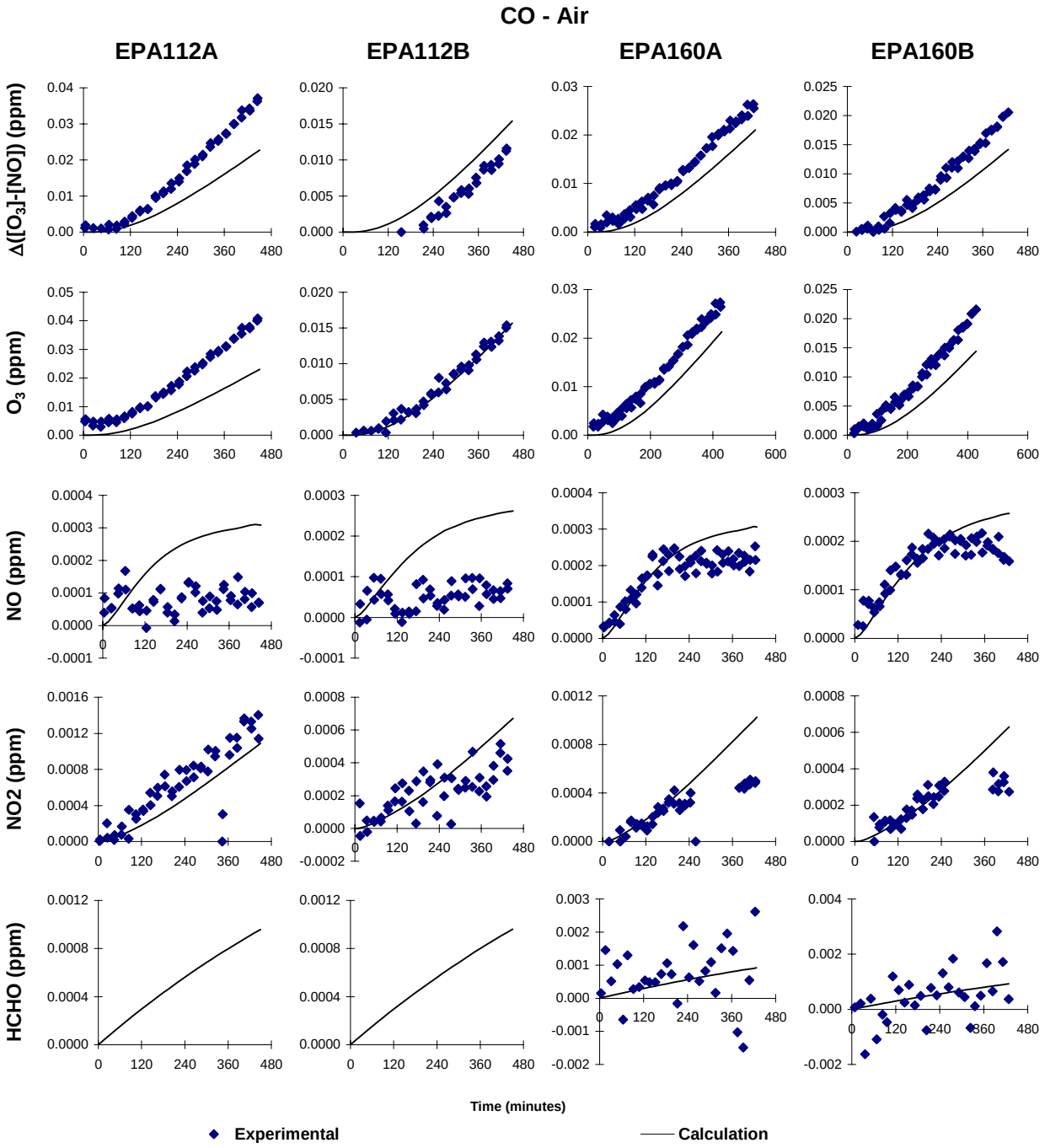

Figure B-4. Experimental and calculated concentration-time plots for selected compounds in the CO - air experiments EPA112 and EPA160.

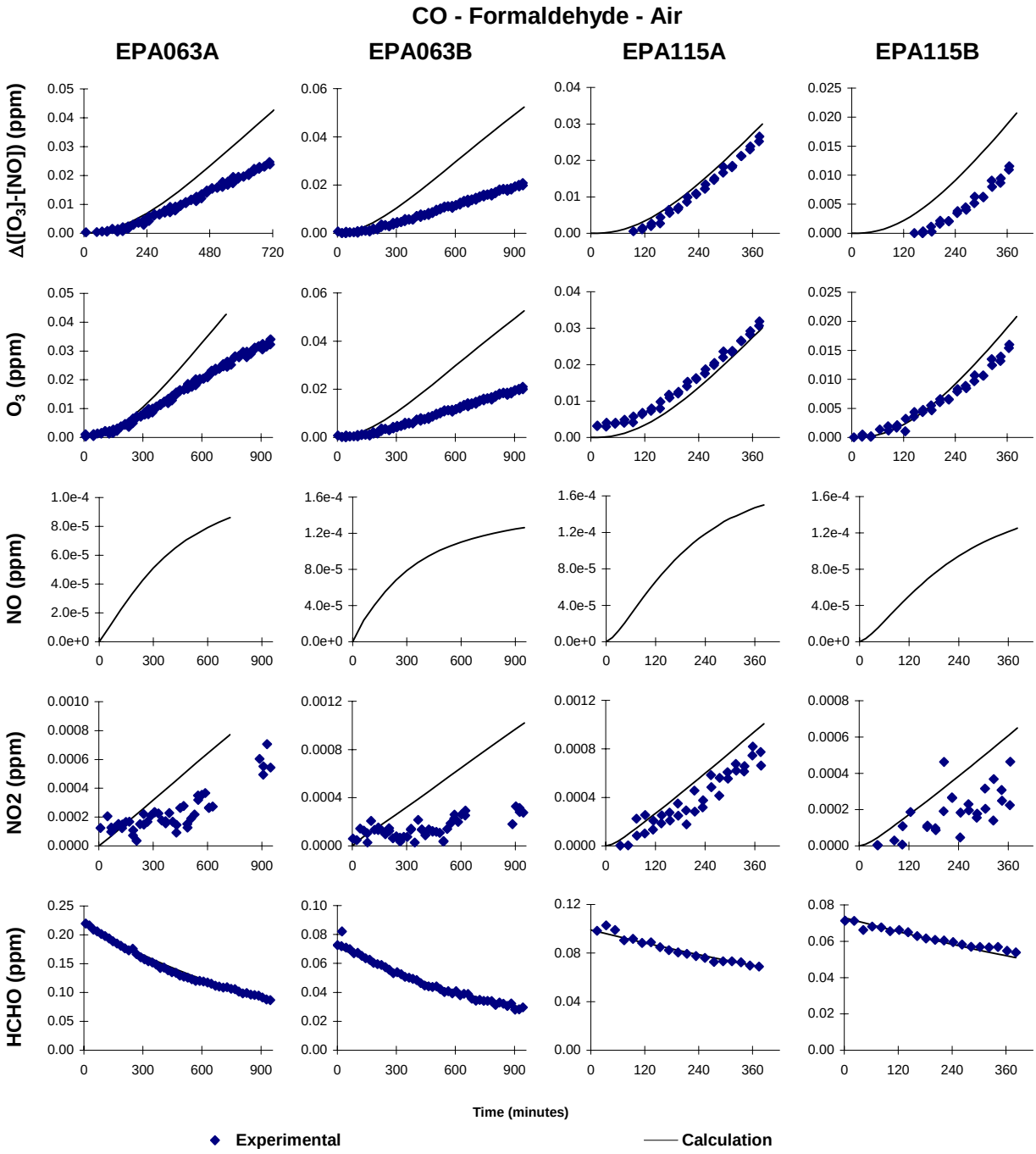

Figure B-5. Experimental and calculated concentration-time plots for selected compounds in the CO – formaldehyde – air experiments EPA063 and EPA115.

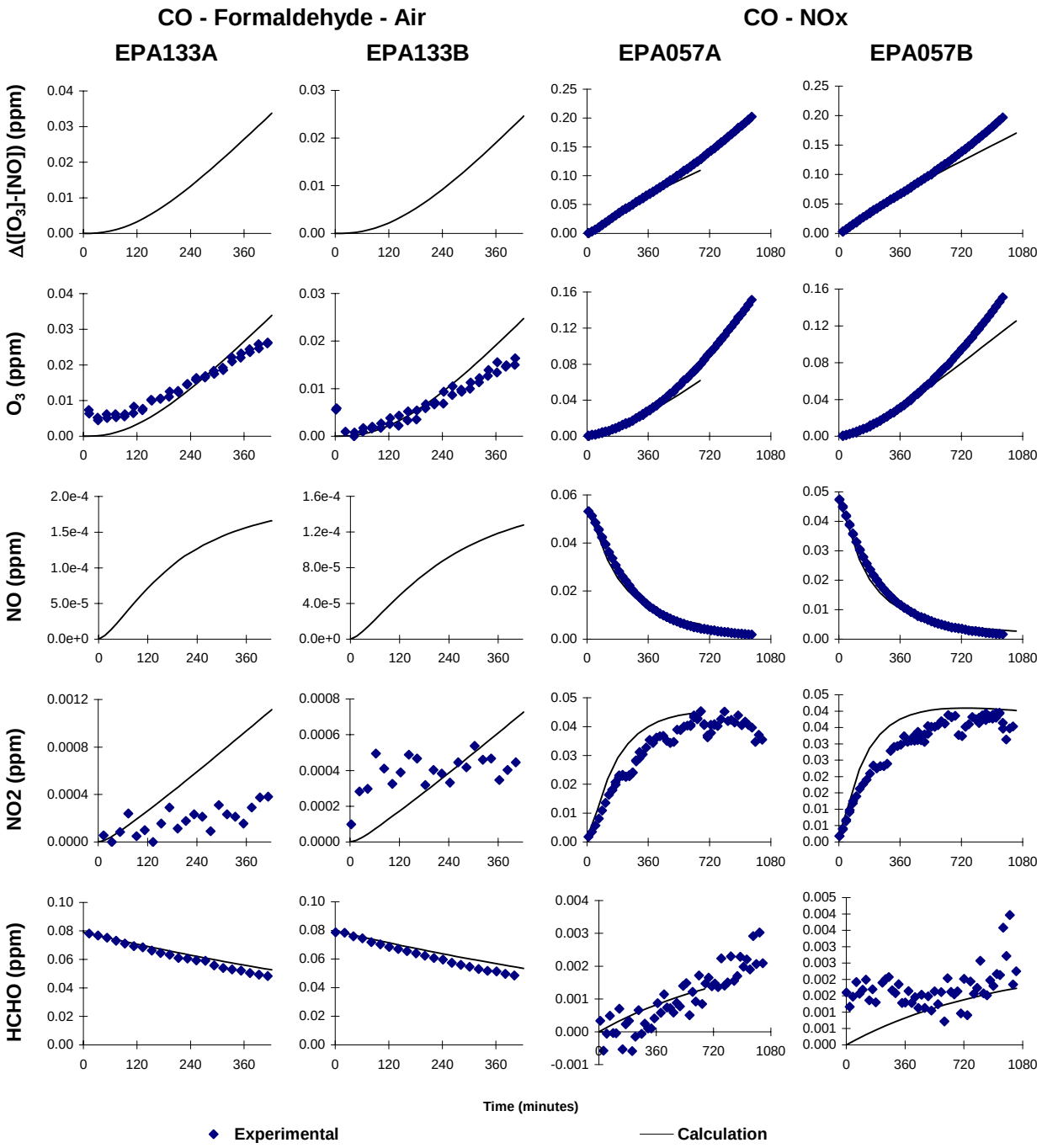

Figure B-6. Experimental and calculated concentration-time plots for selected compounds in the CO - formaldehyde - air experiment EPA133 and the CO - NO experiment EPA057.

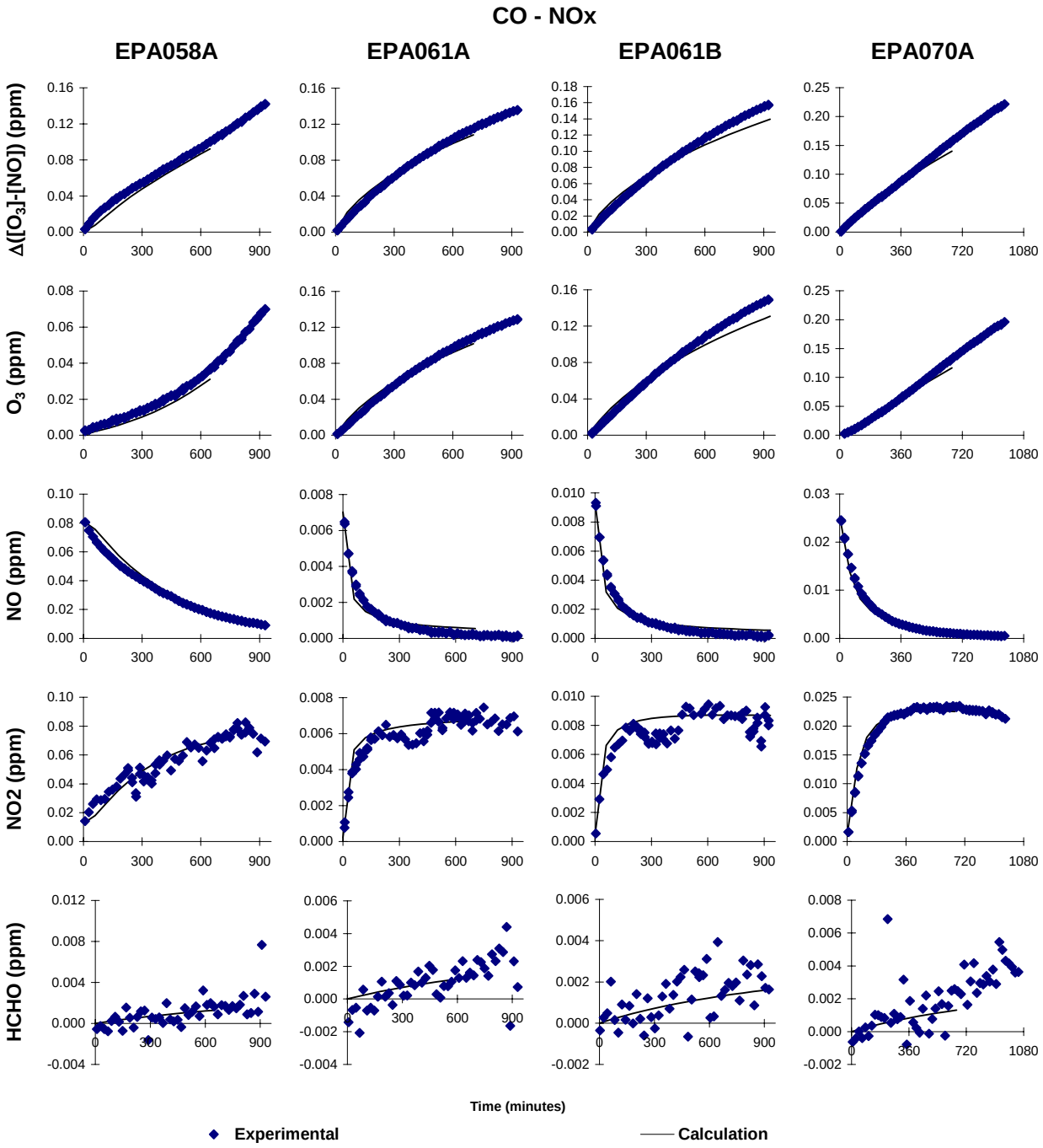

Figure B-7. Experimental and calculated concentration-time plots for selected compounds in the CO - NO experiments EPA058A, EPA061, and EPA070A

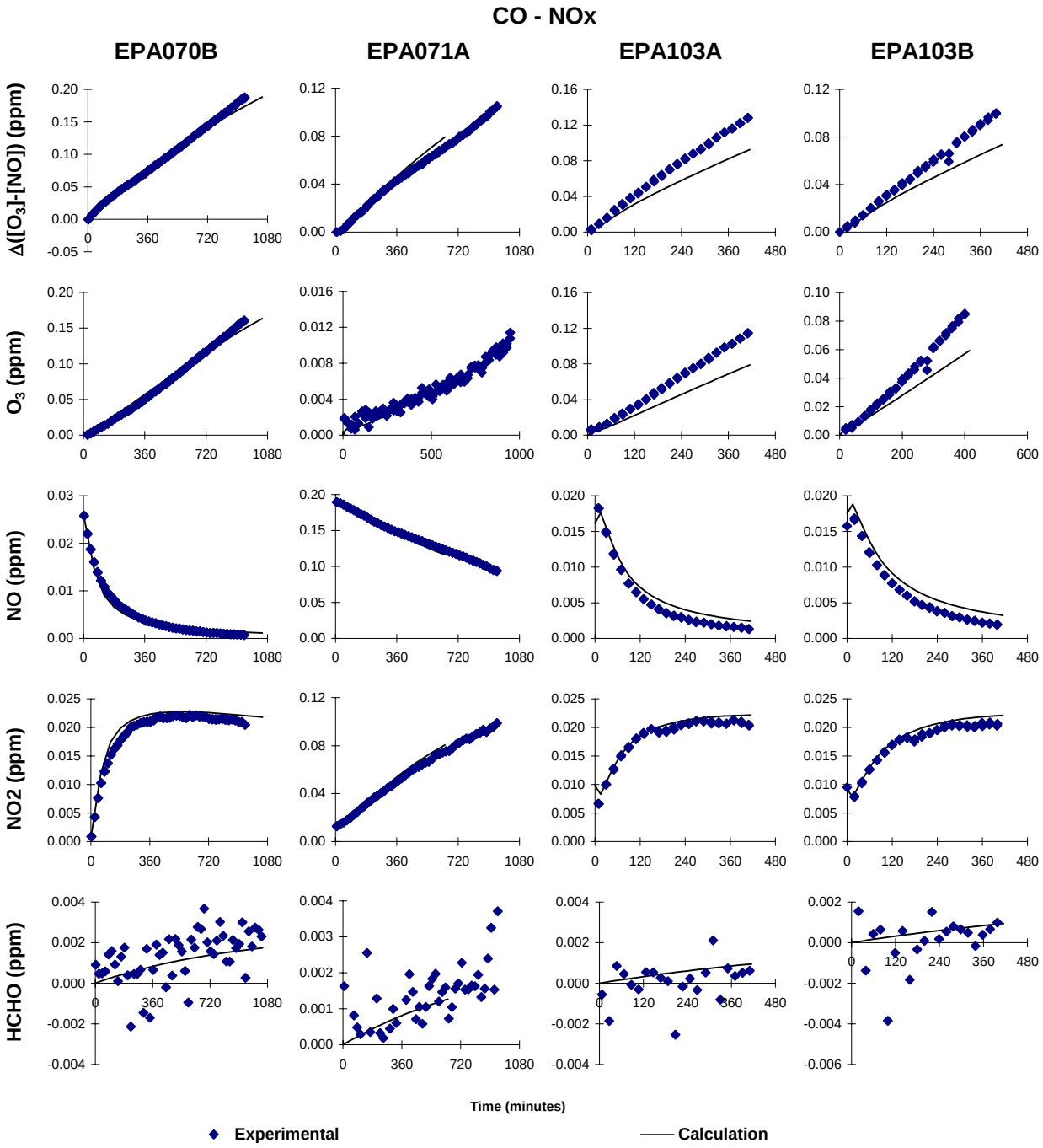

Figure B-8. Experimental and calculated concentration-time plots for selected compounds in the CO - NO experiments EPA070B, EPA071A, and EPA103.

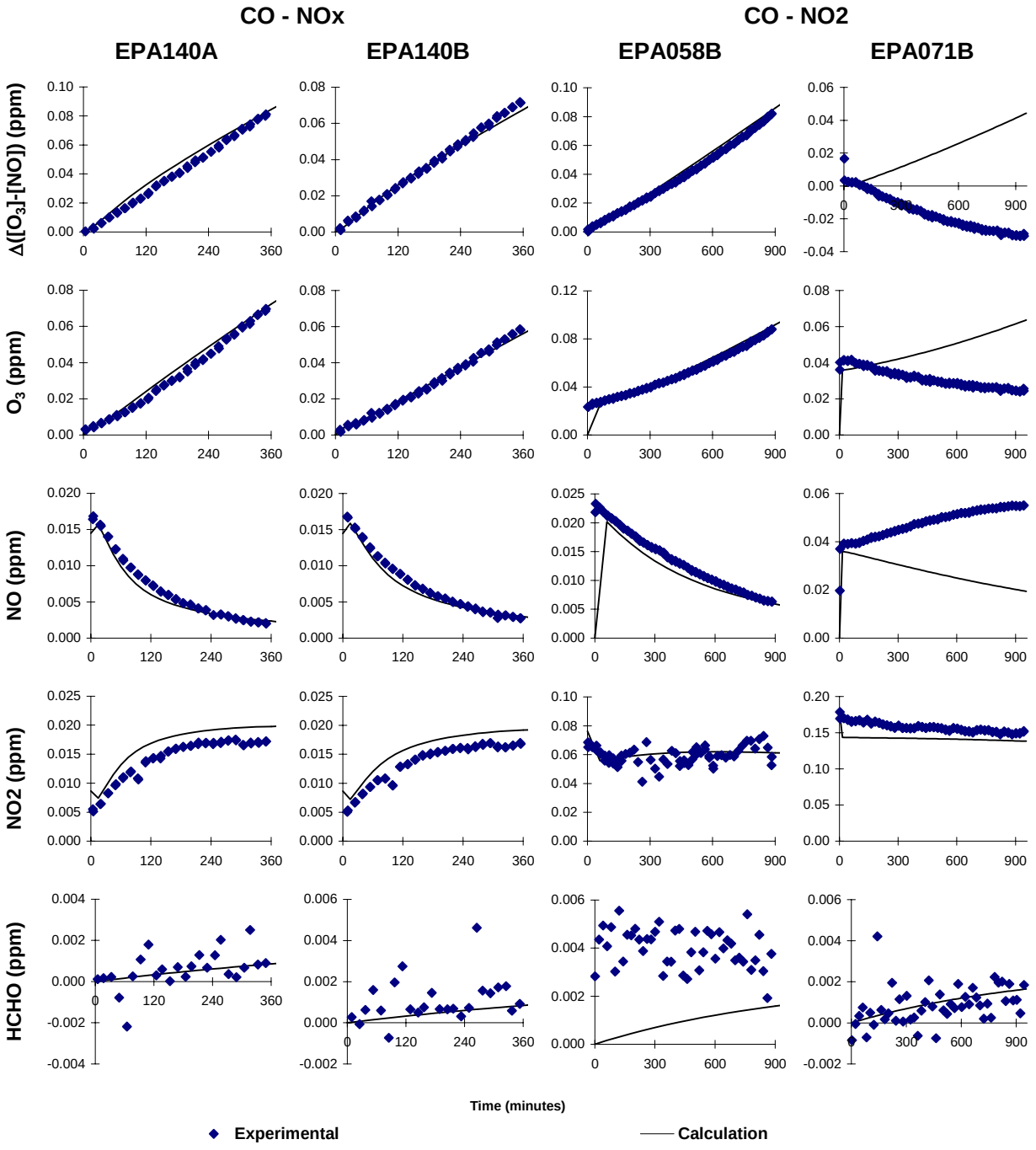

Figure B-9. Experimental and calculated concentration-time plots for selected compounds in the CO - NO experiments EPA140 and the CO - NO_2 experiments EPA058B and EPA071B.

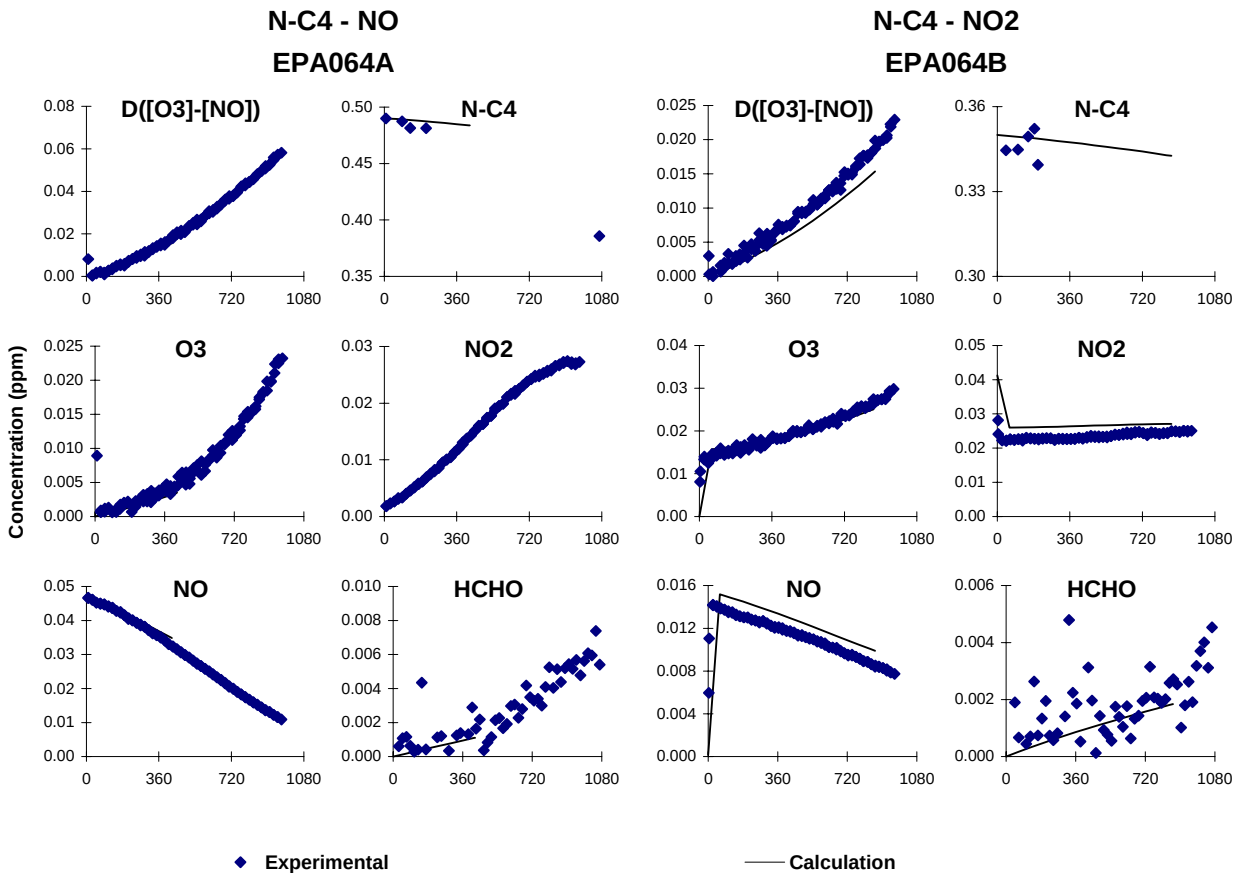

Figure B-10. Experimental and calculated concentration-time plots for selected compounds in the n-butane - NO_x experiment EPA064.

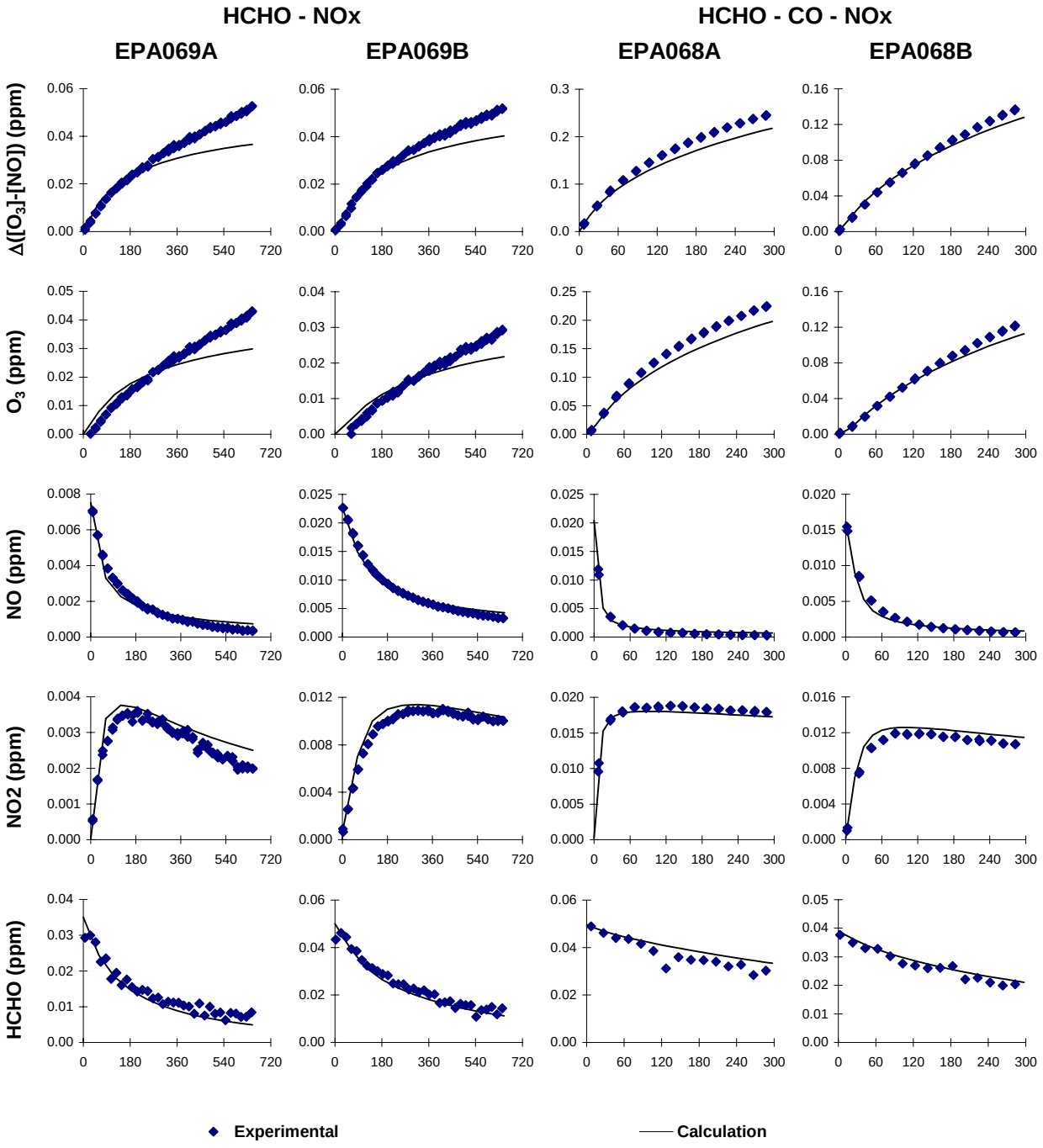

Figure B-11. Experimental and calculated concentration-time plots for selected compounds in the formaldehyde - NO_x experiment EPA068 and the formaldehyde - CO - NO_x experiment EPA069.

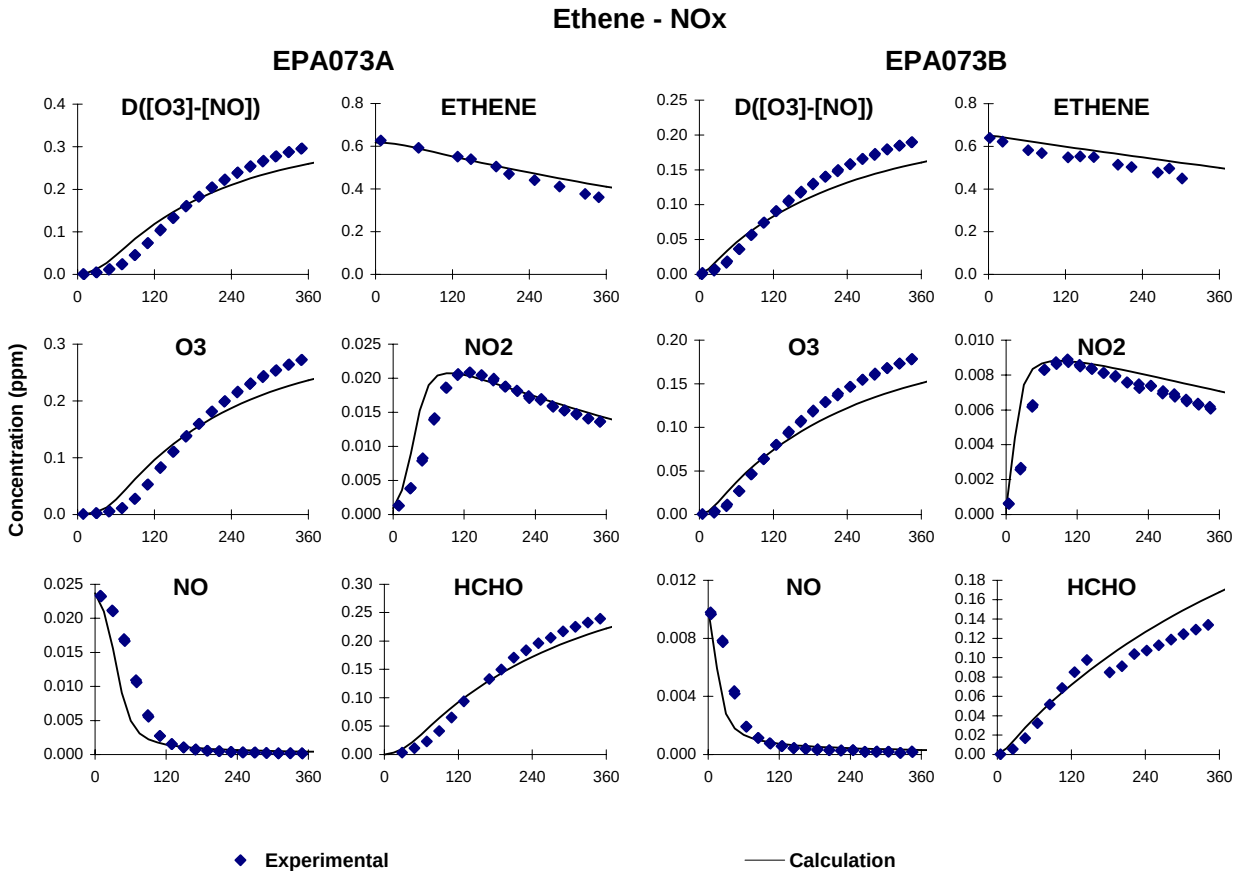

Figure B-12. Experimental and calculated concentration-time plots for selected compounds in the ethene - NO_x experiment EPA073.

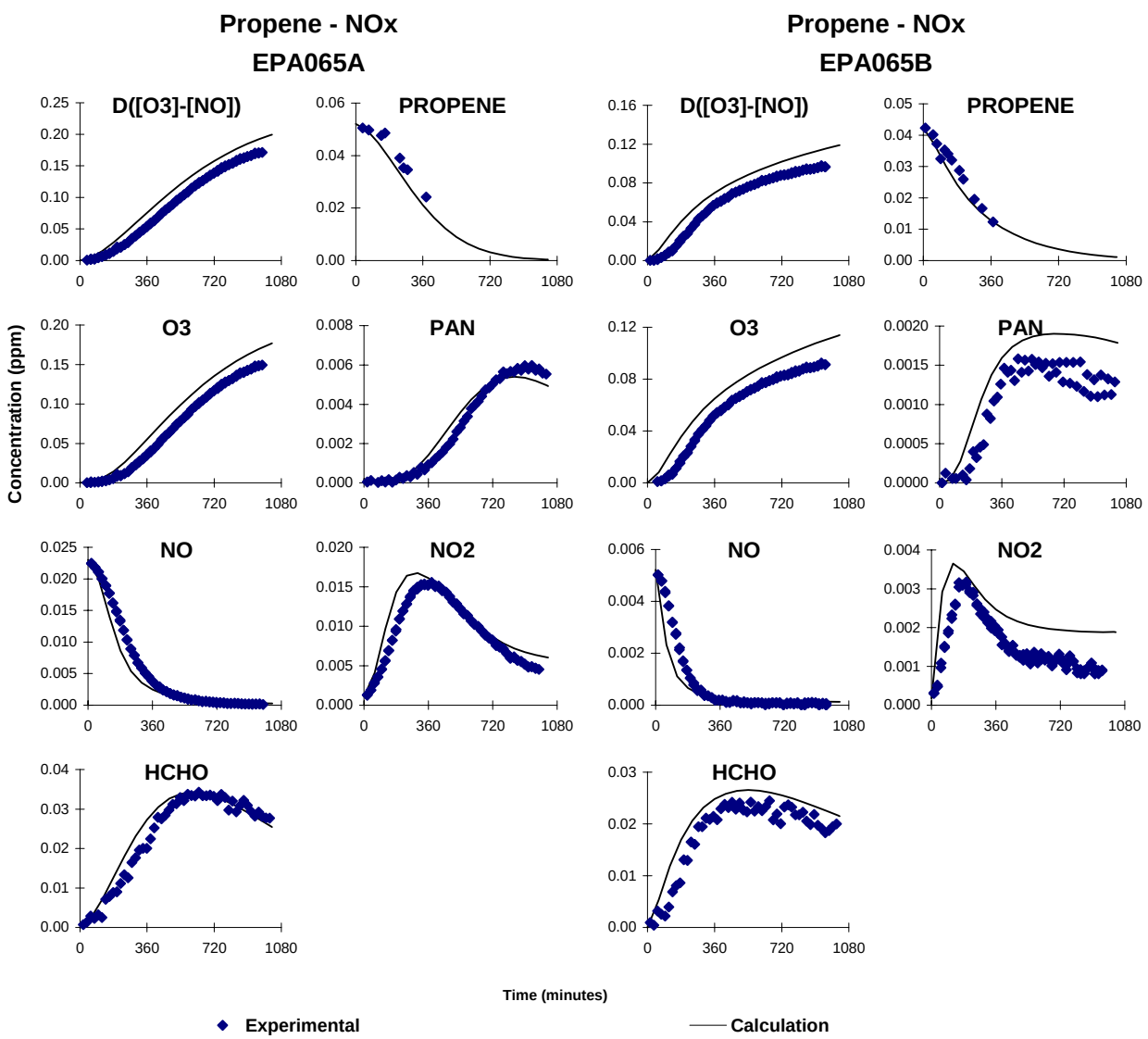

Figure B-13. Experimental and calculated concentration-time plots for selected compounds in the propene - NO_x experiment EPA065.

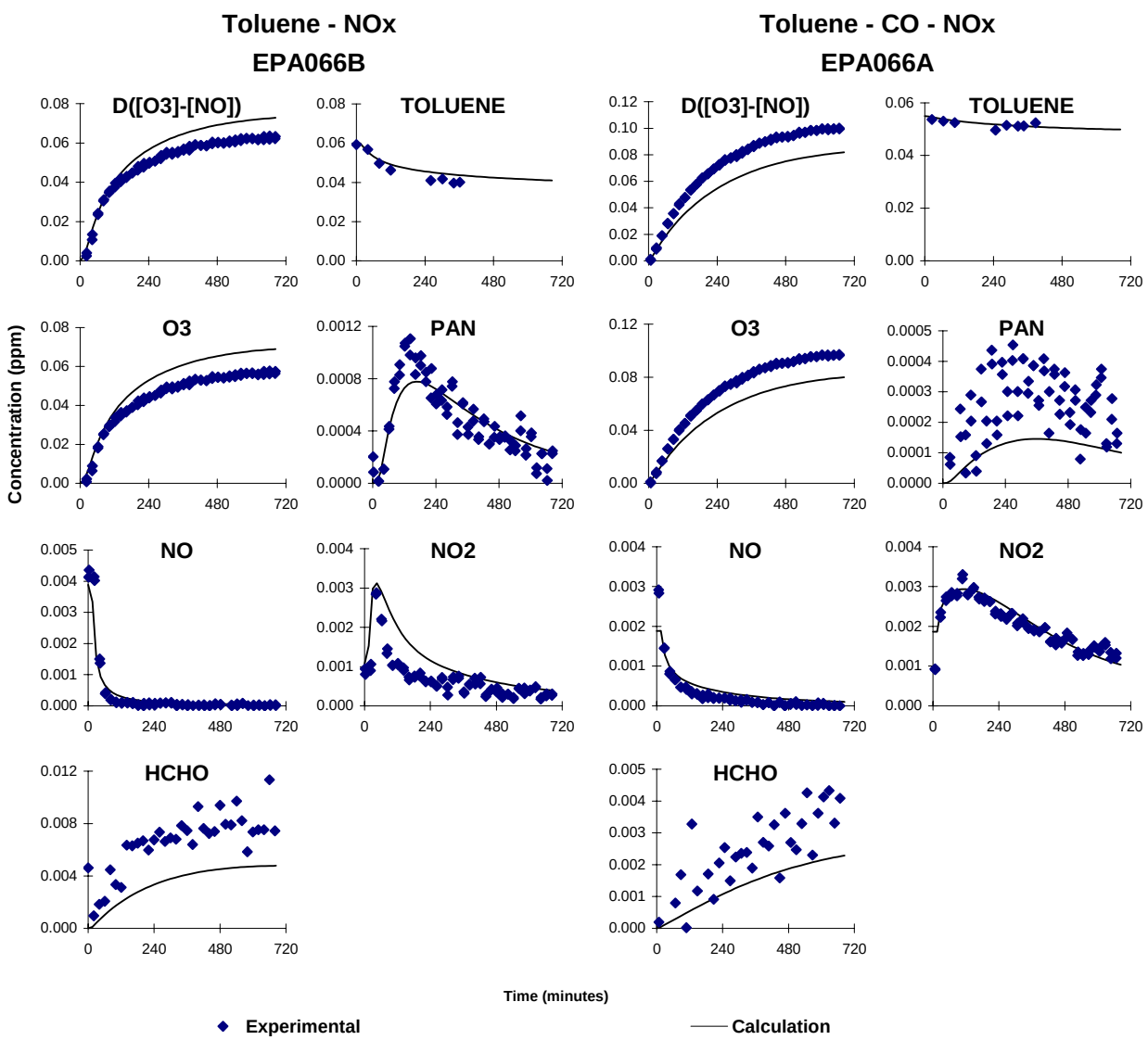

Figure B-14. Experimental and calculated concentration-time plots for selected compounds in the toluene and toluene – CO - NO_x experiment EPA066.

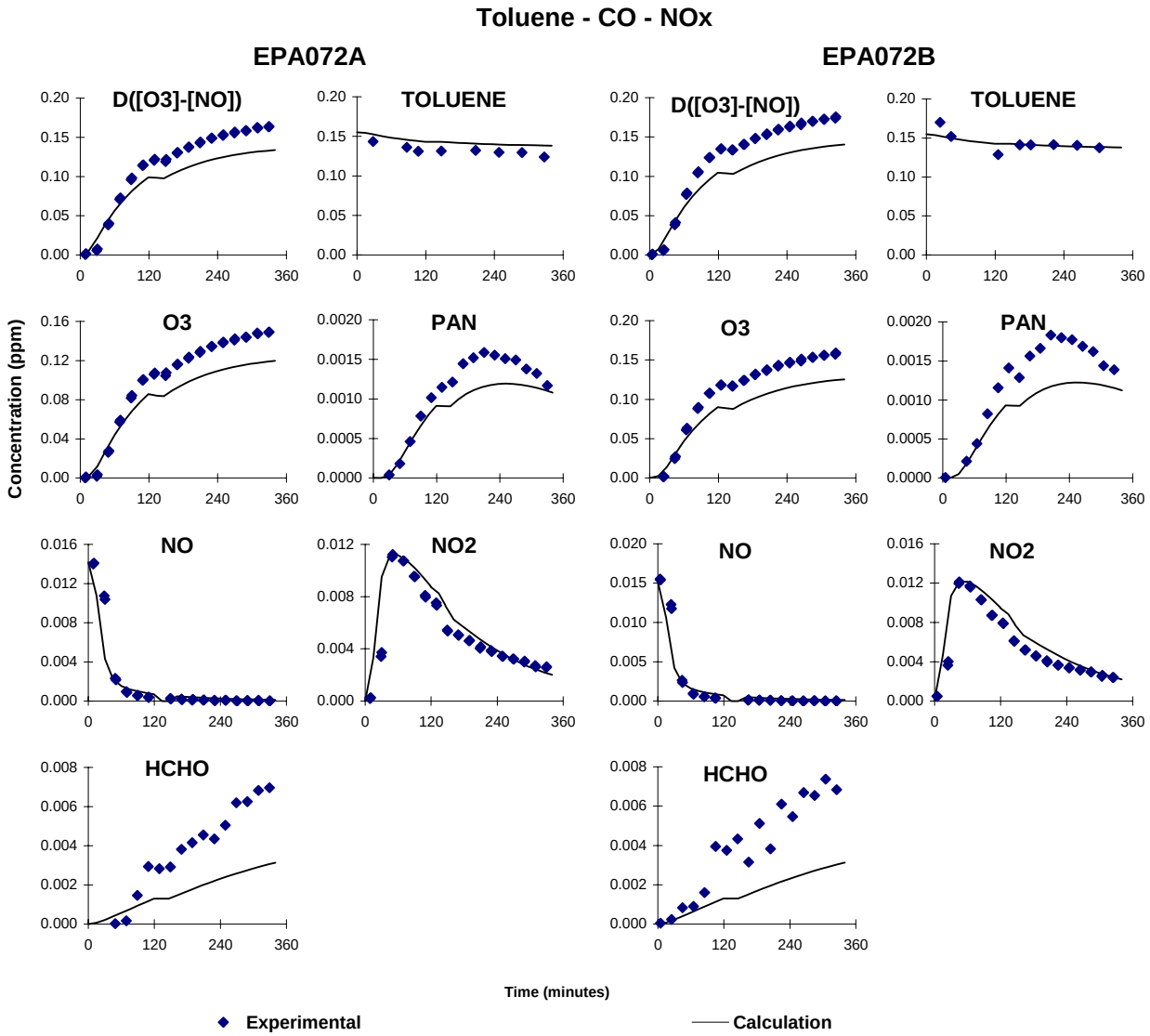

Figure B-15. Experimental and calculated concentration-time plots for selected compounds in the toluene – CO - NO_x experiment EPA072.

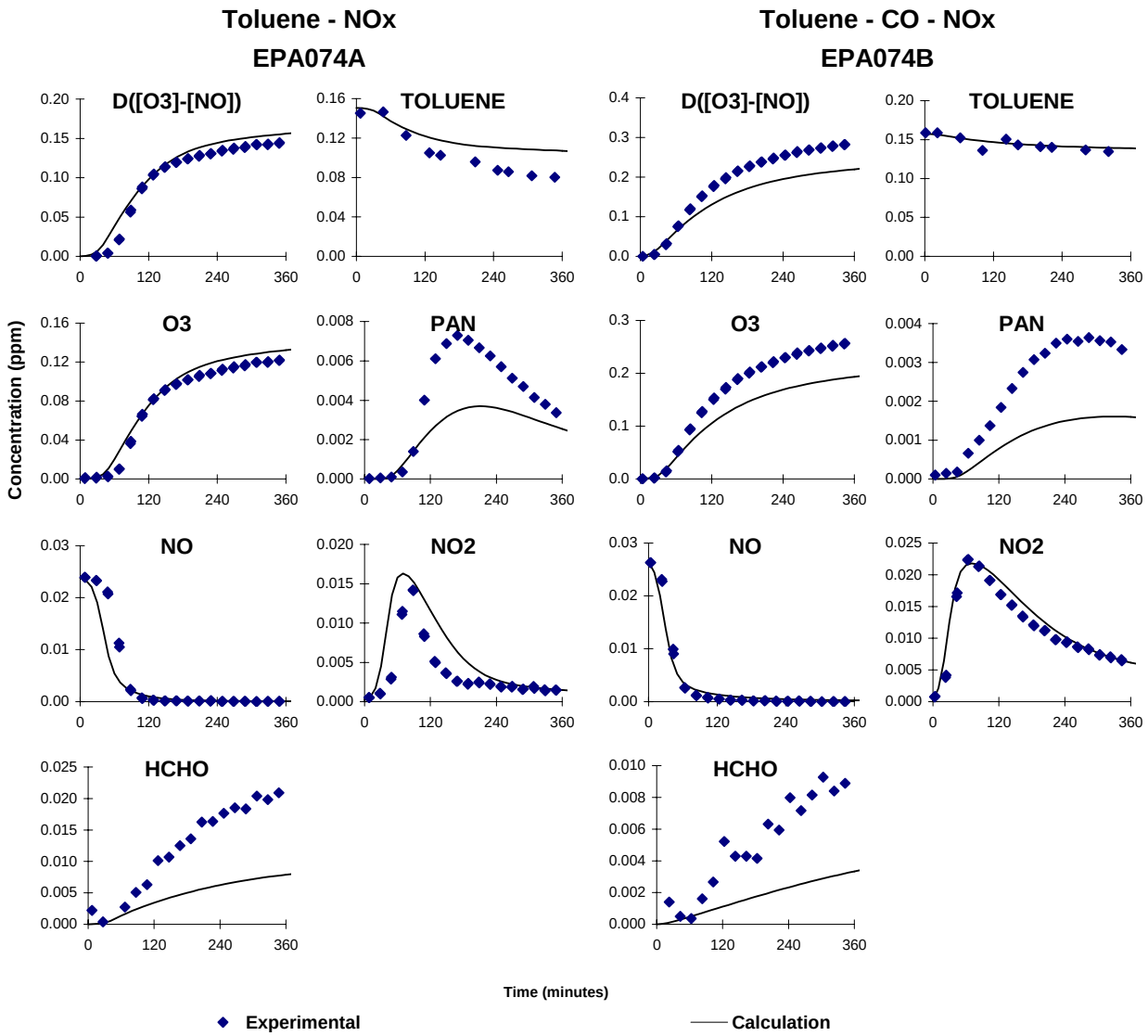

Figure B-16. Experimental and calculated concentration-time plots for selected compounds in the toluene and toluene – CO - NO_x experiment EPA074.

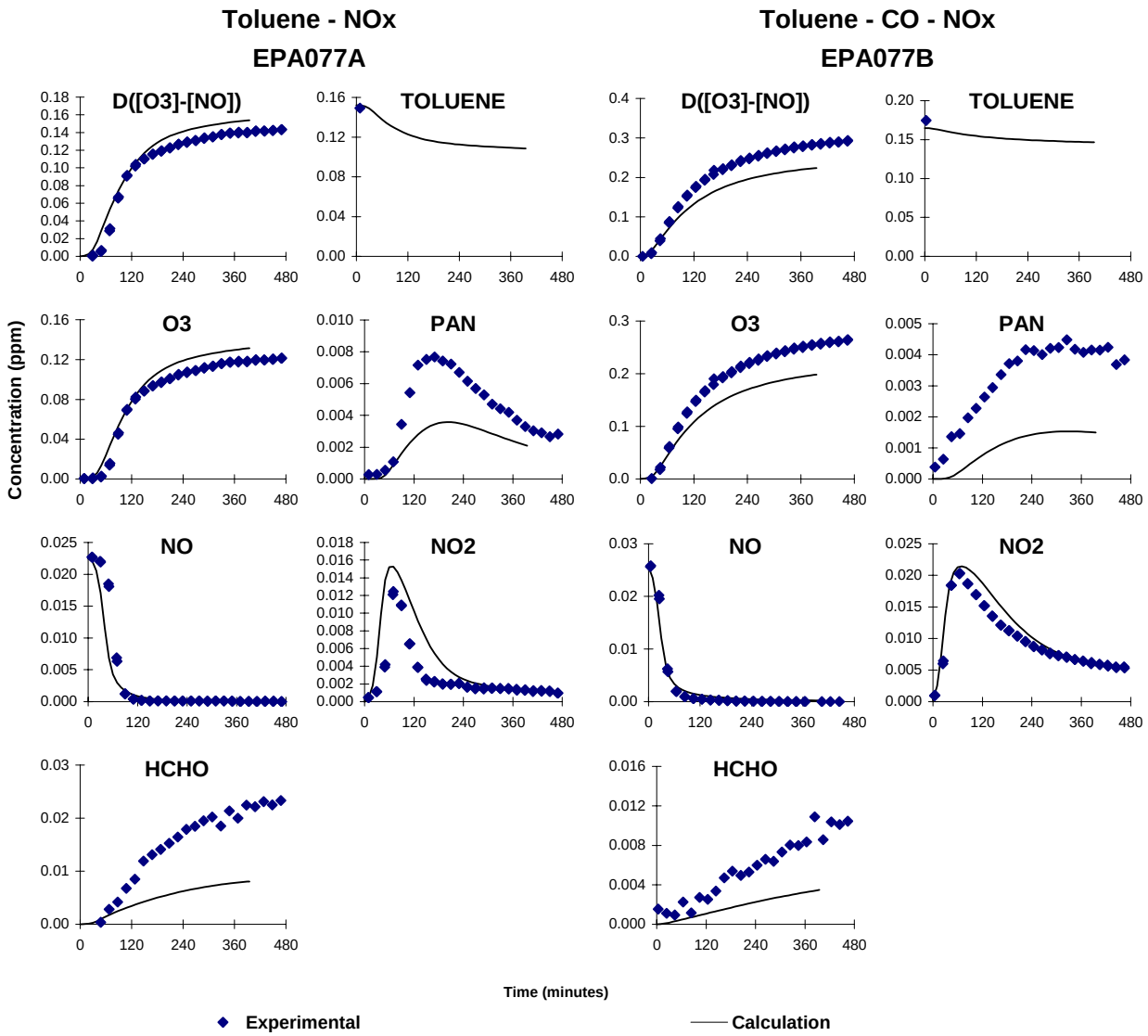

Figure B-17. Experimental and calculated concentration-time plots for selected compounds in the toluene and toluene – CO - NO_x experiment EPA077.

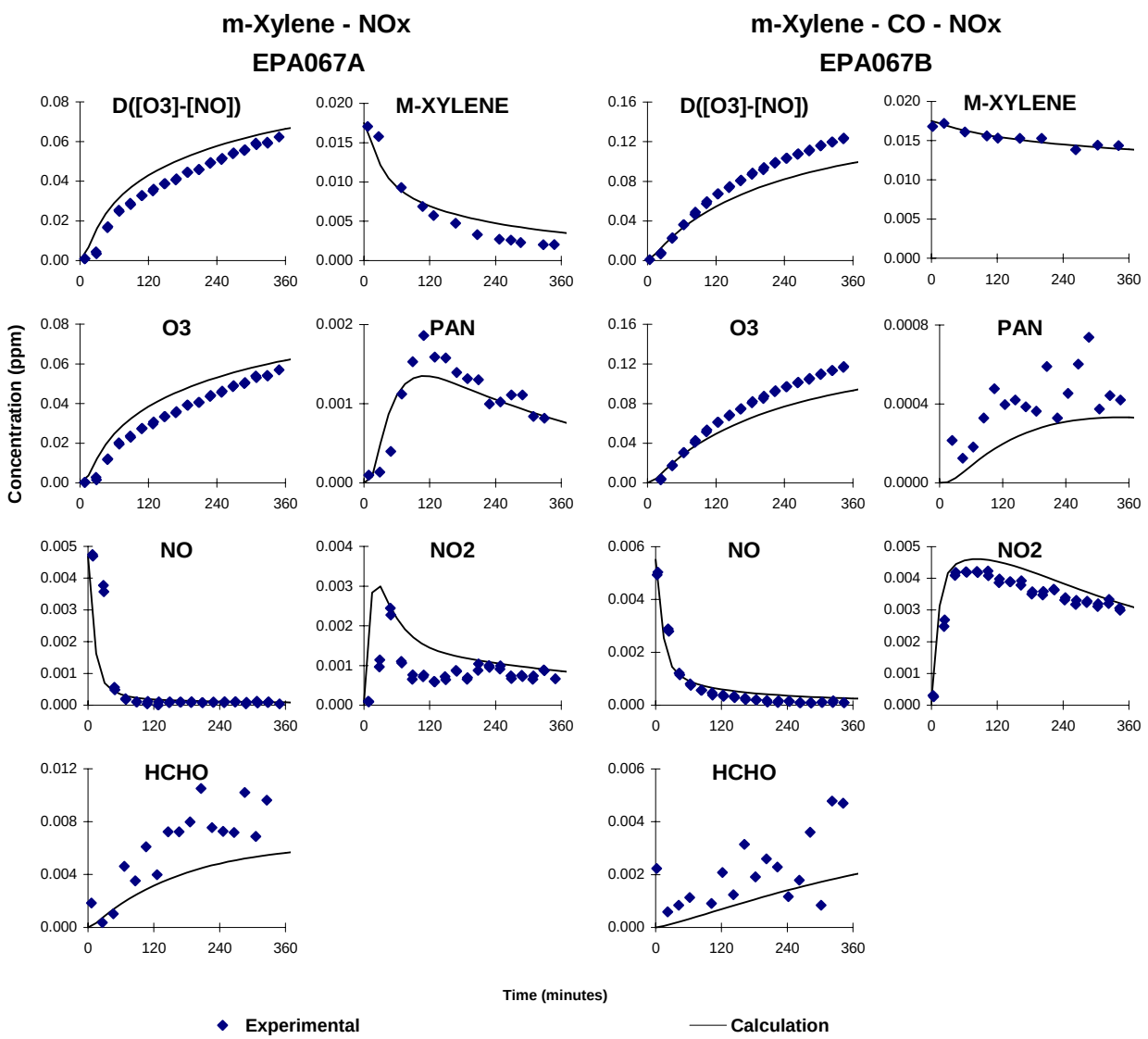

Figure B-18. Experimental and calculated concentration-time plots for selected compounds in the m-xylene and m-xylene – CO - NO_x experiment EPA066.

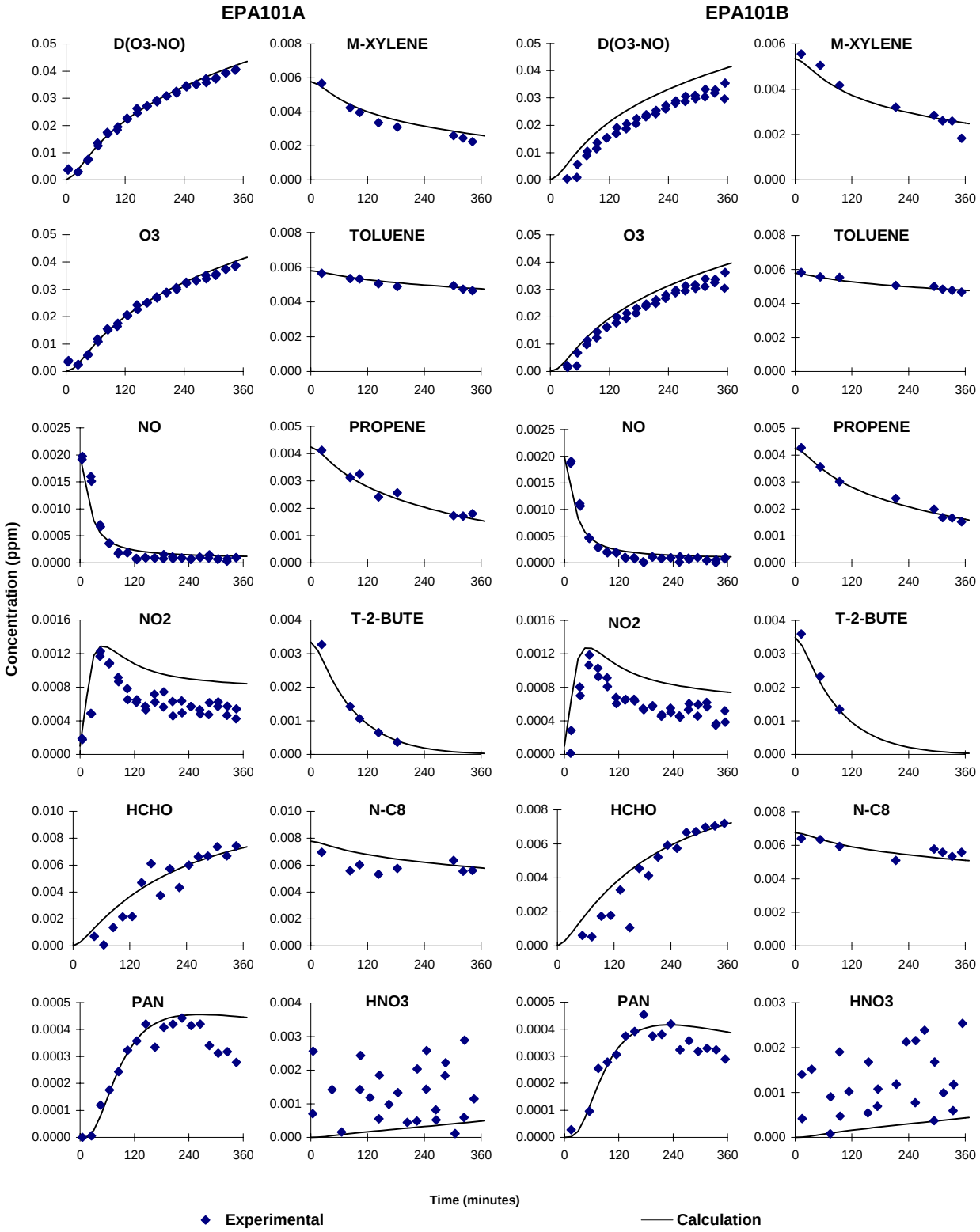

Figure B-19. Experimental and calculated concentration-time plots for most monitored compounds in the low NO_x surrogate - NO_x experiment EPA101.

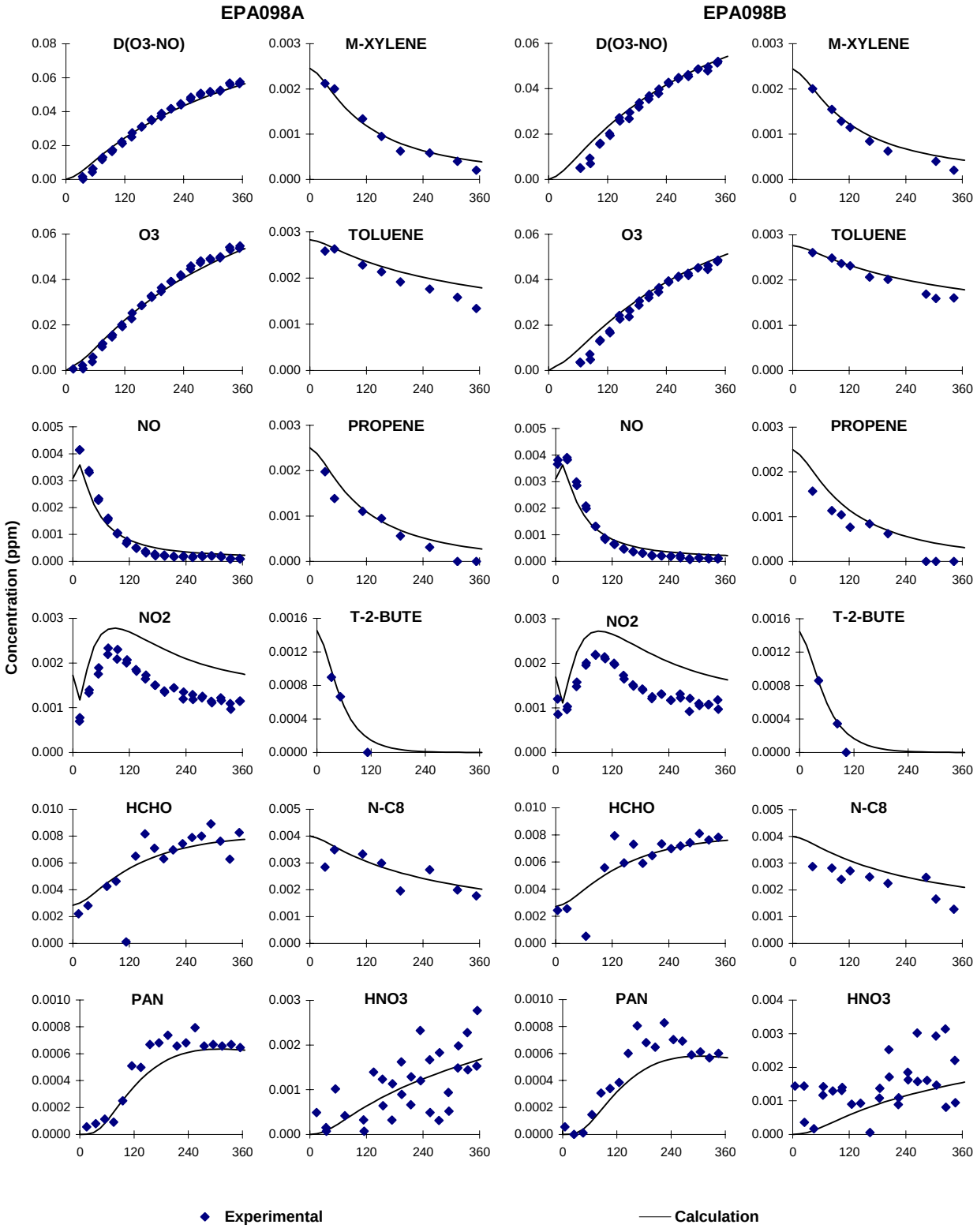

Figure B-20. Experimental and calculated concentration-time plots for most monitored compounds in the low NO_x surrogate - NO_x experiment EPA098.

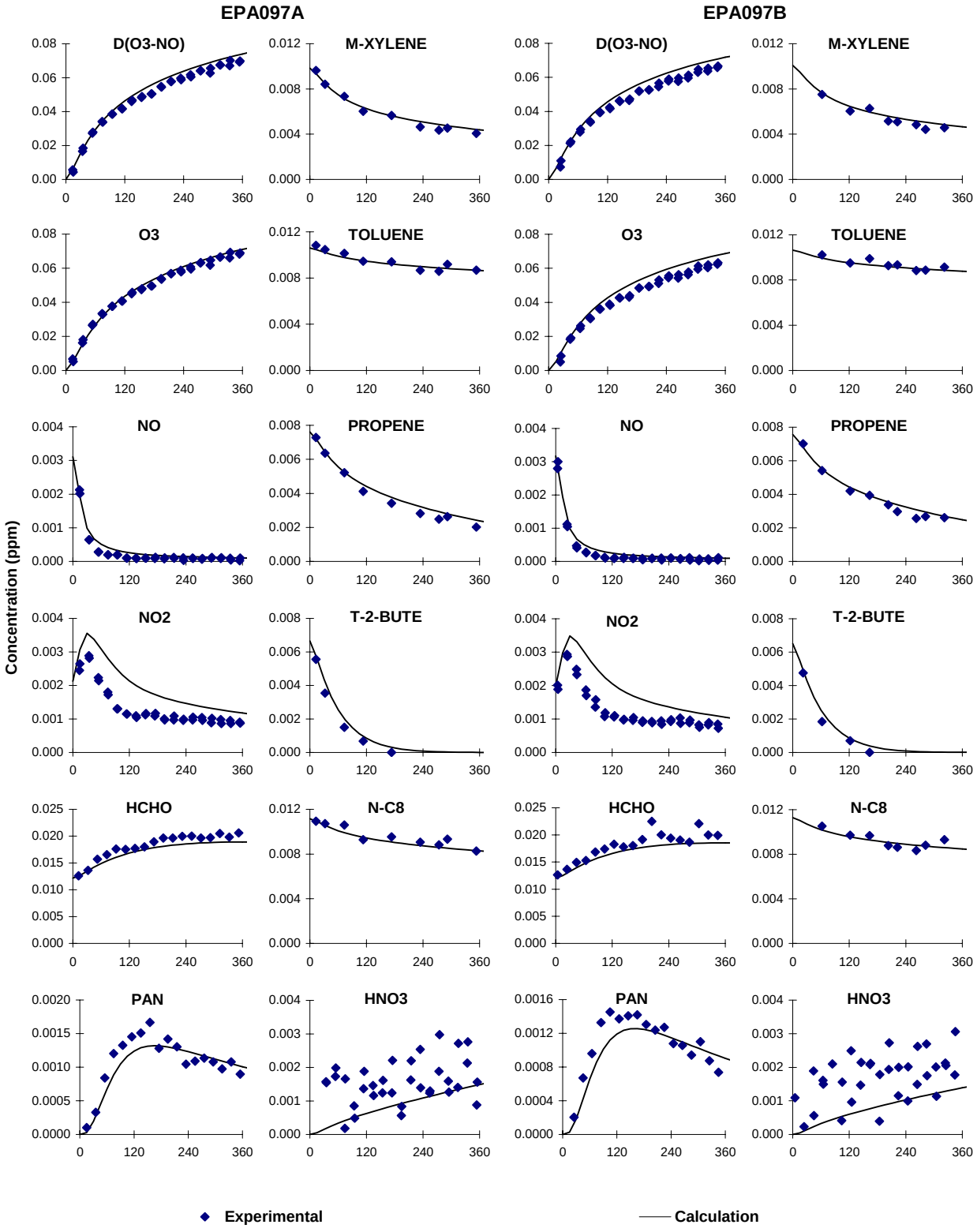

Figure B-21. Experimental and calculated concentration-time plots for most monitored compounds in the low NO_x surrogate - NO_x experiment EPA097.

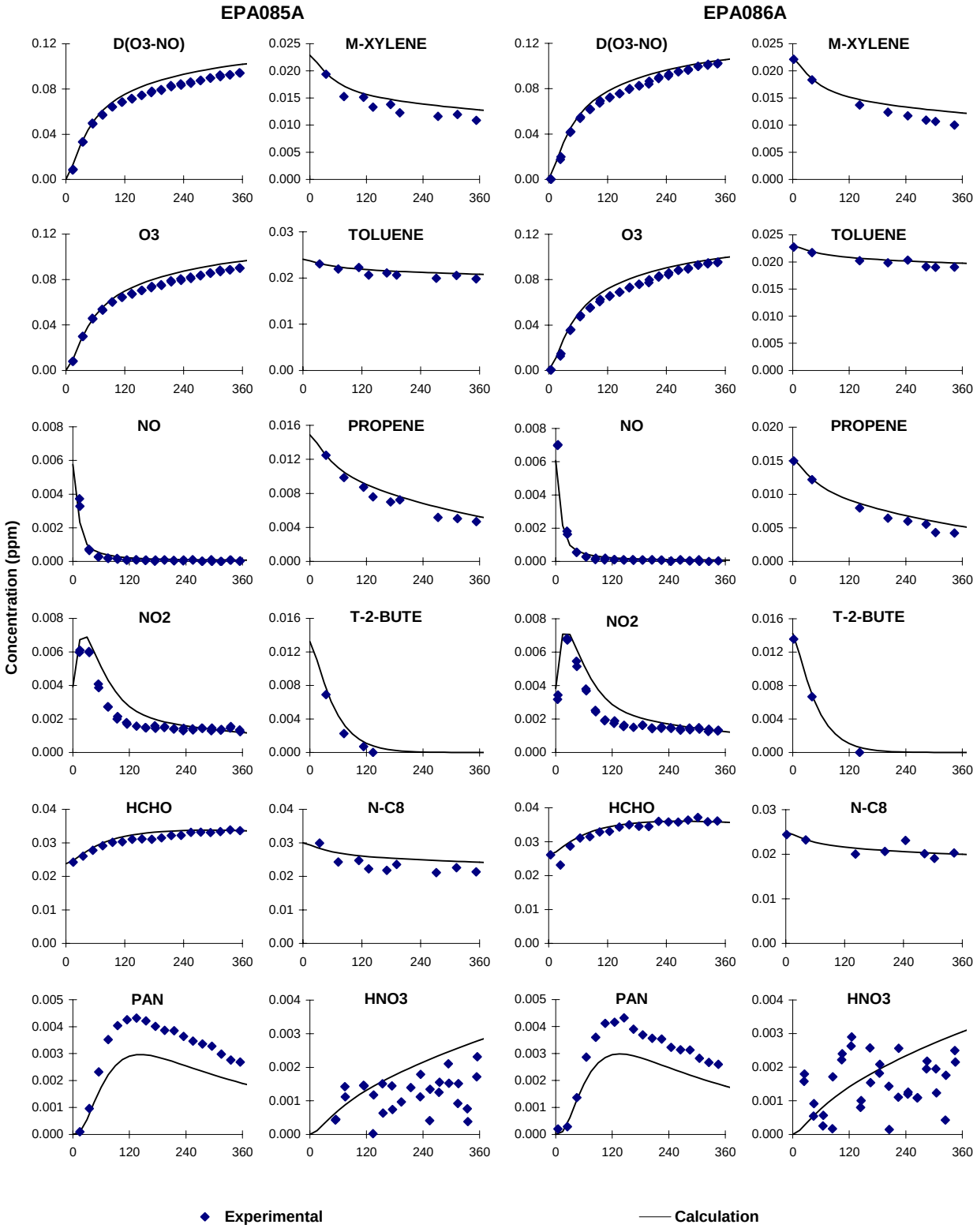

Figure B-22. Experimental and calculated concentration-time plots for most monitored compounds in the low NO_x surrogate - NO_x experiments EPA085A and EPA86A.

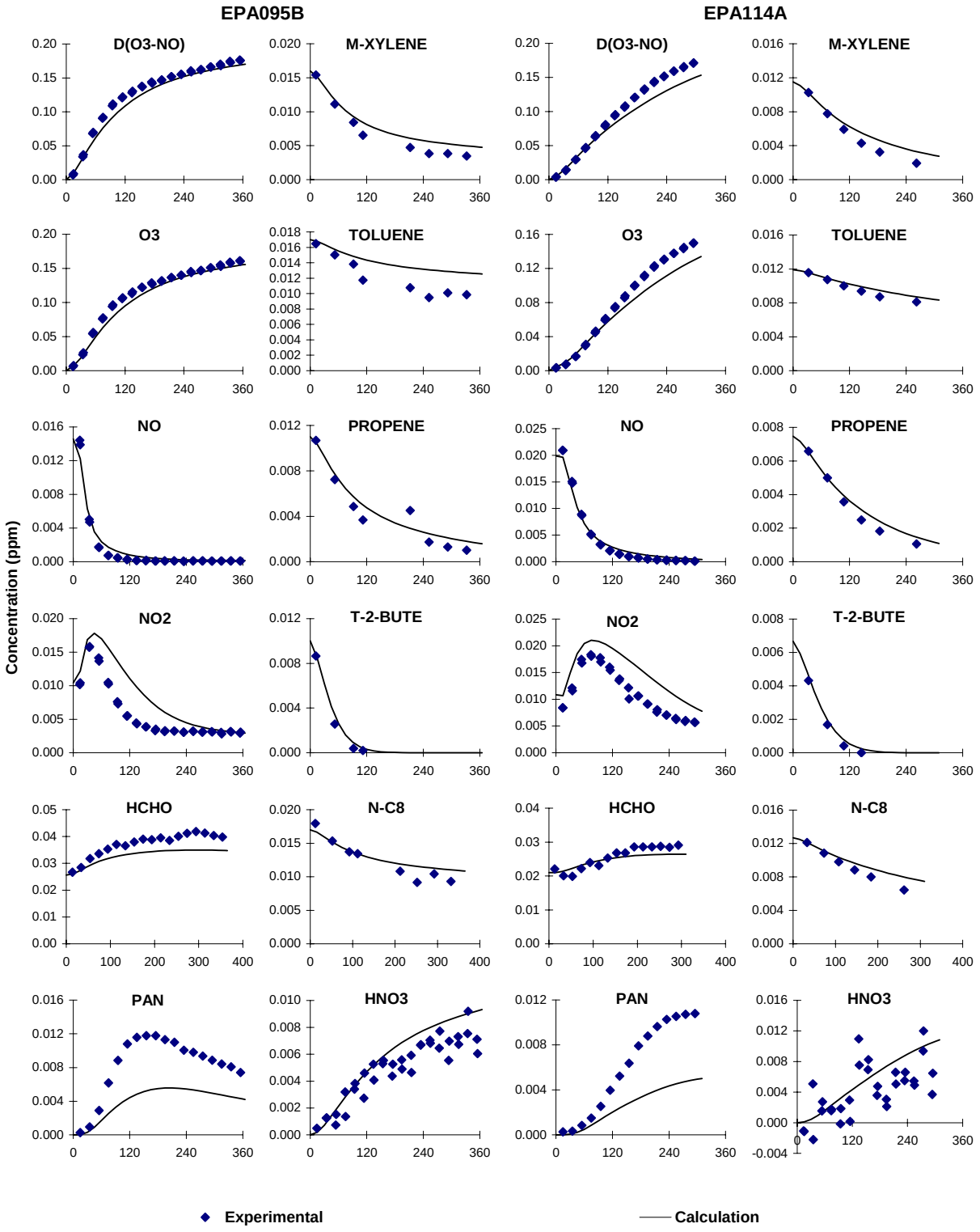

Figure B-23. Experimental and calculated concentration-time plots for most monitored compounds in the surrogate - NO_x experiments EPA095B and EPA114A.

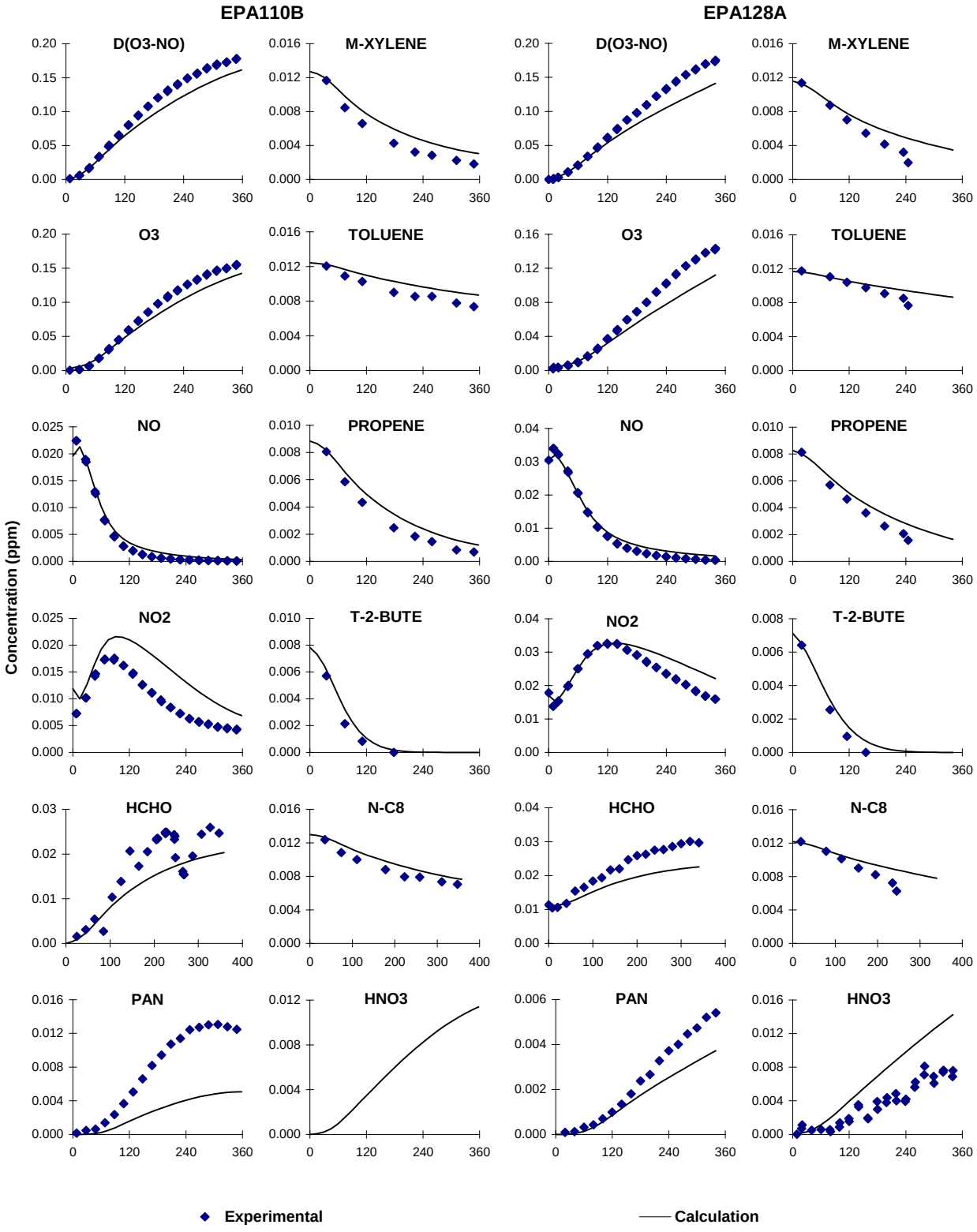

Figure B-24. Experimental and calculated concentration-time plots for most monitored compounds in the surrogate - NO_x experiments EPA110B and EPA128A.

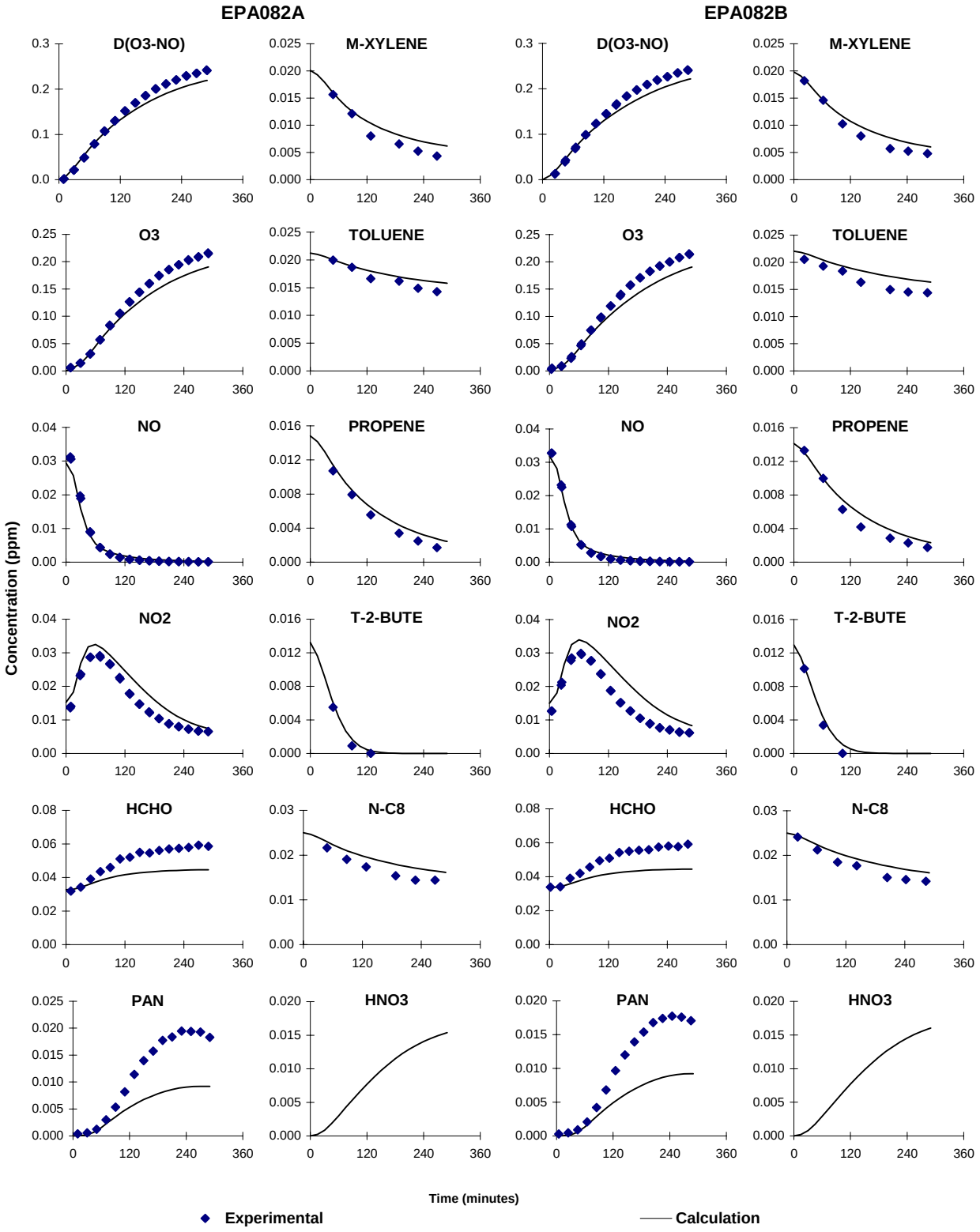

Figure B-25. Experimental and calculated concentration-time plots for most monitored compounds in the surrogate - NO_x experiment EPA082.

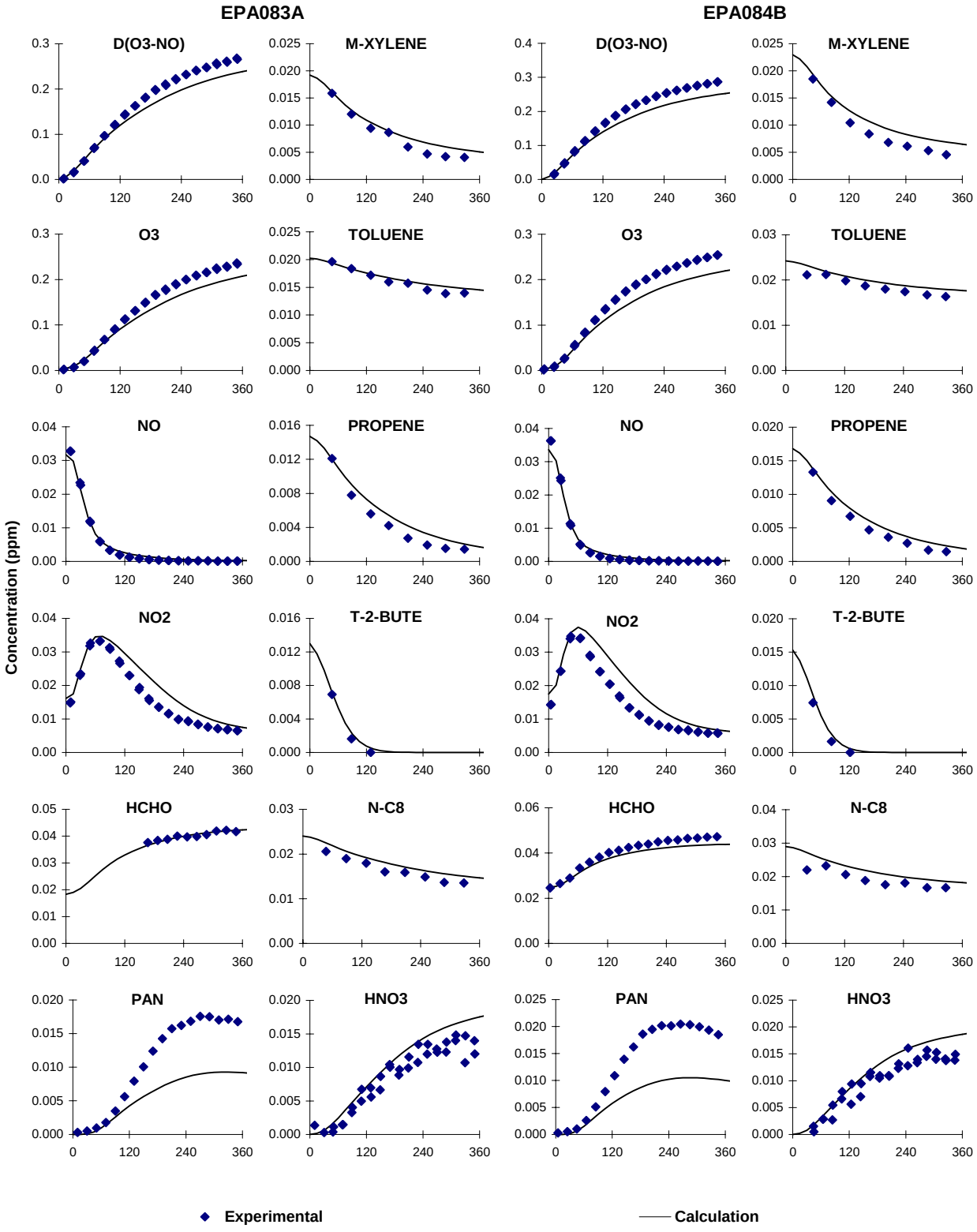

Figure B-26. Experimental and calculated concentration-time plots for most monitored compounds in the surrogate - NO_x experiments EPA083A and EPA084B.

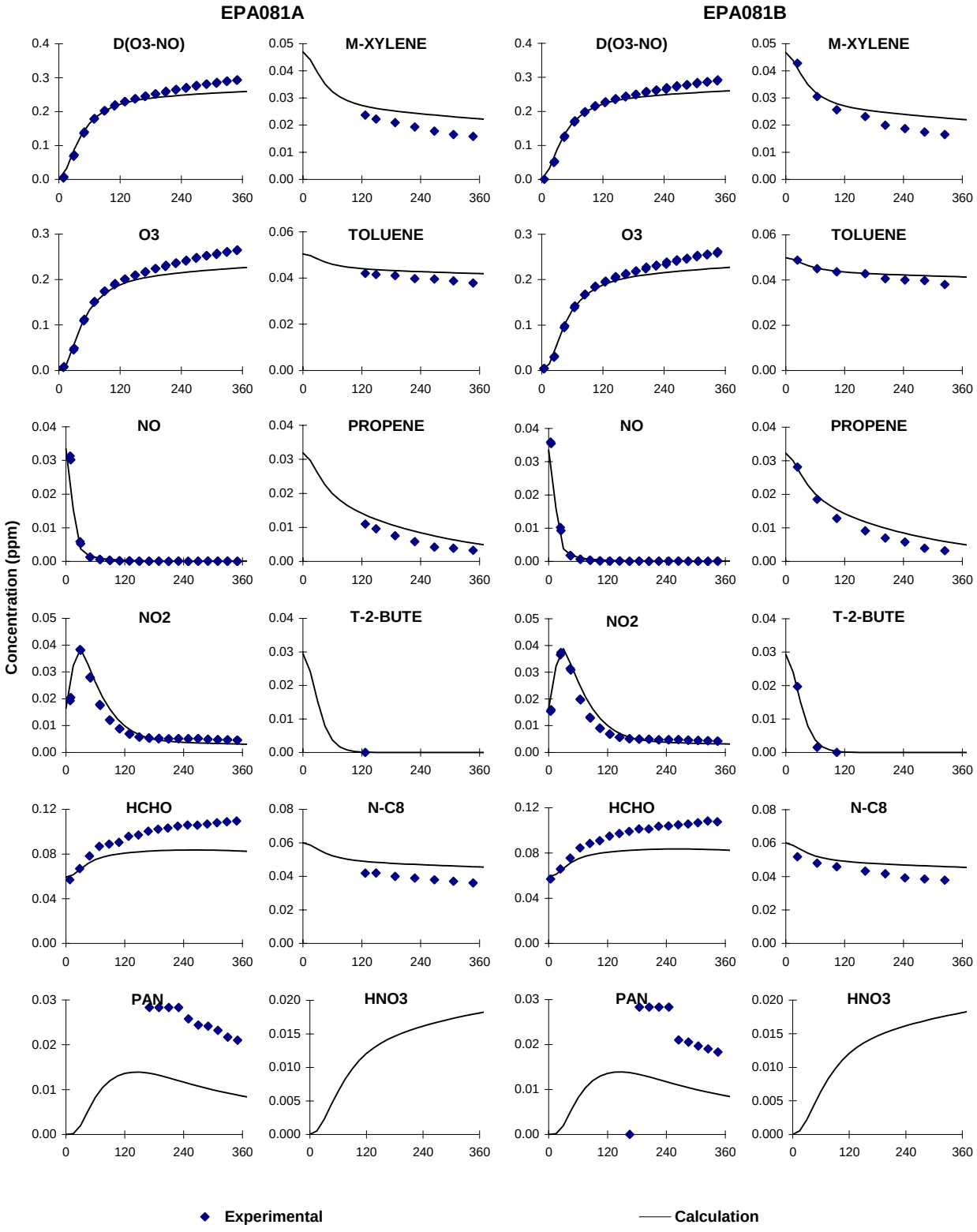

Figure B-27. Experimental and calculated concentration-time plots for most monitored compounds in the surrogate - NO_x experiment EPA081.

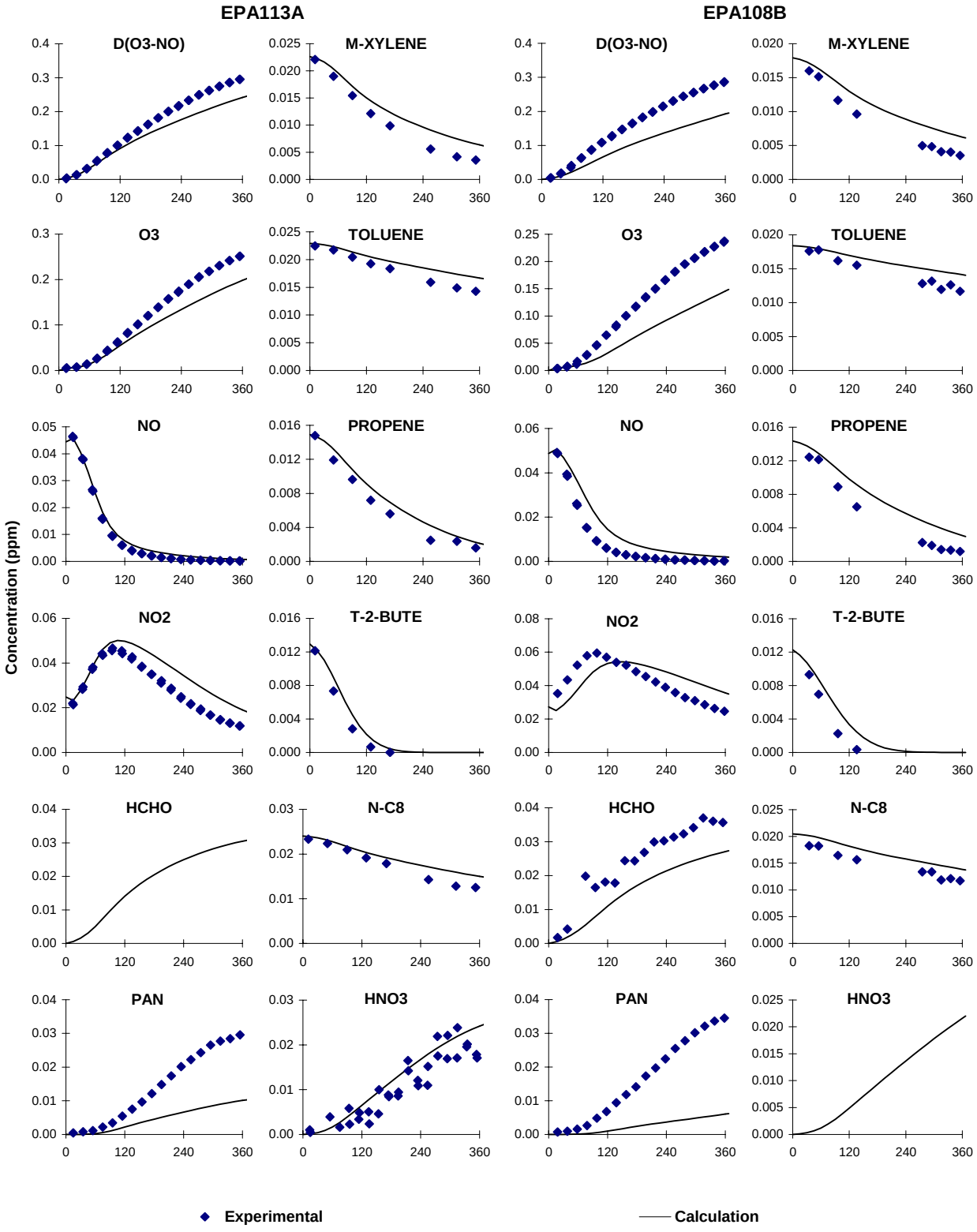

Figure B-28. Experimental and calculated concentration-time plots for most monitored compounds in the surrogate - NO_x experiments EPA113A and EPA108B.

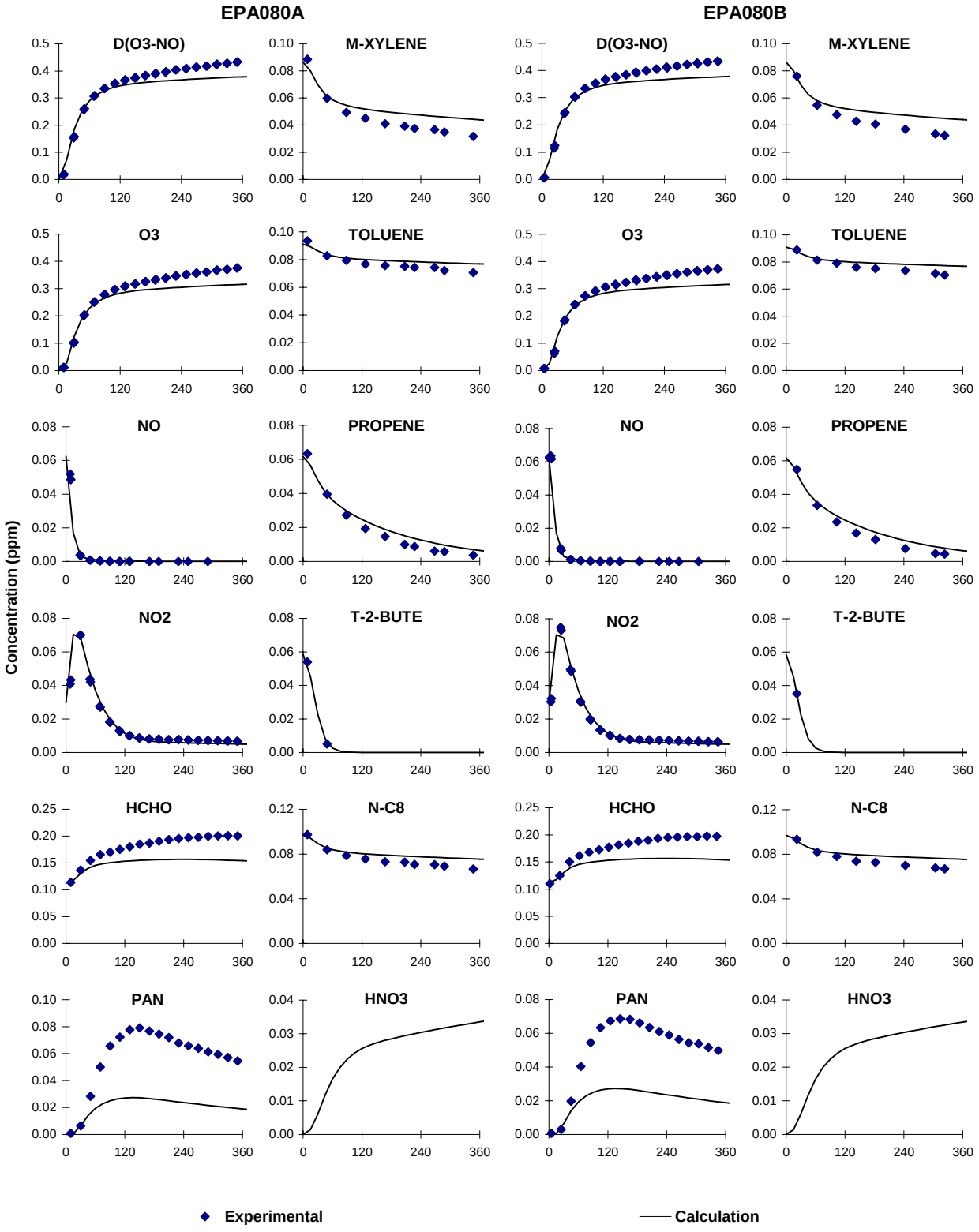

Figure B-29. Experimental and calculated concentration-time plots for most monitored compounds in the surrogate - NO_x experiment EPA080.

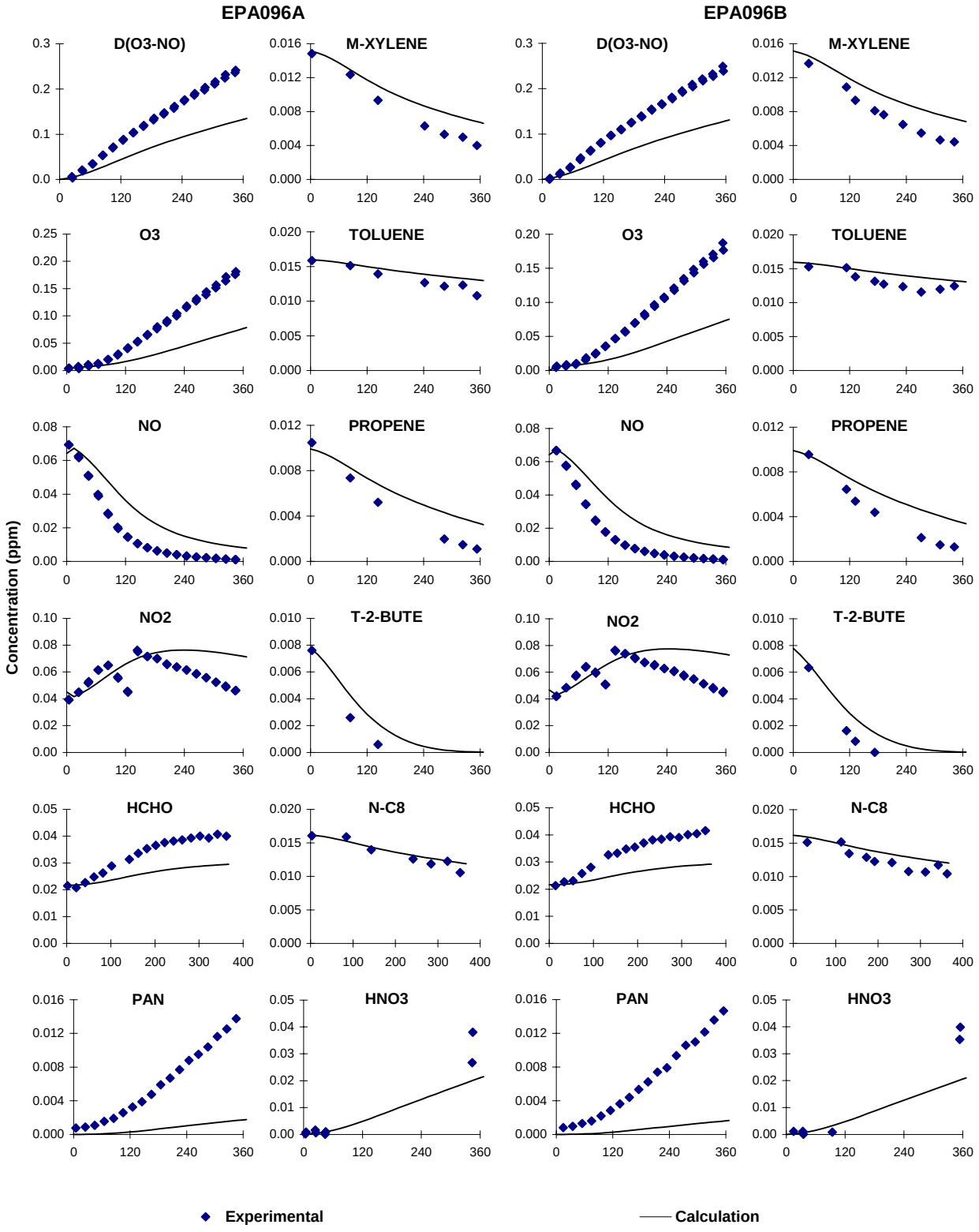

Figure B-30. Experimental and calculated concentration-time plots for most monitored compounds in the surrogate - NO_x experiment EPA096.

TVA Chamber Experiments

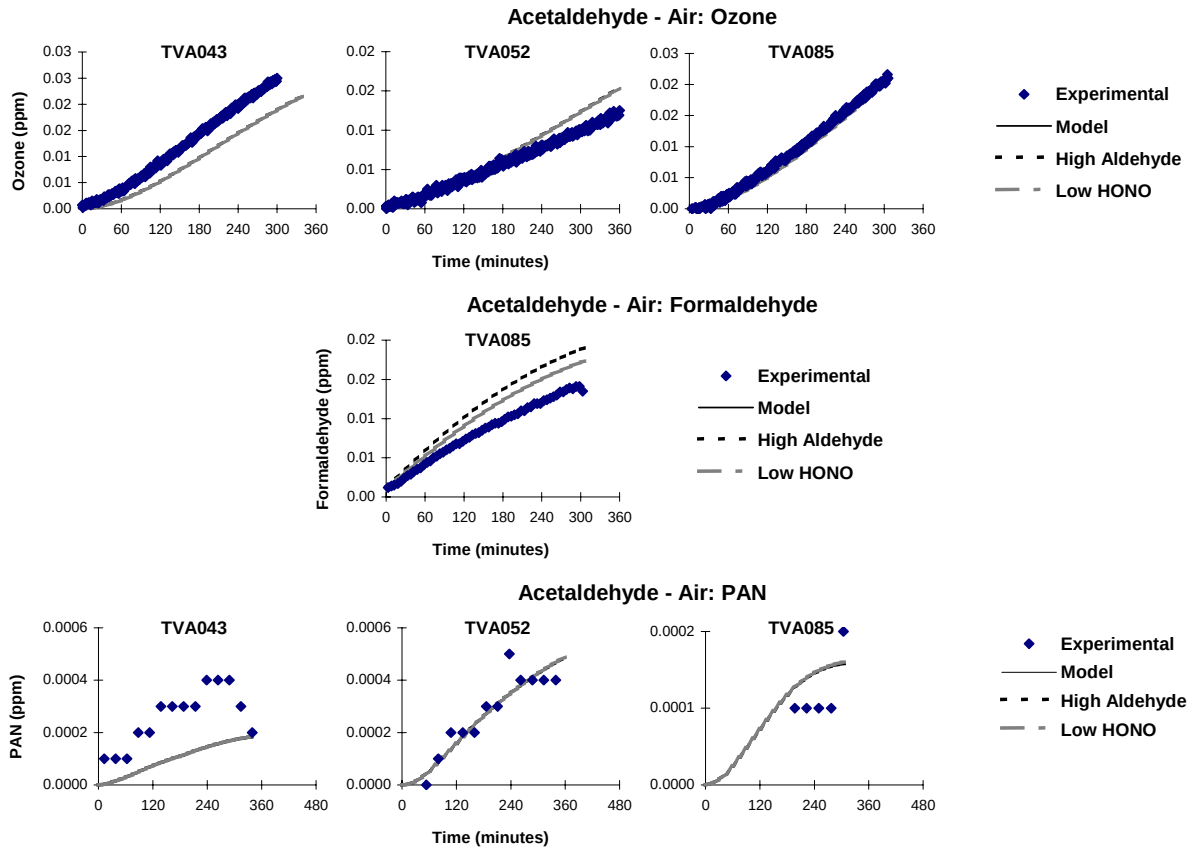

Figure B-31. Plots of experimental and calculated ozone, formaldehyde (where available) and PAN results of the TVA acetaldehyde - air experiments.

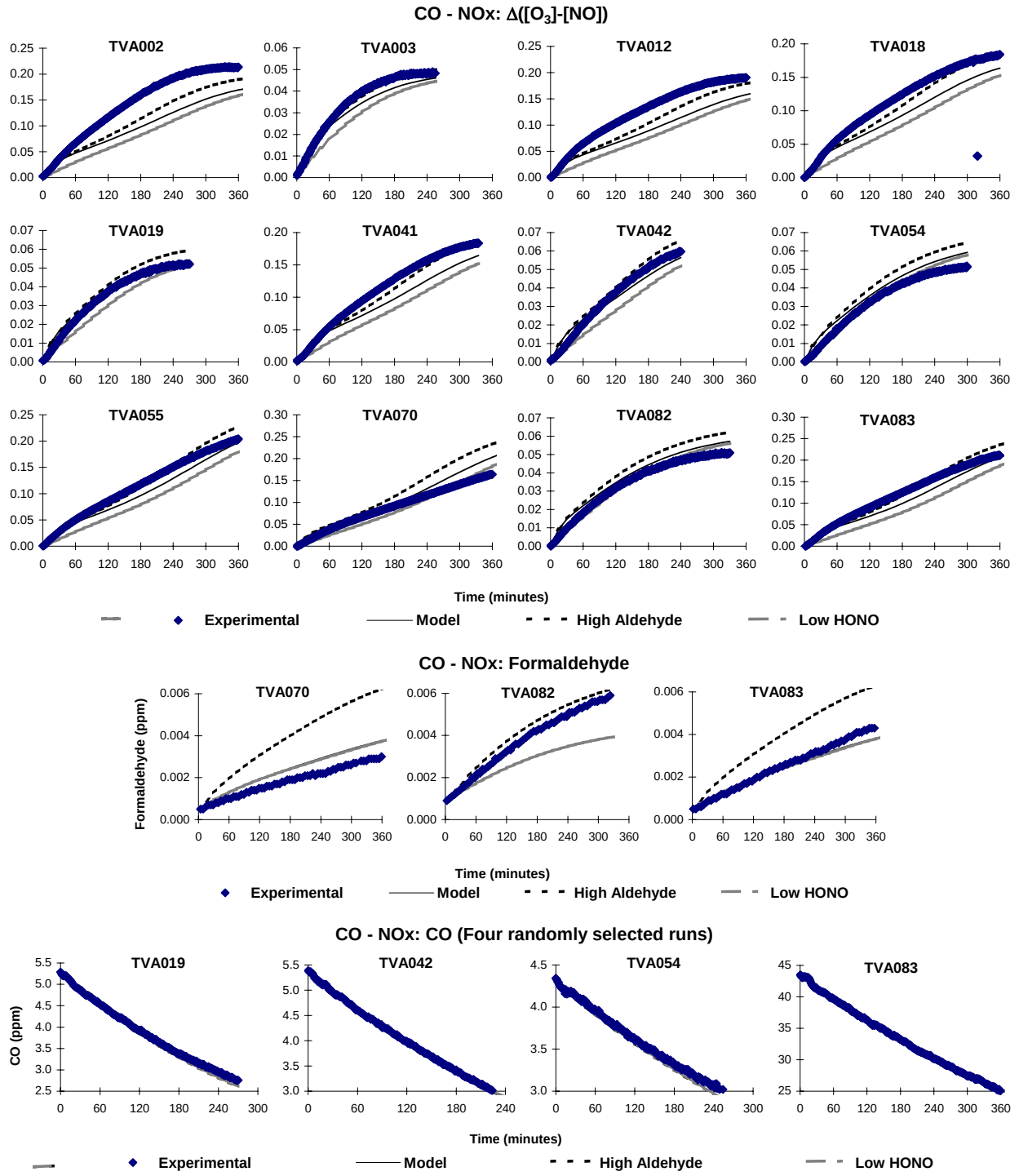

Figure B-32. Plots of experimental and calculated Δ([O3]-[NO]), formaldehyde (where available) and representative CO results of the TVA CO - NO_x experiments. (Model data do not show where they overlap the experimental data.)

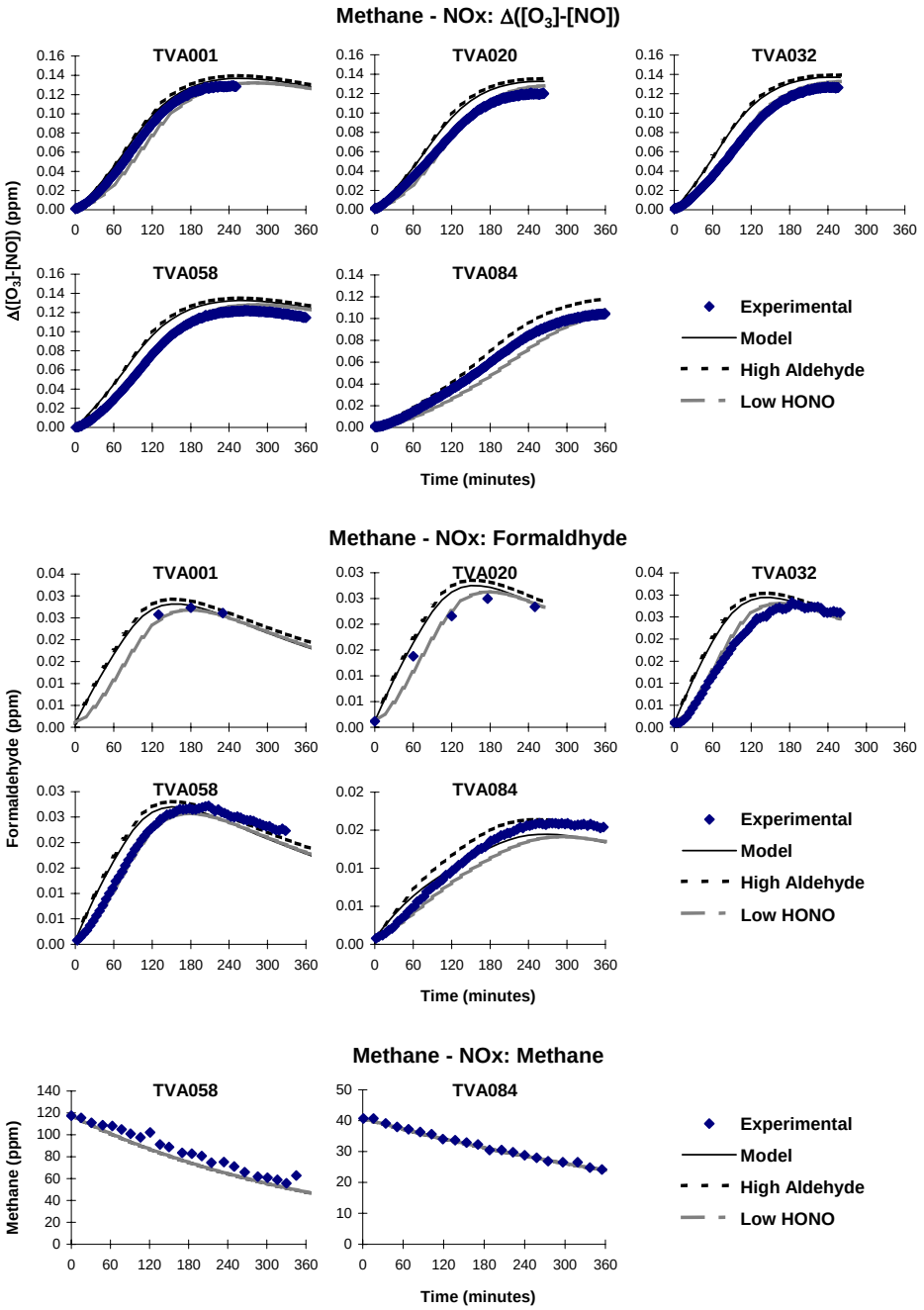

Figure B-33. Plots of experimental and calculated Δ([O3]-[NO]), formaldehyde (where available) and methane (where available) results of the TVA Methane - NO_x experiments.

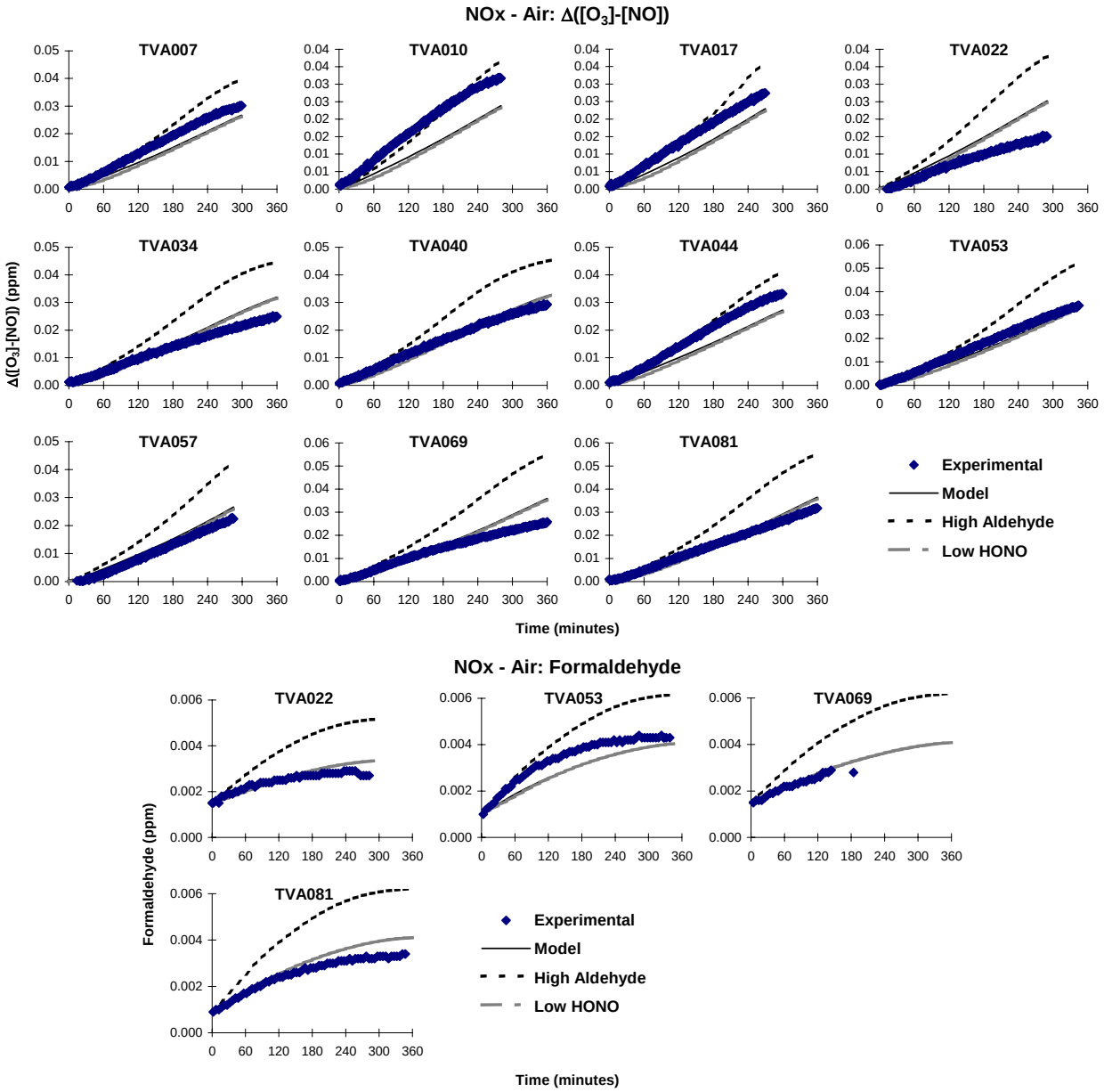

Figure B-34. Plots of experimental and calculated Δ([O3]-[NO]) and formaldehyde (where available) results of the TVA NO_x - air experiments.

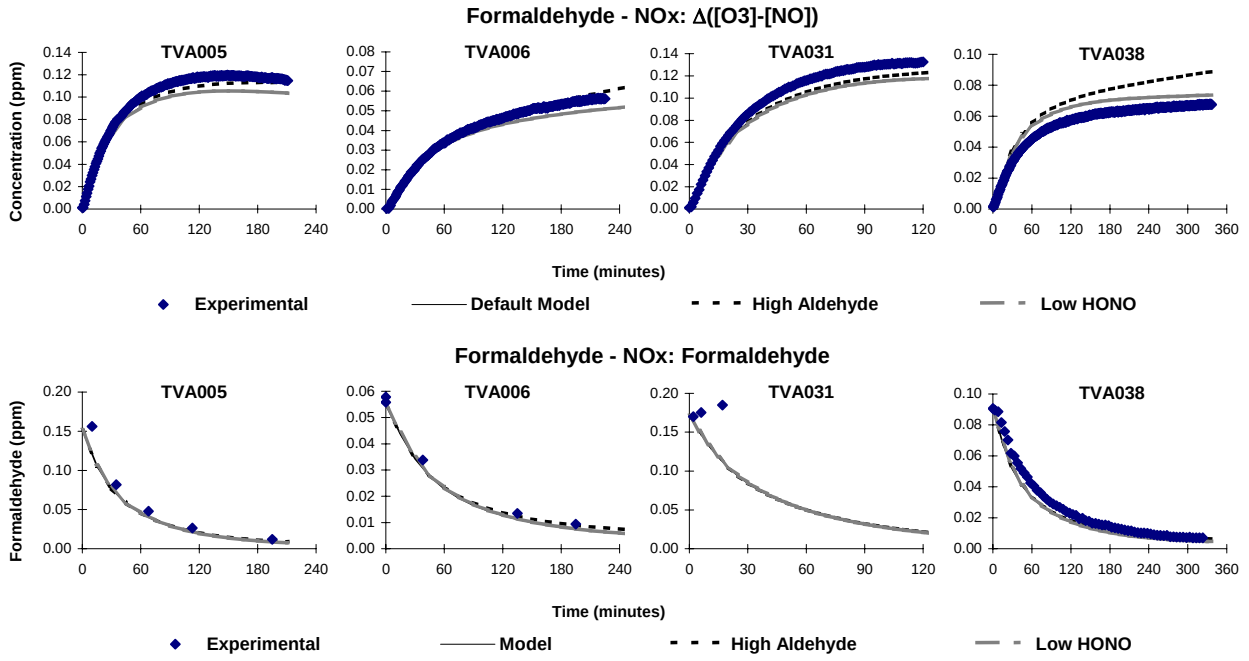

Figure B-35. Plots of experimental and calculated Δ([O_3]-[NO]) and formaldehyde results of the TVA formaldehyde - NO_x experiments.

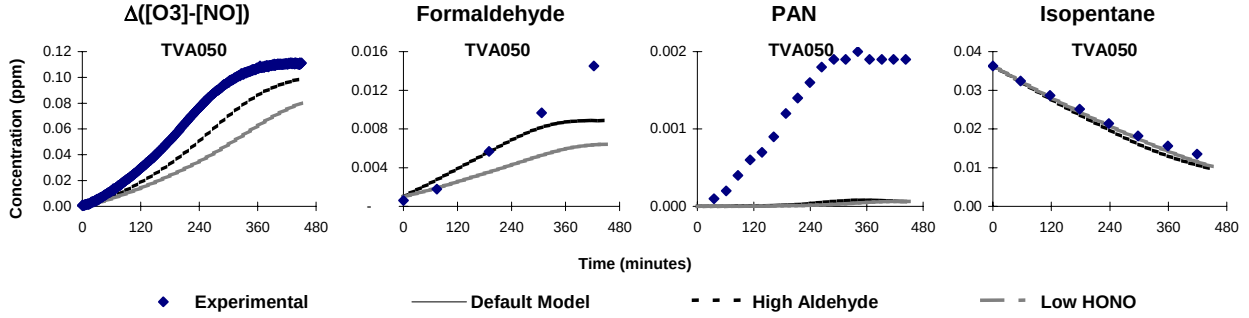

Figure B-36. Plots of experimental and calculated Δ([O_3]-[NO]), formaldehyde, isopentane, and PAN results of the TVA isopentane - NO_x experiment.

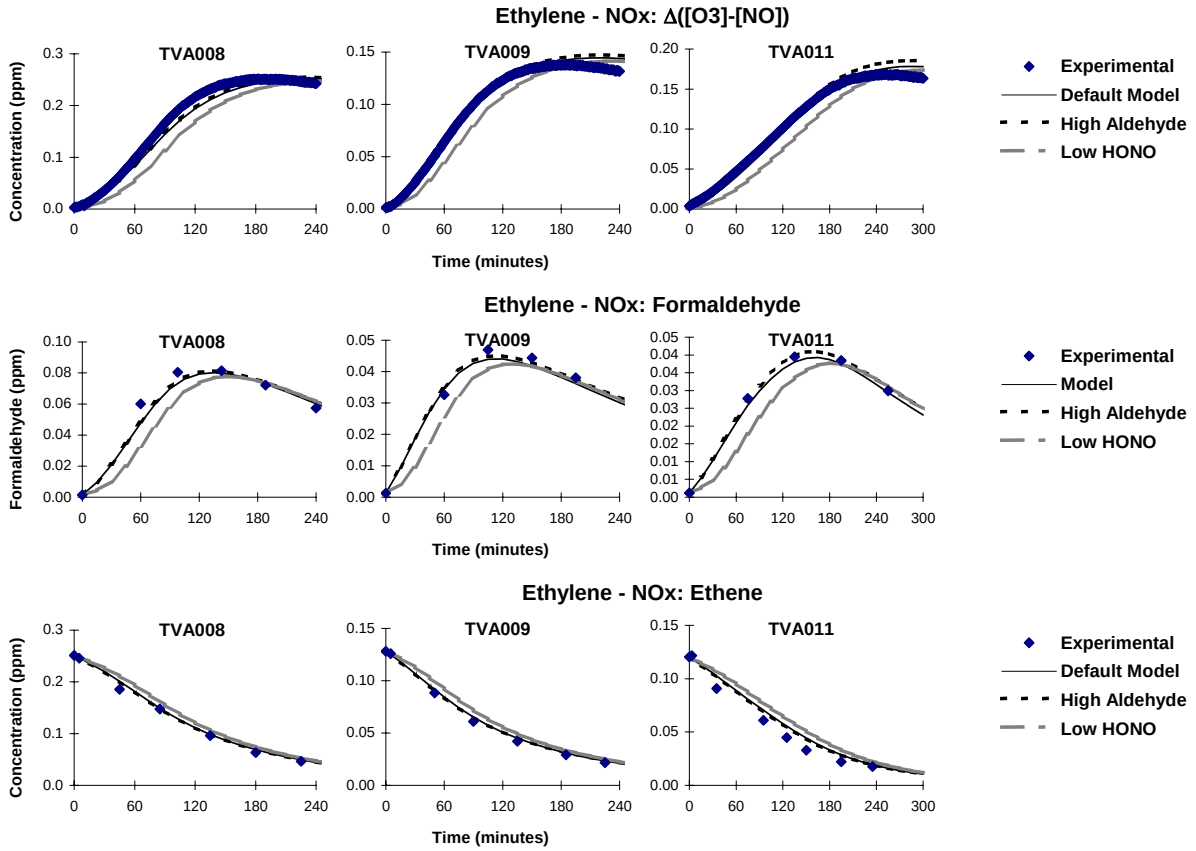

Figure B-37. Plots of experimental and calculated Δ([O3]-[NO]), formaldehyde and ethylene results of the TVA ethylene - NO_x experiments.

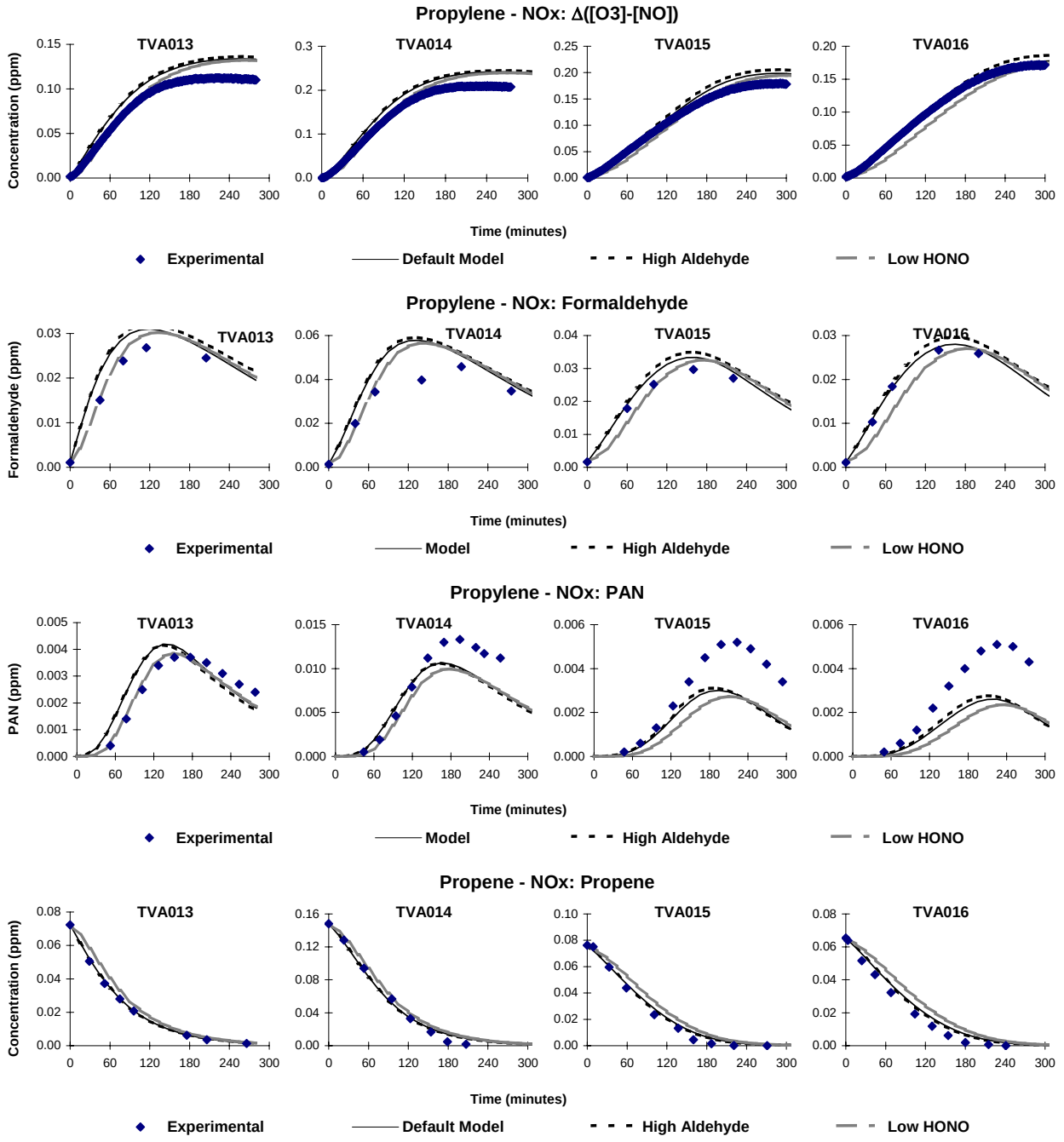

Figure B-38. Plots of experimental and calculated Δ([O3]-[NO]), formaldehyde, PAN and propylene results of the TVA propylene - NO_x experiments.

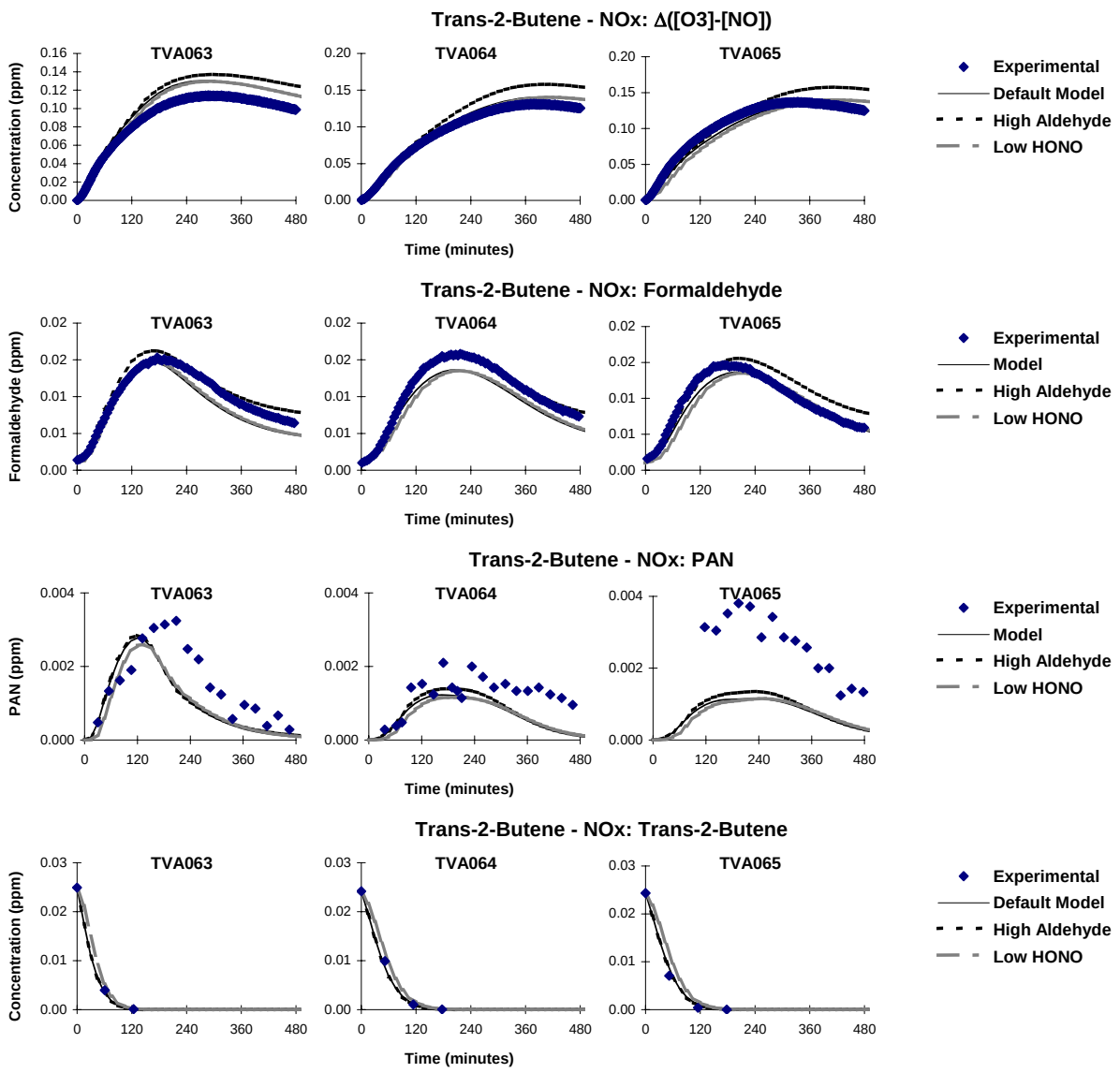

Figure B-39. Plots of experimental and calculated Δ([O3]-[NO]), formaldehyde, PAN and transs-2-butene results of the TVA trans-2-butene - NO_x experiments.

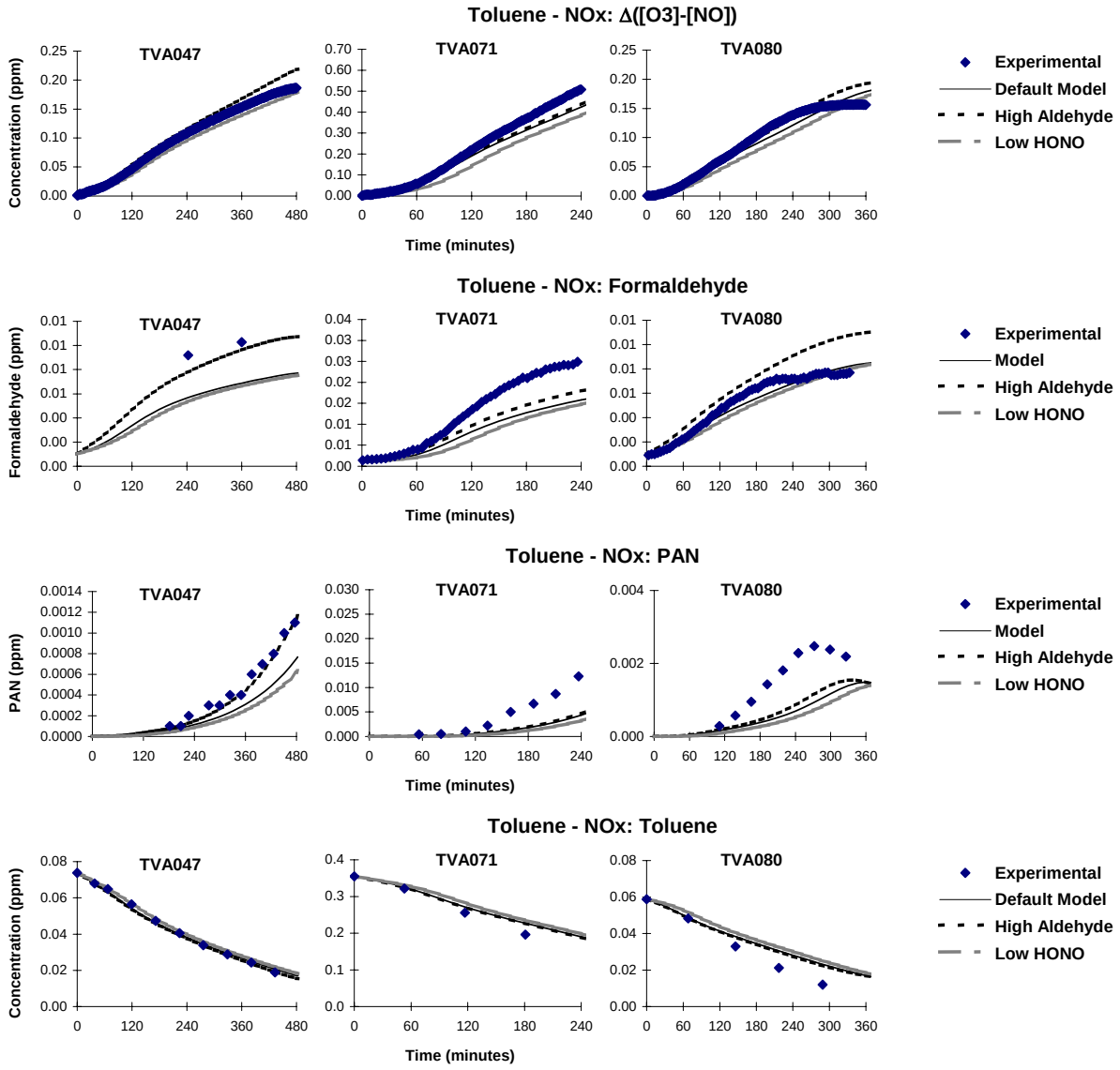

Figure B-40. Plots of experimental and calculated Δ([O3]-[NO]), formaldehyde, PAN, and toluene results of the TVA toluene - NO_x experiments.

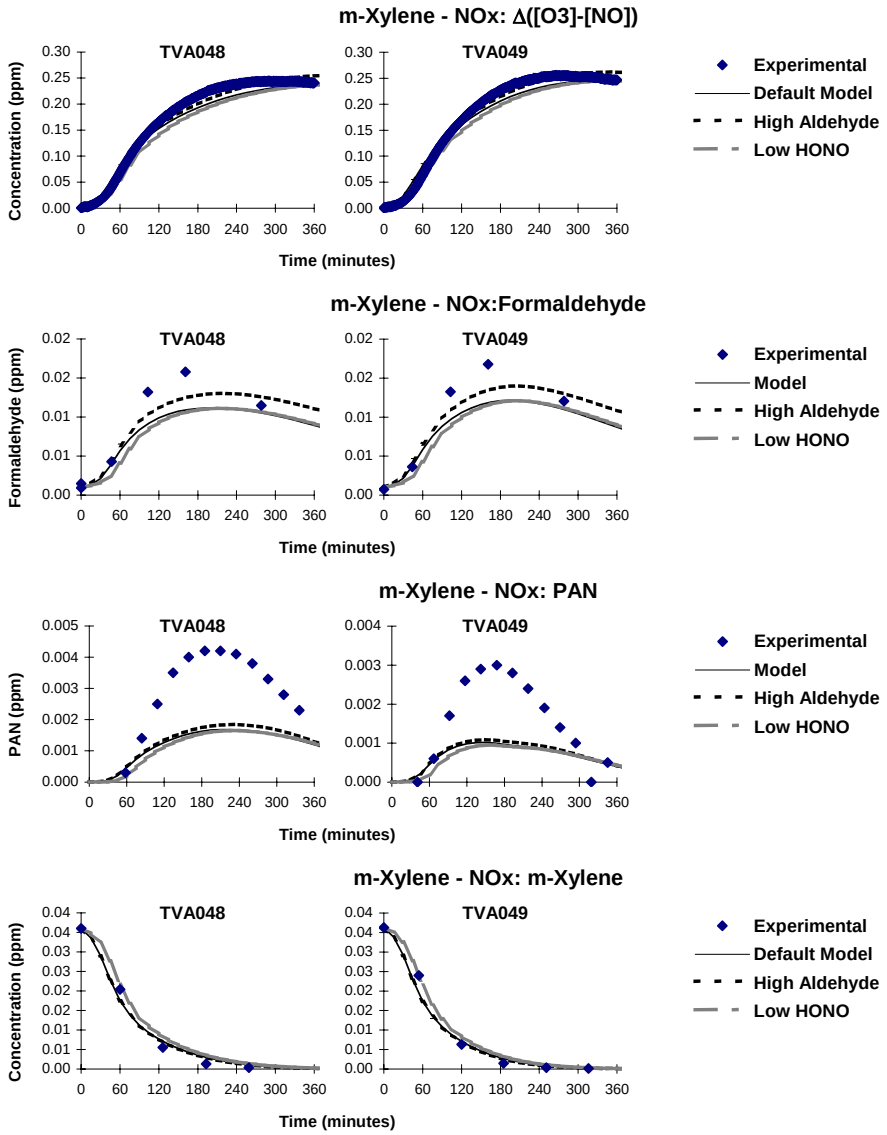

Figure B-41. Plots of experimental and calculated Δ([O3]-[NO]), formaldehyde, and m-xylene results of the TVA m-xylene - NO_x experiments.

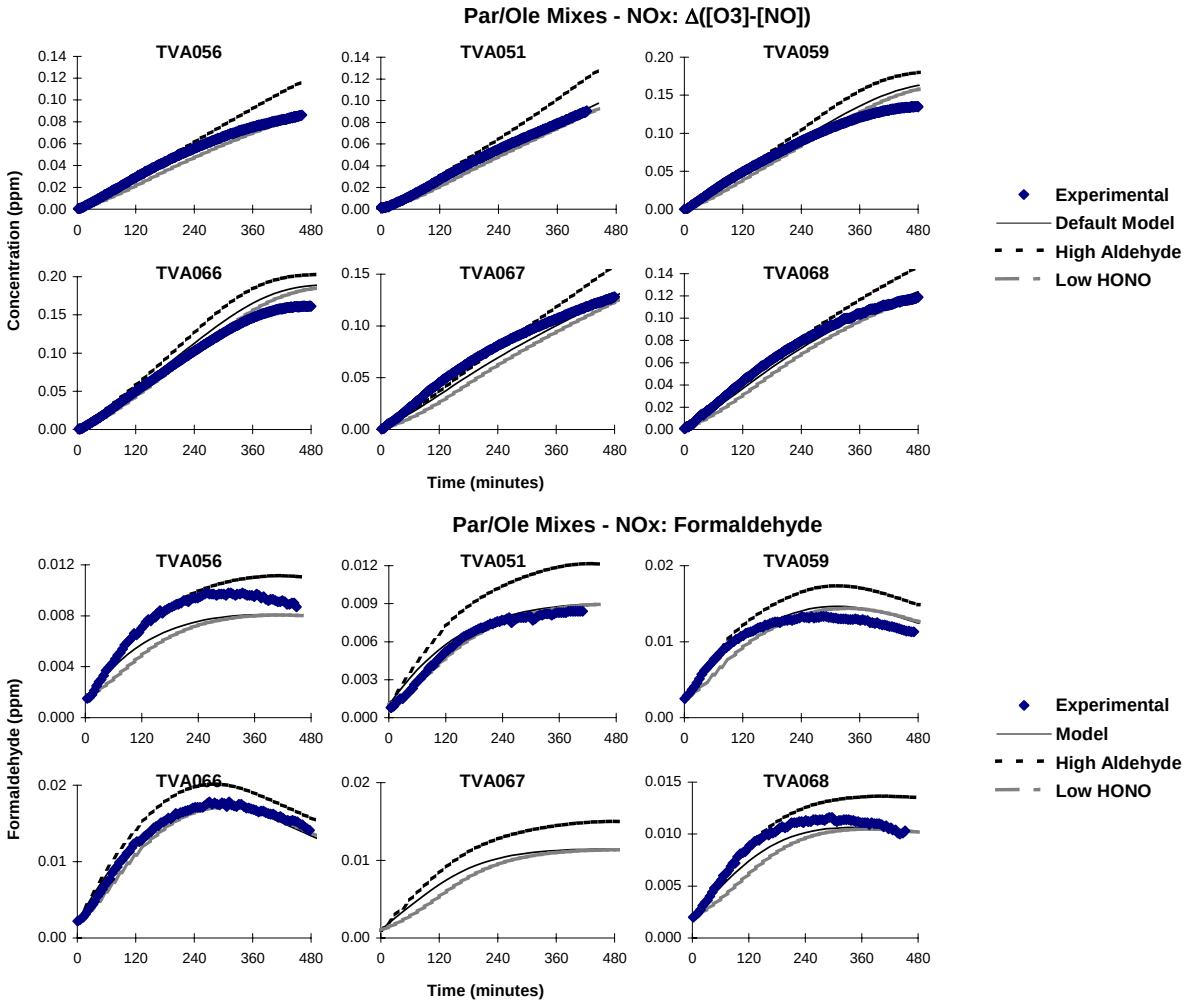

Figure B-42. Plots of experimental and calculated Δ([O3]-[NO]) and formaldehyde results of the TVA paraffin and olefin mix experiments.

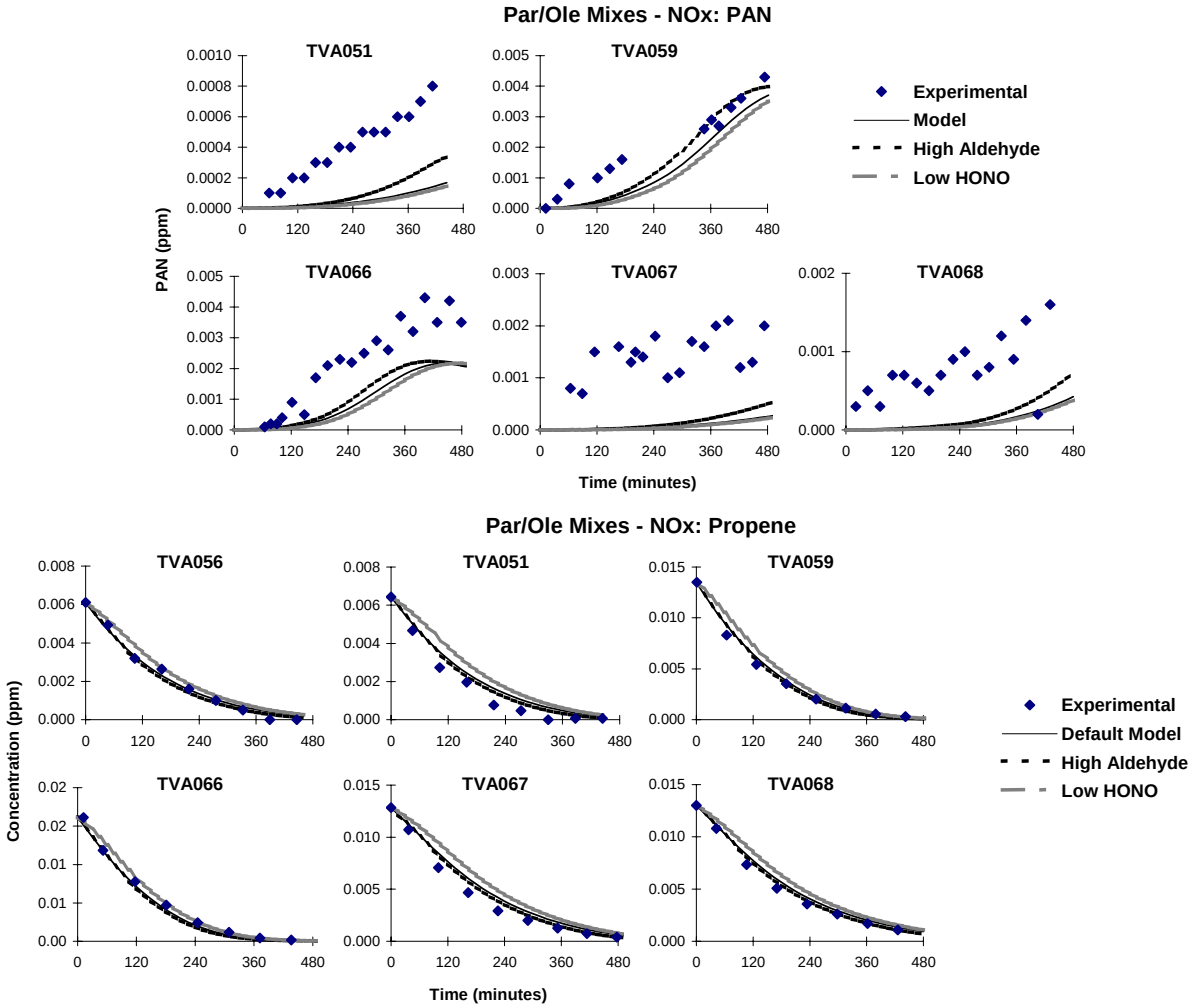

Figure B-43. Plots of experimental and calculated PAN (where available) and propene results of the TVA paraffin and olefin mix experiments.

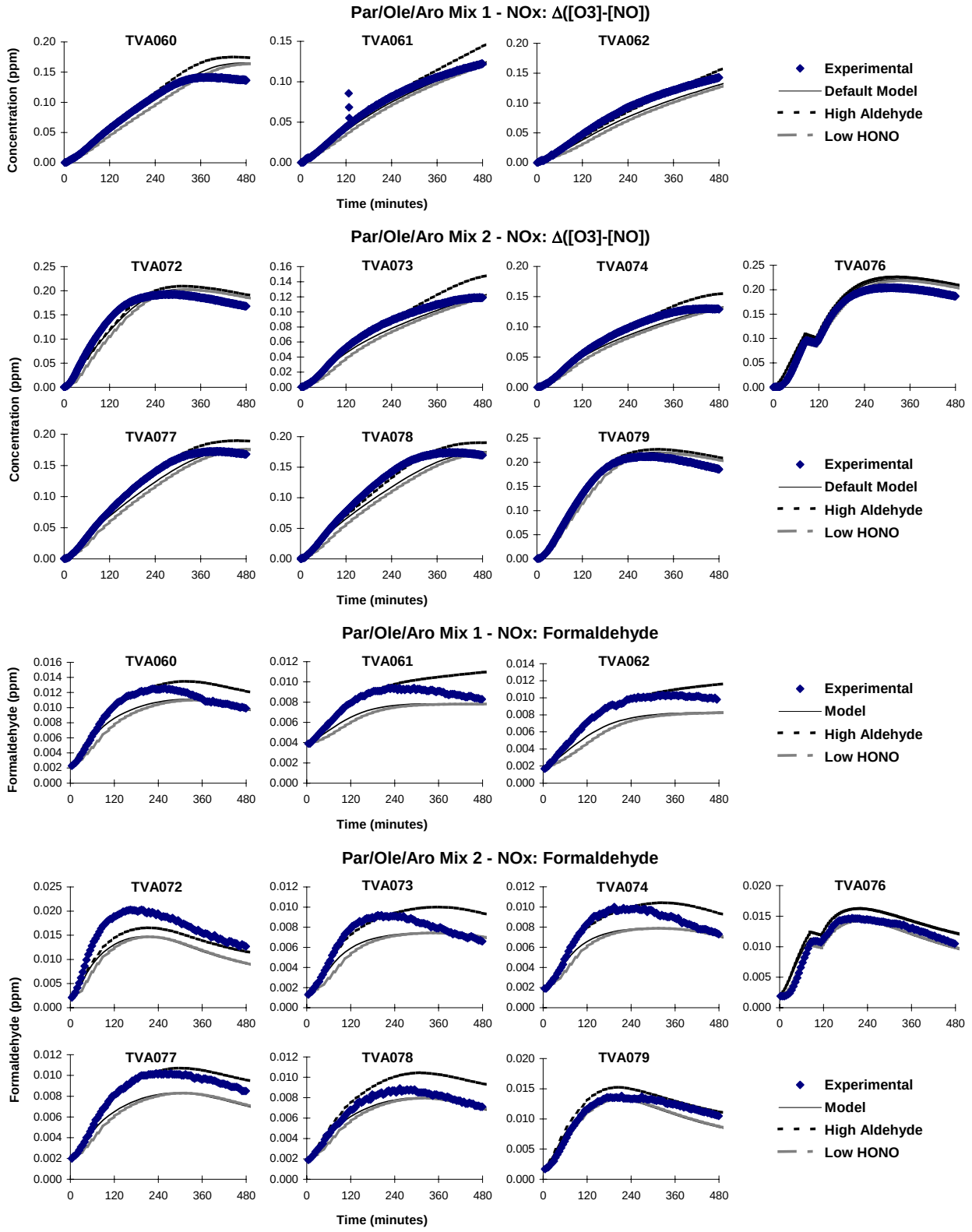

Figure B-44. Plots of experimental and calculated Δ([O3]-[NO]) and formaldehyde results of the TVA paraffin, olefin and aromatic mix experiments.

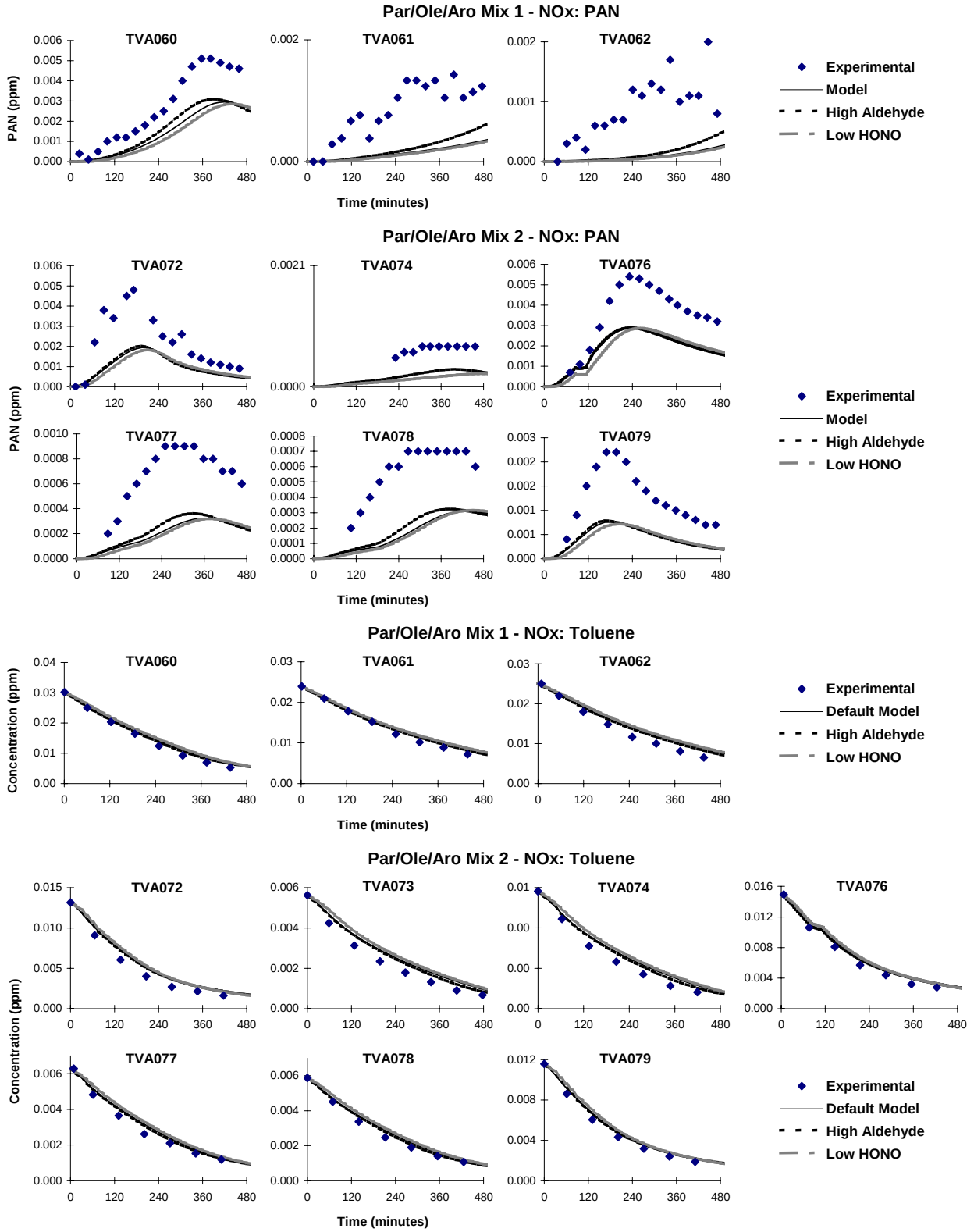

Figure B-45. Plots of experimental and calculated PAN and toluene results of the TVA paraffin, olefin and aromatic mix experiments.

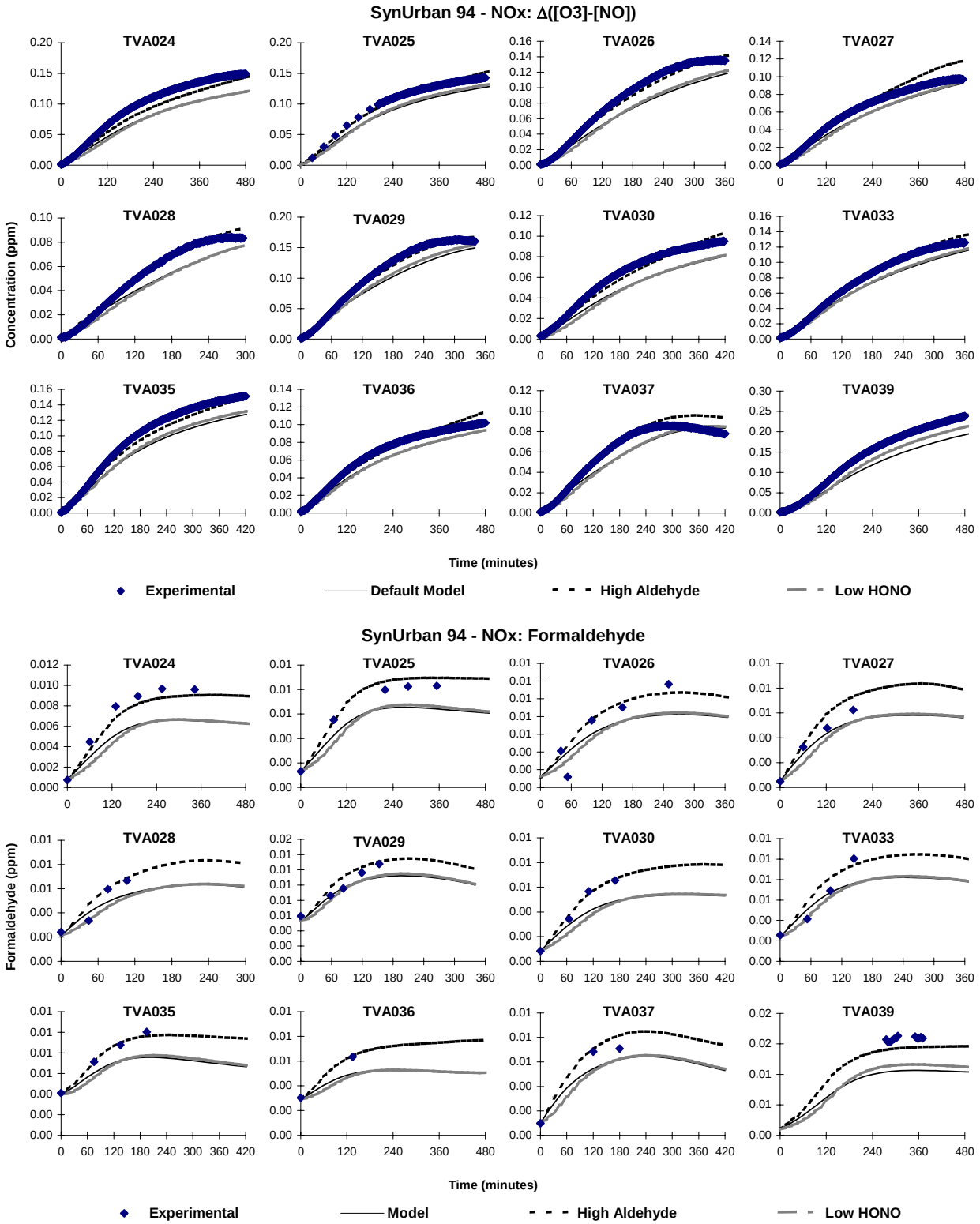

Figure B-46. Plots of experimental and calculated Δ([O3]-[NO]) and formaldehyde results of the TVA synthetic urban mix experiments.

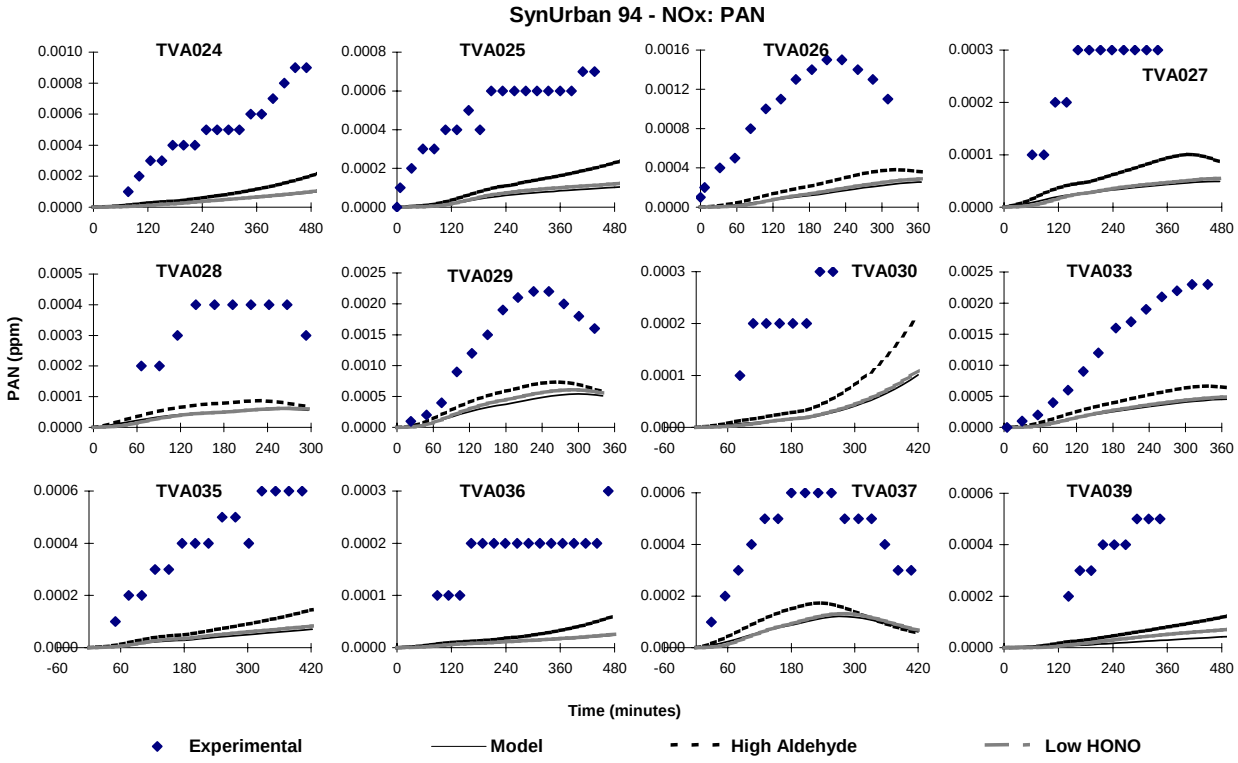

Figure B-47. Plots of experimental and calculated PAN results of the TVA synthetic urban mix experiments.

CSIRO Chamber Experiments

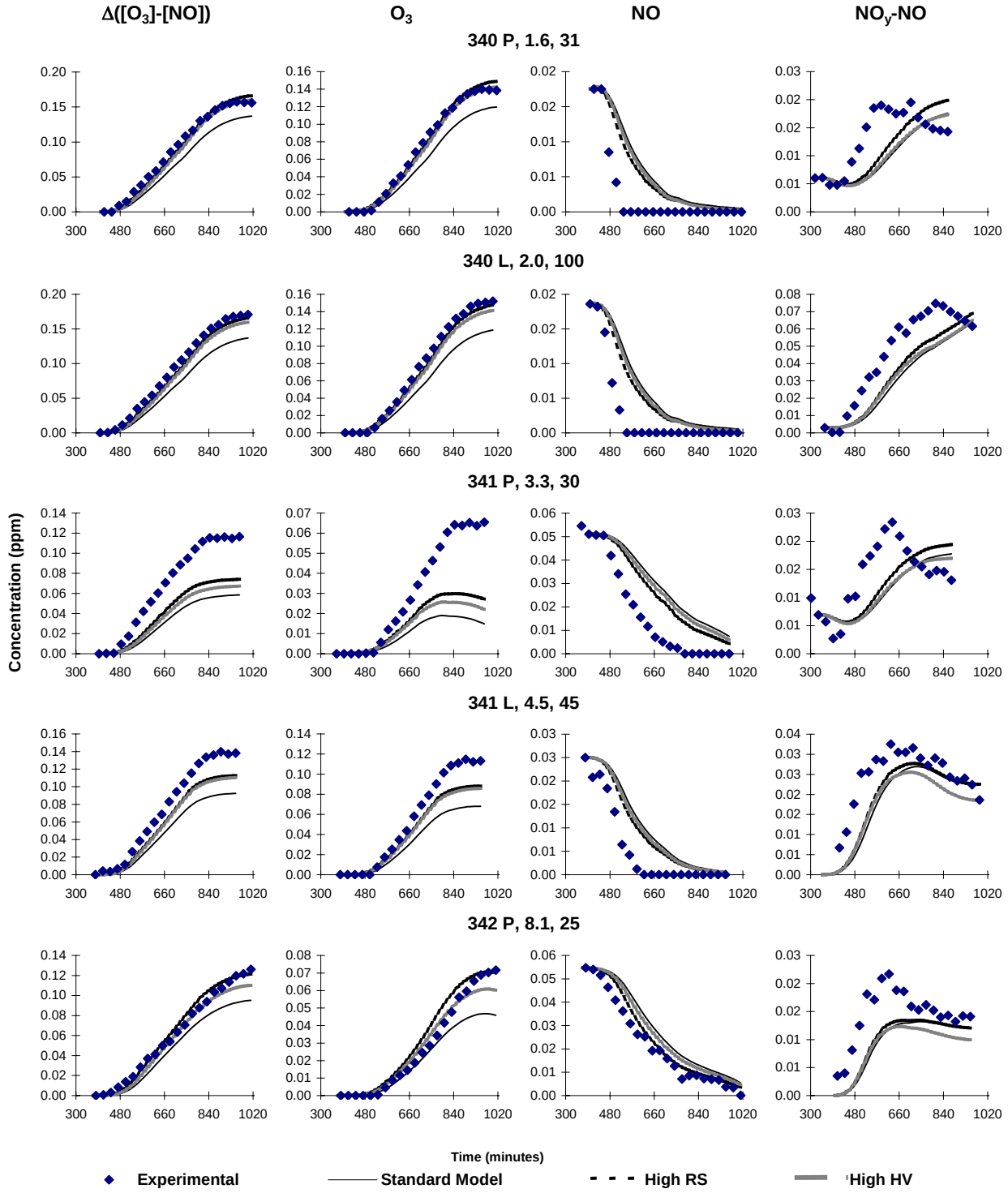

Figure B-48. Experimental and calculated Δ([O_3]-[NO]), O_3, NO, and NO_y-NO data for the CSIRO experiments 340, 342, and Side P of 342. The labels give Run ID, initial VOC in ppmC, and initial NOx in ppb.

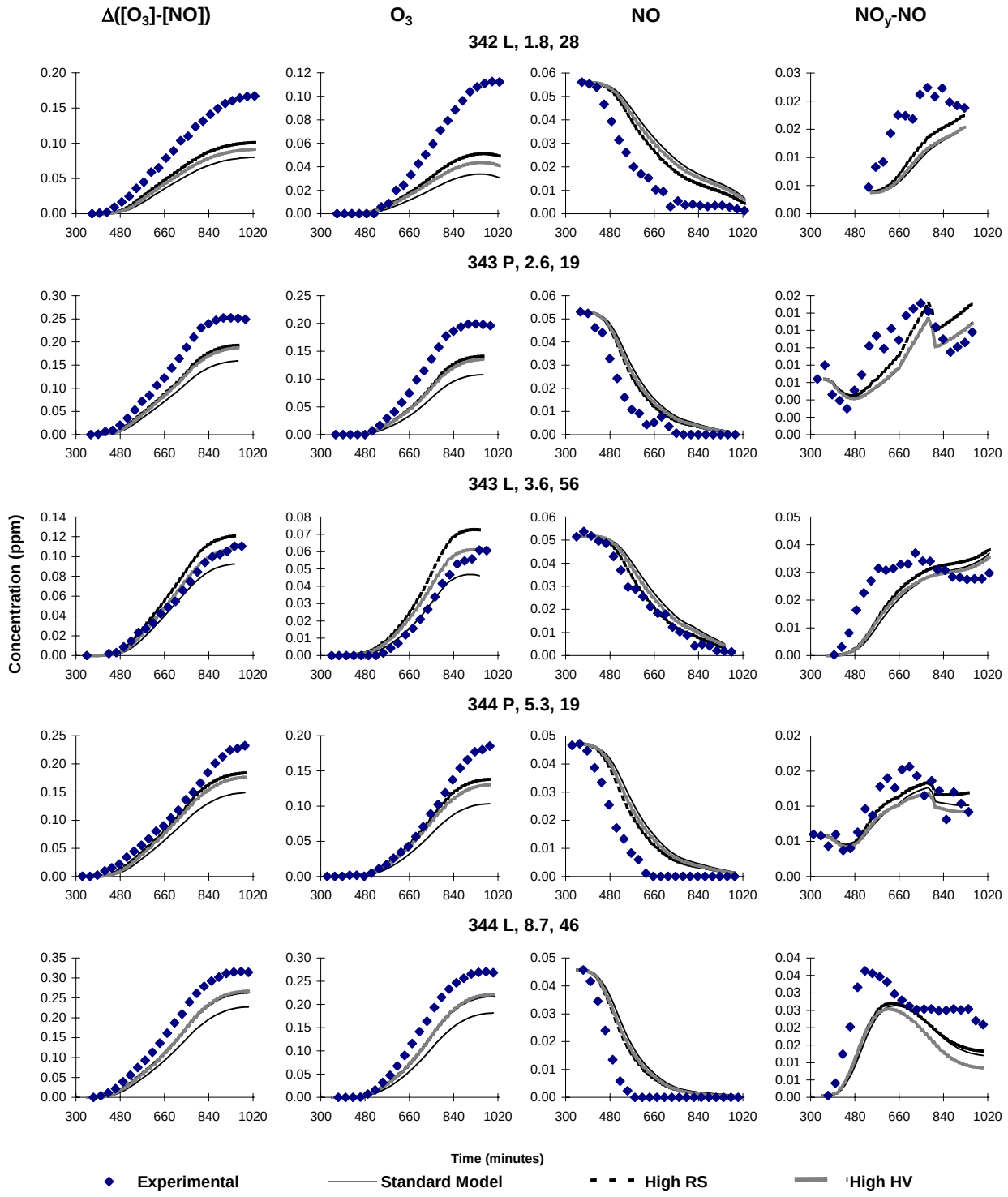

Figure B-49. Experimental and calculated Δ([O_3]-[NO]), O_3, NO, and NO_y-NO data for the CSIRO experiments 342 (Side L), 343 and 344. The labels give Run ID, initial VOC in ppmC, and initial NOx in ppb.

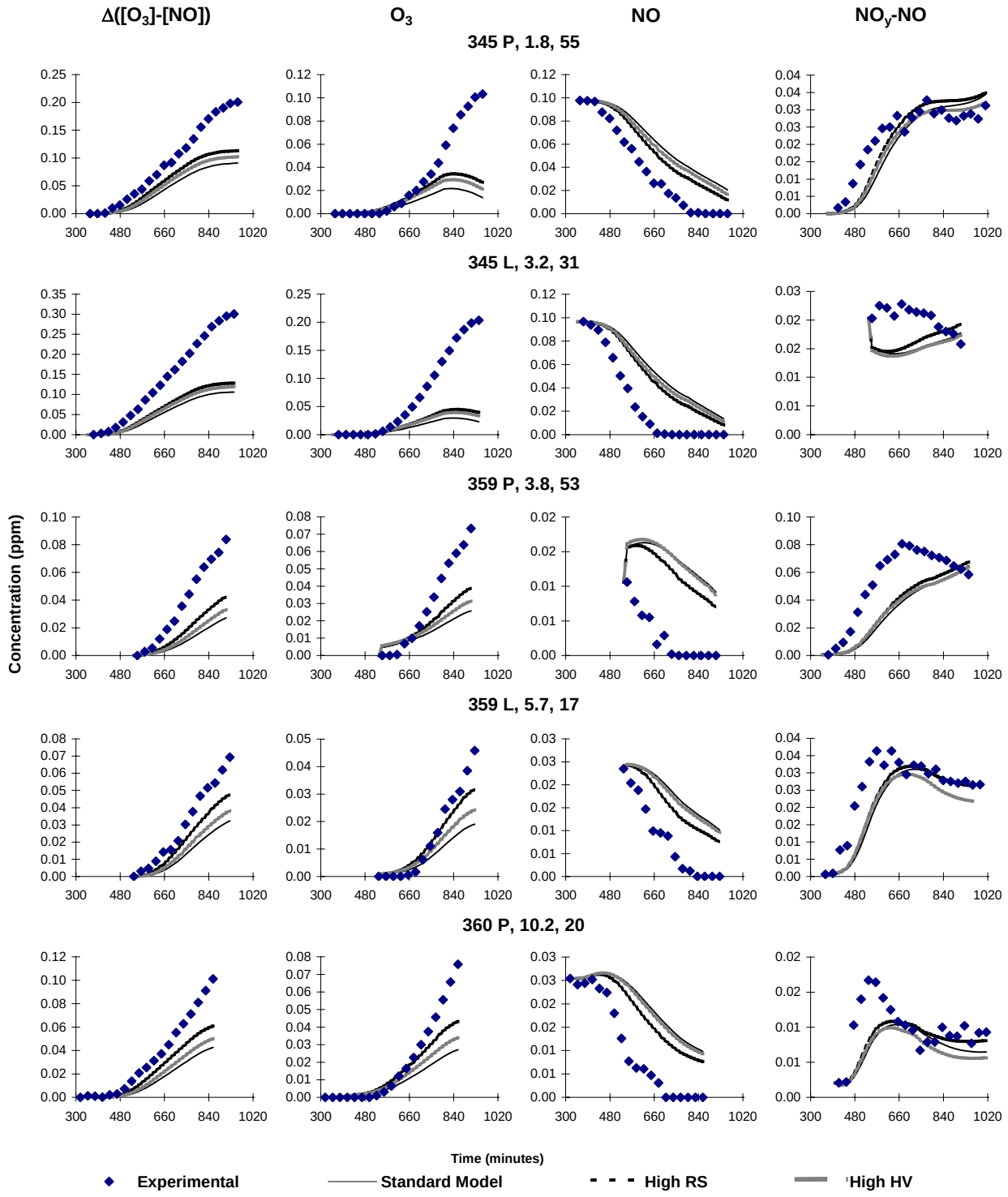

Figure B-50. Experimental and calculated Δ([O_3]-[NO]), O_3, NO, and NO_y-NO data for the CSIRO experiments 345, 359, and Side P of 360. The labels give Run ID, initial VOC in ppmC, and initial NOx in ppb.

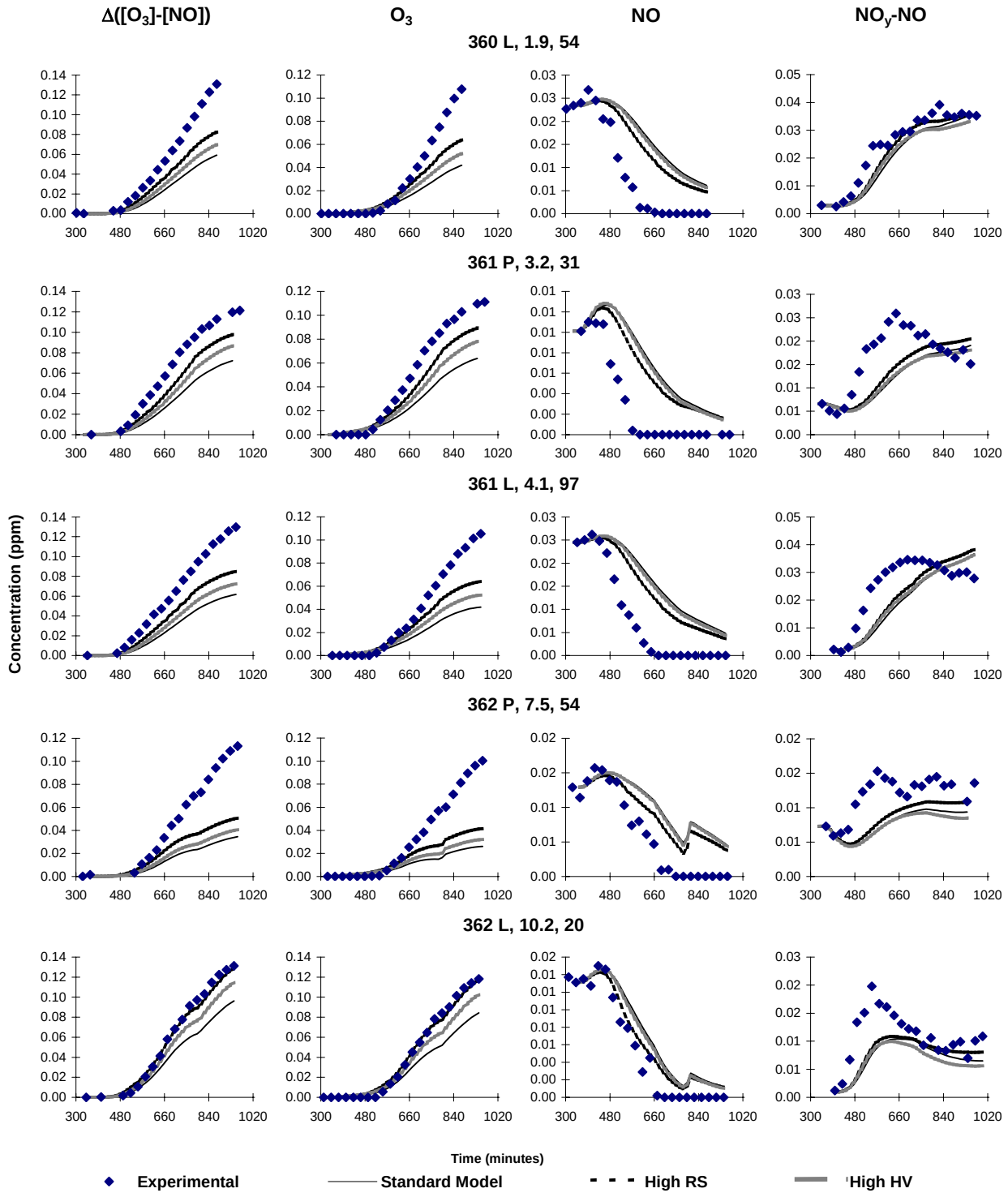

Figure B-51. Experimental and calculated $\Delta([O_3]-[NO])$, O_3, NO, and NO_y-NO data for the CSIRO experiments 360 (Side L), 361 and 362. The labels give Run ID, initial VOC in ppmC, and initial NOx in ppb.